

Development of a multi-disciplinary toolkit to study time cells in the hippocampus

A Thesis

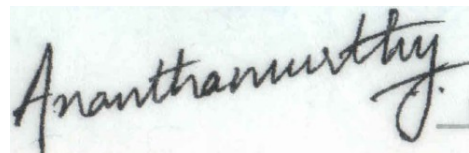
Submitted to the
Tata Institute of Fundamental Research,
Mumbai
for the degree of **Doctor of Philosophy**
in **Biology**

by
Kambadur Gundu Ananthamurthy
National Centre for Biological Sciences,
Tata Institute of Fundamental Research,
Bangalore
April, 2023

DECLARATION

This thesis is a presentation of my original research work. Wherever contributions of others are involved, every effort is made to indicate this clearly, with due reference to the literature, and acknowledgment of collaborative research and discussions.

The work was done under the guidance of Professor Upinder S. Bhalla, at the National Centre for Biological Sciences, Tata Institute of Fundamental Research, Bangalore.

A handwritten signature in black ink, appearing to read "Ananthamurthy J." followed by a short horizontal line.

Kambadur Gundu Ananthamurthy

In my capacity as supervisor of the candidate's thesis, I certify that the above statements are true to the best of my knowledge.

A handwritten signature in black ink, appearing to read "Upinder S. Bhalla".

Prof. Upinder S. Bhalla

Date: 21st April, 2023

43 Acknowledgments

44

45 Projects like the ones described in this thesis cannot be accomplished
46 without good, strong leadership. I thank Upi for the opportunity to learn
47 and grow in his lab, and his patience to see me through tough
48 moments.

49 I thank Shona and Mukund for advice and help over the past decade.

50 I thank my seniors Mehrab, Ashesh, Partha, and Subha. I hope I can
51 make them proud, someday.

52 I thank my colleagues Sahil, Dilawar, Oliver, and Aditya for helping me
53 whenever I asked.

54 I thank Sriram, Manoj, Krishna, and Amit for everything I learnt in CIFF.

55 I thank Mohini, Mugdha, Sebastien, Arnab, and Terence, for being my
56 friends for as long as they could.

57 I thank Supriya, Harini, Anupratap, Sohail, and Prabahan, my well-
58 wishers from Shona lab.

59 I thank KS Krishnan. His absence cannot be filled with anything else.

60 I thank Sanjay, Axel, Panic, Vatsala, Uma, Madan, and Jitu, for always
61 bringing a breath of inspiration to my life and my work.

62 I thank Dr. Shane Heiney for showing me the way with trace eye-blink
63 conditioning, and Dr. Daniel Dombeck for the chronic hippocampus
64 preparation.

65 I'm indebted to the Animal Care and Resource Center (ACRC), the
66 Central Imaging and Flow Facility (CIFF), Dorababu & the Electronics
67 Workshop, Devakumar & the Mechanical Workshop, for anything and
68 everything I have been able to make or create.

69 I thank Swarna and Nikhila for teaching me Tennis. I also thank the
70 Football group, the Badminton group, the Music group, the Theater
71 group, and the Improv group, for always giving me a chance to
72 explore.

73 I thank Neha Panwar for being there in the end.

74 "Very little" is what I'd have achieved without my parents. I hope to be
75 a good person and live up to the values they have taught me.
76 I thank the canteen, the sports facility and gym, hospitality,
77 instrumentation, and admin, for helping me with everything else.

78

for Archana && Bujju,

Index of Tables

Table 1: Summary table of behaviour protocols attempted and essential results.....	99
Table 2: Recipe for ready-to-use cortex buffer. The buffer is typically prepared and stored in aliquots to be used each week. The correct pH range of the buffer was often a crucial factor ensuring the success of the hippocampal preparation.	108

Table of Figures

Figure 1: A schematic representation of the Trisynaptic Pathway as observed with coronal slices along the longitudinal axis of the hippocampus. Image adapted from the webpage for the Neural Circuits and Memory Lab, University of Wisconsin (Milwaukee) [https://sites.lsa.umich.edu/diba-lab/neural-circuits-of-the-hippocampus/].....	26
Figure 2: Water delivery calibration to reward the animal consistently with the same volume of water.....	68
Figure 3: Optoisolator circuit to amplify +5V DC input to +12V DC output.....	70
Figure 4: Lick detector circuit based on a MOSFET design. Whenever the animal performed a lick, a +5V DC Output would be read out.....	71
Figure 5: Typical trial structure with the various phases. Each trial was followed by a randomized Inter-Trial Interval (ITI).....	73
Figure 6: Performance evaluation for two example mice trained to Protocol 1.1 and 1.2. Percentage of total licks in the various trial phases (Pre-Tone, Tone, CT, and ITI), across all sessions of training (coloured bar plots) for A) Mouse 3, and B) Mouse 4.....	74
Figure 7: Performance evaluation for two example mice trained to Protocol 2. Percentage of total licks in the various trial phases (Pre-Tone, Tone, CT, and ITI), across all sessions of training (coloured bar plots), for (A) Mouse S1, and (B) Mouse S2.....	78
Figure 8: Schematic representation of the experimental setup for a simple detection task where the animal must perform a	

lick upon correctly detecting the presence of the conditioned stimulus (CS; from a range of modalities).....	81
Figure 9: Typical trial structure with the various phases and lick dependent relationships.....	82
Figure 10: (A) Performance traces for all the animals individually shown in dashed grey lines. Mean + SEM in black. (B) Mean Performance (%) and Mean Go Tone Lick Percentage (%) with Session for the Go/No-Go Task, plotted in black and green, respectively.....	83
Figure 11: The number of licks in the pre-tone (blue), no-go tone (red), and go tone (green) phases, in a representative animal, in a session with maximum Performance (%).	84
Figure 12: Schematic representation to showcase the two main subtypes of Classical Conditioning (Eye-Blink Conditioning, for our experiments) based on the relative timing and presentation of the CS and US.....	86
Figure 13: Trial by trial (left), and trial-averaged running speed (right) for two example animals, (A) M2 Session 12, and (B) M5 Session 12.....	89
Figure 14: Schematic representation of (A) the behaviour rig with 2-Photon imaging, to train head-fixed mice on a Trace Eye-Blink Conditioning (TEC) task, and (B) relative time intervals between the CS and US.....	91
Figure 15: A picture of a head-fixed mouse clamped on the behaviour rig, with key components: 1) Red LED Illumination, 2) Blue LED CS, 3) Air-puff port directed to the left eye, and 4) Height-adjustable Treadmill.....	92
Figure 16: Steps from behaviour video frame to Fraction of Eye-Closed (FEC) analysis.....	93
Figure 17: Conditioned Responses (CRs) are small amplitude eye-blinks triggered by the CS, and develop with multiple training sessions, while Unconditioned Responses are large eye-blinks to the US, typically consistent across sessions. (A,B) Trial-by-trial FEC traces for (A) M11 Session 2, and (B) Session 4. (C,D) Trial-averaged FEC traces for (C) Session 2 and (D) Session 4, with paired (red) and probe (green) trials.	94
Figure 18: Performance in terms of the percentage of Hit Trials to total trials across sessions, including an ISI switch from 250 ms to 350 ms.....	95
Figure 19: Conditioned Responses (CRs) are preserved for previously learnt ISIs, and switching the ISI to longer intervals results in Complex (multi-CR) eye-blink responses.	

(A,B) Trial-by-trial FEC scores for (A) 250 ms ISI (left) and (B) 500 ms ISI. (C,D) Trial-averaged FEC traces for (C) 250 ms ISI (left) and (D) 500 ms ISI (right), with paired (red) and probe (green) trials.....	96
Figure 20: Conditioned Response (CR) onset timing is maintained across ISI switches. Representative examples from a short ISI switch from (A) 250 ms to (B) 350 ms (right).	97
Figure 21: Bar plots for Conditioned Response (CR) onset across multiple sessions of training after ISI switch from 250 ms to 350 ms, irrespective of how strongly the animals learnt the task. (A) red, strong learner, and (B) blue, weak learner.	97
Figure 22: Representative example of mice trained to 550 ms ISI (Session 6) and 750 ms (Session 4). (A,B), Trial-by-trial FEC responses for (A) 550ms ISI, and (B) 750ms ISI. (C,D) Trial-averaged FEC responses for (C) 550 ms ISI, and (D) 750 ms ISI, with paired (red) and probe trials (green).....	98
Figure 23: (A) A schematic of the rodent brain, showcasing the two hippocampi, one in each hemisphere. The hippocampi lie ~1 mm (mice) below the cortical surface. (B) The hippocampal preparation allows optical access to the deep lying hippocampal CA1 cells, relative to the skull/cortex. The CA1 cell bodies arrange in a laminar fashion, as a tight cell body layer that can be visualized by fluorescence (using either OGB-1 or GCaMP).....	106
Figure 24: Schematic representation for stereotaxic viral injection.....	111
Figure 25: (A) Representative Two-Photon Calcium Image of a plane of Hippocampal CA1 cells, bolus loaded with Oregon Green Bapta-1 (OGB-1), at an instant in time. Example cells marked out post-hoc as pink, green, blue and red. Scale bar 20 μ m. (B) Representative dF/F (%) traces for the calcium activity recorded in a single 10s video for example cells pink, green, blue, and red. Scale bar (1 sec; 10% dF/F).....	113
Figure 26: Tissue Degradation over time. Representative Two-Photon Calcium images of a snapshot in time of the Hippocampal CA1 cell body layer on (A) Day 1 after the surgery and (B) Day 3, after the surgery. Scale bar 30 μ m.	115
Figure 27: Chronic calcium imaging of the same Hippocampal CA1 cells over weeks. Representative 2-Photon images from (A) Day 20, and (B) Day 21, after surgery.	

Landmarks have been marked and were used to confirm frame registration and identify cells. Scale bar 100 μ m.....	116
Figure 28: (A) Representative Two-Photon Calcium Image of a plane of Hippocampal CA1 cells expressing GCaMP6f at an instant in time. Example cells marked out post-hoc in pink, blue, and green, with no-cell background in red. Scale bar 20 μ m. (B) Representative dF/F (%) traces for the calcium activity recorded in a single 10s video for example cells in pink, blue, and green, with no-cell background in red. Scale bar (2 sec; 10% dF/F).....	117
Figure 29: (A) Correlation Coefficients for cell pairs from an example two-photon recording. (B) Meta-K Means clustering with cell pairs using the heuristic that within group pairs would be more similar than between group pairs. In this example, the cells were clustered into two groups, I (red) and II (yellow). (C) Two-Photon image of the field of view of cells; same as Figure 25A. (D) Spatial organization of correlated cell pair groups during spontaneous activity (Modi et al... 2014).....	119
Figure 30: (A) Trial-averaged (25 trials) calcium activity from ~100 CA1 cells in trials where a 5000 Hz tone was presented (red bar). (B) Trial-averaged (18 trials) calcium activity from the same cells in trials where a 5 LPM air-puff to the ipsilateral whiskers was presented (red bar).....	120
Figure 31: (A) Correlation Coefficients for cell pairs from post whisker-puff stimulation periods. (B) Meta-K Means clustering with cell pairs using the heuristic that within group pairs would be more similar than between group pairs. In this example, the cells were clustered into three groups I (red), II (orange), and III (yellow). (D) No clear spatial organization of correlated cell pair groups post whisker stimulation.....	121
Figure 32: (A) Correlation Coefficients for cell pairs from a trial-shuffle control dataset (B) Meta-K Means clustering revealed that there were no cell pair groups identified.....	122
Figure 33: Example Time Cells visualized as event raster plots (A, B, C), along with the trial-summed activity profiles (D, E, F) suggesting ~50% hit trials, for cells 29 and 72 from Session 1 (session type 5) with mouse M26, and slightly lower reliability (~25% hit trials) from cell 105.....	125
Figure 34: Example Other Cells visualized as event raster plots (A, B, C), along with the trial-summed activity profiles	

(D, E, F) for cells 10, 25, and 120 from Session 1 (session type 5) with mouse M26.....	125
Figure 35: Event Time Histograms or tuning curves for Identified Time-Locked Cells with trial-summed peaks in session 4 of training (session type 5) with mouse M26. (A) Unsorted list of Time cells. (B) Peak-sorted list of the same cells. Here, 1 bin = 3 frames = ~210 ms (sampling rate 14.5 Hz without binning; ~5 Hz with binning). As per the (legacy) session type 5 protocol, the CS (50 ms Blue LED flash) was presented in frame bin 39, followed by a stimulus-free trace interval during frame bins 40 and 41, and then the US (50 ms airpuff to ipsilateral eye) was presented in frame bin 42... .126	
Figure 36: Temporal Information (bits) vs Sorted time cell number from the analytically identified Time Cells in Session 4 (session type 5) with mouse M26. No clear trend was observed.....	127
Figure 37: More time cells observed to attain tuning as training sessions. Event Time Histograms of the identified set of time cells between A) Sessions 1 and (B) Session 2, with mouse M26 (session type 5).....	128
Figure 38: Sorted Time Cells form Sequences that develop with learning. Trial-Averaged calcium activity traces for all recorded cells across A) Session 1, B) Session 2, and C) Session 4, with mouse M26 (sessiontype 5). Time 0 ms was aligned to the CS. The CS + Trace + US interval lasted from 0-600 ms, here.....	129
Figure 39: Same/similar tuning across session 1 and session 2 for this example time cell. Blue Event Time Histograms represent the tuning curve for the cell for session 1 (date: 20180508) and Red represent the same but for session 2 (date: 20180509). Pearson's correlation coefficient between the two session pairs was 0.7011.....	130
Figure 40: Three example chronically tracked cell pairs with tuning peaks arriving earlier with training sessions (rows). Blue Event Time Histograms represent the tuning curve for any cell for session 1 (date: 20180508) and Red represent the same but for session 2 (date: 20180509). Pearson's correlation coefficient between the session pairs was 0.6.348, 0.5872 and 0.7027 for A) cell pair 1, B) cell pair 2, and C) cell pair3, respectively.....	131
Figure 41: Example chronically tracked cell pair with de-tuning between session 1 and 4. Blue Event Time Histograms represent the tuning curve for the example cell for session 1	

(date: 20180508) and Red represent the same but for session 4 (date: 20180514). Pearson's correlation coefficient between the two curves was -0.0606.....	132
Figure 42: Comparing chronically tracked time cells across sessions for all matched cell pairs by (A) Correlation Analysis, and (B) Timing of peaks.....	133

Table of Contents

DECLARATION.....	2
Acknowledgments.....	3
Abstract.....	14
Chapter 1 – Introduction.....	16
Projects and overall goals.....	16
Neural systems and behaviour.....	17
Engrams associated with Learning and Memory.....	18
Dynamics in the neural code for engrams.....	20
Theories on the function of the hippocampus.....	23
Space and time in the hippocampus.....	25
“Single-cell, multi-trial” vs. “multi-cell, single-trial” approaches in Neuroscience.....	32
Single-Unit Electrophysiology vs 2-Photon Calcium Imaging to study the Hippocampus.....	36
Calcium imaging by 2-Photon Microscopy.....	38
Automated ROI detection for large-scale Calcium Imaging datasets.....	42
A brief introduction to associative learning.....	42
Short Summaries of the 3 projects.....	45
Project I - How do sensory representations transform with learning?.....	45
Project II - How does the timing of cellular activity adjust to behavioural task variables?.....	46
Project III - What is the best way to detect and score time-tuned cellular activity?.....	47
Code Availability.....	49
Bibliography.....	49
Chapter 2 – Behaviour.....	64
Towards understanding brain activity in a reproducible context.....	64
Operant conditioning [Project I].....	66
Required features.....	66
Water delivery and calibration.....	68
Opto-islator circuit for solenoid control.....	69

Lick detection circuit.....	70
Controlling task details and protocol information.....	71
Head-bar implant, Animal Handling, and Water deprivation.....	72
PROTOCOL 1.1: Stimulus Detection Task.....	72
PROTOCOL 1.2: Stimulus Detection Task with aversive punishment.....	73
Results - Protocol 1.1 and 1.2.....	75
Protocol 2: Stimulus Detection task with timeout box.....	75
Results - Protocol 2.....	77
Protocol 3: Delayed Non-Match to Sample (DNMS).....	79
Results - Protocol 3.....	80
Protocol 4: Go/No-Go Task.....	80
Results - Protocol 4.....	82
Trace Eye-Blink Conditioning [Project II].....	85
Tracking eye-blink responses.....	87
Treadmill and tracking running speed.....	88
Behaviour rig and protocol control - Software.....	89
Analysis - TEC.....	92
Results - TEC.....	94
Bibliography.....	100
Chapter 3 - Imaging.....	102
Physiology in the hippocampus.....	103
Methodology - Acute and chronic imaging [Projects I & II]	105
Preparation of Cortex Buffer.....	107
Oregon Green Bapta-1 injections for acute imaging.....	109
GCaMP and chronic imaging.....	110
Results - Imaging.....	112
2-Photon calcium imaging of hippocampal CA1, <i>in vivo</i>	112
Acute Imaging of OGB-1 loaded hippocampal CA1, <i>in vivo</i>	112
Chronic imaging of hippocampal CA1 using GCaMP.....	114
Spontaneous activity during non-stimulus periods.....	117
Spatial organization of activity correlated cells during spontaneous activity.....	118
Stimulus evoked responses.....	119
Spatial organization of activity correlated cells post whisker-puff stimulation.....	120
Chronic imaging now possible for weeks with the same mouse.....	122
Preliminary analysis to identify time cells.....	123

Tuning, re-tuning, and de-tuning of time cells across sessions.....	127
Bibliography.....	135
Chapter 4 - Analysis.....	140
Chapter 5 - Discussion.....	147
The study of hippocampal CA1 sequences.....	147
Mapping sequences to abstract variables.....	149
Does the brain create or predict?.....	151
Bibliography.....	152
All Bibliography.....	156

80 **Abstract**

81

82 The mammalian Hippocampus is considered important for the
83 formation of several kinds of memory, one of which is the association
84 between stimuli occurring separately in time. Several studies have
85 shown that small populations of Hippocampal CA1 cells fire in time-
86 locked sequences, "bridging" the time gap in temporal tasks (B. Kraus
87 et al., 2013; MacDonald et al., 2011, 2013; Pastalkova et al., 2008),
88 including a single-session version of Trace Eye-Blink Conditioning or
89 TEC (Modi et al., 2014). Such cells are commonly termed time cells
90 (Eichenbaum, 2017; MacDonald et al., 2011).

91 The main goal of the thesis was to be able to study time cells under a
92 variety of behavioural tasks and conditions and elucidate several
93 physiological properties. We standardised a multi-day Trace Eye-Blink
94 Conditioning (TEC) protocol to train head-fixed C57Bl6 mice (Siegel et
95 al., 2015). TEC involves an association between a previously neutral
96 Conditioned Stimulus (CS) with an eye-blink inducing Unconditioned
97 Stimulus (US), across an intervening, stimulus-free, Trace Interval. We
98 were able to observe stable, adaptive learning with our protocols. We
99 also standardized an *in vivo* imaging preparation to record calcium
100 activity from hippocampal CA1 cells, adapted from previously
101 published methods (Dombeck et al., 2010; Modi et al., 2014). We used
102 a custom-built two photon laser-scanning microscope and performed
103 galvo-scans through the imaging window, during TEC. The behaviour
104 and Imaging was conducted simultaneously to record calcium activity
105 as the animals learnt the task. Chronic Calcium Imaging allowed us to
106 track and record the activity of the same cells, confirmed

107 morphologically. We could then identify time cells across sessions, and
108 look for adaptations in tuning curves, along multiple sessions.
109 Furthermore, numerous approaches have been developed to analyse
110 time cells and neuronal activity sequences, but it is not clear if their
111 classifications match, nor how sensitive they are to various sources of
112 data variability. We provided two main contributions to address this: A
113 resource of synthetic 2P Calcium activity data, and a survey of several
114 methods for analyzing time cell data using our synthetic data as
115 ground truth. The synthetic dataset and its generation code are useful
116 for profiling future methods, testing analysis tool-chains, and as input
117 to computational and experimental models of sequence detection. We
118 characterized strengths and weaknesses of several time-cell analysis
119 methods. Finally, we benchmarked how computational requirements
120 scale with large datasets typical of recent recording technologies.

121 Chapter 1 – Introduction

122

123 The vertebrate Central Nervous System (CNS), consisting primarily of
124 the central ganglia (brain) and the spinal cord, samples and receives
125 information from the external world offering top-down control over the
126 activity of all parts of the body. Functions like exploration, food
127 acquisition, and danger aversion, all involve complex coordination
128 between,
129 ● the Sensory Systems (that integrate information from the
130 environment),
131 ● the Memory Systems (that integrate sensory information with
132 prior experience), and
133 ● the Motor Systems (that integrate motor plans and execute
134 movement).

135

136 Projects and overall goals

137

138 The overall focus of the work and experiments described in this thesis
139 was to study Memory Systems, specifically, in terms of,
140

141 **Project I:** How do sensory representations transform with
142 learning?

143

144 **Project II:** How does the timing of cellular activity adjust to
145 behavioural task variables?
146
147 **Project III:** What is the best way to detect and score time-tuned
148 cellular activity?
149
150 Narrowing down, we as a lab were interested in the mammalian
151 hippocampus, a brain structure which is important for consolidating
152 information (from Sensory and other Memory Systems) to enable
153 certain kinds of short-term memory and the translation of short-term
154 memory to long-term.
155

156 **Neural systems and behaviour**
157
158 Ramón y Cajal, one of the pioneers of neuroscience around 1900,
159 utilized Camillo Golgi's staining method to conclusively describe
160 neurons in the brain as independent functional units connected to each
161 other in intricate networks made up of many nodes ($\sim 10^6 - 10^9$). These
162 neurons have since been described not just anatomically, but also on
163 the basis of genetics, development, and neurophysiology.
164
165 In the sub-discipline of Learning and Memory an often studied neuron
166 type is the pyramidal neuron, an example of which is the hippocampal
167 CA1 pyramidal neuron. This thesis describes a toolkit of techniques
168 ranging in a wide, multi-disciplinary scope, assembled with
169 standardized hardware and software routines studying animal
170 behaviour, network neurophysiology, and statistical analyses.

171 The aim of the toolkit was to provide the experimental ability to study
172 the hippocampal CA1 pyramidal neuron network, under strictly
173 controlled behavioural contexts designed to train experimental mice on
174 temporal or episodic memory tasks. Specifically, these tasks such as
175 Trace Eye-Blink Conditioning (TEC) have previously been described to
176 elicit hippocampal CA1 sequences (B. J. Kraus et al., 2015;
177 MacDonald et al., 2011, 2013; Mau et al., 2018; Modi et al., 2014;
178 Pastalkova et al., 2008). This spatiotemporal network activity sequence
179 is dynamic and built from individual hippocampal CA1 pyramidal
180 neurons showcasing time-tuned activity through spiking. These cells
181 are called time cells (Eichenbaum, 2017; MacDonald et al., 2011).
182

183 **Engrams associated with Learning and
184 Memory**

185
186 The term "engram" (coined by Richard Semon) refers to the physical
187 substrate of memory in the organism, used for storing and recalling
188 memories (Josselyn & Tonegawa, 2020). Donald Hebb's theory of
189 Hebbian Plasticity (Hebb, 1949) postulated that memory formation was
190 correlated to modulations in synaptic strength and connectivity. The
191 theory critically emphasized that the pair of neurons connected through
192 the synapse undergoing plasticity to strengthen efficacy, required the
193 spiking activity of both neurons. In subsequent decades, research into
194 the idea led to the theory of spike-timing-dependent plasticity
195 (Caporale & Dan, 2008), a mechanism of synaptic plasticity based on
196 the relative timing of activity of the neurons. It is still a matter of debate
197 whether the biophysical manifestation of the engram is the synapse,

198 the activity of the neurons, biophysical or chemical processes, but it is
199 likely that the engram is distributed across several computational
200 scales in the brain.

201

202 Eric Kandel's experiments with the Aplysia sensory neurons studied gill
203 withdrawal - an aversive but stable, adaptive behaviour (Carew et al.,
204 1971). The reliability of this learned response allowed the experiments
205 to include crucial electrophysiological and neurochemical circuit
206 dissections that ultimately lead to the discovery of the entire neural
207 circuit orchestrating the task, even to the level of cellular signaling.
208 This led to decades of research focused on the plasticity of synapses
209 across nervous systems in the animal kingdom.

210

211 Research exploring causal relationships between the physical or
212 functional integrity of various brain regions and overt behaviour has
213 been crucial to mapping many brain regions to specific functions and
214 motor responses. Technological advancements in molecular
215 neuroscience led to the development of a number of fluorescent
216 sensors, conditional tagging, activators and inhibitors that allowed
217 cellular resolution tracing of the engram (Luo et al., 2018).

218

219 Experiments by Sheena Josselyn, Alcino Silva, and colleagues led to
220 the discovery that the intrinsic excitability of a pyramidal neuron in any
221 network positively biased the probability of recruitment to the engram
222 (Han et al., 2009; Rogerson et al., 2014; Yiu et al., 2014; Y. Zhou et
223 al., 2009), *viz.*, the tagged set of cells were active when memory was
224 learnt and recalled. The engram seemed to be described in terms of
225 the cellular sub-population involved but the experiment could only
226 identify the same over a relatively longer window of time (~mins.). This

227 could lead to only a static list of cells which may even have included
228 False Positives (Type I error). Importantly, any dynamics in the
229 spatiotemporal patterns of activity of the pyramidal neurons were not
230 amenable to study at shorter timescales (~ms.). On the other hand,
231 physiological recordings could describe these dynamics at short
232 timescales, but were rarely translated to chronic measurements of the
233 activity of the same cells across days and sessions, given technical
234 limitations at the time.

235

236 **Dynamics in the neural code for engrams**

237

238 We first discuss some important results that help motivate the study of
239 physiological recordings in the context of engrams, *i.e.*, the dynamical
240 nature of the neural code (~ms to s). In later sections we will describe
241 these dynamics in more detail.

242

243 Place cells and their role in spatial navigation have been studied in
244 great detail through decades of research ever since they were first
245 described by John O'Keefe (O'Keefe & Dostrovsky, 1971). We did not
246 explicitly study place cells in this thesis but some key discoveries in
247 literature require mention, with the goal to build a case for a theory of
248 CA1 ensemble sequences (Modi et al., 2014). Briefly, place cells are
249 pyramidal neurons that showcased a higher than baseline probability
250 of firing action potentials whenever animals navigating spatial
251 environments visited specific locations. The tuning curves or firing
252 fields for these cells often map to the real spatial trajectory of the
253 animal and is thought to be an assimilation of both brain external

254 stimuli such as visual cues, as well as brain internal variables such as
255 motivation, goal orientation, memory, and experience (Ferbinteanu et
256 al., 2011; Ferbinteanu & Shapiro, 2003; Foster, 2017; Frank et al.,
257 2000; Wood et al., 2000).

258

259 As the animal enters these landmark locations in any spatial context,
260 these place cells showcase Phase Precession, firing earlier in phase to
261 cycles of Theta a network rhythm clocked at ~4-10 Hz, as the animal's
262 position changes relative to the landmark. These navigation mapped
263 place cell sequences are called Theta Sequences (Foster & Wilson,
264 2007), typically mapped to a few active neurons at a time.

265

266 In very specific contexts, these place cells express activity sequences
267 synchronized to Sharp Wave Ripples, a different network activity
268 phenomenon clocked at ~10-30 Hz, often not tied to the animal's
269 location, called Replay Sequences (Csicsvari et al., 2007; Foster &
270 Wilson, 2006). These sequences have been described to play out
271 typically in reverse temporal order to models of place cell sequences
272 describing known trajectories in space.

273

274 There is variability in the firing of place cells in any spatial context, and
275 studies have mapped specific sequences to very specific trajectory
276 goals (going towards or away from locations) with modulation by both
277 egocentric and allocentric orientations cues (Davidson et al., 2009;
278 Ferbinteanu et al., 2011; Ferbinteanu & Shapiro, 2003; Frank et al.,
279 2000; Wood et al., 2000) and movement speed based estimates of
280 distance (Kropff et al., 2015).

281

282 Place cell and time cell sequences have many similarities and
283 differences in descriptive neurophysiology, but may emerge from the
284 same memory organization principles (Buzsáki & Llinás, 2017). It is
285 argued that there is significance to the exact phrasing of the CA1
286 sequence in any given context. Furthermore, a very interesting feature
287 observed is Time-stamping, *viz.*, time dependent overlap of ensemble
288 responses to different contexts and behavioural parameters (Cai et al.,
289 2016; Mau et al., 2018).

290

291 Trace Eye-Blink Conditioning is a behavioural context which has been
292 shown to feature CA1 time cell activity sequences. Transient increases
293 in CA1 excitability post acquisition of the task were described up to 4-5
294 days (Moyer et al., 1990) and could be important to the forging of the
295 task specific spatiotemporal sequences during learning. Moreover,
296 Trace Eye-Blink Conditioning in mice has been previously observed to
297 elicit CA1 activity sequences even in a single session of training (Modi
298 et al., 2014).

299

300 Internally driven as opposed to externally driven network models of
301 activity sequences have been proposed as the mechanism driving
302 hippocampal CA1 sequences (Buzsáki & Llinás, 2017; Eichenbaum,
303 2017). The CA1 neurons participating in any sequence may represent
304 physiologically mappable attractors in temporally specific contexts.

305

306 **Theories on the function of the**
307 **hippocampus**

308

309 Four main ideas of hippocampal function studied over the past few
310 decades are,

311 A) Response Inhibition - Studied mostly in the 1960's, this
312 perspective described the Hippocampus as important to the
313 ability of animals to inhibit their impulses and natural, habitual,
314 or dominant behavioral responses to stimuli, in order to select
315 more appropriate responses. This perspective was justified by
316 two observations with regard to animals with hippocampal
317 damage - 1) these animals tended to be hyperactive, and 2)
318 were unable to withhold previously learnt responses. British
319 psychologist Jeffrey Alan Gray developed this perspective to
320 link hippocampal activity with anxiety (McNaughton & Gray,
321 2000).

322

323 B) Episodic Memory – This perspective was popularized by the
324 psychological studies on Patient H. M. (Henry Molaison), who
325 had been suffering from epileptic seizures and had to undergo
326 extensive hippocampectomy (surgical destruction of the
327 hippocampi), as treatment. American neurosurgeon William
328 Beecher Scoville and British-Canadian neuropsychologist
329 Brenda Milner were pioneers of this study and were able to
330 describe severe anterograde and partial retrograde amnesia in
331 the patient post surgery (Scoville & Milner, 1957). Since the late
332 2000's, the discovery and description of time cells (B. Kraus et

333 al., 2013; B. J. Kraus et al., 2015; MacDonald et al., 2011, 2013;
334 Modi et al., 2014; Pastalkova et al., 2008), has reinvigorated this
335 perspective.

336

337 C) Spatial Cognition - Originally popularized by the remarkable
338 work of American-British neuroscientist John O'Keefe and
339 American psychologist Lynn Nadel, the link between
340 hippocampal function and spatial navigation was solidified with
341 the discovery and subsequent descriptions of place cells (Morris
342 et al., 1982; O'Keefe & Dostrovsky, 1971; O'Keefe & Recce,
343 1993). This perspective is the most popular amongst the known
344 and studied functions of the Hippocampus and has been the
345 subject of a large body of work. Indeed, the Nobel Prize in
346 Physiology or Medicine 2014 was awarded to John O'Keefe,
347 May-Britt Moser, and Edvard I. Moser, for "The Brain's
348 Navigational Place and Grid Cell System".

349

350 D) Contextual Mapping – An emerging consensus in the field is
351 that the hippocampus actually builds contextual maps of the
352 environment or perceived events, with expansions to the neural
353 activity code along any relevant dimension of stimuli. Stimuli or
354 events cuing any modality, e.g., spatial, temporal, frequency,
355 etc., may be assimilated, along with more brain internal
356 variables such as (but not limited to) motivation, expected
357 reward status, prior experience in related tasks, and goal-
358 orientation (task specific). This allows the hippocampus to make
359 predictive models that bind new information streams to
360 collectively update predictions (M. R. Cohen & Kohn, 2011;
361 Eichenbaum, 2017; Miller et al., 2023; O'Keefe & Nadel, 1978).

362

363 **Space and time in the hippocampus**

364

365 Damage to the hippocampal system has been shown to cause the
366 impairment of long-term memory or amnesia, in human patients,
367 rodents, and non-human primates. Interestingly, such damage to the
368 Hippocampus seems to have no observable effect on the capacity for
369 acquisition and expression of skilled performance. These two results
370 suggest the role of the Hippocampus in certain kinds of memory, but
371 not all.

372

373 Anatomically, the hippocampal system receives input from, and in turn,
374 projects to the neocortical brain regions that serve as the site to
375 process higher order categories and modalities of information. It is thus
376 suggested that the Hippocampus holds a privileged position in the
377 brain, receiving the outcomes of the computation of the brain's various
378 modules, and relating to them. A large majority of the cortical
379 information is sent to the Hippocampus via the Entorhinal Cortex (EC).
380 This information is processed in roughly three stereotactically and
381 molecularly separable layers of cells in the following order: EC
382 → Dentate Gyrus → CA3 → CA1. This pathway from the EC to the CA1
383 has three separate synaptic connections (across the layers) and is also
384 known as the Trisynaptic Pathway (Figure 1). The output of the CA1 is
385 then sent to other cortical areas.

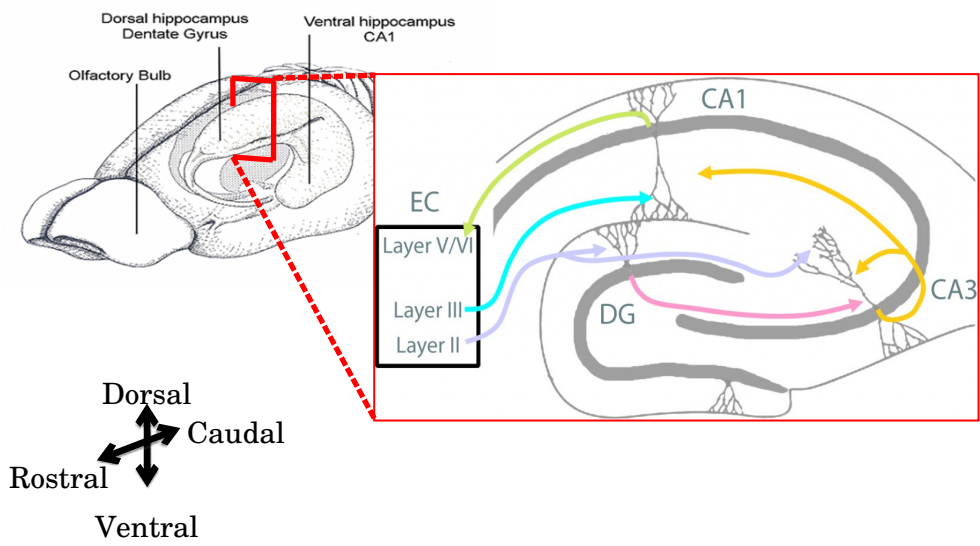


Figure 1: A schematic representation of the Trisynaptic Pathway as observed with coronal slices along the longitudinal axis of the hippocampus. Image adapted from the webpage for the Neural Circuits and Memory Lab, University of Wisconsin (Milwaukee) [<https://sites.lsa.umich.edu/diba-lab/neural-circuits-of-the-hippocampus/>])

387 One of the most significant discoveries in the hippocampal system and
388 surrounding brain structures was the role played in spatial cognition.
389 An enormous corpus of research has conclusively described,
390 • head-direction cells: with tuning curves tied to the direction that
391 experimental animals were oriented to. These cells respond to
392 egocentric vestibular cues as well as allocentric sensory cues
393 (Ranck, 1973; Taube et al., 1990), in the dorsal presubiculum,
394 retrosplenial cortex, entorhinal cortex, thalamus, and striatum,
395 among others.
396 • grid cells: with multi-modal tuning curves at regular spatial
397 positions as a lattice, across the environment being navigated.
398 These cells assimilate information about location, distance, and
399 direction, and are typically found in the entorhinal cortex (Fyhn
400 et al., 2004; Hafting et al., 2005).
401 • boundary vector cells: with tuning curves to the edges of the
402 environment being navigated. These cells are typically found in
403 the subiculum, pre- and para-subiculum, and entorhinal cortex
404 (Bjerknes et al., 2014; Lever et al., 2009; O'Keefe & Burgess,
405 1996; Savelli et al., 2008; Solstad et al., 2008).
406 • speed cells: with modulated firing rates based on the actual
407 running or movement speed of the animals. These cells are
408 typically found in the entorhinal cortex (Kropff et al., 2015).
409 • place cells: with tuning curves to specific locations in the
410 environment (O'Keefe & Dostrovsky, 1971; O'Keefe & Recce,
411 1993). These cells may be found in several hippocampal sub-
412 layers but often studied in the CA1.
413
414 The activity of neurons in the hippocampus of awake, behaving
415 animals is modulated by significant stimuli or objects in the

416 environment as well as relationships between temporally discontiguous
417 but relevant, paired stimuli. With the discovery of place cells, it was
418 clear that the CA1 of animals navigating a spatial environment,
419 showcased location specific firing fields. With the discovery of time
420 cells, it was noted that the CA1 of animals could elicit spatiotemporal
421 sequences of activity whenever the animal was required to make a link
422 between stimuli or events, even with a stimulus-free period in between.
423 Together, these results provided an important physiological parallel
424 between the spatial learning and episode learning deficit seen with
425 damage to the Hippocampus. Curiously, both place cells and time
426 cells, as well as the sequences built up with them were non-
427 topographically mapped, *i.e.*, they may be located anywhere in the
428 hippocampus, with no obvious spatial order (Dombeck et al., 2010;
429 Modi et al., 2014), in contrast to results from the cortex (Dombeck et
430 al., 2009; Ozden et al., 2008).

431

432 In an experiment published in 2008, Eva Pastalkova and colleagues
433 from Gyorgy Buzsaki's lab had rats navigate a figure 8 maze, with the
434 animal being rewarded with water, in between trials, if they managed to
435 alternate between the left and right arms (Pastalkova et al., 2008). As
436 an added nuance in the task, just before launching into the left or right
437 arms, the animal had to spend a fixed amount of time running a
438 treadmill, held in place. This would allow self-motion cues, but with the
439 absence of any other external stimuli. Impressively, single-units
440 recorded from the hippocampal CA1 cells revealed strong correlation
441 with the time spent on the treadmill, despite the absence of external
442 cues, and that different cells tuned to different time points, forming a
443 spatiotemporal sequence of activation (Pastalkova et al., 2008). In a
444 different experiment published in 2011, Christopher J. MacDonald and

445 colleagues from Howard Eichenbaum's lab had rats had to go around
446 a maze and perform a olfactory task (MacDonald et al., 2011). The
447 animals were first presented with an odour, then made to wait for a
448 delay period in a cordoned off section of the maze, before being
449 allowed to either dig for a reward or continue on the maze, depending
450 on the odour presented. As trials progressed, Hippocampal CA1 cells
451 were recorded (single-units) and found to not only be modulated by the
452 decision to be taken, but also to the amount of time spent in the delay
453 period. Experimentally, the delay period could be elongated or
454 shortened, each having an effect on remapping of the tuning fields of
455 the various CA1 cells, but to different extents (MacDonald et al., 2011).

456

457 In 2013, the Eichenbaum group published their findings with head-fixed
458 rats (no movement in space) performing a Delayed Match-To Sample
459 (DMS) task with pairs of odours, where again time-tuned activity could
460 be observed with a sequence of Hippocampal CA1 cell activations, that
461 depended on the identity of the first odour (MacDonald et al., 2013). In
462 2014, Mehrab Modi, Ashesh Dhawale, and Upinder Bhalla published
463 their results with head-fixed mice learning and performing a Trace Eye-
464 Blink Conditioning (TEC), wherein it was observed that Hippocampal
465 CA1 cell activity sequences emerged in close relation to the acquisition
466 of behavioural performance, thus cementing the idea that sub-
467 populations of Hippocampal CA1 cells could bridge temporal gaps
468 between relevant, paired stimuli, and that they did so with the activity
469 of time-tuned cells (Modi et al., 2014).

470

471 Finally, it was important to study if these apparently time-tuned cells
472 were tuned to the actual duration of time in a delay period, or whether
473 it was more important for these cells to track the distance run. In an

474 experiment published in 2013, Benjamin Kraus and colleagues from
475 Howard Eichenbaum's lab again had their rats navigate a figure 8
476 maze, but with a motorized treadmill in the central arm, to
477 experimentally regulate the running speed. With this setup, the study
478 was successful at delineating that both time spent running and
479 distance run were important features, and that different cells could tune
480 to either of the features (B. Kraus et al., 2013). Whenever hippocampal
481 CA1 cells showcased time-tuned activity (as opposed to
482 space/location-tuned activity), such cells were dubbed "Time Cells"
483 (Eichenbaum, 2017; MacDonald et al., 2011).

484

485 Other interesting physiological parallels between the CA1 place cells
486 and time cells are,

- 487 1. Phase Precession: In relation to theta oscillations (6-10 Hz)
488 measured as local field potentials (LFP), individual cells tended
489 to fire action potentials at progressively earlier phases with each
490 successive cycle, described first for place cells (O'Keefe &
491 Recce, 1993), and then also for time cells (Pastalkova et al.,
492 2008).
- 493 2. Temporal Compression: Sequences of place or time cells could
494 be elicited at significantly shorter time scales, with fidelity in the
495 participating cells (Dragoi & Buzsáki, 2006; Foster, 2017).
496 Indeed, with regard to the typically studied regime of ~100-200
497 ms or behaviour time scales, the same sequence may be
498 elicited at ~10 ms as short segments during Sharp Wave
499 Ripples (Dragoi et al., 1999; V. Itskov et al., 2008; Jadhav et al.,
500 2012; O'Keefe & Recce, 1993; Valero et al., 2015) or even as
501 the whole sequences during Replay (Csicsvari et al., 2007; Diba
502 & Buzsáki, 2007; Foster, 2017; Foster & Wilson, 2006; Gupta et

503 al., 2010; Pfeiffer & Foster, 2013, 2015)(Foster, 2017; Foster &
504 Wilson, 2006; Gupta et al., 2010; Pfeiffer & Foster, 2013) or
505 Pre-play (Dragoi & Tonegawa, 2011, 2013).

506 3. Remapping: Systematic changes in the experimental paradigm,
507 such as those to the size of the experimental arena or in the
508 time interval between stimuli or events, would result in
509 systematic changes in the firing fields of place (Muller & Kubie,
510 1989) and time cells (MacDonald et al., 2011).

511 4. Variable Firing Fields: The width of the firing fields for a set of
512 place or time cells, respectively, may be variable. However, an
513 important distinction here is that there is as yet no clearly
514 identified predictor of the widths for place cells to spatial
515 directions, while time cells tuned to later time points in the inter-
516 stimulus or delay periods usually exhibit a widening of firing
517 fields (B. J. Kraus et al., 2015; MacDonald et al., 2011, 2013;
518 Mau et al., 2018; Pastalkova et al., 2008). The significance of
519 firing field density and widths is as yet an open line of inquiry.
520

521 Single-units recorded from the medial entorhinal cortex (MEC) as well
522 as the hippocampal CA1 that were found tuned to specific frequency
523 “landmarks” during frequency sweeps self-initiated by rats (Aronov et
524 al., 2017), suggesting that the CA1 could tune to variables other than
525 space and time. This added even more weight to “Contextual Mapping”
526 as an important function of the hippocampus.

527

528 **“Single-cell, multi-trial” vs. “multi-cell,
529 single-trial” approaches in Neuroscience**

530

531 A dominant, early perspective in neurophysiology had been to record
532 activity from a single cell, over many trials, under a variety of
533 conditions (bath applications in slice physiology, different physiological
534 conditions like stress and genetic background, etc.). For more than one
535 recorded cell, the process would be repeated, till the dataset was
536 complete.

537

538 An intermediate perspective was to record from multiple cells
539 simultaneously, yet treat each cell independently for analysis towards
540 correlation and mechanism studies, across many repeats of
541 experimental conditions or trials (same as above).

542

543 An important and more modern perspective is to record from multiple
544 cells simultaneously, and use this network or population activity to
545 decode single-trial characteristics (position, time, stimulus presence,
546 etc.) using very powerful numerical and mathematical algorithms
547 involving (but not limited to) Bayesian Decoding and Information
548 Theory. The essential idea is that the neuronal code of the brain is not
549 defined just by the activity of single neurons since they may only
550 encode very specific fractions of the experience, but rather that the
551 population encodes the full experience, using a number of distributed
552 and redundant strategies.

- 553 • Bayesian Decoding: Using the activity of multiple,
554 simultaneously recorded neurons to develop a likelihood

555 estimate of the evidence (firing rate combinations) to the
556 experimental parameter (spatial position, relative time, etc.)
557 and combine this with the experimentally determined prior
558 (probability), to obtain estimates of the conditional or
559 posterior probability of a parameter value, given evidence.
560 Bayes' Rule describes

561
$$P(A|B) = P(B|A).P(A)/P(B)$$

562 ... where,

563 A: Parameter value (position, time, etc.)

564 B: Evidence (cellular firing rate)

565 $P(A)$: Prior Probability (experimentally defined)

566 $P(B)$: Probability of evidence (Firing Rate)

567 $P(A|B)$: Posterior probability of parameter value given
568 evidence

569 $P(B|A)$: Likelihood estimate of evidence given parameter
570 value (based on recordings)

571 This methodology has been used to not only successfully
572 predict specific time points in a trial from population activity, but
573 has also been used to observe that the population activity from
574 a session of recording is able to predict time points in trials
575 conducted on subsequent sessions of recording, up unto 3-4
576 sessions (Mau et al., 2018).

- 577 • Information Theory: Using recorded cellular activity to
578 estimate how much information this activity carries about
579 experimental parameters (position, time, stimuli, etc.). Three
580 essential metrics have been used,
 - 581 1. Information per activity spike (I_{spike}), in bits/spike
 - 582 2. Information per unit time (I_{sec}), in bits/sec

583 3. Mutual Information (MI) between evidence and
584 parameter value, in bits

585 William Skaggs, Bruce McNaughton and colleagues published a
586 series of experiments working out the value of Information Theory
587 based approaches to deciphering the hippocampal code, reviewed
588 previously (Skaggs et al., 1996). This idea was later adapted strongly
589 by the field but focus throughout, remained on place cells.

590

591 An interesting study published in 2018 even used synthetic test
592 datasets to go to the extent of estimating place cell detection algorithm
593 performance on the basis of I_{spike} , I_{sec} and MI (Souza et al., 2018). They
594 found,

595 1. MI could outperform the other two in a variety of scenarios.
596 2. I_{spike} and I_{sec} may still be useful in identifying unique
597 subpopulations of place cells.
598 3. Important algorithmic adjustments could be made to the
599 calculations of I_{spike} and I_{sec} , to equalize performance between
600 them and MI.

601 There was clear nuance in the population code that required such a
602 perspective during analysis. Eichenbaum and colleagues popularized
603 the use of such metrics in the context of time cells (Mau et al., 2018),
604 yet a systematic approach to identifying the best algorithms for time
605 cells was requisite.

606

607 Correlation analysis between pairs of recorded cells is one of the most
608 important analytical directions taken by neurophysiologists
609 understanding brain function, and has been reviewed previously (M. R.
610 Cohen & Kohn, 2011). However, such analysis can be subject to False
611 Positives, without appropriate significance studies. Specifically, it is

612 important to look at whether the activity profile or tuning curves for cells
613 (in relation to task variables) is significant above chance or other
614 clearly defined cutoffs, using a large number of randomized surrogates
615 of the recorded activity, generated by adding random timing shifts or
616 bootstraps. Multiple pairwise correlations may not be sufficient to
617 identify synchronous sequential activity in the network, without looking
618 at higher orders of correlation across recorded cells. Ultimately, such
619 studies benefit from simultaneous high-yield recordings, updated
620 analytical procedures utilizing surrogate data for significance analysis,
621 examining repetitions across trials (or trial-to-trial variability), and even
622 the use of multiple analytical strategies, as reviewed previously
623 (Foster, 2017; Grün, 2009).

624

625 Synfire chains (Abeles, 1982, 1991, 2009; Abeles et al., 2004) as
626 sequential neuronal activity patterns or motifs have been described in
627 cortical slices *in vitro* (Reyes, 2003), as well as *in vivo* (Ikegaya et al.,
628 2004). The 2004 study described these sequences as songs (Ikegaya
629 et al., 2004) that can incorporate new information as extensions of the
630 motifs by combining multiple synfire chains (Bienenstock, 1995).

631 However, an important consideration is that the original theoretical
632 ideas behind synfire chains assumed feed-forward connections
633 between layers of neurons, with recognition by subsequent neurons
634 looking only at waves of synchrony, rather than specific individual
635 neuronal identities (Abeles, 2004). Another important perspective is
636 that these cortical sequences could be artifacts elicited just by chance,
637 given the nature of membrane voltage fluctuations (McLelland &
638 Paulsen, 2007; Mokeichev et al., 2007). There is thus some speculation
639 over the significance of “cortical songs”, *in vivo*.

640

641 A major step forward with “multi-cell, single-trial” approaches is the
642 benefit of resolving how each cell and inter-cell interactions contribute
643 to stimulus representation, behavioural task variables, and other brain-
644 intrinsic computation. Technological advances in large-scale
645 neurophysiology recordings such as the increased density of tetrode
646 drives, neuropixels, optical sectioning and microscopy, resonant
647 scanning, etc., have enabled the discovery of well coordinated
648 sequences of cellular activity such as Sharp Wave Ripples (SWRs),
649 Replay, and behavioural timescale spatio-temporal sequences, *in vivo*,
650 among others. This is primarily due to a radical improvement in an
651 experimenter’s ability to simultaneously record from multiple cells
652 (Foster, 2017), going from yields of ~10 cells to even ~10⁴ cells, per
653 animal.
654

655 **Single-Unit Electrophysiology vs 2-Photon 656 Calcium Imaging to study the Hippocampus**

657
658 The most well characterized and studied function of the hippocampus
659 and surrounding tissue (Entorhinal Cortex, Parasubiculum, etc.) was
660 the role these tissue systems played in Spatial Navigation and Coding.
661 Single-Unit Electrophysiology was paramount to being able to isolate
662 the activity from individual cells, and eventually was used to discover
663 and describe properties of place cells (O’Keefe & Dostrovsky, 1971),
664 grid cells (Fyhn et al., 2004; Hafting et al., 2005), head-direction cells
665 (Taube et al., 1990), along with numerous other important
666 physiological discoveries, as detailed previously. However, even with
667 advances in the density of tetrode recordings, the yield of recorded

668 cells from any given animal was often limited to <50 cells. It was only
669 with the invention of Neuropixels (Jun et al., 2017) that this yield could
670 be expanded to ~1000 cells. We had opted to utilize calcium imaging
671 by 2-Photon Microscopy (Denk et al., 1990; Stosiek et al., 2003). This
672 methodology, allowed us to record ~100-150 cells per session with our
673 mice, albeit with significant cost to the recording frame rate on account
674 of the limitations of the technique. We discuss details of our technique
675 along with challenges and preliminary results, in Chapter 3 –
676 “Imaging”.

677

678 The hippocampi (one in each hemisphere) of the mouse brain lie ~1
679 mm below the most superficial layers of cortex (just inside the
680 cranium), a barrier typically too wide for typical 1-photon fluorescence
681 imaging systems (Confocal, Spinning Disk, etc.). This poses a very
682 difficult challenge for imaging preparations since there are hardware
683 and other technical limits to how long the working distance of
684 microscope objectives can be made. The use of 2-photon microscopy
685 combined with combinations of cortical excavations (to aid physical
686 access), microendoscopes, as well as prisms to guide emitted
687 fluorescence, have all been used to achieve deep brain imaging based
688 recordings at cellular resolution, in rodents (Andermann et al., 2013;
689 Attardo et al., 2015; Barreto et al., 2009; Barreto & Schnitzer, 2012;
690 Dombeck et al., 2010; Heys et al., 2014; Murray & Levene, 2012;
691 Velasco & Levene, 2014; Ziv et al., 2013).

692

693 All imaging preparation standardizations described in this thesis invoke
694 2-Photon calcium imaging of hippocampal CA1 cells at cellular
695 resolution (1 pix = ~1 μ m), following cortical excavations just above the
696 left hippocampus (Dombeck et al., 2010).

697 Calcium imaging by 2-Photon Microscopy

698

699 Typically, as cells become activated and elicit action potentials, there is
700 often a large concomitant influx of Ca^{2+} ions through voltage gated
701 calcium channels all around the perisomatic membrane, amongst other
702 cellular compartments. Several organic dyes have been developed that
703 reversibly bind Ca^{2+} ions in the cytosol and either become fluorescent
704 or emit greater fluorescence (often with a red shift) when in this Ca^{2+} -
705 bound state (Paredes et al., 2008). Additionally tremendous advances
706 in molecular biology has seen the deployment of Genetically Encoded
707 Calcium Indicators (GECIs) that may be exogenously incorporated into
708 the genome of target cells. These GECIs serve the same function as
709 organic calcium dyes, but may easily be replenished in the cytosol
710 given the cell's natural machinery for transcription and translation, and
711 whose Fluorescence properties can be engineered for brightness,
712 responsivity, Ca^{2+} binding K_d , and fluorescence emission wavelengths.
713 The number of cells that may be recorded by fluorescence is often only
714 limited to either the spread of the organic dye or the imaging
715 magnification settings, allowing for yields of 100-1000 cells.

716

717 With any Imaging based neurophysiology, there is always a trade-off
718 between yield (number of cells recorded simultaneously) and temporal
719 resolution. Increasing the yield by recording over a larger area of tissue
720 requires many more pixels per imaging frame, resulting in a loss of
721 temporal resolution (frame rate). On the other hand, increasing the
722 frame rate necessitates capturing fewer pixels per frame, decreasing
723 yield. There is even a limitation of simply zooming out, since stable
724 fluorescence intensity fluctuations can only be identified when each

725 cell is defined at least by a certain number of pixels, to allow proper
726 isolation.

727

728 Specifically with calcium imaging, the signal to be recorded
729 corresponds to Ca^{2+} flux in the cytoplasm as measured by the change
730 in emitted fluorescence of reporters such as GCaMP, with a $\tau_{\text{rise}} = 10-$
731 100 ms and $\tau_{\text{fall}} = 100\text{-}300$ ms (Chen et al., 2013). This signal is one or
732 two orders of magnitude slower than the action potential ($\sim 2\text{-}5$ ms).
733 However, this may not necessarily be a limitation since a dominant
734 idea in the field is to simply consider rate coding, or time-averaged
735 spiking activity (Abeles, 2004), bringing down the effective temporal
736 resolution of the electrical record.

737

738 Genetically Encoded Voltage Indicators (GEVIs) that fluoresce with
739 higher emission during membrane voltage dynamics have also been
740 developed. However, their localization onto the membrane of the cell,
741 instead of the cytoplasm, diminishes the total emitted photon flux per
742 unit time, and requires longer bin times to achieve reasonable signal-
743 to-noise, as reviewed previously (Mollinedo-Gajate et al., 2021). This
744 unfortunately brings down the frame rate even more than what can be
745 achieved with GECIs. We avoided GEVIs in the projects described in
746 this thesis.

747

748 A major advancement in Fluorescence Imaging was the invention of
749 Confocal and Multiphoton (typically 2-Photon) Microscopes, which
750 allowed for unprecedented recording signal-to-noise by optical
751 sectioning. 2-Photon Imaging itself was an important development for
752 the neurophysiology of tissue greater than 300 μm in thickness, typical
753 of rodent brain tissue, because it avoids wasteful excitation of imaging

754 planes that are not in focus (out-of-plane). The 2-Photon effect
755 requires two photons of longer wavelength (lower energy per photon),
756 to near instantaneously excite a fluorophore. The photon flux is highest
757 at the focal plane (with an N-squared dependence) of the microscope
758 so only the section of the tissue corresponding to the focal place is
759 allowed to achieve fluorescence. Additionally, longer wavelengths of
760 excitation light can more easily penetrate deeper layers of tissue, due
761 to comparatively lower scattering or Rayleigh effect (Denk et al., 1990;
762 Helmchen & Denk, 2005).

763

764 The hippocampus (specifically the hippocampal CA1) was the main
765 brain structure of interest for all our physiology experiments, and lies
766 under about 1 mm of cortical tissue for mice. This is a depth that is
767 difficult to image even with 2-Photon Microscopy. The typical
768 methodology employed in such cases is to perform a cortical
769 excavation just above the Hippocampus filling the crevice with optically
770 clearer agarose or silicone elastomer. Even so, the hippocampal CA1
771 cell body layer (*Stratum Pyramidale*) still lies about 150-300 μm below
772 the external capsule and corpus callosum fibers (left intact for chronic
773 imaging). Accordingly, we combined cortical excavation with 2-Photon
774 microscopy, using a long working distance objective with a wide field of
775 view, imaging cytosolic Ca^{2+} activity with the help of either an organic
776 dye (OGB-1; acute imaging) or a GECI (GCaMP6f; chronic imaging).

777

778 An important perspective that has motivated the use of Imaging based
779 physiology recordings (as opposed to Electrophysiological methods)
780 other than potential yield, is that imaging provides anatomical
781 confirmation of any particular recorded cell, and this in turn allows for,

- 782 A) Unambiguous isolation of the same cell across multiple imaging
783 sessions (across days and weeks). Single-Units are ultimately
784 only algorithmically resolved and this can be done only for cells
785 that are active and are represented in multiple spatially
786 separated electrodes. However, very recently, Ashesh Dhawale
787 and colleagues from Bence Olveczky's lab have devised a
788 solution to track the movement of electrodes in tissue over time
789 and use this information to ensure chronic recording of the
790 same units (Dhawale et al., 2017). This technique was not
791 available at the time when experiments for this thesis were
792 started.
- 793 B) Unambiguous detection of the lack of activity in an otherwise
794 recorded cell. Since the cell can be anatomically identified
795 independent of activity, it is possible to observe the absence of
796 Ca^{2+} activity. Automated cell ROI detection (Francis et al., 2012;
797 Maruyama et al., 2014; Mukamel et al., 2009; Pachitariu et al.,
798 2017; Pnevmatikakis et al., 2016) simplifies the pre-processing
799 step of cell isolation even over large batch sizes. These
800 procedures inherently require the use of the calcium activity
801 profiles of recorded cells, viz., inactive cells (though
802 anatomically visible), may not be isolated.

803

804 **Automated ROI detection for large-scale**

805 **Calcium Imaging datasets**

806

807 A number of automated ROI detection algorithms have been cited in
808 literature that require minimal user intervention, perform relatively fast
809 identification for a large number of identified sources (putative cells).

810 Some popular algorithms include PCA/ICA (Mukamel et al., 2009),
811 Suite2p (Pachitariu et al., 2017), and Non-Negative Matrix
812 Factorization (NNMF)(Pnevmatikakis et al., 2016), which all have been
813 developed to the extent where comparable or oftentimes much better
814 ROI detection is achieved than as compared to the more tedious hand-
815 drawn ROIs which scales very poorly with orders of cells recorded.

816 We have strictly followed Suite2p (Pachitariu et al., 2017) for all
817 physiological ROI (cell sources) described in this thesis.

818

819 **A brief introduction to associative learning**

820

821 The ability to physiologically record cells is insufficient without placing
822 the experimental animals in precisely defined, stable behavioural
823 contexts. Only in this way can neural activity be checked for
824 correlations or mapping to distinct changes in external behaviour
825 variables and the decisions that the animal makes, accordingly.

826 Combining behaviour and recording was considered an important
827 guiding principle in all our experiments.

828

829 Prior to the early 20th century, Structuralism was a dominant
830 perspective in Psychology, insisting on introspection - the observation
831 and report of one's own mind and thoughts. Experiments and
832 discoveries by Ivan Pavlov at the Military Medical Academy in
833 Petrograd (St. Petersburg), eventually led to a dramatic shift in
834 perspective, with the birth of Classical Conditioning, a type of
835 associative learning. Following the very same methodology advocated
836 by Francis Bacon (early 17th century), quantitative data from carefully
837 conducted animal experiments were recorded, with the idea to narrow
838 down on a small number of hypotheses that could explain experimental
839 observations.

840

841 Ivan Pavlov provided essential demonstrations of anticipation and
842 made tremendous progress in understanding the circumstances on
843 which anticipation depends, and this is why Classical Conditioning is
844 also often referred to as Pavlovian Conditioning. Following Pavlov's
845 studies (Pavlov, 1927), it was proposed that Classical Conditioning
846 was a prototypical example of Association. While it does have caveats
847 such as covert learning when observable behaviour may be blocked
848 (Dickinson et al., 1983; Krupa & Thompson, 2003), Associative
849 learning is rich with a variety of animals and association tasks that
850 have been crucial to study memory and learning over the past century.

851

852 Typically, animals require no prior training to elicit a behavioural or
853 motor movement to biologically potent stimulus (appetitive or aversive),
854 called an Unconditioned Stimulus (US). Examples include food, water,
855 electrical shock, temperature shock, etc.. Without pairing with a US, a
856 neutral stimulus elicits no observable response from an animal, and

857 such a stimulus is called a Conditioned Stimulus (CS). Examples
858 include simple auditory tones, flashes of light, among others.
859

860 Classical Conditioning is both the behavioural procedure as well as the
861 learning process that results from the pairing of a previously neutral
862 stimulus (CS) with a biologically potent stimulus (US). Repeated
863 pairing allows animals to make implicit associations between the CS
864 and US, and essentially anticipate the occurrence of the US, once the
865 CS is observed. Animals report this forecasting feat by producing the
866 same response that they would to a US, albeit often a milder version.
867 Typical protocols for Classical Conditioning, follow the regime of
868 Forward pairing, *viz.*, - the CS is presented before the US, and this
869 temporal structure will be followed unanimously across all behaviour
870 experiments described in this thesis.

871

872 The standardization of the behavioural task, physiological recording
873 (imaging) preparation, as well as the custom analysis routines to look
874 for various physiological features are described in this thesis.
875 Combining these multi-disciplinary approaches allowed us to develop a
876 toolkit to study time cells in the hippocampus, under strict behavioural
877 contexts. It is important to note, however, that spatiotemporal
878 sequences of activity as measured by calcium imaging based
879 simultaneous recordings of a large number of cells, are not limited to
880 the hippocampus, being studied even in the visual cortex (Pachitariu et
881 al., 2017; Poort et al., 2015), somatosensory cortex (Petersen, 2019),
882 entorhinal cortex (Heys et al., 2014), and even in the cerebellum
883 (Giovannucci et al., 2017). Essentially, the analytical methods
884 developed can easily be adapted to other neuronal network recordings
885 where time-tuning may be applicable.

886

887 **Short Summaries of the 3 projects**

888 **Project I - How do sensory representations transform
889 with learning?**

890 Sensory Systems Neuroscience is a very popular field spanning
891 studies looking at numerous brain regions and sub-regions in the
892 cortex and hippocampus, *in vivo* (R. A. Andersen et al., 1993; Fassihi
893 et al., 2017; Khan et al., 2010; Meeks et al., 2010; Petersen, 2019;
894 Poort et al., 2015; Voelcker et al., 2022), among several others. Many
895 if not most of these studies describe neural activity in animals with
896 expert levels of behavioural learning and performance to the presented
897 stimuli. Lacunae still remain as to mechanisms deployed during active
898 or online learning especially in the early stages of behavioural training.
899

900 We deployed our experiments with the intention to study how Calcium
901 Imaging by 2-Photon Microscopy could reveal finer population level
902 details of network activity as the animals were tested on the learning of
903 an Operant Conditioning or lick behaviour task. We were able to,

- 904 1. Prototype OGB-1 based calcium imaging *in vivo*, from head-
905 fixed mice in a manner suited to combined behaviour and
906 recording experiments, and
- 907 2. Study preliminary data from animals that correlation based
908 functional activity clusters of recorded CA1 cells have spatial
909 organization during bouts of spontaneous activity.

910

911 However, we were not satisfied with the level and rate of learning in
912 our Operant Conditioning protocols, eventually leading to a search for
913 more stable behavioural paradigms, in mice. Additionally, the use of
914 OGB-1 as the Calcium Indicator also had to be abandoned since this
915 fundamentally disallowed multi-day tracking of the same cells. We
916 discuss our prototyping efforts and preliminary data for this project in
917 detail, in the first few sections each of Chapters 2 (“Behaviour”) and 3
918 (“Imaging”).

919

920 **Project II - How does the timing of cellular activity adjust
921 to behavioural task variables?**

922

923 Research on the cerebellum has made substantial progress in the
924 elucidation of network mechanisms correlating well with external
925 stimulus timing based variables, as animals learn Trace Eye-Blink
926 Conditioning and Delay Conditioning (Kalmbach, Davis, et al., 2010;
927 Kalmbach, Ohyama, et al., 2010; Medina et al., 2000; Ohyama et al.,
928 2003; Siegel & Mauk, 2013). The predominant studies on time cells in
929 the hippocampus have focused on the context of appetitive reinforcing
930 stimuli (Eichenbaum, 2004, 2017; B. Kraus et al., 2013; B. J. Kraus et
931 al., 2015; MacDonald et al., 2011, 2013; Mau et al., 2018; Pastalkova
932 et al., 2008). Time cells in the behavioural context of Trace Eye-Blink
933 conditioning, an aversive learning paradigm, have been explored (Modi
934 et al., 2014), but details such as correlations with rates of behavioural
935 learning, tuning adaptability, and long-term stability (~weeks) of the
936 time cell sequences are yet to be studied.

937

938 We prototyped a GCaMP6f based *in vivo* hippocampal preparation that
939 allowed for chronic, longitudinal recordings of hippocampal CA1, by 2-
940 Photon Calcium Imaging (Dombeck et al., 2010) that could be
941 combined with a stable and adaptable learning protocols of Trace Eye-
942 Blink Conditioning (Siegel et al., 2015).

943 From our preliminary set of recordings we were able to,

- 944 1. Detect time cells in our population recordings,
- 945 2. Observe signs of expansion of the time cell sub-population over
946 early stages of learning, and
- 947 3. Observe shifts in the timing of peak for known, chronically
948 tracked time cells, typically moving away from the US and
949 towards the CS.

950

951 Technical difficulties prevented us from expanding our experimental
952 recording datasets to the point where these results could be looked at
953 more critically and the results may be sufficient for publication. We
954 discuss our prototyping efforts and preliminary data for this project in
955 detail, in the last few sections each of Chapters 2 (“Behaviour”) and 3
956 (“Imaging”).

957

958 **Project III - What is the best way to detect and score
959 time-tuned cellular activity?**

960

961 Given that we had collected a reasonable sample of multi-day tracked
962 cells while head-fixed mice were being trained to a Trace Eye-Blink
963 Conditioning (TEC) task, we wished to move forward to identifying time

964 cells in the most reliable way, with the aim to drawing quality
965 conclusions from the physiology recordings.

966

967 The paper entitled “Synthetic Data Resource and Benchmarks for Time
968 Cell Analysis and Detection Algorithms” (Ananthamurthy & Bhalla,
969 2023) was a consolidation of our progress to analyse physiology data
970 from real and synthetic cells expressed as calcium activity trials and
971 sessions.

972

973 Here, we used a computational approach and developed categorically
974 labelled, user definable, large scale synthetic datasets, as a test bed to
975 compare and benchmark the predictions made by popular time cell
976 detection algorithms. We were able to study the sensitivity of these
977 computational algorithms across a wide array of experimental
978 recording parameters, and could ultimately conclude the best
979 operational regimes for each of them. All of the code base for this
980 project is freely available online
981 (<https://github.com/bhallalab/TimeCellAnalysis>) and is intended to be a
982 resource to researchers.

983

984 The paper is attached as Chapter 4 (“Analysis”).

985 **Code Availability**

986

987 All our code for Synthetic Data generation and time cell Analysis is
988 available at <https://www.github.com/bhallalab/TimeCellAnalysis>.

989

990 All our code for conducting Trace Eye-Blink Conditioning (TEC)
991 behaviour is available at
992 <https://www.github.com/ananthamurthy/eyeBlinkBehaviour>.

993

994 Analysis scripts for evaluating TEC performance are available at
995 <https://github.com/ananthamurthy/MATLAB/tree/master/TECAnalysis>.

996 **Bibliography**

997

998 Abeles, M. (1982). *Local Cortical Circuits: An Electrophysiological*
999 *Study*. Springer-Verlag. <https://books.google.co.in/books?id=s25lwEACAAJ>

1000 Abeles, M. (1991). *Corticonics: Neural Circuits of the Cerebral Cortex*.
1001 Cambridge University Press. <https://doi.org/DOI:10.1017/CBO9780511574566>

1002 Abeles, M. (2004). Time Is Precious. *Science*, 304(5670), 523–524.
1003 <https://doi.org/10.1126/science.1097725>

1004 Abeles, M. (2009). *Synfire Chains* (L. R. B. T.-E. of N. Squire (ed.); pp.
1005 829–832). Academic Press.
1006 <https://doi.org/https://doi.org/10.1016/B978-008045046-9.01437-6>

1007 Abeles, M., Hayon, G., & Lehmann, D. (2004). Modeling
1008 compositionality by dynamic binding of synfire chains. *Journal of*
1009 *Computational Neuroscience*, 17(2), 179–201.
1010 <https://doi.org/10.1023/B:JCNS.0000037682.18051.5f>

- 1013 Ananthamurthy, K. G., & Bhalla, U. S. (2023). Synthetic Data Resource
1014 and Benchmarks for Time Cell Analysis and Detection Algorithms.
1015 *ENeuro*, ENEURO.0007-22.2023.
1016 <https://doi.org/10.1523/ENEURO.0007-22.2023>
- 1017 Andermann, M. L., Gilfoy, N. B., Goldey, G. J., Sachdev, R. N. S.,
1018 Wölfel, M., McCormick, D. A., Reid, R. C., & Levene, M. J. (2013).
1019 Chronic Cellular Imaging of Entire Cortical Columns in Awake
1020 Mice Using Microprisms. *Neuron*, 80(4), 900–913.
1021 <https://doi.org/10.1016/j.neuron.2013.07.052>
- 1022 Andersen, R. A., Snyder, L. H., Li, C.-S., & Stricanne, B. (1993).
1023 Coordinate transformations in the representation of spatial
1024 information. *Current Opinion in Neurobiology*, 3(2), 171–176.
1025 [https://doi.org/https://doi.org/10.1016/0959-4388\(93\)90206-E](https://doi.org/https://doi.org/10.1016/0959-4388(93)90206-E)
- 1026 Aronov, D., Nevers, R., & Tank, D. W. (2017). Mapping of a non-spatial
1027 dimension by the hippocampal-entorhinal circuit. *Nature*,
1028 543(7647), 719–722. <https://doi.org/10.1038/nature21692>
- 1029 Attardo, A., Fitzgerald, J. E., & Schnitzer, M. J. (2015). Impermanence
1030 of dendritic spines in live adult CA1 hippocampus. *Nature*,
1031 523(7562), 592–596. <https://doi.org/10.1038/nature14467>
- 1032 Barreto, R. P. J., Messerschmidt, B., & Schnitzer, M. J. (2009). In vivo
1033 fluorescence imaging with high-resolution microlenses. *Nature
Methods*, 6(7), 511–512. <https://doi.org/10.1038/nmeth.1339>
- 1035 Barreto, R. P. J., & Schnitzer, M. J. (2012). In vivo optical
1036 microendoscopy for imaging cells lying deep within live tissue.
1037 *Cold Spring Harbor Protocols*, 2012(10), 1029–1034.
1038 <https://doi.org/10.1101/pdb.top071464>
- 1039 Bienenstock, E. (1995). A model of neocortex. *Network: Computation
in Neural Systems*, 6(2), 179–224. https://doi.org/10.1088/0954-898X_6_2_004
- 1042 Bjerknes, T. L., Moser, E. I., & Moser, M.-B. (2014). Representation of
1043 Geometric Borders in the Developing Rat. *Neuron*, 82(1), 71–78.
1044 <https://doi.org/10.1016/j.neuron.2014.02.014>

- 1045 Buzsáki, G., & Llinás, R. (2017). Space and time in the brain. *Science*
1046 (New York, N.Y.), 358(6362), 482–485.
1047 <https://doi.org/10.1126/science.aan8869>
- 1048 Cai, D. J., Aharoni, D., Shuman, T., Shobe, J., Biane, J., Song, W.,
1049 Wei, B., Veshkini, M., La-Vu, M., Lou, J., Flores, S. E., Kim, I.,
1050 Sano, Y., Zhou, M., Baumgaertel, K., Lavi, A., Kamata, M.,
1051 Tuszyński, M., Mayford, M., ... Silva, A. J. (2016). A shared neural
1052 ensemble links distinct contextual memories encoded close in
1053 time. *Nature*, 534(7605), 115–118.
1054 <https://doi.org/10.1038/nature17955>
- 1055 Caporale, N., & Dan, Y. (2008). Spike timing-dependent plasticity: a
1056 Hebbian learning rule. *Annual Review of Neuroscience*, 31, 25–
1057 46. <https://doi.org/10.1146/annurev.neuro.31.060407.125639>
- 1058 Carew, T. J., Castellucci, V. F., & Kandel, E. R. (1971). An Analysis of
1059 Dishabituation and Sensitization of The Gill-Withdrawal Reflex In
1060 Aplysia. *International Journal of Neuroscience*, 2(2), 79–98.
1061 <https://doi.org/10.3109/00207457109146995>
- 1062 Chen, T.-W., Wardill, T. J., Sun, Y., Pulver, S. R., Renninger, S. L.,
1063 Baohan, A., Schreiter, E. R., Kerr, R. A., Orger, M. B., Jayaraman,
1064 V., Looger, L. L., Svoboda, K., & Kim, D. S. (2013). Ultrasensitive
1065 fluorescent proteins for imaging neuronal activity. *Nature*,
1066 499(7458), 295–300. <https://doi.org/10.1038/nature12354>
- 1067 Cohen, M. R., & Kohn, A. (2011). Measuring and interpreting neuronal
1068 correlations. *Nature Neuroscience*, 14(7), 811–819.
1069 <https://doi.org/10.1038/nn.2842>
- 1070 Csicsvari, J., O'Neill, J., Allen, K., & Senior, T. (2007). Place-selective
1071 firing contributes to the reverse-order reactivation of CA1
1072 pyramidal cells during sharp waves in open-field exploration. *The*
1073 *European Journal of Neuroscience*, 26(3), 704–716.
1074 <https://doi.org/10.1111/j.1460-9568.2007.05684.x>
- 1075 Davidson, T. J., Kloosterman, F., & Wilson, M. A. (2009). Hippocampal
1076 replay of extended experience. *Neuron*, 63(4), 497–507.
1077 <https://doi.org/10.1016/j.neuron.2009.07.027>

- 1078 Denk, W., Strickler, J. H., & Webb, W. W. (1990). Two-photon laser
1079 scanning fluorescence microscopy. *Science (New York, N.Y.)*,
1080 248(4951), 73–76. <https://doi.org/10.1126/science.2321027>
- 1081 Dhawale, A. K., Poddar, R., Wolff, S. B. E., Normand, V. A.,
1082 Kopelowitz, E., & Ölveczky, B. P. (2017). Automated long-term
1083 recording and analysis of neural activity in behaving animals.
1084 *eLife*, 6, e27702. <https://doi.org/10.7554/eLife.27702>
- 1085 Diba, K., & Buzsáki, G. (2007). Forward and reverse hippocampal
1086 place-cell sequences during ripples. *Nature Neuroscience*, 10(10),
1087 1241–1242. <https://doi.org/10.1038/nn1961>
- 1088 Dickinson, A., Nicholas, D. J., & Mackintosh, N. J. (1983). A re-
1089 examination of one-trial blocking in conditioned suppression. *The
1090 Quarterly Journal of Experimental Psychology B: Comparative
1091 and Physiological Psychology*, 35, 67–79.
1092 <https://doi.org/10.1080/14640748308400914>
- 1093 Dombeck, D. A., Graziano, M. S., & Tank, D. W. (2009). Functional
1094 clustering of neurons in motor cortex determined by cellular
1095 resolution imaging in awake behaving mice. *The Journal of
1096 Neuroscience : The Official Journal of the Society for
1097 Neuroscience*, 29(44), 13751–13760.
1098 <https://doi.org/10.1523/JNEUROSCI.2985-09.2009>
- 1099 Dombeck, D. A., Harvey, C. D., Tian, L., Looger, L. L., & Tank, D. W.
1100 (2010). Functional imaging of hippocampal place cells at cellular
1101 resolution during virtual navigation. *Nature Neuroscience*, 13(11),
1102 1433–1440. <https://doi.org/10.1038/nn.2648>
- 1103 Dragoi, G., & Buzsáki, G. (2006). Temporal encoding of place
1104 sequences by hippocampal cell assemblies. *Neuron*, 50(1), 145–
1105 157. <https://doi.org/10.1016/j.neuron.2006.02.023>
- 1106 Dragoi, G., Carpi, D., Recce, M., Csicsvari, J., & Buzsáki, G. (1999).
1107 Interactions between hippocampus and medial septum during
1108 sharp waves and theta oscillation in the behaving rat. *The Journal
1109 of Neuroscience : The Official Journal of the Society for*

- 1110 *Neuroscience*, 19(14), 6191–6199.
1111 <http://www.ncbi.nlm.nih.gov/pubmed/10407055>
- 1112 Dragoi, G., & Tonegawa, S. (2011). Preplay of future place cell
1113 sequences by hippocampal cellular assemblies. *Nature*,
1114 469(7330), 397–401. <https://doi.org/10.1038/nature09633>
- 1115 Dragoi, G., & Tonegawa, S. (2013). Distinct preplay of multiple novel
1116 spatial experiences in the rat. *Proceedings of the National
1117 Academy of Sciences of the United States of America*, 110(22),
1118 9100–9105. <https://doi.org/10.1073/pnas.1306031110>
- 1119 Eichenbaum, H. (2004). Hippocampus: Cognitive processes and
1120 neural representations that underlie declarative memory. *Neuron*,
1121 44(1), 109–120. <https://doi.org/10.1016/j.neuron.2004.08.028>
- 1122 Eichenbaum, H. (2017). On the Integration of Space, Time, and
1123 Memory. *Neuron*, 95(5), 1007–1018.
1124 <https://doi.org/10.1016/j.neuron.2017.06.036>
- 1125 Fassihi, A., Akrami, A., Pulecchi, F., Schönfelder, V., & Diamond, M. E.
1126 (2017). Transformation of Perception from Sensory to Motor
1127 Cortex. *Current Biology : CB*, 27(11), 1585-1596.e6.
1128 <https://doi.org/10.1016/j.cub.2017.05.011>
- 1129 Ferbinteanu, J., & Shapiro, M. L. (2003). Prospective and retrospective
1130 memory coding in the hippocampus. *Neuron*, 40(6), 1227–1239.
1131 [https://doi.org/10.1016/s0896-6273\(03\)00752-9](https://doi.org/10.1016/s0896-6273(03)00752-9)
- 1132 Ferbinteanu, J., Shirvalkar, P., & Shapiro, M. L. (2011). Memory
1133 Modulates Journey-Dependent Coding in the Rat Hippocampus.
1134 *The Journal of Neuroscience*, 31(25), 9135 LP – 9146.
1135 <https://doi.org/10.1523/JNEUROSCI.1241-11.2011>
- 1136 Foster, D. J. (2017). Replay Comes of Age. *Annual Review of
1137 Neuroscience*, 40, 581–602. <https://doi.org/10.1146/annurev-neuro-072116-031538>
- 1139 Foster, D. J., & Wilson, M. A. (2006). Reverse replay of behavioural
1140 sequences in hippocampal place cells during the awake state.
1141 *Nature*, 440(7084), 680–683. <https://doi.org/10.1038/nature04587>

- 1142 Foster, D. J., & Wilson, M. A. (2007). Hippocampal theta sequences.
1143 *Hippocampus*, 17(11), 1093–1099.
1144 <https://doi.org/10.1002/hipo.20345>
- 1145 Francis, M., Qian, X., Charbel, C., Ledoux, J., Parker, J. C., & Taylor,
1146 M. S. (2012). Automated region of interest analysis of dynamic
1147 Ca²⁺ signals in image sequences. *American Journal of*
1148 *Physiology. Cell Physiology*, 303(3), C236-43.
1149 <https://doi.org/10.1152/ajpcell.00016.2012>
- 1150 Frank, L. M., Brown, E. N., & Wilson, M. (2000). Trajectory encoding in
1151 the hippocampus and entorhinal cortex. *Neuron*, 27(1), 169–178.
1152 [https://doi.org/10.1016/s0896-6273\(00\)00018-0](https://doi.org/10.1016/s0896-6273(00)00018-0)
- 1153 Fyhn, M., Molden, S., Witter, M. P., Moser, E. I., & Moser, M.-B.
1154 (2004). Spatial representation in the entorhinal cortex. *Science*
1155 (*New York, N.Y.*), 305(5688), 1258–1264.
1156 <https://doi.org/10.1126/science.1099901>
- 1157 Giovannucci, A., Badura, A., Deverett, B., Najafi, F., Pereira, T. D.,
1158 Gao, Z., Ozden, I., Kloth, A. D., Pnevmatikakis, E., Paninski, L.,
1159 De Zeeuw, C. I., Medina, J. F., & Wang, S. S.-H. (2017).
1160 Cerebellar granule cells acquire a widespread predictive feedback
1161 signal during motor learning. *Nature Neuroscience*, 20(5), 727–
1162 734. <https://doi.org/10.1038/nn.4531>
- 1163 Grün, S. (2009). Data-Driven Significance Estimation for Precise Spike
1164 Correlation. *Journal of Neurophysiology*, 101(3), 1126–1140.
1165 <https://doi.org/10.1152/jn.00093.2008>
- 1166 Gupta, A. S., van der Meer, M. A. A., Touretzky, D. S., & Redish, A. D.
1167 (2010). Hippocampal Replay Is Not a Simple Function of
1168 Experience. *Neuron*, 65(5), 695–705.
1169 <https://doi.org/https://doi.org/10.1016/j.neuron.2010.01.034>
- 1170 Hafting, T., Fyhn, M., Molden, S., Moser, M.-B., & Moser, E. I. (2005).
1171 Microstructure of a spatial map in the entorhinal cortex. *Nature*,
1172 436(7052), 801–806. <https://doi.org/10.1038/nature03721>
- 1173 Han, J.-H., Kushner, S. A., Yiu, A. P., Hsiang, H.-L. L., Buch, T.,
1174 Waisman, A., Bontempi, B., Neve, R. L., Frankland, P. W., &

- 1175 Josselyn, S. A. (2009). Selective erasure of a fear memory.
1176 *Science (New York, N.Y.)*, 323(5920), 1492–1496.
1177 <https://doi.org/10.1126/science.1164139>
- 1178 Hebb, D. O. (1949). The organization of behavior; a
1179 neuropsychological theory. In *The organization of behavior; a*
1180 *neuropsychological theory*. Wiley.
- 1181 Helmchen, F., & Denk, W. (2005). *Deep tissue two-photon microscopy*.
1182 2(12), 9. <https://doi.org/10.1038/nmeth818>
- 1183 Heys, J. G., Rangarajan, K. V., & Dombeck, D. A. (2014). The
1184 Functional Micro-organization of Grid Cells Revealed by Cellular-
1185 Resolution Imaging. *Neuron*, 84(5), 1079–1090.
1186 <https://doi.org/10.1016/j.neuron.2014.10.048>
- 1187 Ikegaya, Y., Aaron, G., Cossart, R., Aronov, D., Lampl, I., Ferster, D.,
1188 & Yuste, R. (2004). Synfire chains and cortical songs: temporal
1189 modules of cortical activity. *Science (New York, N.Y.)*, 304(5670),
1190 559–564. <https://doi.org/10.1126/science.1093173>
- 1191 Itskov, V., Pastalkova, E., Mizuseki, K., Buzsaki, G., & Harris, K. D.
1192 (2008). Theta-mediated dynamics of spatial information in
1193 hippocampus. *The Journal of Neuroscience : The Official Journal*
1194 *of the Society for Neuroscience*, 28(23), 5959–5964.
1195 <https://doi.org/10.1523/JNEUROSCI.5262-07.2008>
- 1196 Jadhav, S. P., Kemere, C., German, P. W., & Frank, L. M. (2012).
1197 Awake hippocampal sharp-wave ripples support spatial memory.
1198 *Science (New York, N.Y.)*, 336(6087), 1454–1458.
1199 <https://doi.org/10.1126/science.1217230>
- 1200 Josselyn, S. A., & Tonegawa, S. (2020). Memory engrams: Recalling
1201 the past and imagining the future. *Science (New York, N.Y.)*,
1202 367(6473). <https://doi.org/10.1126/science.aaw4325>
- 1203 Jun, J. J., Steinmetz, N. A., Siegle, J. H., Denman, D. J., Bauza, M.,
1204 Barbarits, B., Lee, A. K., Anastassiou, C. A., Andrei, A., Aydin, Ç.,
1205 Barbic, M., Blanche, T. J., Bonin, V., Couto, J., Dutta, B., Gratiy,
1206 S. L., Gutnisky, D. A., Häusser, M., Karsh, B., ... Harris, T. D.
1207 (2017). Fully integrated silicon probes for high-density recording of

- 1208 neural activity. *Nature*, 551(7679), 232–236.
1209 <https://doi.org/10.1038/nature24636>
- 1210 Kalmbach, B. E., Davis, T., Ohyama, T., Riusech, F., Nores, W. L., &
1211 Mauk, M. D. (2010). Cerebellar Cortex Contributions to the
1212 Expression and Timing of Conditioned Eyelid Responses. *Journal*
1213 *of Neurophysiology*, 103(4), 2039–2049.
1214 <https://doi.org/10.1152/jn.00033.2010>
- 1215 Kalmbach, B. E., Ohyama, T., & Mauk, M. D. (2010). Temporal
1216 Patterns of Inputs to Cerebellum Necessary and Sufficient for
1217 Trace Eyelid Conditioning. *Journal of Neurophysiology*, 104(2),
1218 627–640. <https://doi.org/10.1152/jn.00169.2010>
- 1219 Khan, A. G., Parthasarathy, K., & Bhalla, U. S. (2010). Odor
1220 representations in the mammalian olfactory bulb. *Wiley*
1221 *Interdisciplinary Reviews. Systems Biology and Medicine*, 2(5),
1222 603–611. <https://doi.org/10.1002/wsbm.85>
- 1223 Kraus, B. J., Brandon, M. P., Robinson, R. J., Connerney, M. A.,
1224 Hasselmo, M. E., & Eichenbaum, H. (2015). During Running in
1225 Place, Grid Cells Integrate Elapsed Time and Distance Run.
1226 *Neuron*, 88(3), 578–589.
1227 <https://doi.org/10.1016/j.neuron.2015.09.031>
- 1228 Kraus, B., Robinson, R., White, J., Eichenbaum, H., & Hasselmo, M.
1229 (2013). Hippocampal “Time Cells”: Time versus Path Integration.
1230 *Neuron*, 78(6), 1090–1101.
1231 <https://doi.org/10.1016/j.neuron.2013.04.015>
- 1232 Kropff, E., Carmichael, J. E., Moser, M.-B., & Moser, E. I. (2015).
1233 Speed cells in the medial entorhinal cortex. *Nature*, 523(7561),
1234 419–424. <https://doi.org/10.1038/nature14622>
- 1235 Krupa, D., & Thompson, R. (2003). Inhibiting the Expression of a
1236 Classically Conditioned Behavior Prevents Its Extinction. *The*
1237 *Journal of Neuroscience : The Official Journal of the Society for*
1238 *Neuroscience*, 23, 10577–10584.
1239 <https://doi.org/10.1523/JNEUROSCI.23-33-10577.2003>

- 1240 Lever, C., Burton, S., Jeewajee, A., O'Keefe, J., & Burgess, N.
1241 (2009). Boundary Vector Cells in the Subiculum of the
1242 Hippocampal Formation. *The Journal of Neuroscience*, 29(31),
1243 9771 LP – 9777. <https://doi.org/10.1523/JNEUROSCI.1319-09.2009>
- 1245 Luo, L., Callaway, E. M., & Svoboda, K. (2018). Genetic Dissection of
1246 Neural Circuits: A Decade of Progress. *Neuron*, 98(2), 256–281.
1247 <https://doi.org/https://doi.org/10.1016/j.neuron.2018.03.040>
- 1248 MacDonald, C. J., Carrow, S., Place, R., & Eichenbaum, H. (2013).
1249 Distinct hippocampal time cell sequences represent odor
1250 memories in immobilized rats. *The Journal of Neuroscience : The
1251 Official Journal of the Society for Neuroscience*, 33(36), 14607–
1252 14616. <https://doi.org/10.1523/JNEUROSCI.1537-13.2013>
- 1253 MacDonald, C. J., Lepage, K. Q., Eden, U. T., & Eichenbaum, H.
1254 (2011). Hippocampal “time cells” bridge the gap in memory for
1255 discontiguous events. *Neuron*, 71(4), 737–749.
1256 <https://doi.org/10.1016/j.neuron.2011.07.012>
- 1257 Maruyama, R., Maeda, K., Moroda, H., Kato, I., Inoue, M., Miyakawa,
1258 H., & Aonishi, T. (2014). Detecting cells using non-negative matrix
1259 factorization on calcium imaging data. *Neural Networks : The
1260 Official Journal of the International Neural Network Society*, 55,
1261 11–19. <https://doi.org/10.1016/j.neunet.2014.03.007>
- 1262 Mau, W., Sullivan, D. W., Kinsky, N. R., Hasselmo, M. E., Howard, M.
1263 W., & Eichenbaum, H. (2018). The Same Hippocampal CA1
1264 Population Simultaneously Codes Temporal Information over
1265 Multiple Timescales. *Current Biology*, 28(10), 1499-1508.e4.
1266 <https://doi.org/10.1016/j.cub.2018.03.051>
- 1267 McLelland, D., & Paulsen, O. (2007). Cortical Songs Revisited: A
1268 Lesson in Statistics. *Neuron*, 53(3), 319–321.
1269 <https://doi.org/https://doi.org/10.1016/j.neuron.2007.01.020>
- 1270 McNaughton, N., & Gray, J. A. (2000). Anxiolytic action on the
1271 behavioural inhibition system implies multiple types of arousal

- 1272 contribute to anxiety. *Journal of Affective Disorders*, 61(3), 161–
1273 176. [https://doi.org/10.1016/s0165-0327\(00\)00344-x](https://doi.org/10.1016/s0165-0327(00)00344-x)
- 1274 Medina, J. F., Garcia, K. S., Nores, W. L., Taylor, N. M., & Mauk, M. D.
1275 (2000). Timing mechanisms in the cerebellum: testing predictions
1276 of a large-scale computer simulation. *The Journal of
1277 Neuroscience : The Official Journal of the Society for
1278 Neuroscience*, 20(14), 5516–5525.
1279 <https://doi.org/10.1523/JNEUROSCI.20-14-05516.2000>
- 1280 Meeks, J. P., Arnson, H. A., & Holy, T. E. (2010). Representation and
1281 transformation of sensory information in the mouse accessory
1282 olfactory system. *Nature Neuroscience*, 13(6), 723–730.
1283 <https://doi.org/10.1038/nn.2546>
- 1284 Miller, A. M. P., Jacob, A. D., Ramsaran, A. I., De Snoo, M. L.,
1285 Josselyn, S. A., & Frankland, P. W. (2023). Emergence of a
1286 predictive model in the hippocampus. *Neuron*.
1287 <https://doi.org/10.1016/j.neuron.2023.03.011>
- 1288 Modi, M. N., Dhawale, A. K., & Bhalla, U. S. (2014). CA1 cell activity
1289 sequences emerge after reorganization of network correlation
1290 structure during associative learning. *eLife*, 3, e01982–e01982.
1291 <https://doi.org/10.7554/eLife.01982>
- 1292 Mokeichev, A., Okun, M., Barak, O., Katz, Y., Ben-Shahar, O., &
1293 Lampl, I. (2007). Stochastic Emergence of Repeating Cortical
1294 Motifs in Spontaneous Membrane Potential Fluctuations In Vivo.
1295 *Neuron*, 53, 413–425.
1296 <https://doi.org/10.1016/j.neuron.2007.01.017>
- 1297 Mollinedo-Gajate, I., Song, C., & Knöpfel, T. (2021). Genetically
1298 Encoded Voltage Indicators. *Advances in Experimental Medicine
1299 and Biology*, 1293, 209–224. https://doi.org/10.1007/978-981-15-8763-4_12
- 1301 Morris, R. G. M., Garrud, P., Rawlins, J. N. P., & O'Keefe, J. (1982).
1302 Place navigation impaired in rats with hippocampal lesions.
1303 *Nature*, 297(5868), 681–683. <https://doi.org/10.1038/297681a0>

- 1304 Moyer, J. R., Deyo, R. A., & Disterhoft, J. F. (1990). Hippocampectomy
1305 disrupts trace eye-blink conditioning in rabbits. *Behavioral*
1306 *Neuroscience*, 104(2)(Apr 1990), 243–252.
1307 <https://doi.org/10.1037/0735-7044.104.2.243>
- 1308 Mukamel, E. A., Nimmerjahn, A., & Schnitzer, M. J. (2009). Automated
1309 analysis of cellular signals from large-scale calcium imaging data.
1310 *Neuron*, 63(6), 747–760.
1311 <https://doi.org/10.1016/j.neuron.2009.08.009>
- 1312 Muller, R. U., & Kubie, J. L. (1989). The firing of hippocampal place
1313 cells predicts the future position of freely moving rats. *The*
1314 *Journal of Neuroscience : The Official Journal of the Society for*
1315 *Neuroscience*, 9(12), 4101–4110.
1316 <https://doi.org/10.1523/JNEUROSCI.09-12-04101.1989>
- 1317 Murray, T. A., & Levene, M. J. (2012). Singlet gradient index lens for
1318 deep in vivo multiphoton microscopy. *Journal of Biomedical*
1319 *Optics*, 17(2), 021106. <https://doi.org/10.1117/1.JBO.17.2.021106>
- 1320 O'Keefe, J., & Burgess, N. (1996). Geometric determinants of the
1321 place fields of hippocampal neurons. *Nature*, 381(6581), 425–428.
1322 <https://doi.org/10.1038/381425a0>
- 1323 O'Keefe, J., & Dostrovsky, J. (1971). The hippocampus as a spatial
1324 map. Preliminary evidence from unit activity in the freely-moving
1325 rat. *Brain Research*, 34(1), 171–175. [https://doi.org/10.1016/0006-8993\(71\)90358-1](https://doi.org/10.1016/0006-8993(71)90358-1)
- 1327 O'Keefe, J., & Nadel, L. (1978). The Hippocampus as a Cognitive Map.
1328 In *Philosophical Studies* (Vol. 27).
1329 <https://doi.org/10.5840/philstudies19802725>
- 1330 O'Keefe, J., & Recce, M. L. (1993). Phase relationship between
1331 hippocampal place units and the EEG theta rhythm.
1332 *Hippocampus*, 3(3), 317–330.
1333 <https://doi.org/10.1002/hipo.450030307>
- 1334 Ohyama, T., Nores, W. L., Murphy, M., & Mauk, M. D. (2003). What
1335 the cerebellum computes. *Trends in Neurosciences*, 26(4), 222–
1336 227. [https://doi.org/10.1016/S0166-2236\(03\)00054-7](https://doi.org/10.1016/S0166-2236(03)00054-7)

- 1337 Ozden, I., Lee, H. M., Sullivan, M. R., & Wang, S. S.-H. (2008).
1338 Identification and Clustering of Event Patterns From In Vivo
1339 Multiphoton Optical Recordings of Neuronal Ensembles. *Journal*
1340 *of Neurophysiology*, 100(1), 495–503.
1341 <https://doi.org/10.1152/jn.01310.2007>
- 1342 Pachitariu, M., Stringer, C., Dipoppa, M., Schröder, S., Rossi, L. F.,
1343 Dalgleish, H., Carandini, M., & Harris, K. D. (2017). Suite2p:
1344 beyond 10,000 neurons with standard two-photon microscopy.
1345 *BioRxiv*, 61507. <https://doi.org/10.1101/061507>
- 1346 Paredes, R. M., Etzler, J. C., Watts, L. T., Zheng, W., & Lechleiter, J.
1347 D. (2008). Chemical calcium indicators. *Methods (San Diego,*
1348 *Calif.)*, 46(3), 143–151.
1349 <https://doi.org/10.1016/j.ymeth.2008.09.025>
- 1350 Pastalkova, E., Itskov, V., Amarasingham, A., & Buzsaki, G. (2008).
1351 Internally Generated Cell Assembly Sequences in the Rat
1352 Hippocampus. *Science*, 321(5894), 1322–1327.
1353 <https://doi.org/10.1126/science.1159775>
- 1354 Pavlov, I. P. (1927). Conditioned reflexes: an investigation of the
1355 physiological activity of the cerebral cortex. In *Conditioned*
1356 *reflexes: an investigation of the physiological activity of the*
1357 *cerebral cortex*. Oxford Univ. Press.
- 1358 Petersen, C. C. H. (2019). Sensorimotor processing in the rodent
1359 barrel cortex. *Nature Reviews. Neuroscience*, 20(9), 533–546.
1360 <https://doi.org/10.1038/s41583-019-0200-y>
- 1361 Pfeiffer, B. E., & Foster, D. J. (2013). Hippocampal place-cell
1362 sequences depict future paths to remembered goals. *Nature*,
1363 497(7447), 74–79. <https://doi.org/10.1038/nature12112>
- 1364 Pfeiffer, B. E., & Foster, D. J. (2015). Autoassociative dynamics in the
1365 generation of sequences of hippocampal place cells. *Science*,
1366 349(6244), 180–183. <https://doi.org/10.1126/science.aaa9633>
- 1367 Pnevmatikakis, E. A., Soudry, D., Gao, Y., Machado, T. A., Merel, J.,
1368 Pfau, D., Reardon, T., Mu, Y., Lacefield, C., Yang, W., Ahrens, M.,
1369 Bruno, R., Jessell, T. M., Peterka, D. S., Yuste, R., & Paninski, L.

- 1370 (2016). Simultaneous Denoising, Deconvolution, and Demixing of
1371 Calcium Imaging Data. *Neuron*, 89(2), 285–299.
1372 <https://doi.org/https://doi.org/10.1016/j.neuron.2015.11.037>
- 1373 Poort, J., Khan, A. G., Pachitariu, M., Nemri, A., Orsolic, I., Krupic, J.,
1374 Bauza, M., Sahani, M., Keller, G. B., Mrsic-Flogel, T. D., & Hofer,
1375 S. B. (2015). Learning Enhances Sensory and Multiple Non-
1376 sensory Representations in Primary Visual Cortex. *Neuron*, 86(6),
1377 1478–1490. <https://doi.org/10.1016/j.neuron.2015.05.037>
- 1378 Ranck, J. B. (1973). Studies on single neurons in dorsal hippocampal
1379 formation and septum in unrestrained rats: Part I. Behavioral
1380 correlates and firing repertoires. *Experimental Neurology*, 41(2),
1381 462–531. [https://doi.org/https://doi.org/10.1016/0014-4886\(73\)90290-2](https://doi.org/https://doi.org/10.1016/0014-4886(73)90290-2)
- 1383 Reyes, A. D. (2003). Synchrony-dependent propagation of firing rate in
1384 iteratively constructed networks in vitro. *Nature Neuroscience*,
1385 6(6), 593–599. <https://doi.org/10.1038/nn1056>
- 1386 Rogerson, T., Cai, D. J., Frank, A., Sano, Y., Shobe, J., Lopez-Aranda,
1387 M. F., & Silva, A. J. (2014). Synaptic tagging during memory
1388 allocation. *Nature Reviews Neuroscience*, 15(3), 157–169.
1389 <https://doi.org/10.1038/nrn3667>
- 1390 Savelli, F., Yoganarasimha, D., & Knierim, J. J. (2008). Influence of
1391 boundary removal on the spatial representations of the medial
1392 entorhinal cortex. *Hippocampus*, 18(12), 1270–1282.
1393 <https://doi.org/10.1002/hipo.20511>
- 1394 Scoville, W. B., & Milner, B. (1957). Loss of recent memory after
1395 bilateral hippocampal lesions. In *Journal of Neurology,*
1396 *Neurosurgery & Psychiatry* (Vol. 20, pp. 11–21). BMJ Publishing
1397 Group. <https://doi.org/10.1136/jnnp.20.1.11>
- 1398 Siegel, J. J., & Mauk, M. D. (2013). Persistent Activity in Prefrontal
1399 Cortex during Trace Eyelid Conditioning: Dissociating Responses
1400 That Reflect Cerebellar Output from Those That Do Not. *The
1401 Journal of Neuroscience*, 33(38), 15272 LP – 15284.
1402 <https://doi.org/10.1523/JNEUROSCI.1238-13.2013>

- 1403 Siegel, J. J., Taylor, W., Gray, R., Kalmbach, B., Zemelman, B. V.,
1404 Desai, N. S., Johnston, D., & Chitwood, R. A. (2015). Trace
1405 Eyeblink Conditioning in Mice Is Dependent upon the Dorsal
1406 Medial Prefrontal Cortex, Cerebellum, and Amygdala: Behavioral
1407 Characterization and Functional Circuitry. *ENeuro*, 2(4),
1408 ENEURO.0051-14.2015. <https://doi.org/10.1523/ENEURO.0051-14.2015>
- 1410 Skaggs, W., McNaughton, B., Gothard, K., & Markus, E. (1996). An
1411 Information-Theoretic Approach to Deciphering the Hippocampal
1412 Code. *Neural Inf. Process Syst.*, 5.
- 1413 Solstad, T., Boccara, C. N., Kropff, E., Moser, M.-B., & Moser, E. I.
1414 (2008). Representation of Geometric Borders in the Entorhinal
1415 Cortex. *Science*, 322(5909), 1865–1868.
1416 <https://doi.org/10.1126/science.1166466>
- 1417 Souza, B. C., Pavão, R., Belchior, H., & Tort, A. B. L. (2018). On
1418 Information Metrics for Spatial Coding. *Neuroscience*, 375, 62–73.
1419 <https://doi.org/10.1016/j.neuroscience.2018.01.066>
- 1420 Stosiek, C., Garaschuk, O., Holthoff, K., & Konnerth, A. (2003). In vivo
1421 two-photon calcium imaging of neuronal networks. *Proceedings of
1422 the National Academy of Sciences of the United States of
1423 America*, 100(12), 7319–7324.
1424 <https://doi.org/10.1073/pnas.1232232100>
- 1425 Taube, J. S., Muller, R. U., & Ranck, J. B. J. (1990). Head-direction
1426 cells recorded from the postsubiculum in freely moving rats. I.
1427 Description and quantitative analysis. *The Journal of
1428 Neuroscience : The Official Journal of the Society for
1429 Neuroscience*, 10(2), 420–435.
1430 <https://doi.org/10.1523/JNEUROSCI.10-02-00420.1990>
- 1431 Valero, M., Cid, E., Averkin, R. G., Aguilar, J., Sanchez-Aguilera, A.,
1432 Viney, T. J., Gomez-Dominguez, D., Bellistri, E., & de la Prida, L.
1433 M. (2015). Determinants of different deep and superficial CA1
1434 pyramidal cell dynamics during sharp-wave ripples. *Nature
1435 Neuroscience*. <https://doi.org/10.1038/nn.4074>

- 1436 Velasco, M. G. M., & Levene, M. J. (2014). In vivo two-photon
1437 microscopy of the hippocampus using glass plugs. *Biomedical*
1438 *Optics Express*, 5(6), 1700–1708.
1439 <https://doi.org/10.1364/BOE.5.001700>
- 1440 Voelcker, B., Pancholi, R., & Peron, S. (2022). Transformation of
1441 primary sensory cortical representations from layer 4 to layer 2.
1442 *Nature Communications*, 13(1), 5484.
1443 <https://doi.org/10.1038/s41467-022-33249-1>
- 1444 Wood, E. R., Dudchenko, P. A., Robitsek, R. J., & Eichenbaum, H.
1445 (2000). Hippocampal Neurons Encode Information about Different
1446 Types of Memory Episodes Occurring in the Same Location.
1447 *Neuron*, 27(3), 623–633.
1448 [https://doi.org/https://doi.org/10.1016/S0896-6273\(00\)00071-4](https://doi.org/https://doi.org/10.1016/S0896-6273(00)00071-4)
- 1449 Yiu, A. P., Mercaldo, V., Yan, C., Richards, B., Rashid, A. J., Hsiang,
1450 H.-L. L., Pressey, J., Mahadevan, V., Tran, M. M., Kushner, S. A.,
1451 Woodin, M. A., Frankland, P. W., & Josselyn, S. A. (2014).
1452 Neurons are recruited to a memory trace based on relative
1453 neuronal excitability immediately before training. *Neuron*, 83(3),
1454 722–735. <https://doi.org/10.1016/j.neuron.2014.07.017>
- 1455 Zhou, Y., Won, J., Karlsson, M. G., Zhou, M., Rogerson, T., Balaji, J.,
1456 Neve, R., Poirazi, P., & Silva, A. J. (2009). CREB regulates
1457 excitability and the allocation of memory to subsets of neurons in
1458 the amygdala. *Nature Neuroscience*, 12(11), 1438–1443.
1459 <https://doi.org/10.1038/nn.2405>
- 1460 Ziv, Y., Burns, L. D., Cocker, E. D., Hamel, E. O., Ghosh, K. K., Kitch,
1461 L. J., El Gamal, A., & Schnitzer, M. J. (2013). Long-term dynamics
1462 of CA1 hippocampal place codes. *Nature Neuroscience*, 16(3),
1463 264–266. <https://doi.org/10.1038/nn.3329>

1464 **Chapter 2 – Behaviour**

1465

1466 **Towards understanding brain activity in a 1467 reproducible context**

1468

1469 Our understanding of memory and learning depends upon the type of
1470 learning that is studied (Schreurs, 1989). Two important categories of
1471 memory and learning experiments are,

- 1472 1. Non-associative (Habituation and Sensitization), and
- 1473 2. Associative learning (Classical and Operant Conditioning).

1474

1475 Non-associative learning paradigms provide information about how an
1476 organism responds to repeated presentations of a single stimulus
1477 (Brown, 1998). However, it was of interest to us to study how animals
1478 responded to a number of events and stimuli being associated, and
1479 how the activity of the brain relates to this. Hence, we chose to design
1480 our experiments to incorporate associative learning, which is a
1481 relatively permanent change in behaviour that results from the
1482 temporal conjunction of two or more events or stimuli.

1483

1484 Empirically, reproducible behaviour depends on strong associations
1485 between the events or stimuli being paired, and may often require
1486 many repeated pairings or trials. Additionally, having the animal
1487 engage in the behavioural task and pay attention to the stimuli being

1488 presented, is crucial to look for important correlations between the
1489 experiment conditions (external) and brain activity (internal).

1490

1491 Anaesthetized animals have been previously used to study brain
1492 activity and led to important discoveries, e.g. - visual representation of
1493 moving bars in the visual cortex (Hubel & Wiesel, 1962), habituation in
1494 the Hippocampus (Deshmukh & Bhalla, 2003). However, it was clear
1495 that similar experiments repeated in awake animals did not result in the
1496 same observations. Indeed, animals needed to navigate a known
1497 environment before the discovery of place cells (O'Keefe &
1498 Dostrovsky, 1971), grid cells (Fyhn et al., 2004; Hafting et al., 2005),
1499 and head-direction cells (Ranck, 1973; Taube et al., 1990), among
1500 others, could be made.

1501

1502 The reliability of the overt behavioural responses of the experiment
1503 animals then sets the conditions and parameter list to study physiology
1504 within the confines of reproducible behavioural contexts, and was
1505 considered an important mandate for the standardization of any of the
1506 behavioural tasks described in this chapter. Under the umbrella of
1507 associative learning, we began our experiments with various protocols
1508 related to Operant Conditioning wherein the reinforcing signal for
1509 learning was a water reward to correctly timed licks. As will be
1510 discussed in the next few sections, we later switched to aversive
1511 conditioning with Trace Eye-Blink Conditioning.

1512

1513 **Operant conditioning [Project I]**

1514

1515 Operant conditioning is both the procedure and a type of associative
1516 learning process through which the strength of a voluntarily performed
1517 behaviour is modified positively (appetitively) by reward (water,
1518 sucrose, food, etc.), or negatively (aversively) by punishment (air-puff
1519 to the eye, electrical shocks, etc.). For example, if the animal responds
1520 to a presented stimulus by performing a lick onto a water spout, then a
1521 water reward would strengthen the behaviour while Lithium Chloride
1522 solution (which is aversive) would weaken it.

1523

1524 We now describe our experiments and results with regard to Operant
1525 Conditioning, in more detail.

1526

1527 **Required features**

1528

1529 For Project I, the goal was to study how the association of a neutral
1530 stimulus with a water reward modified the neurophysiological activity of
1531 the hippocampal CA1. For this, we required the following.

1532 1. An assortment of different stimuli and modalities (light, tone, etc.)
1533 to be presented to the animal.

1534 2. The animal must withhold any motor movement during the
1535 presentation of the stimuli, to study pure stimulus responses.

1536 3. The animal must perform a lick for a water reward after the end of
1537 the stimulus presentation.

1538 4. The animal must be able to make the association between stimuli
1539 and water reward within 7 days of training (at the time we did not have
1540 the ability to record for multiple days).

1541

1542 The behavioural state of the animal, in terms of anxiety, motivation,
1543 attention, etc., may be variable when a naïve animal is presented with
1544 different stimuli. This may cause a large variability in the activity of
1545 cells, since the animal may not be paying attention to it. Also, if the
1546 animal were rewarded for performing the task it is expected that there
1547 would be motivation to pay attention to the stimuli presented. Finally,
1548 such a task would involve the animal associating the stimuli that it is
1549 trained to with a behavioural task and this would provide an apt context
1550 to study association related changes in stimulus responses.

1551

1552 In this section, we discuss some important protocols that we tried and
1553 tested and a list of the various kinds of behavioural tasks we employed
1554 for head-fixed mice.

1555

1556 For Project I, we tried several variations of Operant Conditioning
1557 including Stimulus Detection tasks, Delayed Non-Match to Sample
1558 (DNMS), as well as Go/No-Go tasks. Each of these tasks requires
1559 animals to perform licks to the Conditioned Stimuli and for them to be
1560 rewarded (2-3 µL water) or punished based on the task demands and
1561 protocol design.

1562

1563 **Water delivery and calibration**

1564

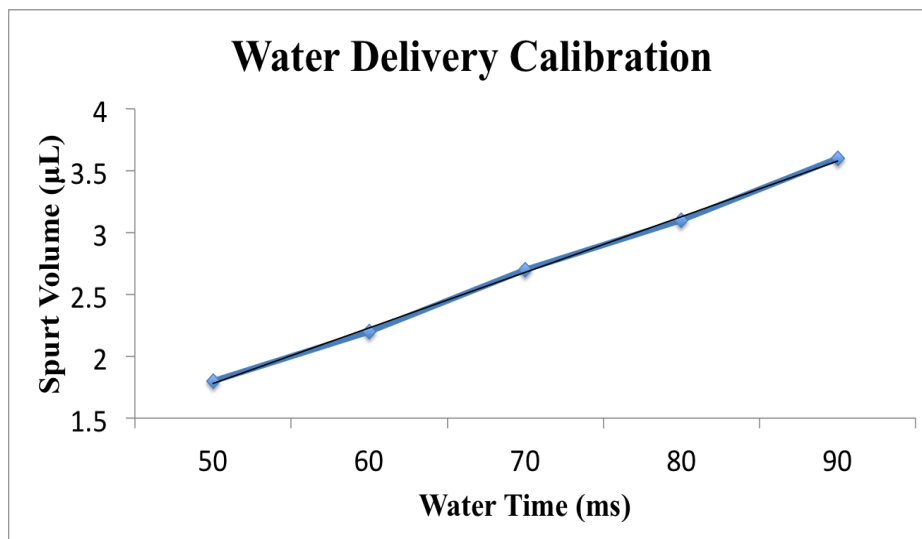


Figure 2: Water delivery calibration to reward the animal consistently with the same volume of water.

1565 The lick port was made from a trimmed and smoothed 16 gauge
1566 syringe, connected to a water reservoir with small diameter tubing. A
1567 solenoid valve clamped onto this tubing, gated by a 12V DC signal.
1568 When this gate was opened, the volume of water could be regulated by
1569 the duration of the 12V DC signal. We calibrated the duration of gate
1570 opening to achieve ~2 μ L per pulse or spurt (Jaramillo & Zador, 2014).
1571 The weight of 100 spurts was measured and then divided by 100 to get
1572 the weight of 1 spurt. 65 ms was found corresponding to 2.5 μ L (this
1573 value was used for all Operant Conditioning experiments). In the figure
1574 below (Figure 2), the measured volumes/weights are plotted as blue
1575 filled diamonds, error bars are presented as Standard Error and the
1576 linear trendline is shown in black.

1577 **Opto-islator circuit for solenoid control**

1578

1579 To be able to programmatically control the 12V DC line to the solenoid
1580 valve, we used the following circuit (Figure 3), which accepted a 5V
1581 digital input from the DAQ (NI USB-6001) interfacing the lab computer
1582 to the behaviour rig.

1583

1584 **Parts list**

1585 1. 470 ohm resistor
1586 2. 15 kohm resistor
1587 3. MCT2e
1588 4. ULN2003
1589 5. Bases (adaptors for MCT2e and ULN2003)
1590 6. +5V and +12V DC inputs from a Power Supply)
1591 7. Source of +5V DC input (DAQ, etc.)
1592 8. Connecting wires
1593 9. Load Resistance (Solenoid, etc.)

1594

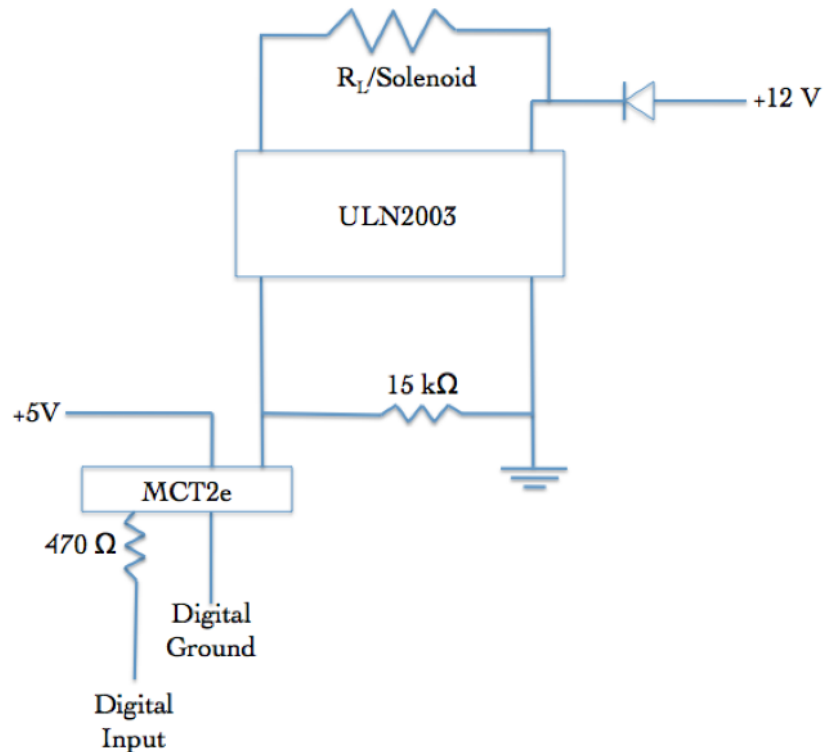


Figure 3: Optoisolator circuit to amplify +5V DC input to +12V DC output.

1596

1597 Lick detection circuit

1598

1599 To be able to monitor the presence or absence of licks to the port, the
 1600 conductive part (metal) of the lick port syringe was connected to a
 1601 MOSFET such that a 5V DC voltage could be read out, whenever the
 1602 animal would make contact with the port. This was designed as a
 1603 readout to Stimulus Detection by the animal. The circuit diagram is
 1604 shown below (Figure 4):

1605

1606 **Parts list**

- 1607 1. +5V Power Supply
- 1608 2. 4.7 kohm resistor
- 1609 3. 22 Mohm resistor
- 1610 4. IN4007 Diode
- 1611 5. NPN Transistor IRF540N (MOSFET)
- 1612

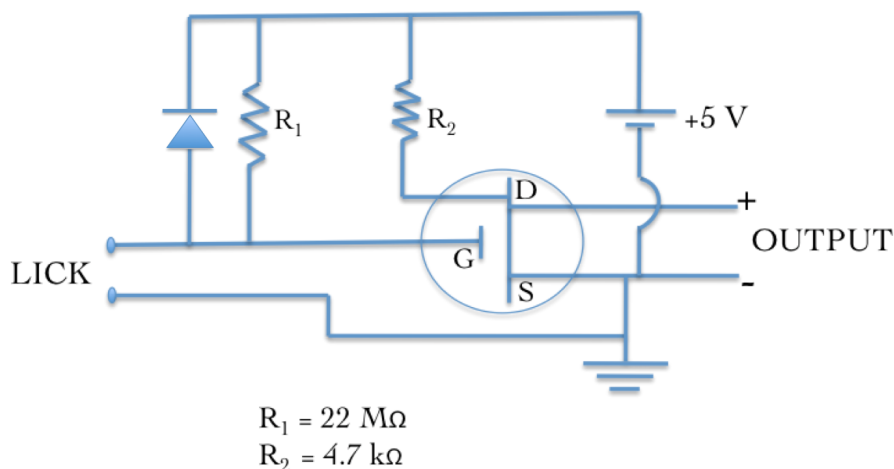


Figure 4: Lick detector circuit based on a MOSFET design. Whenever the animal performed a lick, a +5V DC Output would be read out.

1614 **Controlling task details and protocol information**

1615

- 1616 All protocols were controlled using custom scripts written in NI LabVIEW 8. These scripts were run on a lab desktop which interfaced with the DAQ (NI USB-6001) via USB. The DAQ,
 - 1619 1. Sent the 5V digital input to switch on the solenoid valve
 - 1620 regulating water delivery, and

1621 2. Received the 5V digital output of the lick detection circuit
1622 whenever a lick was produced by the animal.

1623

1624 **Head-bar implant, Animal Handling, and Water
1625 deprivation**

1626

1627 All experiments were planned to be conducted on head-fixed C57Bl/6
1628 mice, with the eventual intention to perform *in vivo* imaging on these
1629 animals. For this, we surgically implanted metal head-bars on the skull
1630 of the animals while they were maintained on 1-2% Isoflurane, above a
1631 heating pad (35°C). Surgeries would last no longer than 30 mins per
1632 animal.

1633

1634 After 1-7 days of recovery after surgery, we handled the animals gently
1635 for 2 days till the animals would appear comfortable with lifting and
1636 gentle collar grabbing. Next, for 3-4 days, we kept the animals head-
1637 clamped on the behavioural setup (Figure 8). We restricted our
1638 animals to ~1ml of water per day, keeping check that their body weight
1639 did not fall to below 80% of the weight on day 1.

1640

1641 **PROTOCOL 1.1: Stimulus Detection Task**

1642

1643 We first tried the simplest version of the lick task wherein an auditory
1644 tone was followed by a water reward. The animal would have to
1645 withhold licking till the end of the stimulus presentation, and then
1646 perform the lick for the reward (Figure 5).

1647 **Total number of trials**: 600/session; 1 session/day

1648 **Trial phases**:

1649 1. Stimulus free pre-tone (PT): 1 s

1650 2. Tone: 5 kHz for 1 s

1651 3. Critical timeout (CT): 100 ms

1652 4. Inter-trial Interval (ITI): randomized between 2 s to 5



Figure 5: Typical trial structure with the various phases. Each trial was followed by a randomized Inter-Trial Interval (ITI).

1654 Only licks during the critical timeout (CT) phase immediately after the
1655 Tone phase were rewarded while licks in other phases resulted in a
1656 phase restart.

1657

1658 **PROTOCOL 1.2: Stimulus Detection Task with aversive
1659 punishment**

1660

1661 **Total number of trials**: 600/session; 1 session/day

1662

1663 Only licks during the critical timeout (CT) phase immediately after the
1664 Tone phase were rewarded while licks in other phases resulted in an
1665 aversive punishment, *viz.*, 100 ms air-puff to the body of the animal,
1666 before a phase restart. For Mouse 3 we started Protocol 1.2 from
1667 Session 3 while for Mouse 4 we started Protocol 1.2 from Session 2.

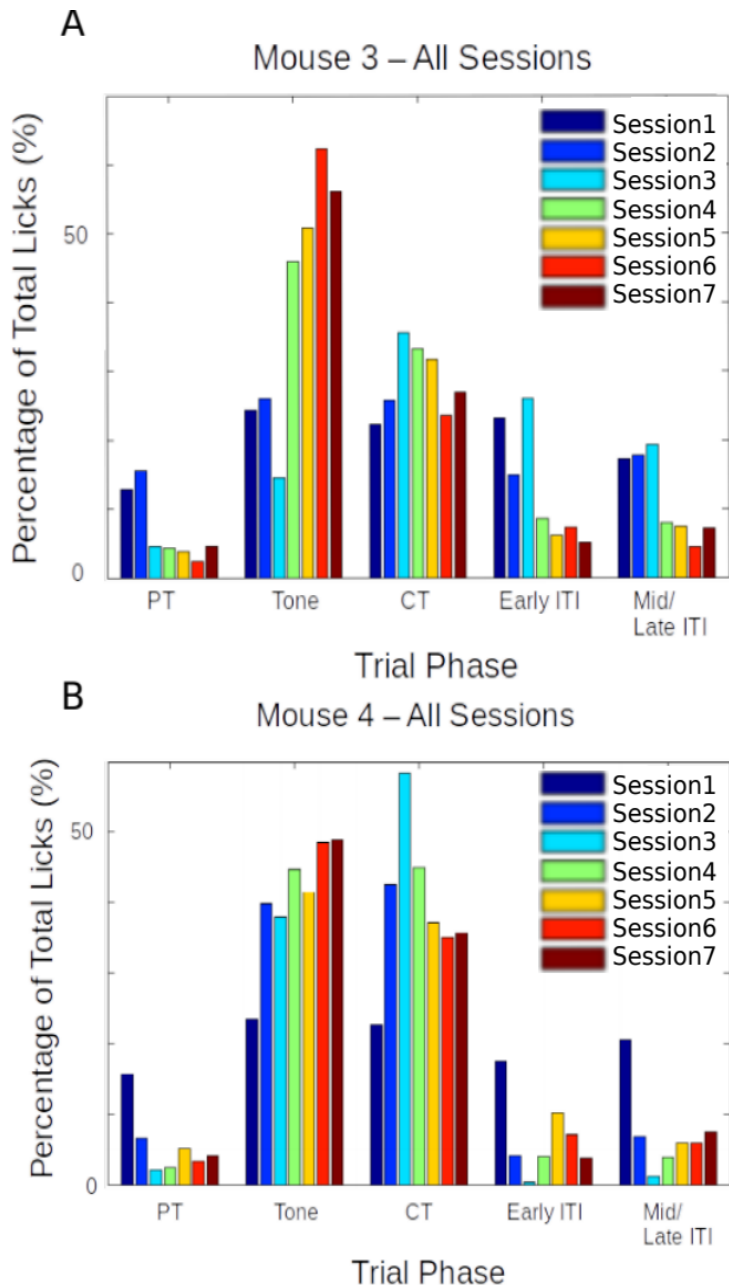


Figure 6: Performance evaluation for two example mice trained to Protocol 1.1 and 1.2. Percentage of total licks in the various trial phases (Pre-Tone, Tone, CT, and ITI), across all sessions of training (coloured bar plots) for A) Mouse 3, and B) Mouse 4

1669 **Results – Protocol 1.1 and 1.2**

1670

1671 The behavioural performance for each of the experiment animals was
1672 evaluated using custom analysis scripts written in MATLAB 2011. Here
1673 are the results from two mice trained based on Protocols 1.1 and 1.2
1674 (Figure 6).

1675 In both the examples shown, animals would typically produce a great
1676 percentage of total licks even during the Tone period. This failure to
1677 withhold licks carried on for 7-14 sessions, and the task was ultimately
1678 unsuccessful.

1679

1680 **Total animals trained:** 2

1681 **Conclusion:** Fail

1682

1683 **Protocol 2: Stimulus Detection task with timeout box**

1684

1685 We also tried the same Stimulus Detection protocol, without an air-puff
1686 punishment, but with incorrect licks punished by a trial abort and a
1687 stimulus-free timeout phase, which the animal could escape from if it
1688 withheld licking. We decided to train the animals in blocks, each with a
1689 specific goal that the animal had to achieve.

1690

1691 **Trial phases:**

1692 1 Stimulus-free pre-tone (PT): 1 s

1693 2 Tone: 5 kHz for a variable duration (based on Block)

1694 3 Critical timeout (CT): 1000 ms

1695 4 Inter-trial Interval (ITI): randomized between 2 s to 5 s

1696

1697 Only licks during the critical timeout (CT) phase immediately after the
1698 Tone phase were rewarded while licks in other phases resulted in a
1699 phase restart.
1700
1701 **Block 1:** Unconditional Water to get the animal to associate the tone
1702 - ~20 trials
1703 - 100 or 200 ms Tone duration
1704 - Unconditional water provided at the end of the tone, irrespective of
1705 lick
1706
1707 **Block 2:** Conditional Water to get the animal to learn that licking
1708 with/after tone is going to be rewarded
1709 - 100 or 200 ms Tone duration
1710 - 1000 ms Reward phase
1711 - Lick during/after tone (Reward phase) = reward
1712 - No lick = no reward
1713 - Lick during pre-tone = no reward/abortion of trial
1714 - Lick during ITI = no reward/abortion of trial
1715 - Animals graduate to the next Block of training only after achieving at
1716 least 70-80% success rates
1717
1718 **Block 3:** Training the animal to learn "when" to lick
1719 - 1000 ms pre-tone, 100 or 200 ms Tone, 1000 ms Reward phase, 3-5
1720 s randomized ITI
1721 - Lick during Reward phase = reward
1722 - Any lick during the pre-tone or the tone, aborts the trial and sends the
1723 program to a Timeout phase (lasting, 2-3 s)
1724 - The timeout phase ends only when there is a 2-3 s (specified) interval
1725 of no licking

1726 - If the timeout phase ends, a new trial begins
1727 - Licks during ITI are also "punished" accordingly
1728 - Animals graduate to the next Block of training only after achieving 70-
1729 80% success rates

1730

1731 **Block 4:** Same as Block 3, but with a gradually increasing tone
1732 duration in steps of 50/100 ms
1733 - The tone duration is gradually increased, the increase being tailored
1734 to the performance of the animal
1735 - It will be attempted to get the animals to learn to wait for 500-700 ms
1736 - Animals graduate to the next Block of the experiment only after
1737 achieving 70-80% success rates

1738

1739 **Results – Protocol 2**

1740

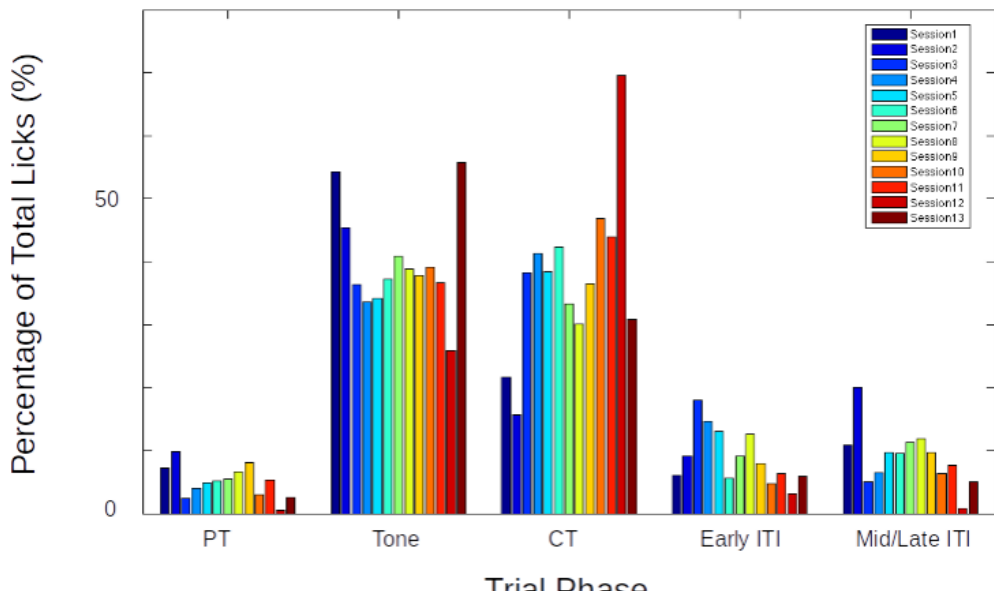
1741 The behavioural performance for each of the experiment animals was
1742 evaluated using custom analysis scripts written in MATLAB. Here are
1743 two representative examples of mice trained based on Protocol 2 –
1744 Block 3 (Figure 7).

1745

1746

A

Mouse S1 – All Sessions



B

Mouse S2 – All Sessions

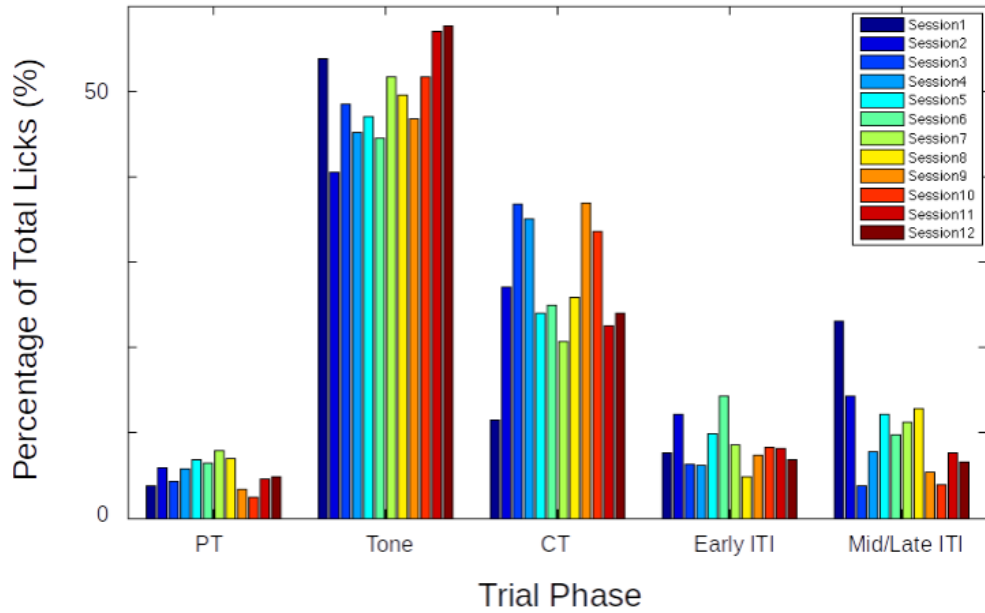


Figure 7: Performance evaluation for two example mice trained to Protocol 2. Percentage of total licks in the various trial phases (Pre-Tone, Tone, CT, and ITI), across all sessions of training (coloured bar plots), for (A) Mouse S1, and (B) Mouse S2.

1748 Again, as is clear from the examples above, that while the mice
1749 eventually produced a decent percentage of total licks in the critical
1750 timeout (CT) phase to get a water reward, they did not learn to
1751 withhold licks during the Tone phase, even after >10 sessions. The
1752 task was ultimately unsuccessful.

1753

1754 **Total animals trained:** 4

1755 **Conclusion:** Fail

1756

1757 **Protocol 3: Delayed Non-Match to Sample (DNMS)**

1758

1759 Delayed Non-Match to Sample (DNMS) is a task that is ideally suited
1760 to study working memory and recognition (Binder et al., 2009), but we
1761 decided to try it. This task involves trial-by-trial presentation of two
1762 stimuli separated by a stimulus-free delay interval. For any given trial,
1763 If the two pseudorandomly chosen pairs of stimuli were identical, then
1764 licks would not be rewarded. However, if the pair of stimuli were
1765 different, then licks would be rewarded with 2 μ L water.

1766

1767 We tried to incorporate more tones, in the hope that this may improve
1768 the chances of the animals focusing on the task specifics, instead of
1769 producing licks to just any particular stimulus.

1770

1771 **Tones used:** 6000 Hz, 8500 Hz, 10000 Hz, and 11500 Hz

1772 **Trial phases:**

- 1773 1. Pre-Tone duration (ms): 1000 ms
- 1774 2. CS 1 duration (ms): 350 ms

1775 3. Delay Interval duration (ms): 250 ms
1776 4. CS 2 duration (ms): 350 ms (unless a correct lick is
1777 elicited)
1778 5. ITI duration (s): randomized from 1 s to 3 s
1779 **Punishment:** Timeout Box (minimum of 3s of no licks to escape)
1780 **Reward:** 2 µL of water

1781

1782 **Results – Protocol 3**

1783
1784 >70-80% of the trials had to be aborted because the animals would not
1785 withhold licking after the 1st of the pair of tones was presented. This
1786 did not change even after 7 days (sessions) of training.

1787

1788 **Total animals trained:** 6

1789 **Conclusion:** Fail

1790

1791 **Protocol 4: Go/No-Go Task**

1792

1793 In an attempt to simplify the behavioural task, we decided to
1794 reconfigure the DNMS task to a simpler Go/No-Go task. Here, we
1795 would again present the animal with two stimuli, but with the only
1796 condition being that the animal would have to lick after the second
1797 stimulus, and not before. This simplifies the behaviour to a certain
1798 extent, because the animals need only use the first stimulus as a cue
1799 for the second. Failure to perform this task could more easily then be
1800 attributed to a lack of attention in that trial. Only the data from the trials

1801 where the animal succeeds to do the task would be considered for
1802 analysis. Training related changes in actual stimulus representations
1803 would be carefully dissected out. Furthermore, such a task would
1804 control for the behavioural state of the animal and help provide
1805 important datasets.

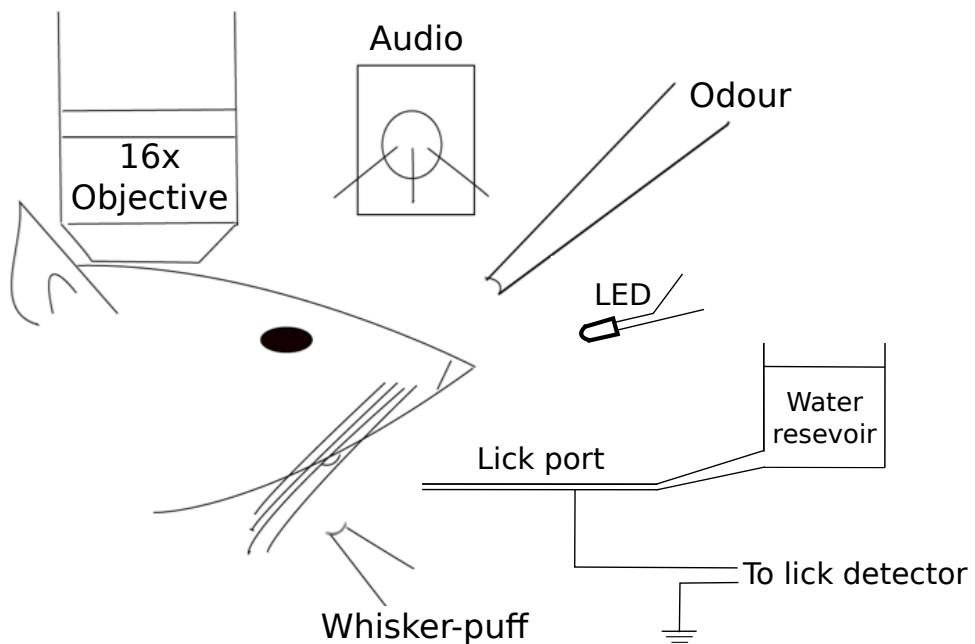


Figure 8: Schematic representation of the experimental setup for a simple detection task where the animal must perform a lick upon correctly detecting the presence of the conditioned stimulus (CS; from a range of modalities).

1807 In terms of imaging, we hoped to use the no-go stimulus to record a
1808 clean stimulus response without the possible contamination of
1809 movement (licking behaviour), and the go stimulus to verify attention
1810 (Figure 8).

1811 Trials were designed to go through the following phases and have the
1812 animal graduate to subsequent phases, only after correctly performing
1813 the behaviour:
1814 1. Pre-tone: Stimulus-free period; no lick
1815 2. No-go tone: 7kHz tone period; no lick
1816 3. Go tone: 10kHz tone period; lick for reward
1817 If the animal would perform an incorrect lick, the particular phase
1818 currently occurring was restarted. Only licks to the Go tone were
1819 rewarded (Figure 9).

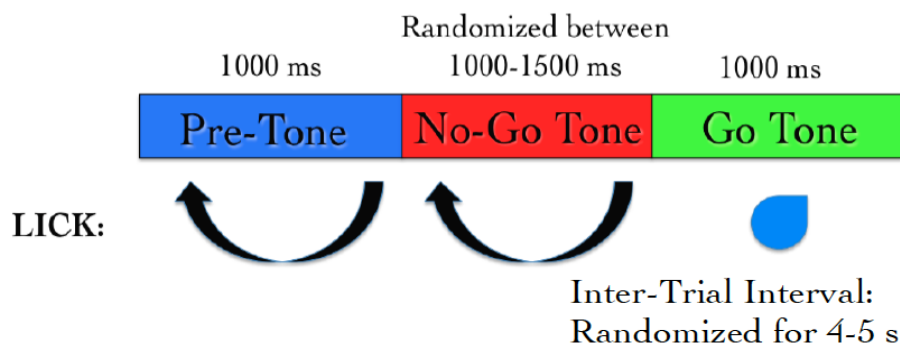


Figure 9: Typical trial structure with the various phases and lick dependent relationships.

1821 Results – Protocol 4

1822
1823 The behavioural performance improves only after ~3-4 sessions of
1824 training (Figure 10A). This is primarily due to an increase in the
1825 percentage of trials with a correct Go tone lick, as shown (Figure 10B).
1826

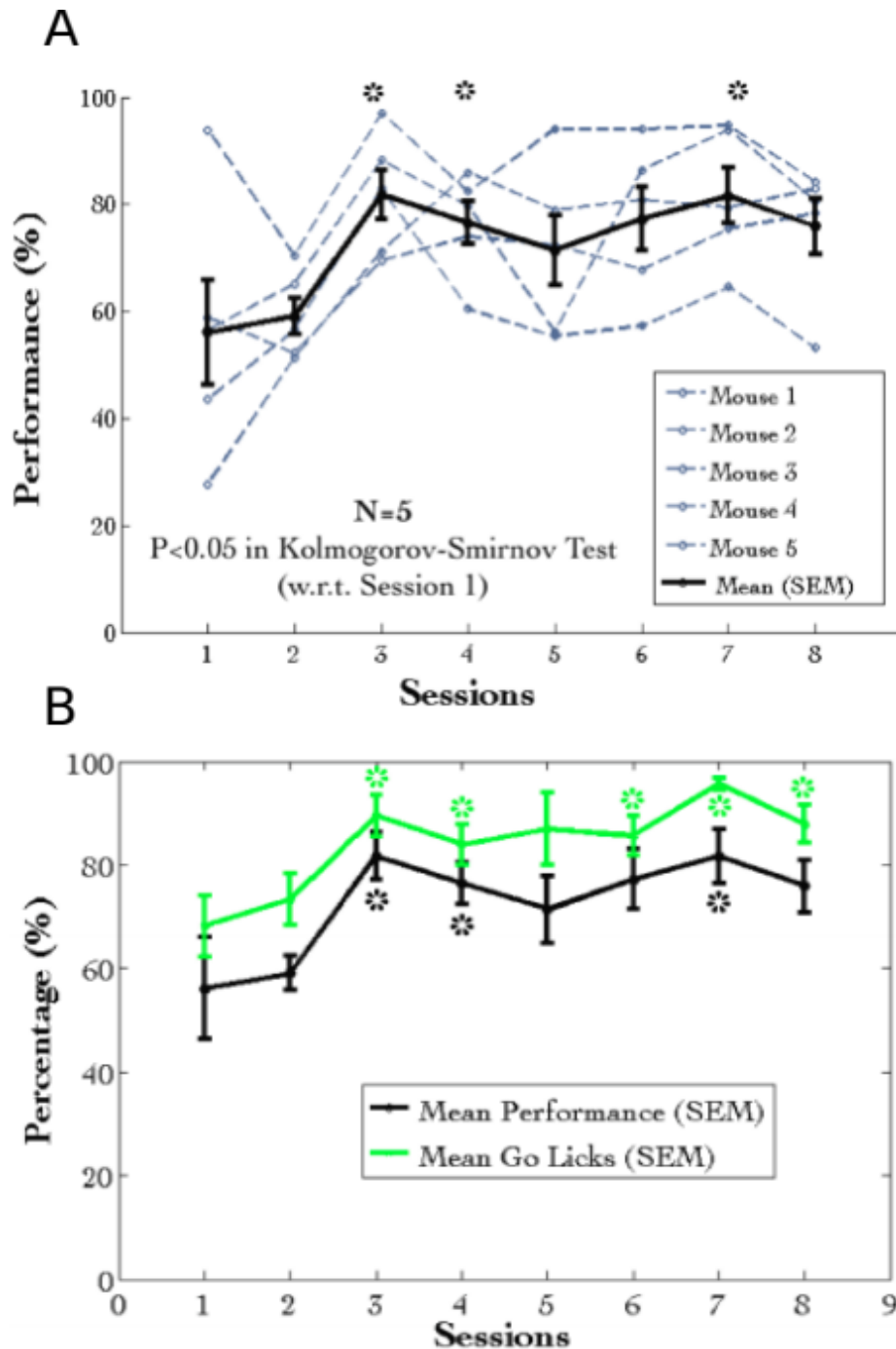


Figure 10: (A) Performance traces for all the animals individually shown in dashed grey lines. Mean + SEM in black. (B) Mean Performance (%) and Mean Go Tone Lick Percentage (%) with Session for the Go/No-Go Task, plotted in black and green, respectively.

1828 A plot of the lick histogram for the various trial phases revealed that
1829 despite reaching the maximum success rate, the animals continued to
1830 lick during the no-go tone phase (incorrect lick) for a long duration of
1831 time (Figure 11). There was no difference in the amounts of time spent
1832 in the pre-tone or no-go tone phases. This suggested that the animals
1833 did not discriminate between the Go and no-go tones. Accordingly, the
1834 current protocol was not being learnt as expected.

1835

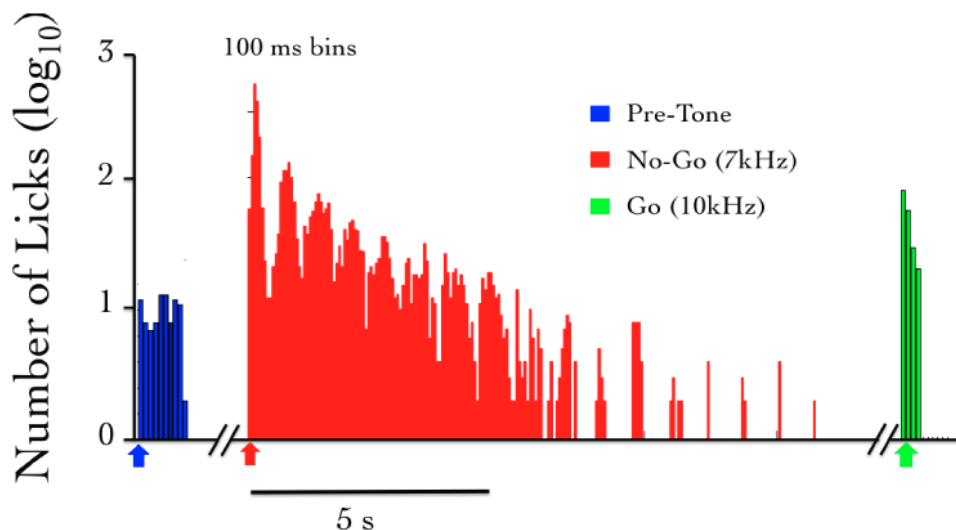


Figure 11: The number of licks in the pre-tone (blue), no-go tone (red), and go tone (green) phases, in a representative animal, in a session with maximum Performance (%).

1837 We were not able to get discriminatory detection. Animals would resort
1838 to performing licks continuously and agnostically to the go and no-go
1839 stimulus. In a study published many years later, it was determined that
1840 discriminatory tasks such as the one described above, could often
1841 require 3-4 weeks of training (Guo et al., 2014), since the animal was
1842 not punished with anything more than a delay or phase restart.

1843

1844 **Total animals trained:** 5

1845 **Conclusion:** Fail

1846

1847 Eventually, we had to abandon these experiments, to switch to an
1848 aversive conditioning task, *viz.*, Trace Eye-Blink Conditioning (TEC).

1849 With the change in the main behavioural task we also changed the
1850 project goals. The TEC task was standardized with the intention to
1851 work on Project II which is to study how animals make complex
1852 associations between different types of stimuli and how they adapt to
1853 changes to the inter-stimulus interval (ISI).

1854

1855 **Trace Eye-Blink Conditioning [Project II]**

1856

1857 Eye-blink Conditioning is a class of Classical Conditioning and requires
1858 the presentation of a neutral stimulus (Conditioned Stimulus, CS) along
1859 with an eye-blink eliciting, mildly aversive stimulus (Unconditioned
1860 Stimulus, US). Depending on whether the CS presentation overlaps
1861 with the US presentation or if the two stimuli are separated by a
1862 stimulus free interval in between (Trace interval), the concomitant
1863 procedure is called Delay Conditioning or Trace Conditioning,
1864 respectively (Figure 12). In either case, precise timing of the CS and
1865 US is mandated.

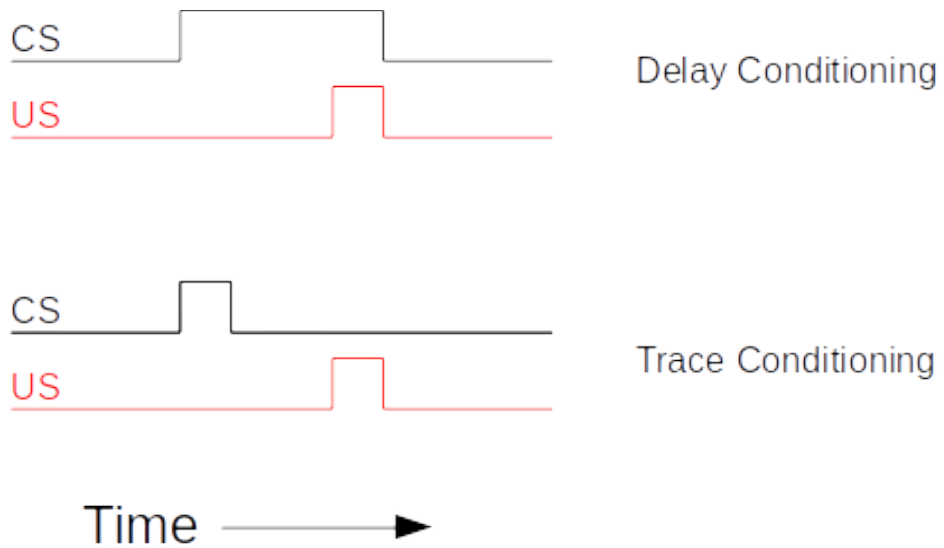


Figure 12: Schematic representation to showcase the two main subtypes of Classical Conditioning (Eye-Blink Conditioning, for our experiments) based on the relative timing and presentation of the CS and US.

1867 The CS is usually an auditory tone or a visual stimulus (e.g.- LED
 1868 Flash), while the US is typically a mild air-puff to the cornea, or a
 1869 gentle electric shock to the eye-lid. Naive animals (rabbits, rodents,
 1870 monkeys, etc.) produce a robust, reflexive eye-blink to the US
 1871 (Unconditioned Response, UR) and ignore the CS, in early trials.
 1872 However, with repeated pairing of CS and US, the animals are able to
 1873 associate the two, and use the CS as a cue to predict the US,
 1874 producing a partial, preemptive eye-blink just before the expected time
 1875 of the US (Conditioned Response, CR). The CR develops in amplitude
 1876 over multiple pairings or training sessions. In well trained animals, the
 1877 CR begins at a time point closer and closer to the CS onset, and
 1878 usually merges with the UR. The animals produce this CR in an
 1879 attempt to avoid the US.
 1880

1881 Traditionally, Trace Eye-Blink Conditioning has been an important
1882 hippocampus-dependent behavioural task, and has been adapted to a
1883 variety of different species, spanning rabbits, rats, and mice.

1884

1885 Damage or inhibition of the hippocampus has been shown to limit task
1886 acquisition without affecting other non-hippocampus dependent tasks
1887 such as Delay Conditioning. As per published literature, Ibotenic Acid
1888 was used in a session dependent fashion, to observe both limitations
1889 in first acquiring the Trace Conditioning task, as well as detriments to
1890 behavioural recall, even after animals learn the task to a high degree of
1891 proficiency, suggesting the pivotal role that the hippocampus plays in
1892 temporal tasks of this nature (Tseng et al., 2004).

1893

1894 A single session of Trace Eye-Blink Conditioning, with strong stimuli
1895 (CS and US), has been previously employed (Modi et al., 2014), but
1896 with only upto 50% of the animals learning the task. Typically animals
1897 require around 3-7 sessions (~200-600 trials) to robustly learn the task.
1898 Accordingly, we designed and standardized a multi-session version of
1899 TEC, to allow more animals to learn and acquire the task, based on
1900 previously published work (Siegel et al., 2015).

1901

1902 **Tracking eye-blink responses**

1903

1904 The most foolproof way to track eye-blink responses (especially with
1905 head-fixed animals) chronically (for multiple sessions across days), is
1906 to use a video camera. We used a Point Grey Chameleon3 1.3 MP
1907 Monochrome USB3.0 camera) for this purpose. It is cost effective and
1908 with proper scaling of the resolution and field of view, can achieve

1909 recording rates of >200 frames per second (FPS). An important criteria
1910 for getting faster frame rates is to have better illumination, so that the
1911 camera may be set to lower exposure settings. We used a set of 5-10
1912 Red colour LEDs as the light source, and these are run using a 12V
1913 DC line, with current limited resistors in series. Additionally, we used
1914 an IR-blocking filter to avoid capturing the 2-Photon excitation light
1915 (910-920 nm) when conduction behaviour and imaging experiments
1916 simultaneously. Finally, to focus the light from the eye of the animal
1917 onto the camera sensor, we used a Tamron M118FM16 lens (1/1.8,
1918 16mm F/1.4).

1919 **Treadmill and tracking running speed**

1920
1921 Allowing the head-fixed animals to run on a treadmill was an important
1922 behaviour rig consideration, as this allows the animals to be more
1923 comfortable and less stressed. We used a 6 inch cylindrical massage
1924 roller with a stainless steel axle running along the length. This axle had
1925 ball bearings on the two ends, to allow for free rotation against clamps.
1926 Additionally, we used linear actuators to be able to adjust the height of
1927 the treadmill relative to the head-fixing clamps.

1928
1929 On one side of the treadmill, we used a printed pattern of black
1930 squares (side length: 1cm) along the circumference (Siegel et al.,
1931 2015). This allowed an IR LED - Photodetector pair to catch the edges
1932 of the black printed squares. The number of edges detected per unit
1933 time, then gave us the run speed of the animals being trained (Figure
1934 13).

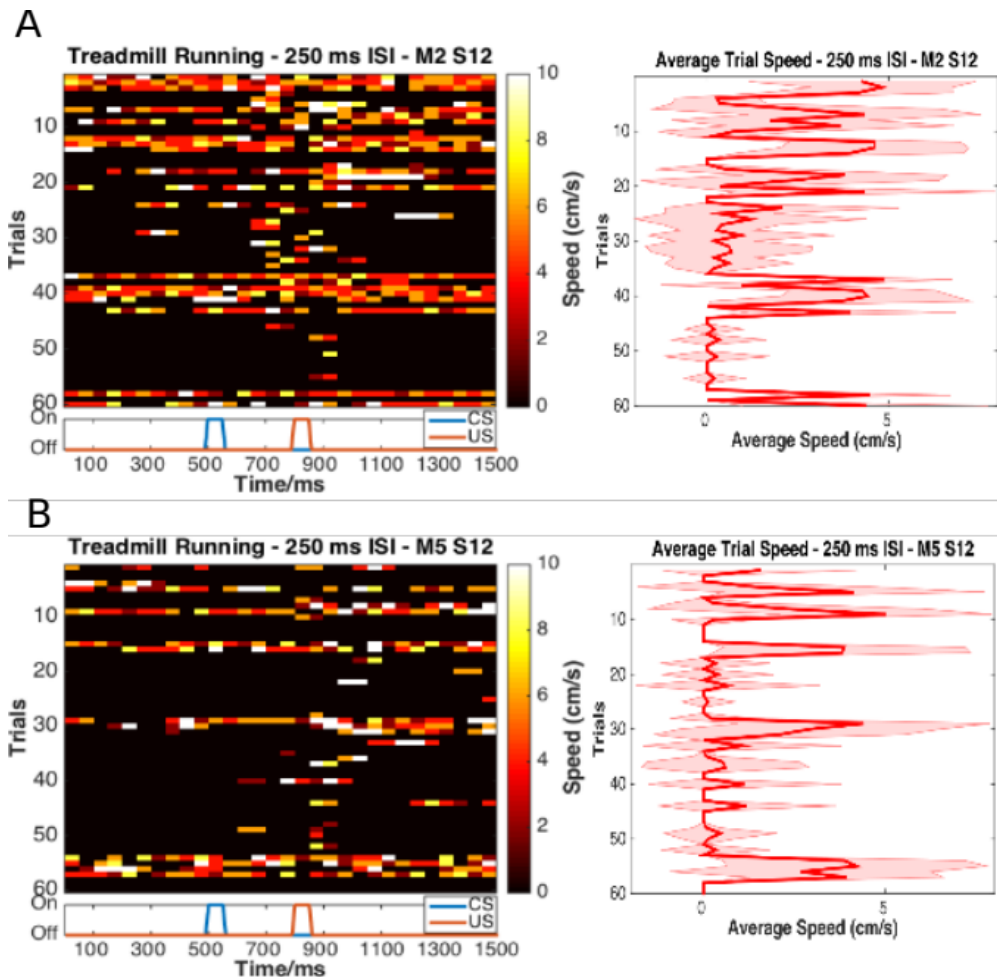


Figure 13: Trial by trial (left), and trial-averaged running speed (right) for two example animals, (A) M2 Session 12, and (B) M5 Session 12.

1936 Behaviour rig and protocol control - Software

1937

1938 For our initial experiments we used the open-source behaviour
 1939 controlling software suite Bonsai (Windows version). Later on, we were
 1940 able to implement our own custom codes that allowed integration of
 1941 the video camera, Arduino for stimulus delivery and treadmill tracking,

1942 and the software side of the protocols. Dilawar S. Rajput was
1943 instrumental in setting up the camera pipeline and integrating it into the
1944 Arduino code. The Camera server was implemented in C++ with
1945 Spinnaker API (Point Grey) and this fetched frames from the camera.
1946 The camera client was written in Python, and this read the frames to
1947 produce a copy to monitor the video feed live, as well as write the
1948 video frames to disk as .tif files.
1949 With this setup, the maximum memory usage was ~1.3 GB RAM, and
1950 the code (available at <https://github.com/BhallaLab/PointGreyCamera>)
1951 had the following dependencies:
1952 • libopencv-dev, python-opencv
1953 • cmake, g++, gnu-make
1954 • libtiff-dev, python-tifffile, python-numpy
1955 • python-gnuplotlib, gnuplot-x11
1956
1957 An important requirement for our behaviour experiment design was to
1958 be able to train the animals systematically under reproducible
1959 conditions, with the aim to have stable behavioural training and animal
1960 performance. We used a blue LED as the Conditioned Stimulus (CS,
1961 50 ms flash) with an air-puff to the eye serving as the Unconditioned
1962 Stimulus (US, 50 ms pulse). We used an Arduino to orchestrate
1963 stimulus delivery and protocol design. All experiments were performed
1964 on head-fixed C57Bl6 mice, since we planned to use a stationary,
1965 custom-built two-microscope to image hippocampal CA1 activity during
1966 task acquisition and recall (Figure 14; Figure 15).

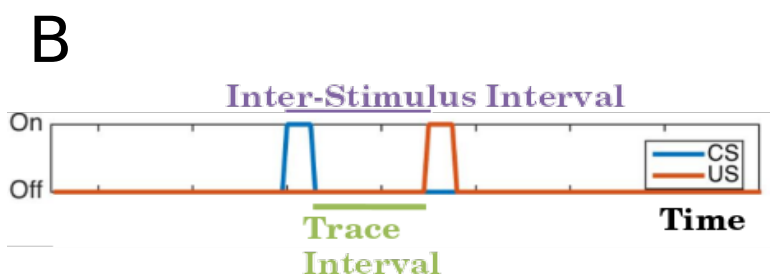
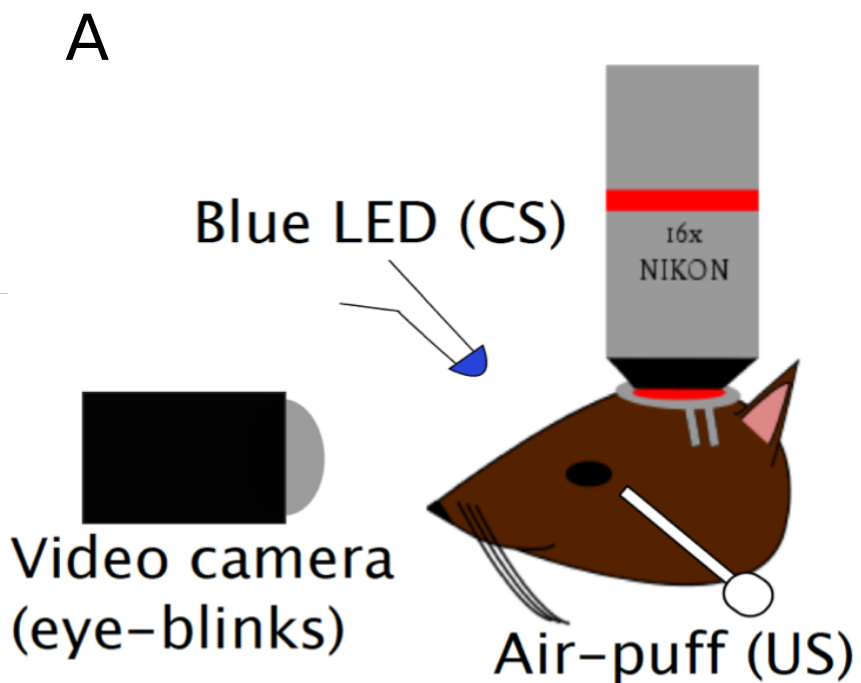


Figure 14: Schematic representation of (A) the behaviour rig with 2-Photon imaging, to train head-fixed mice on a Trace Eye-Blink Conditioning (TEC) task, and (B) relative time intervals between the CS and US.

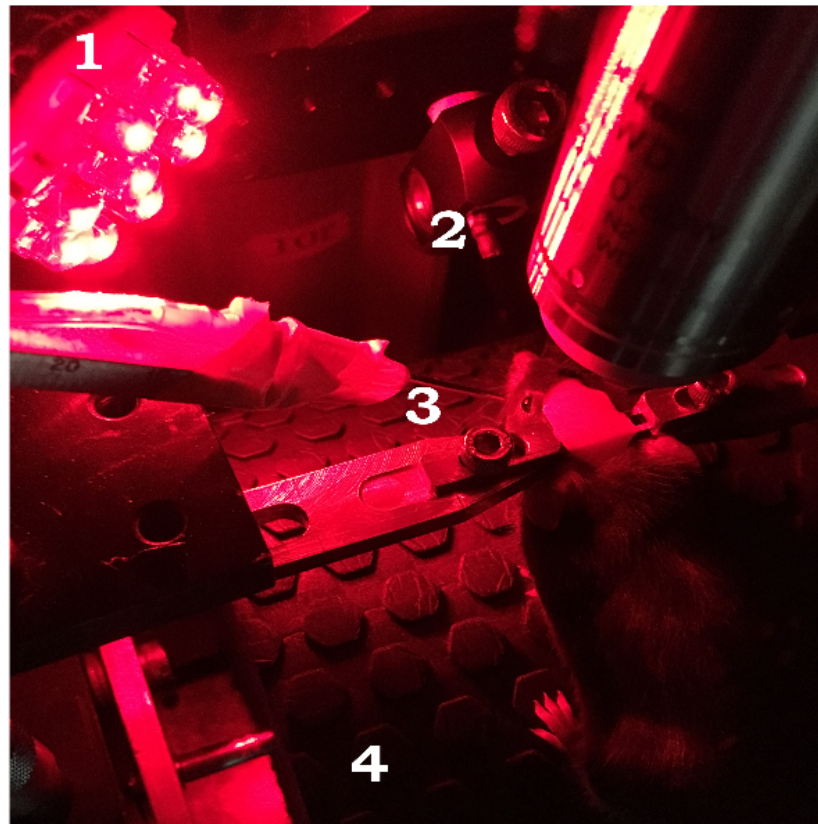


Figure 15: A picture of a head-fixed mouse clamped on the behaviour rig, with key components: 1) Red LED Illumination, 2) Blue LED CS, 3) Air-puff port directed to the left eye, and 4) Height-adjustable Treadmill

1968 Analysis - TEC

1969

1970 Once the .tif movies of the eye of the animal being trained were saved,
1971 they were analyzed by a custom script written in MATLAB, wherein for
1972 every frame we (Figure 16),

- 1973 1. Adjust contrast (optional)
- 1974 2. Apply a median filter (optional)
- 1975 3. Crop out the pixels defining the eye and surrounding
1976 (identical number of pixels for all trials and animals)

- 1977 4. Binarize the image of the eye to get black pixels defining the
 1978 visible (opened) portion of the eye
 1979 5. Count the relative proportion of open vs closed eye pixels in
 1980 the cropped image, and
 1981 6. Assign each frame with a Fraction of Eye Closure (FEC)
 1982 score.
 1983

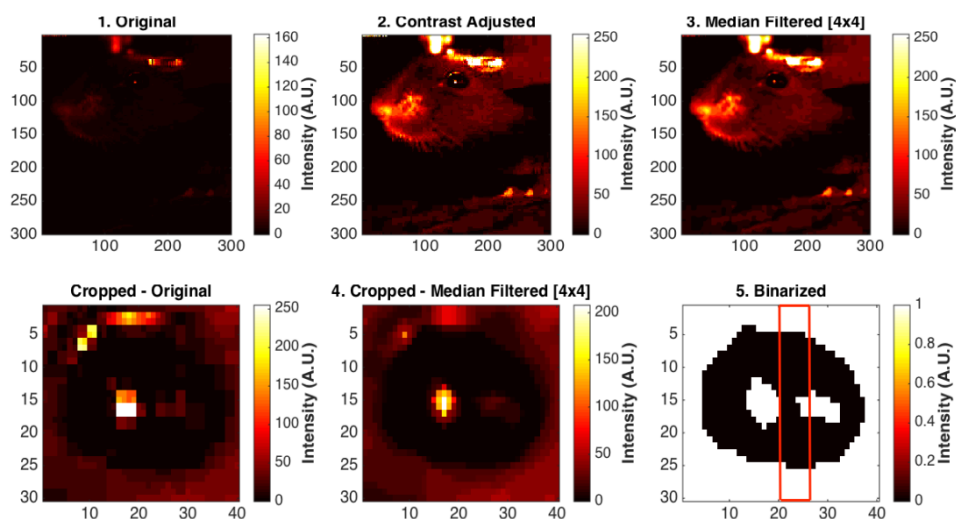


Figure 16: Steps from behaviour video frame to Fraction of Eye-Closed (FEC) analysis

1985 The FEC score then allowed us to analyse each trial's worth of frames
 1986 for eye-blanks. There are many features of the eye-blink that could be
 1987 used to gauge the overall performance of the animal in terms of both
 1988 the Conditioned Response (CR) as well as the Unconditioned
 1989 Response (UR), but for our experiments, we chose to use Eye-Blink
 1990 Amplitude (Siegel et al., 2015). Additionally, we studied whether the
 1991 animals could produce CRs in the absence of the US, by
 1992 pseudorandomly selecting 10% trials to skip the US (Probe Trials).
 1993

1994 Results - TEC

1995

- 1996 1. Animals showcase task acquisition by performing Conditioned
1997 Responses (CRs), observed as pre-emptive blinks timed to
1998 avoid the aversive US. The kinetics of the CR (timing,
1999 amplitude, etc.) are dependent on the amount of training, but
2000 are identical across paired and probe trials (Figure 17).

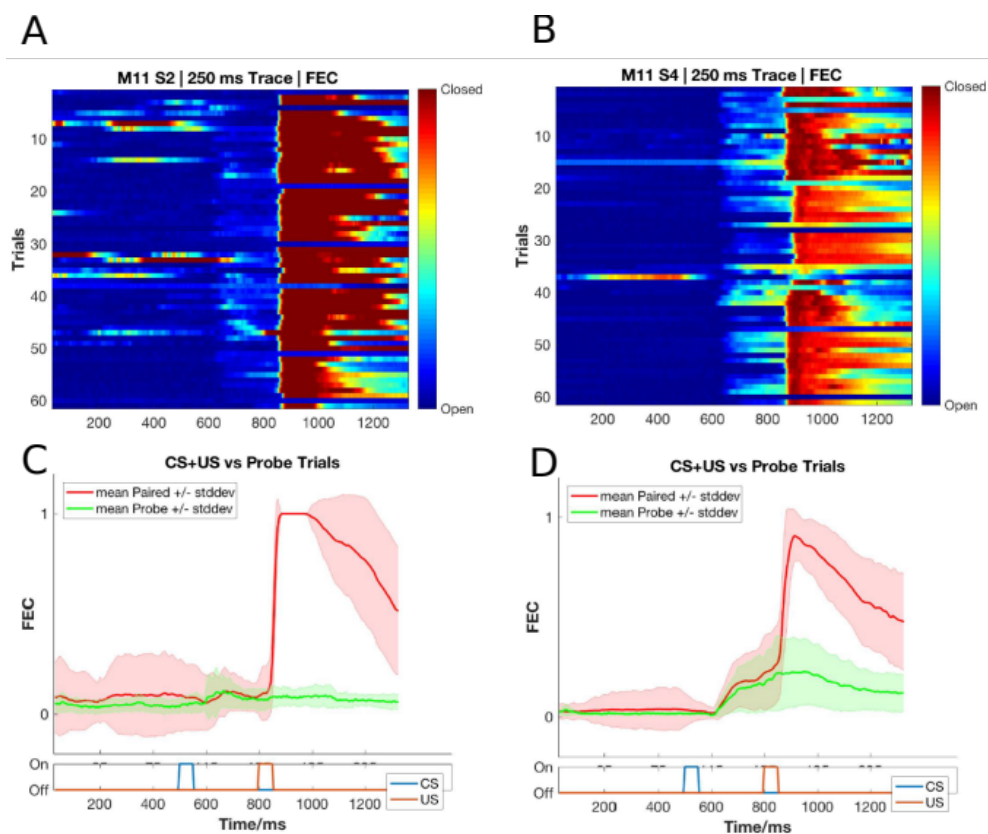


Figure 17: Conditioned Responses (CRs) are small amplitude eye-blanks triggered by the CS, and develop with multiple training sessions, while Unconditioned Responses are large eye-blanks to the US, typically consistent across sessions. (A,B) Trial-by-trial FEC traces for (A) M11 Session 2, and (B) Session 4. (C,D) Trial-averaged FEC traces for (C) Session 2 and (D) Session 4, with paired (red) and probe (green) trials.

- 2002 2. Most animals can pick up the task within 4-7 sessions (1 session/day, 60 trials/session), even if on water deprivation.
- 2003
- 2004 Animals can also be subsequently trained to different inter-stimulus intervals. Using the Conditioned Response (CR) amplitude, each trial can be binarized to whether a CR was elicited (Hit Trial) or not (Miss Trial), by thresholding at mean trial FEC + 2*Std. Dev.. Performance for the session is then estimated as the ratio of Hit Trials to Total Trials (Figure 18).
- 2005
- 2006
- 2007
- 2008
- 2009
- 2010

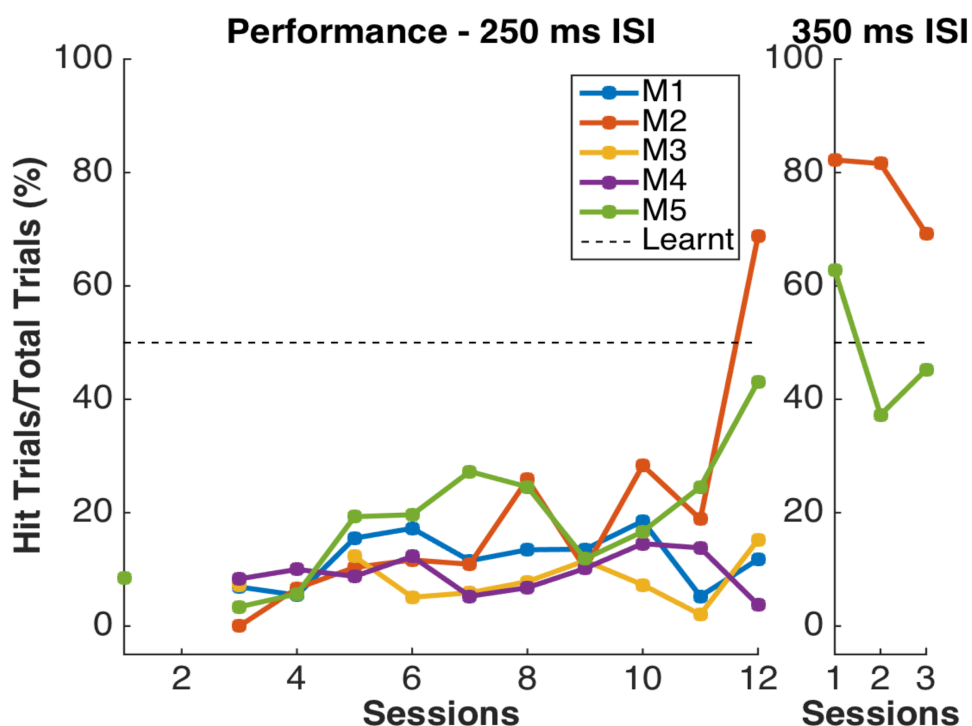


Figure 18: Performance in terms of the percentage of Hit Trials to total trials across sessions, including an ISI switch from 250 ms to 350 ms.

- 2012 3. Animals that learn multiple ISIs, especially when the second ISI is $\geq 2x$ the first ISI, showcase complex eye-blinks without extinction of the previously learnt CRs. Once an animal
- 2013
- 2014

2015 showcases the ability to produce Conditioned Responses (CRs)
 2016 to one inter-stimulus interval (ISI), this interval can be
 2017 elongated. In the example shown below we first trained the
 2018 animal to a 250 ms ISI, and then switched to a 500 ms ISI
 2019 (Figure 19).

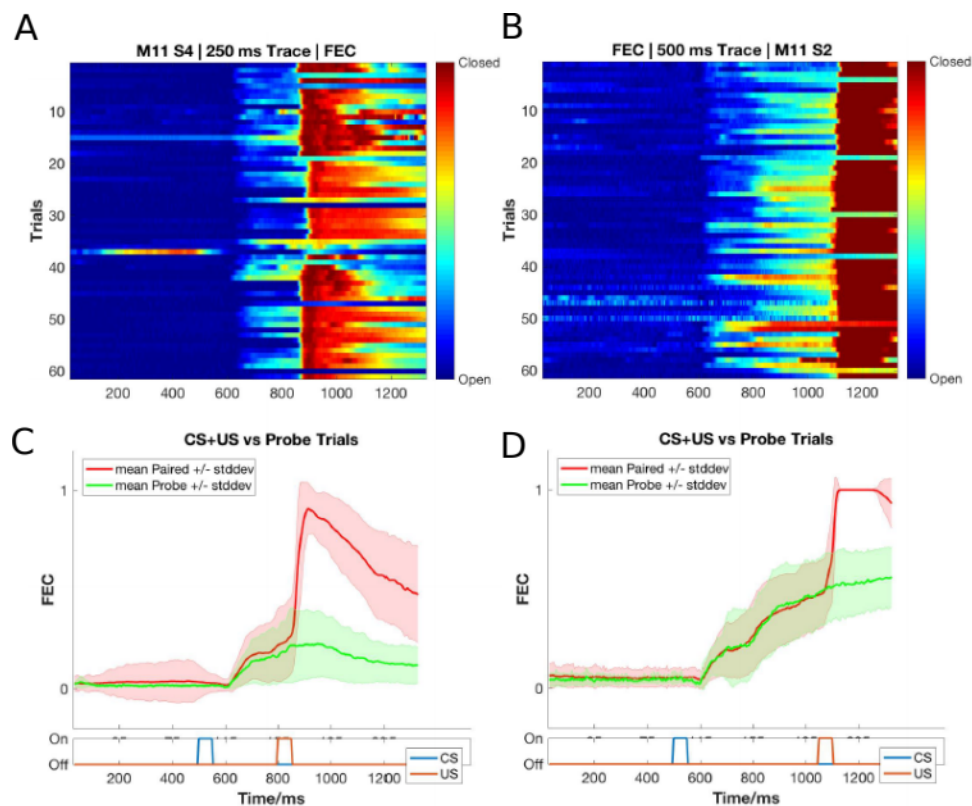


Figure 19: Conditioned Responses (CRs) are preserved for previously learnt ISIs, and switching the ISI to longer intervals results in Complex (multi-CR) eye-blink responses. (A,B) Trial-by-trial FEC scores for (A) 250 ms ISI (left) and (B) 500 ms ISI. (C,D) Trial-averaged FEC traces for (C) 250 ms ISI (left) and (D) 500 ms ISI (right), with paired (red) and probe (green) trials.

2021 4. The onset of the Conditioned Response (CR) is not affected by
 2022 the ISI switch, irrespective of how strongly the animals learn the

task. CRs during paired and probe trials were near identical, showcasing that the animal (Figure 20; Figure 21).

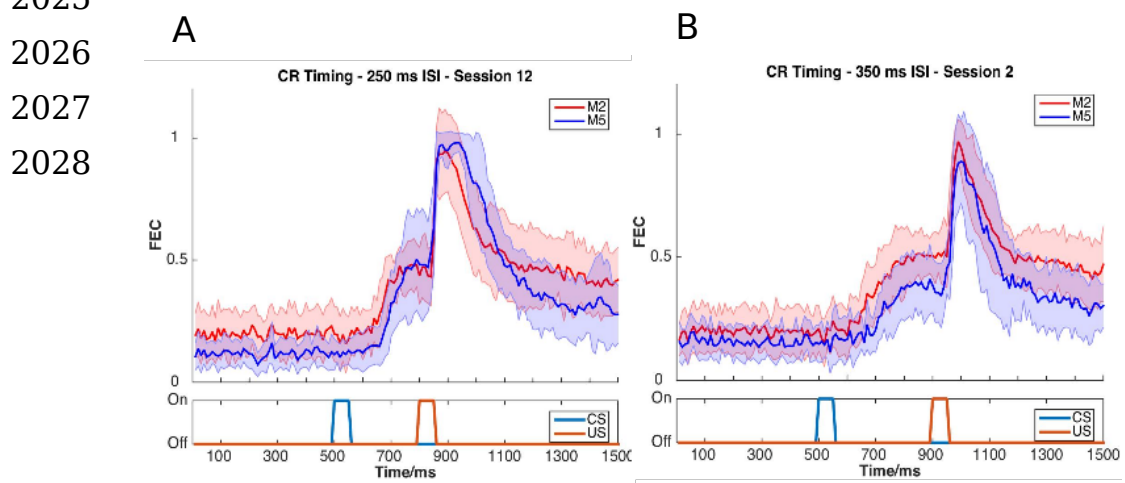


Figure 20: Conditioned Response (CR) onset timing is maintained across ISI switches. Representative examples from a short ISI switch from (A) 250 ms to (B) 350 ms (right).

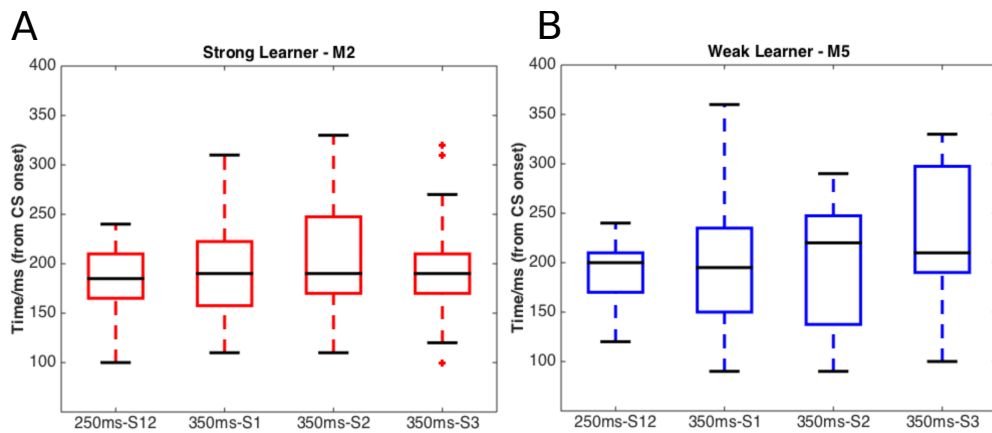


Figure 21: Box plots for Conditioned Response (CR) onset across multiple sessions of training after ISI switch from 250 ms to 350 ms, irrespective of how strongly the animals learnt the task. (A) red, strong learner, and (B) blue, weak learner.

2031 5. Animals can also be trained to very long ISIs from Session 1,
2032 with acquisition taking <10-14 days. Here we tried to train
2033 animals to either a 550 ms ISI or a 750 ms ISI. Note, however,
2034 that unless multiple ISIs are taught to the same animal, the CR
2035 eye-blink is singular (Figure 22).
2036

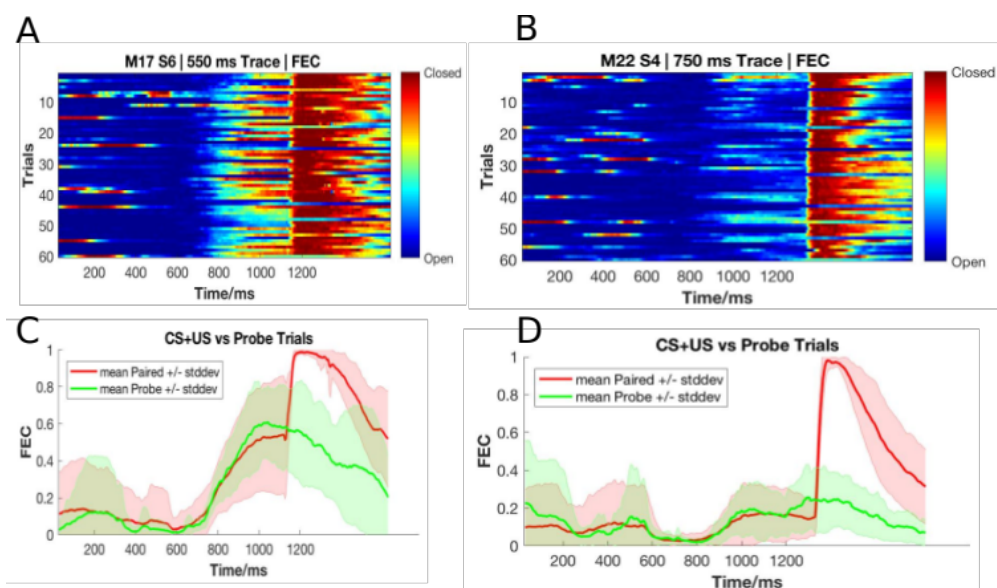


Figure 22: Representative example of mice trained to 550 ms ISI (Session 6) and 750 ms ISI (Session 4). (A,B), Trial-by-trial FEC responses for (A) 550ms ISI, and (B) 750ms ISI. (C,D) Trial-averaged FEC responses for (C) 550 ms ISI, and (D) 750 ms ISI, with paired (red) and probe trials (green).

2038 **Total animals trained:** 18 [Conditioned Responses visible]
2039 **Conclusion:** Success
2040
2041 Ultimately, we were satisfied with the Trace Eye-Blink Conditioning
2042 paradigm since we could observe stable conditioned responses that
2043 developed over a reasonably short period of training time (<1 week),
2044 and adaptable conditioned responses to behaviour parameter

2045 modulations, in head-fixed mice that could be subjected to
2046 simultaneous 2-Photon calcium imaging.

2047

Table 1: Summary table of behaviour protocols attempted and essential results

NAME	PUNISHMENT TYPE	REMARKS
Operant Protocol 1.1 (Stimulus Detection)	No water reward for incorrect licks.	Lack of water reward for incorrect licks not enough for behavioural discrimination at <1 week of training.
Operant Protocol 1.2 (Stimulus Detection)	Air-puff punishment for incorrect licks.	Strong punishment for incorrect licks not enough for behavioural discrimination at <1-2 weeks of training.
Operant Protocol 2 (Stimulus Detection)	Timeout (3s) punishment for incorrect licks.	Alternate or weaker punishment attempted but not enough for behavioural discrimination at <1-2 weeks of training, even with behavioural shaping in blocks of training.
Operant Protocol 3 (DNMS)	Timeout (3s) punishment for incorrect licks.	Alternate punishment attempted but not enough for behavioural discrimination at <1 week of training. No obvious effect of adding delay intervals between stimulus presentations.
Operant Protocol 4 (Go/No-Go) Aversive Protocol (Trace Eye-Blink Conditioning)	Trial phase repeat punishment for incorrect licks. No punishment.	Alternate punishment attempted but not enough for behavioural discrimination at <1 week of training Animals learn the task and produce stable, adaptable conditioned responses (CRs) within 1 week of training.

2048

2049 Bibliography

- 2050 Brown, G. D. (1998). Nonassociative learning processes affecting
2051 swimming probability in the seashell Tritonia diomedea:
2052 habituation, sensitization and inhibition. *Behavioural Brain
2053 Research*, 95(2), 151–165.
2054 [https://doi.org/https://doi.org/10.1016/S0166-4328\(98\)00072-2](https://doi.org/https://doi.org/10.1016/S0166-4328(98)00072-2)
- 2055 Deshmukh, S. S., & Bhalla, U. S. (2003). Representation of odor
2056 habituation and timing in the hippocampus. *The Journal of
2057 Neuroscience : The Official Journal of the Society for
2058 Neuroscience*, 23(5), 1903–1915.
2059 <https://doi.org/10.1523/JNEUROSCI.23-05-01903.2003>
- 2060 Fyhn, M., Molden, S., Witter, M. P., Moser, E. I., & Moser, M.-B.
2061 (2004). Spatial representation in the entorhinal cortex. *Science
2062 (New York, N.Y.)*, 305(5688), 1258–1264.
2063 <https://doi.org/10.1126/science.1099901>
- 2064 Guo, Z. V, Hires, S. A., Li, N., O'Connor, D. H., Komiyama, T., Ophir,
2065 E., Huber, D., Bonardi, C., Morandell, K., Gutnisky, D., Peron, S.,
2066 Xu, N., Cox, J., & Svoboda, K. (2014). Procedures for Behavioral
2067 Experiments in Head-Fixed Mice. *PLOS ONE*, 9(2), e88678.
2068 <https://doi.org/10.1371/journal.pone.0088678>
- 2069 Hafting, T., Fyhn, M., Molden, S., Moser, M.-B., & Moser, E. I. (2005).
2070 Microstructure of a spatial map in the entorhinal cortex. *Nature*,
2071 436(7052), 801–806. <https://doi.org/10.1038/nature03721>
- 2072 Hubel, D. H., & Wiesel, T. N. (1962). Receptive fields, binocular
2073 interaction and functional architecture in the cat's visual cortex.
2074 *The Journal of Physiology*, 160(1), 106–154.
2075 <https://doi.org/10.1113/jphysiol.1962.sp006837>
- 2076 Jaramillo, S., & Zador, A. M. (2014). Mice and rats achieve similar
2077 levels of performance in an adaptive decision-making task . In
2078 *Frontiers in Systems Neuroscience* (Vol. 8).
2079 <https://www.frontiersin.org/articles/10.3389/fnsys.2014.00173>
- 2080

- 2081 O'Keefe, J., & Dostrovsky, J. (1971). The hippocampus as a spatial
2082 map. Preliminary evidence from unit activity in the freely-moving
2083 rat. *Brain Research*, 34(1), 171–175. [https://doi.org/10.1016/0006-8993\(71\)90358-1](https://doi.org/10.1016/0006-8993(71)90358-1)
- 2085 Ranck, J. B. (1973). Studies on single neurons in dorsal hippocampal
2086 formation and septum in unrestrained rats: Part I. Behavioral
2087 correlates and firing repertoires. *Experimental Neurology*, 41(2),
2088 462–531. [https://doi.org/https://doi.org/10.1016/0014-4886\(73\)90290-2](https://doi.org/https://doi.org/10.1016/0014-4886(73)90290-2)
- 2090 Schreurs, B. G. (1989). Classical conditioning of model systems: A
2091 behavioral review. *Psychobiology*, 17(2), 145–155.
2092 <https://doi.org/10.3758/BF03337830>
- 2093 Siegel, J. J., Taylor, W., Gray, R., Kalmbach, B., Zemelman, B. V.,
2094 Desai, N. S., Johnston, D., & Chitwood, R. A. (2015). Trace
2095 Eyeblink Conditioning in Mice Is Dependent upon the Dorsal
2096 Medial Prefrontal Cortex, Cerebellum, and Amygdala: Behavioral
2097 Characterization and Functional Circuitry. *ENeuro*, 2(4),
2098 ENEURO.0051-14.2015. <https://doi.org/10.1523/ENEURO.0051-14.2015>
- 2100 Taube, J. S., Muller, R. U., & Ranck, J. B. J. (1990). Head-direction
2101 cells recorded from the postsubiculum in freely moving rats. I.
2102 Description and quantitative analysis. *The Journal of
2103 Neuroscience : The Official Journal of the Society for
2104 Neuroscience*, 10(2), 420–435.
2105 <https://doi.org/10.1523/JNEUROSCI.10-02-00420.1990>

2106 **Chapter 3 – Imaging**

2107

2108 The mammalian hippocampus is considered important in the formation
2109 of new memories about experienced events (episodic or
2110 autobiographical memory), general declarative memory (memories that
2111 can be explicitly verbalized), spatial memory and navigation, and
2112 associations between stimuli that are distinct in time, among other
2113 functions. To achieve this, the Hippocampus must integrate information
2114 from different areas of the cortex.

2115

2116 Much of the cortical information that enters the Hippocampus (at the
2117 Dentate Gyrus), comes through the Entorhinal Cortex, along the
2118 Perforant Path (Hjorth-Simonsen & Jeune, 1972). The Dentate Gyrus
2119 cell network then relays this information to the CA3 cell network
2120 through Mossy Fibers, which in turn relays the information to CA1
2121 cells, through the Schaffer Collateral Fibers. This is popularly known as
2122 the Trisynaptic Circuit or Pathway (Figure 1 from Chapter 1 -
2123 "Introduction") and there is scope and evidence for computation and
2124 information processing at every step (MacDonald et al., 2011;
2125 McHugh et al., 2007; Modi et al., 2014; Nakashiba et al., 2008; Suh et
2126 al., 2011). Finally, the CA1 cells have their outputs to other brain
2127 regions. It is important to note, however, that regions like the CA1 are
2128 known to have access to information directly from other brain regions,
2129 as well (P. Andersen et al., 2006).

2130

2131 Literature in the field suggests that naïve animals may have some
2132 sensory gating of "Neutral" stimuli at the level of the CA1 (Abe et al.,

2133 2014; Bellistri et al., 2013; Kamondi, 1998). The source of this
2134 inhibition (at least the step before the local interneurons) seems to be
2135 the Medial Septum, through Fimbria-Fornix (Abe et al., 2014). Also,
2136 behavioural relevance allows the CA1 to elicit depolarizations that can
2137 be mapped to brain external stimuli (Dombeck et al., 2010; Harvey et
2138 al., 2009; P. M. Itskov et al., 2011; MacDonald et al., 2011, 2013; Modi
2139 et al., 2014; Pastalkova et al., 2008).

2140

2141 The Hippocampus consists of ventral and dorsal portions both of which
2142 are of similar composition but are parts of different neural circuits
2143 (Moser & Moser, 1998). The dorsal hippocampus performs primarily
2144 cognitive functions and in memory function, while the ventral
2145 hippocampus modulates emotional and affective processes (Fanselow
2146 & Dong, 2010).

2147

2148 **Physiology in the hippocampus**

2149

2150 The Hippocampus is located deep in the medial temporal lobe of
2151 mammals and is defined by several sub-structures, including the
2152 Dentate Gyrus (one site for information input to the hippocampus) and
2153 the Hippocampus Proper constituted by the CA1, CA2, CA3 and CA4
2154 cellular levels.

2155

2156 Using extracellular tungsten microelectrodes in naïve unanesthetized
2157 rabbits serially exposed to multimodal stimuli (Vinogradova, 2001), it
2158 was reported that in the CA1,

2159 1. A major fraction the reactive neurons have unimodal responses
2160 (41-44%)
2161 2. Multimodal neurons are modality-unspecific but have
2162 differentiated responses to stimuli of different modalities and even to
2163 various stimuli within a single modality
2164 3. Many neurons respond by Phasic (evoked responses last for the
2165 duration and as long as the stimulus) and Specific (stimulus-specific
2166 pattern) responses
2167 4. Neurons with inhibitory responses are encountered less
2168 frequently than those with various types of excitatory
2169 5. Habituation (non-responsiveness to repeatedly presented stimuli) is
2170 present though not among all the responsive cells (71-75%) and is
2171 often gradual
2172
2173 Imaging based activity studies have the advantage of being able to
2174 capture many more cells (>100 from the same animal) during
2175 experiments (Dombeck et al., 2010; Pachitariu et al., 2017; Peron et
2176 al., 2015; Poort et al., 2015; Sofroniew et al., 2016) as compared to
2177 typical electrophysiological measurements. Imaging provides an
2178 unambiguous method to identify cells that are not active during a
2179 period of interest. Another advantage is that it provides anatomical
2180 confirmation to help track the same cell over multiple days of
2181 recording, without ambiguity, for longitudinal studies. Finally, imaging
2182 techniques have gained momentum in the study of the hippocampal
2183 CA1 various spatial scales, from cellular resolution somatic studies
2184 (Dombeck et al., 2010; Modi et al., 2014), to dendritic (Mizrahi, 2004;
2185 Sheffield & Dombeck, 2014), axonic boutons terminating on the CA1
2186 interneuron populations (Kaifosh et al., 2013; Lovett-Barron et al.,
2187 2014), as well as spines (Attardo et al., 2015), *in vivo*.

2188
2189 We designed our imaging studies (for this thesis), with the aim to
2190 understand the network and cellular mechanisms of the hippocampal
2191 CA1 that corresponded with behavioral learning induced changes. We
2192 started by looking for CA1 responses to neutral stimuli in naive
2193 animals, *in vivo*. Subsequently, we planned to subject these animals to
2194 behavioural training and study if and how the same cells would
2195 respond.

2196
2197 Depending on the intended duration of the imaging experiments, *viz.*, a
2198 few hours (single session) or a few days and weeks (multiple
2199 sessions), we were able to standardize both an Acute as well as a
2200 Chronic *in vivo* hippocampal preparation. We now discuss the *in vivo*
2201 hippocampal preparation, physiology recordings, and a brief summary
2202 of the results. An important perspective for our experiments was to
2203 study how sensory stimulus responses of hippocampal CA1 develop
2204 with associative learning.

2205

2206 **Methodology – Acute and chronic imaging** 2207 **[Projects I & II]**

2208
2209 The overall experiment deals with optically measuring the activity of
2210 the dorsal CA1 hippocampal neurons when different stimulus
2211 modalities are presented to a male C57BL/6 mouse. The thesis covers
2212 experiments conducted acutely (lasting <10 hours) using OGB-1 as a
2213 calcium sensor), as well as chronically (~7-21 days) using a genetically
2214 encoded calcium indicator, GCaMP6f).

2215

2216 The 2-Photon excitation wavelength for OGB-1 experiments was set to
2217 810 nm (scattering coefficient: $\sim 3 \text{ rad}^2/\text{mm}$) and the same for
2218 GCaMP6f was set to 910 nm (scattering coefficient: $\sim 2 \text{ rad}^2/\text{mm}$) to
2219 image cell bodies (Min et al., 2017) in the CA1, *in vivo*. However,
2220 despite the relatively low scattering of longer wavelengths, the
2221 hippocampus cannot be imaged directly, through the cortex since the
2222 layer of cortex is too thick ($\sim 1\text{-}1.5 \text{ mm}$) to allow proper excitation of the
2223 sample. These infra-red (IR) photons are expected to be scattered
2224 almost completely, well before the imaging depth of the CA1 cell body
2225 layer. These layers of cortex have to accordingly be carefully suctioned
2226 out to allow the microscope objective to have optical access to the
2227 exposed tissue (Figure 23).

2228

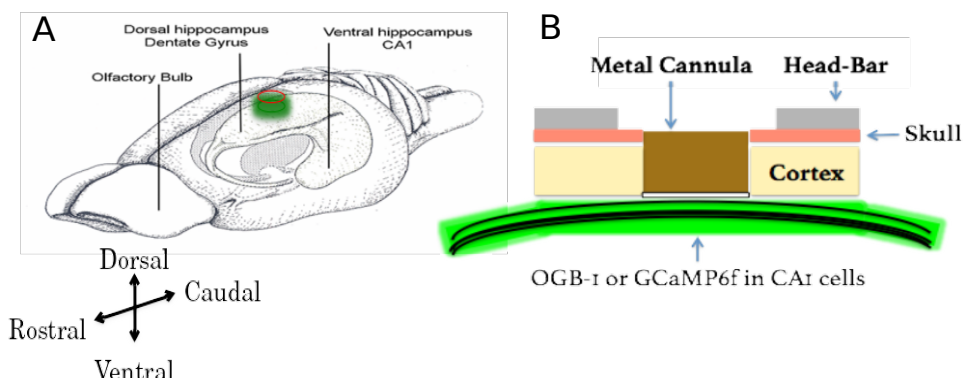


Figure 23: (A) A schematic of the rodent brain, showcasing the two hippocampi, one in each hemisphere. The hippocampi lie $\sim 1 \text{ mm}$ (mice) below the cortical surface. (B) The hippocampal preparation allows optical access to the deep lying hippocampal CA1 cells, relative to the skull/cortex. The CA1 cell bodies arrange in a laminar fashion, as a tight cell body layer that can be visualized by fluorescence (using either OGB-1 or GCaMP).

2230 We first put the animal under anesthesia using a vapor chamber
2231 saturated with 3% isoflurane. Next, the animal was cheek-clamped and
2232 a light state of anesthesia was maintained using 1-2% isoflurane,
2233 provided directly to the nozzle of the animal, keeping track of ~1 Hz
2234 breathing rate and a body temperature of 35-37 °C (with heating pad).
2235 The animal was given a haircut and a circular incision of ~5 cm
2236 circumference was made on the scalp, revealing the skull below. We
2237 then affixed head-bars and skull screws with the help of dental cement,
2238 to be able to clamp the animal post surgery on the 2-Photon
2239 Microscope.

2240

2241 The left, dorsal hippocampus was targeted with a 3-5 mm circular
2242 craniotomy aimed at 1.5 mm left and 2.0 mm behind bregma, tearing
2243 and peeling out the Dura to reveal the cortex. We then carefully
2244 aspirated out the cortex (part of the somatosensory cortex) under
2245 repeated washes of Cortex Buffer (see table 1 for recipe), until the
2246 horizontal CC fibre layer was visible. Finally, we added a drop of low
2247 gelling agarose and a 5 mm coverslip (for acute preps); Kwik-Sil and
2248 inserted a 3 mm metal cannula with a coverslip attached at the bottom
2249 (for chronic preps). We used different sensors depending on the
2250 requirement for the preparation, *viz.*, acute (OGB-1) or chronic imaging
2251 (GCaMP6f). We refer to this series of steps as the hippocampal
2252 preparation.

2253 **Preparation of Cortex Buffer**

2254

2255 We prepared cortex buffer by weighing out the required amount of the
2256 salts, NaCl, KCl, Glucose and HEPES (see table 2 for recipe) and

2257 making up the volume of the solution with Milli Q Water to ~1000 ml.
2258 We then set the pH of the buffer with the help of a calibrated pH meter
2259 to 7.35, using 1M NaOH_(aq).
2260 Lastly, the contents were filtered through a 0.22 um membrane using a
2261 vacuum filtration, and stored at 6 °C.
2262

Table 2: Recipe for ready-to-use cortex buffer. The buffer is typically prepared and stored in aliquots to be used each week. The correct pH range of the buffer was often a crucial factor ensuring the success of the hippocampal preparation.

Ingredient	Concentration (mM)	Amount (g/L or ml/L)
NaCl (s)	125	7.31 g
KCl (s)	5	0.373 g
Glucose (s)	10	1.8 g
HEPES (s)	10	2.38 g
CaCl ₂ (aq)	2	1.6 ml of 1.25 M stock solution
MgCl ₂ (aq)	2	1.5 ml of 1.3 M stock solution0

2263 **Oregon Green Bapta-1 injections for acute**
2264 **imaging**

2265

2266 To prepare Oregon Green Bapta-1 (OGB-1) dye for microinjections, we
2267 first dissolved a 50 µg tube of OGB-1 in 5 µl of Pluronic Acid, and
2268 vortex the mix for 5 minutes. Separately, we diluted 20 µl of Phenol
2269 Red into 500 µl of cortex buffer, and transferred 45 µl of this solution to
2270 the OGB-1 mix. Next, we sonicated the 50 µl solution for 20 mins.,
2271 followed by centrifugation at 10000 RPM for 5 seconds. The remaining
2272 supernatant was split into 7 aliquots (7 µl), and stored at -20 C for a
2273 maximum of one week (7 days).

2274

2275 For acute/single-day experiments, we injected OGB-1 using pulled,
2276 dye loaded micropipettes (~2 MΩ resistance, ~2 µm diameter) at a
2277 depth of 100-150 µm (Figure 23) from the topmost layer of exposed
2278 tissue, till a slow but detectable pulse of dye (visualized as a red/pink
2279 solution) was visible just below the tissue surface. This allowed the dye
2280 to be soaked up by the basal dendrites of the CA1 and takes 30-60
2281 mins for incorporation into the cytoplasm. We typically allowed the
2282 animal 1-2 hours of respite before the subsequent imaging session.
2283 High pressure ejection of the dye into the tissue may damage the
2284 neuropil, while very low pressures or clogs in the pipette affected the
2285 spread of the dye across the tissue. We aimed to image ~100 x 100
2286 µm² of the tissue in any particular ROI, and achieved this with 5 minute
2287 injections for each micropipette aiming to load the dye at 2-3, well
2288 separated positions spread across the entire exposed dorsal surface.
2289 We estimated that the dye volume was <1000 nl/injection. After the

2290 injection cycle with any micropipette, we left the tissue undisturbed for
2291 at least 5-10 mins before pulling the micropipette out of the tissue.

2292

2293 Once all the injections were complete, the exposure was sealed using
2294 5% low gelling agarose making sure the temperature was cool enough
2295 to avoid heat-related tissue damage.

2296

2297 OGB-1 is eventually cleared from the cytoplasm but allows for a limited
2298 window for imaging studies (Stosiek et al., 2003). Reopening the
2299 agarose seal and re-injections were never attempted to prevent
2300 unnecessary damage to the underlying tissue. Additionally, the
2301 agarose plug itself was found to be unstable beyond 1-3 days. This
2302 resulted in the imaging possibility being limited to the same day as the
2303 surgery (acute imaging).

2304

2305 **GCaMP and chronic imaging**

2306

2307 For chronic/multi-day experiments, we standardized a stereotaxic viral
2308 injection step, where we inject the gene for GCaMP5 or GCaMP6f into
2309 the dorsal hippocampus at -1.5 mm lateral, 2 mm posterior, and 1.3
2310 mm dorsal from bregma on the skull surface (Figure 24).

2311

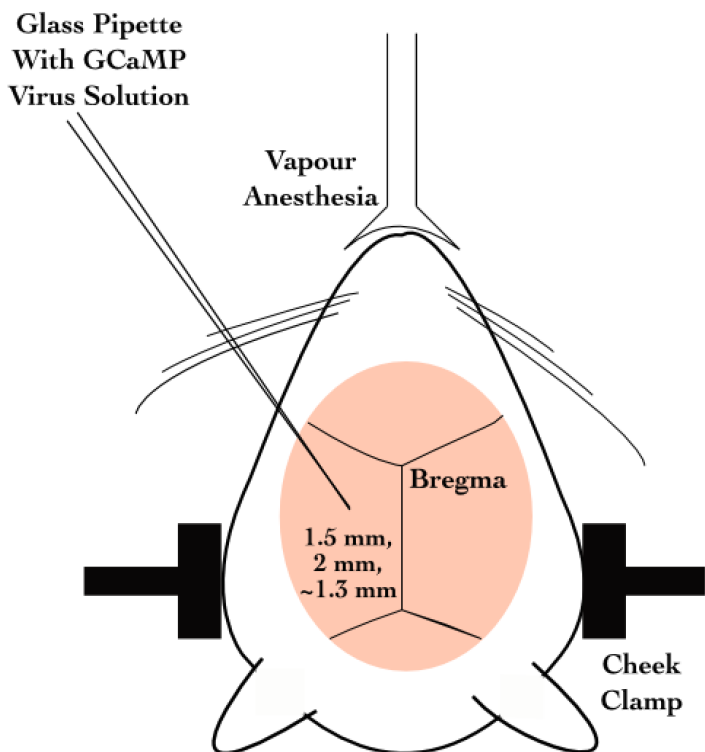


Figure 24: Schematic representation for

2312 stereotaxic viral injection.

2313

2314 Later on, we switched to directly using GCaMP6f transgenic mice

2315 (background: C56BL/6) that express GCaMP6f in the Hippocampus

2316 [Tg(Thy1-

2317 GCaMP6f)GP5.17Dkim JAX stock #025393]. This helped us

2318 circumvent the dye loading or viral injection steps, aiding in the

2319 potential success of the preparations, by way of tissue health and

2320 recording quality. A thin layer of Kwik-Sil instead of agarose, helped

2321 keep the imaging window optically transparent for imaging.

2322

2323 **Results - Imaging**

2324

2325 **2-Photon calcium imaging of hippocampal CA1, *in vivo***

2326

2327 The CA1 cell body layer is ~200 µm deep, in through the hippocampal
2328 surface. At these depths, scattering of excitation as well as emission
2329 light is significant. However, we are able to image at these depths with
2330 Two-Photon Imaging LASER Scanning Imaging (810 nm for OGB-1
2331 and 910 nm for GCaMP5/GCaMP6f), where a high intensity pulsed
2332 LASER allows for two photons to near instantaneously excite
2333 fluorophores in a thin z-slice plane which is the focal plane of the
2334 Objective. Our LASER, the Coherent Chameleon Ultra II emits ~3 W at
2335 810 nm, and ~2 W at 910 nm. At these depths, there was scattering of
2336 emitted photons. However, since only the focal plane was excited any
2337 and all emitted photons that we captured were considered part of the
2338 signal. We used a Nikon 16x water immersion, 0.8 NA, 3 mm working
2339 distance Objective (N16XLWD-PF), to get a large field of view.

2340

2341 **Acute Imaging of OGB-1 loaded hippocampal CA1, *in*
2342 *vivo***

2343

2344 We injected OGB-1 dye into brain tissue for our acute imaging
2345 experiments (see Methodology for details). OGB-1 spreads throughout
2346 the cytoplasm and neuropil, and infiltrates the cell nucleus, giving the
2347 cells the appearance of solid circles (cells). The cell body (soma)

2348 ranges from 10-15 μm depending on the orientation of the imaging
2349 layer in 3D tissue space (Figure 25A).

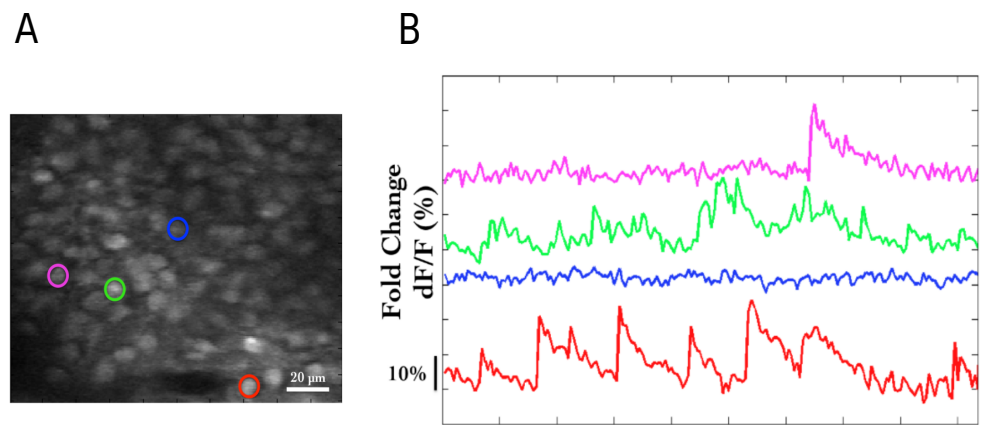


Figure 25: (A) Representative Two-Photon Calcium Image of a plane of Hippocampal CA1 cells, bolus loaded with Oregon Green Bapta-1 (OGB-1), at an instant in time. Example cells marked out post-hoc as pink, green, blue and red. Scale bar 20 μm . (B) Representative dF/F (%) traces for the calcium activity recorded in a single 10s video for example cells pink, green, blue, and red. Scale bar (1 sec; 10% dF/F).

2350 Each cell in the recorded region of interest (ROI), was identified and
2351 marked out (in pixel identity), based on local activity of correlated
2352 pixels in the time series movies. The average intensity of the pixels
2353 corresponding to each cell for each frame in each recording video, was
2354 saved as the raw calcium fluorescence trace. Next, these raw calcium
2355 traces were baseline normalized to equate the baselines for each cell
2356 at 0, and describe the dynamic range of the intensity values as 0 to 1,
2357 or 1 to 100%. The corresponding time series of baseline normalized
2358 dF/F for the representative example cells are shown (Figure 25B;
2359 Figure 28B).
2360

2361 **Chronic imaging of hippocampal CA1 using GCaMP**

2362

2363 For chronic imaging, tissue health was of paramount concern since it
2364 could easily degrade in time (Figure 26). With practice and
2365 standardization, we were able to get the preparations to survive for 2-4
2366 weeks at very good signal-to-noise. Preparations that resulted in very
2367 poor signal-to-noise were often recorded but these datasets have not
2368 been showcased in this thesis. While preparations can sometimes last
2369 even months, typically it is crucial to consider if the ROI for recording
2370 could provide >20 cells, to continue the experiment.

2371 GCaMP is designed to be cytosolic and does not typically cross into
2372 the cell nucleus. GCaMP labeled cell bodies appear as doughnuts in
2373 the imaging slice (Figure 26A; Figure 27).

2374

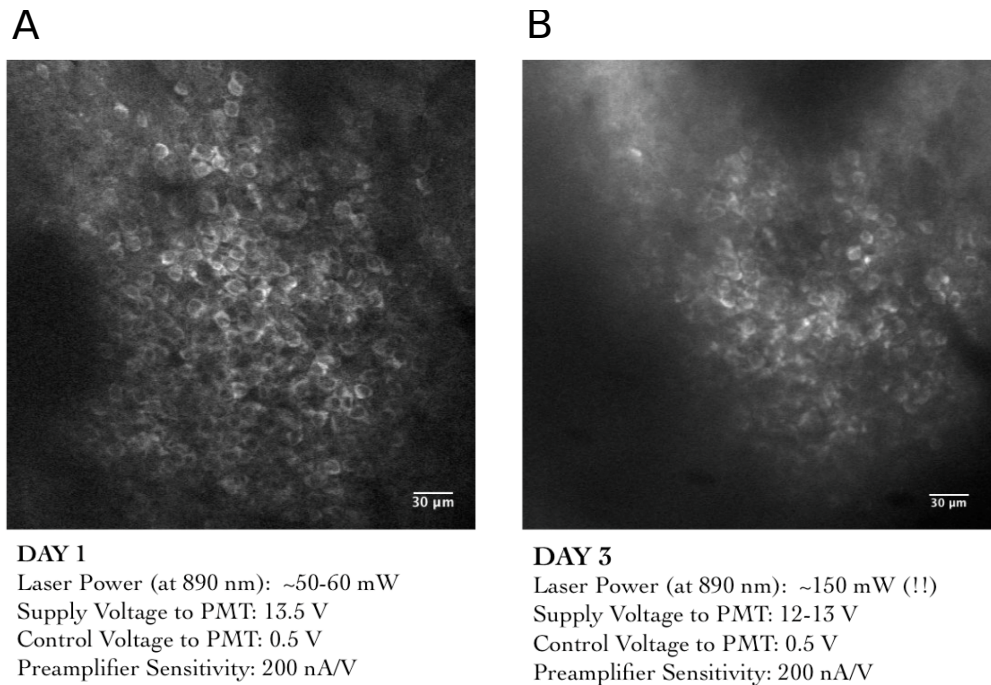


Figure 26: Tissue Degradation over time. Representative Two-Photon Calcium images of a snapshot in time of the Hippocampal CA1 cell body layer on (A) Day 1 after the surgery and (B) Day 3, after the surgery. Scale bar 30 μ m.

2376 Recordings with very good signal-to-noise, where the same chronically
 2377 labeled CA1 cells could be anatomically identified on subsequent days
 2378 even >2-3 weeks post surgery (Figure 27) were eventually acquired,
 2379 and are featured in the data presented in Chapter 4.
 2380

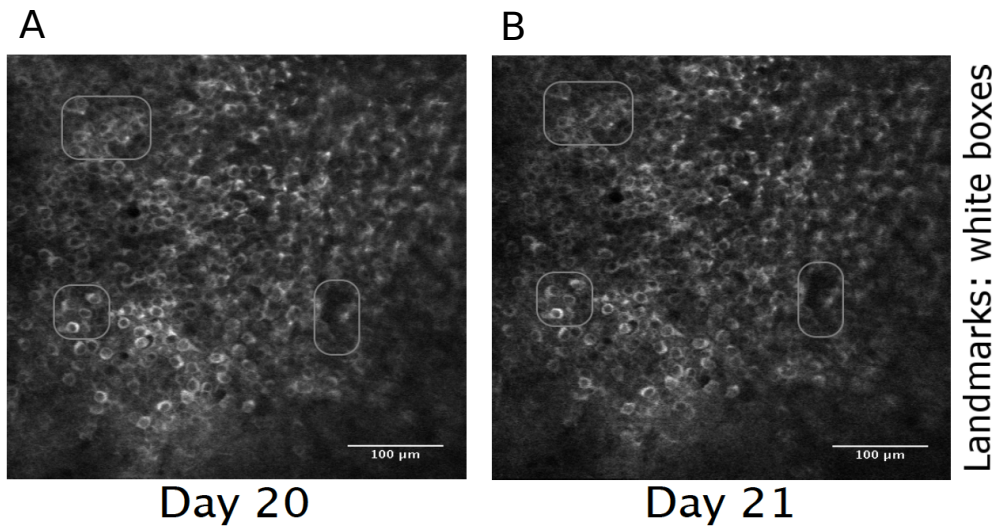


Figure 27: Chronic calcium imaging of the same Hippocampal CA1 cells over weeks. Representative 2-Photon images from (A) Day 20, and (B) Day 21, after surgery. Landmarks have been marked and were used to confirm frame registration and identify cells. Scale bar 100 μm .

2382 The magnification and resolution of the field of view are important
 2383 parameters to consider when balancing magnification for the resolution
 2384 and the maximization of the number of cells being simultaneously
 2385 recorded from (Figure 25A; Figure 28A).
 2386
 2387 While recording at high frame rates for live imaging, we captured a
 2388 relatively large number of cells (~100) in time-series imaging frames, at
 2389 frame rates of around 10-15 frames per second (FPS). Subsequently,
 2390 we subjected the animal to various stimuli across trials and saved
 2391 these images for analysis.
 2392

2393

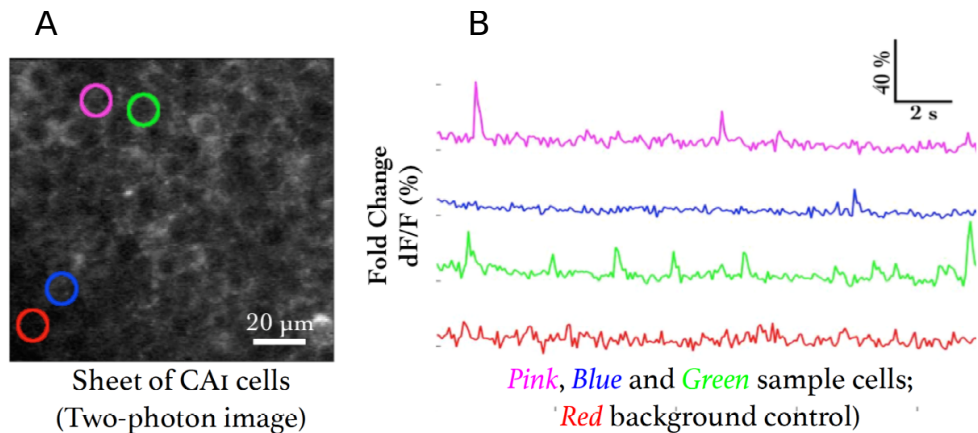


Figure 28: (A) Representative Two-Photon Calcium Image of a plane of Hippocampal CA1 cells expressing GCaMP6f at an instant in time. Example cells marked out post-hoc in pink, blue, and green, with no-cell background in red. Scale bar 20 μ m. (B) Representative $dF/F (\%)$ traces for the calcium activity recorded in a single 10s video for example cells in pink, blue, and green, with no-cell background in red. Scale bar (2 sec; 10% dF/F).

2395 Spontaneous activity during non-stimulus periods

2396

2397 We recorded the calcium activity from a large number of hippocampal
 2398 CA1 cell bodies, while presenting various neutral and conditioning
 2399 stimuli, including fairly large periods of time before and after stimulus
 2400 presentation. Activity of cells, typically observed *in vivo*, in these
 2401 periods is termed spontaneous activity. Cells may showcase variable
 2402 rate (number of calcium events per sec) and timing. Given proper
 2403 signal isolation for identified cells in an ROI, each source or “cell” may
 2404 be considered independent, *i.e.* - there is minimized cross talk between
 2405 the fluorescence emitted by each cell body.

2406

2407 **Spatial organization of activity correlated cells during**
2408 **spontaneous activity**

2409

2410 As part of our Acute Imaging experiments using OGB-1, we studied the
2411 Pearson's Correlation Coefficient for the activity traces across all cell
2412 pairs, during bouts of spontaneous activity, viz., all frames from the
2413 beginning of the trial till the presentation of the stimulus, across all
2414 trials. Cell pairs showcased a range of correlation coefficients (Figure
2415 29) and we were able to cluster cells based on activity using Meta-K
2416 Means (Modi et al., 2014; unpublished data from Dhawale, 2013).

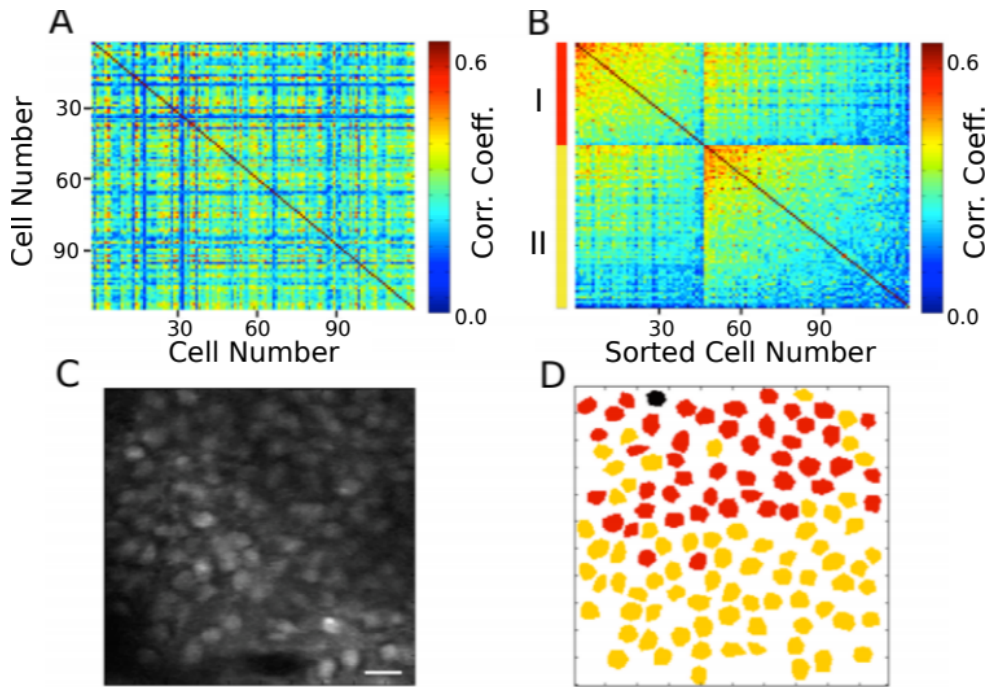


Figure 29: (A) Correlation Coefficients for cell pairs from an example two-photon recording. (B) Meta-K Means clustering with cell pairs using the heuristic that within group pairs would be more similar than between group pairs. In this example, the cells were clustered into two groups, I (red) and II (yellow). (C) Two-Photon image of the field of view of cells; same as Figure 25A. (D) Spatial organization of correlated cell pair groups during spontaneous activity (Modi et al., 2014).

2418 Stimulus evoked responses

2419

2420 We also recorded calcium activity from the same cells during
 2421 presentation of various neutral stimuli to the animals. Here are the
 2422 results of the auditory (tone) and somatosensory (whisker) stimulus
 2423 experiments.

2424

2425 A neutral auditory tone at 5000 Hz (for 1 sec) was presented to the
 2426 animals N= 6 animals; 25 trials). We observed no clear signs of cell
 2427 activity modulation by neutral tones. Below, we show an example
 2428 animal with trial-averaged calcium traces as dF/F (%), across all
 2429 recorded cells with a 1 sec tone presentation (Figure 30A). We also
 2430 presented animals to whisker stimulation by playing a 1s long air-puff
 2431 (5 LPM) to the ipsilateral (left) whisker (N = 5 animals; 25 trials). In this
 2432 case, we observed whisker-stimulation based cell activity modulation.
 2433 Below, we show the trial-averaged calcium traces as dF/F (%) of the
 2434 same example animal as above, presented with a 1 sec whisker-puff
 2435 (Figure 30B).

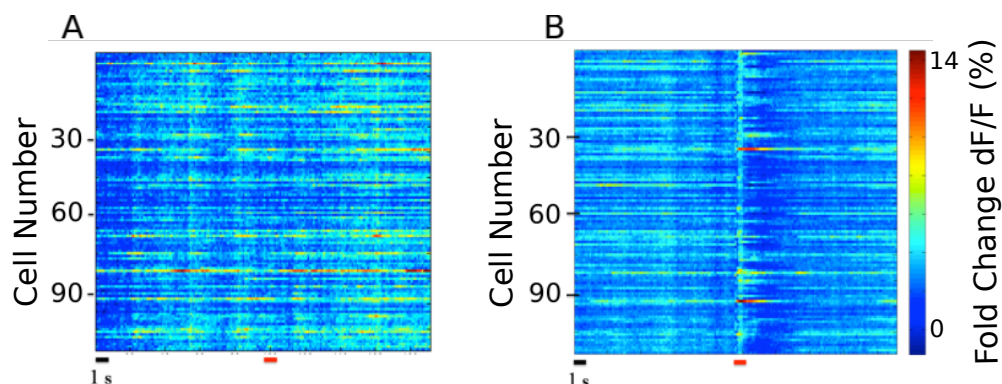


Figure 30: (A) Trial-averaged (25 trials) calcium activity from ~100 CA1 cells in trials where a 5000 Hz tone was presented (red bar). (B) Trial-averaged (18 trials) calcium activity from the same cells in trials where a 5 LPM air-puff to the ipsilateral whiskers was presented (red bar).

2437 **Spatial organization of activity correlated cells post whisker-puff**
 2438 **stimulation**
 2439
 2440 We attempted the same clustering analysis using Meta-K-Means on
 2441 the activity profiles of all the cells post presentation of the whisker-puff

2442 till the end of the trial, across all trials. These functionally correlated
2443 cell pair groups were found distributed across the imaging plane with
2444 no clear sign of spatial clustering (Figure 31).
2445 Comparing Figure 29D and Figure 31C, we observed that the whisker-
2446 puff stimulation results in a change in the spatial map of correlated
2447 activity, in the same network of cells.

2448

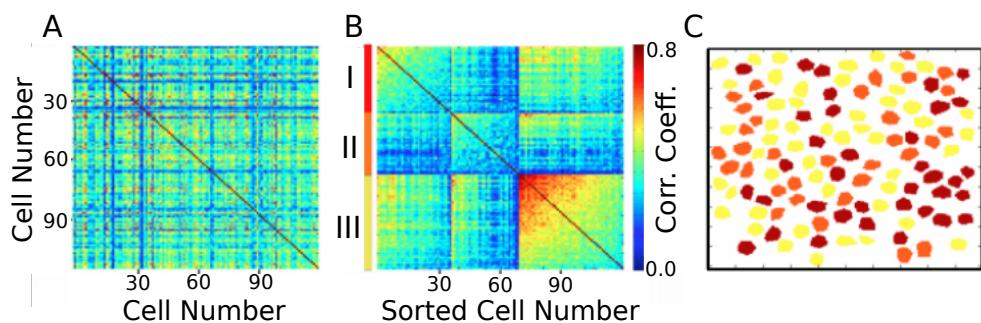


Figure 31: (A) Correlation Coefficients for cell pairs from post whisker-puff stimulation periods. (B) Meta-K Means clustering with cell pairs using the heuristic that within group pairs would be more similar than between group pairs. In this example, the cells were clustered into three groups I (red), II (orange), and III (yellow). (D) No clear spatial organization of correlated cell pair groups post whisker stimulation

2450 As a control, we shuffled the trial time points for each cell
2451 pseudorandomly, to artificially break activity correlations. No functional
2452 clusters were identified using the same Meta-K-Means clustering on
2453 this surrogate dataset (Figure 32). This suggested that the cell pair
2454 groups under other conditions (Figure 29; Figure 31) were not artifacts
2455 of the algorithm or implementation.

2456

2457

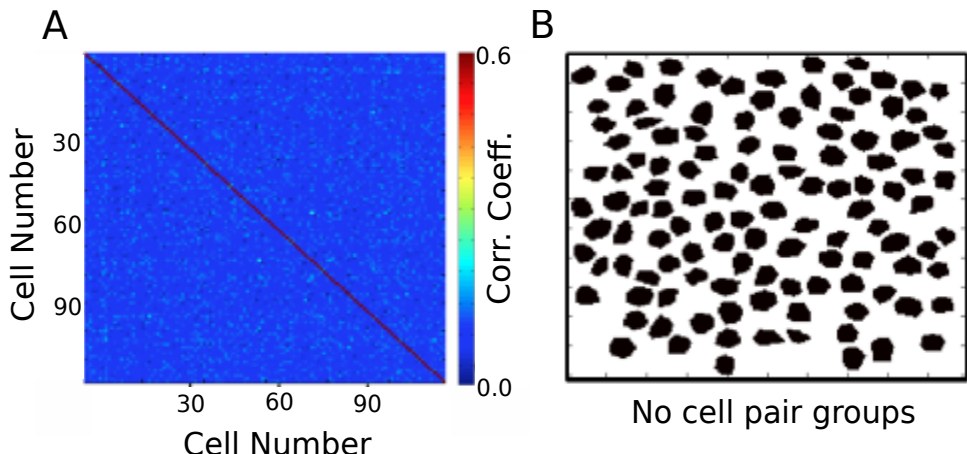


Figure 32: (A) Correlation Coefficients for cell pairs from a trial-shuffle control dataset (B) Meta-K Means clustering revealed that there were no cell pair groups identified.

2459 **Chronic imaging now possible for weeks with the same**
 2460 **mouse**
 2461
 2462 The need for multi-day tracking was mandated for recordings through
 2463 behavioural training, since the animals typically only learn Trace Eye-
 2464 Blink Conditioning (TEC; Chapter 2) over the course of 3-7 days
 2465 (Siegel et al., 2015). A different experiment design would have been to
 2466 train animals and then perform the hippocampal preparation to record
 2467 CA1 neural activity while the animal(s) exhibit learnt Conditioned
 2468 Responses (CRs). However, we argued against this experimental
 2469 design, on account of the following.
 2470 1. The actual cellular and network mechanisms that allow for the
 2471 animal to learn the behavioural task would be very difficult to study
 2472 given that the learning period would have passed.

2473 2. The success rate of the hippocampal preparation is typically very
2474 low (estimated at ~33-50% based on the last 200 attempts), given
2475 potential sources of failures such as tissue decay, bleeding into the
2476 imaging window from damaged parts of the hippocampus, implant
2477 instability especially with stressed or unsettled experiment animals,
2478 and photobleaching from the 2-P excitation LASER over multiple
2479 imaging sessions. TEC is typically learnt by >50% animals (Modi et al.,
2480 2014; Siegel et al., 2015). We had argued for exposing the
2481 hippocampus for imaging before behavioural training since any
2482 successful preparations could then be subjected to the relatively more
2483 consistent behavioural training.

2484 3. Having the preparation performed before training minimizes the
2485 number of times the animal would be subjected to surgery (to just the
2486 once), improving chances of animal health through the experiment.

2487

2488 Next, we discuss some preliminary results from the chronic imaging
2489 datasets. A non-overlapping set of results that feature in “Chapter 4 -
2490 Analysis” of this thesis, have been skipped here for brevity.

2491

2492 **Preliminary analysis to identify time cells**

2493

2494 The analysis algorithm pertaining only to the results presented here in
2495 “Chapter 3 - Imaging”, was adapted from William Mau’s Temporal
2496 Information method (Mau et al., 2018; Chapter 4 - “Analysis”). This
2497 version of the algorithm is expected to be subject to some degree of
2498 Type I (false positives) and Type II (false negative) errors.
2499 Subsequently, the algorithm was developed to the extent of the

2500 Python/C++ implementation featured in “Chapter 4 – Analysis”, with
2501 much superior prediction performance.
2502

2503 1. We applied a filter to select for cells that had activity in >25% of
2504 trials (irrespective of tuning)

2505 2. We then develop Peri-stimulus Time Histograms (PSTH), using
2506 Area Under the Curve for a binsize of 3 frames, centering the “0
2507 ms” to the onset of the Conditioned Stimulus for visualization.

2508 3. Next, we estimate Temporal Information (TI), using

2509
$$TI = 1/\lambda * \sum_j \lambda_j \log_2 (\lambda_j / \lambda) P_j$$

2510 where,

2511 λ : Average Transient rate for each cell

2512 λ_j : Average transient rate for each cell in bin “j”

2513 P_j : Probability that the mouse was in time bin “j”

2514 For every trial, we also random shuffled the frame points to develop a
2515 random activity model (1000 times) and ensure that $\lambda > \lambda_{rand}$ in more
2516 than 99% of the models. Filtering for cells active in >25% trials with a λ
2517 $> \lambda_{rand}$ in >99% shuffles along with the estimation of TI, provided us a
2518 handle on reliability.

2519

2520 **Time Cells**

2521

2522 During the experience of temporally organized events or stimuli, in this
2523 case post training to Trace Eye-Blink Conditioning, a rough contingent
2524 of ~20% of the total cells recorded, were observed to showcase time-
2525 locked calcium activity mapping the Blue LED or Conditioned Stimulus
2526 (CS) to the air-puff or Unconditioned Stimulus (US). These cells were
2527 classified as time cells. Here are some example time cells (Figure 33).

2528

2529

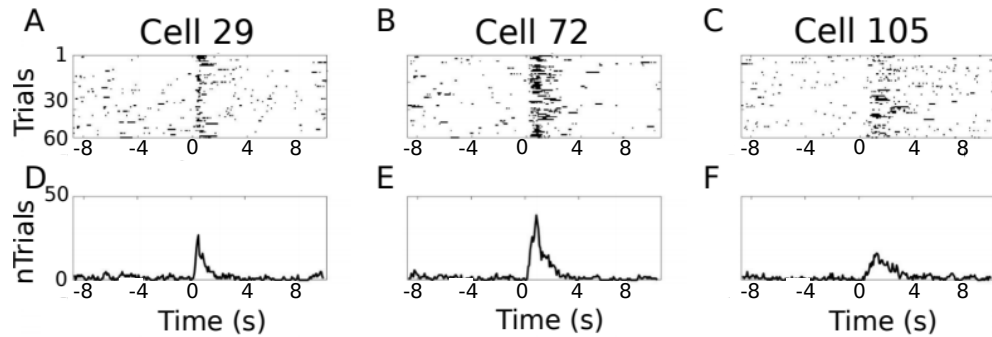


Figure 33: Example Time Cells visualized as event raster plots (A, B, C), along with the trial-summed activity profiles (D, E, F) suggesting ~50% hit trials, for cells 29 and 72 from Session 1 (session type 5) with mouse M26, and slightly lower reliability (~25% hit trials) from cell 105.

2530 **Other Cells**

2531

2532 On the other hand, most cells did not clear our analysis algorithm
2533 checkpoints and were classified as other cells. Here are some example
2534 Other Cells (Figure 34) from the same session with mouse M26
2535 (Session 1; session type 5).

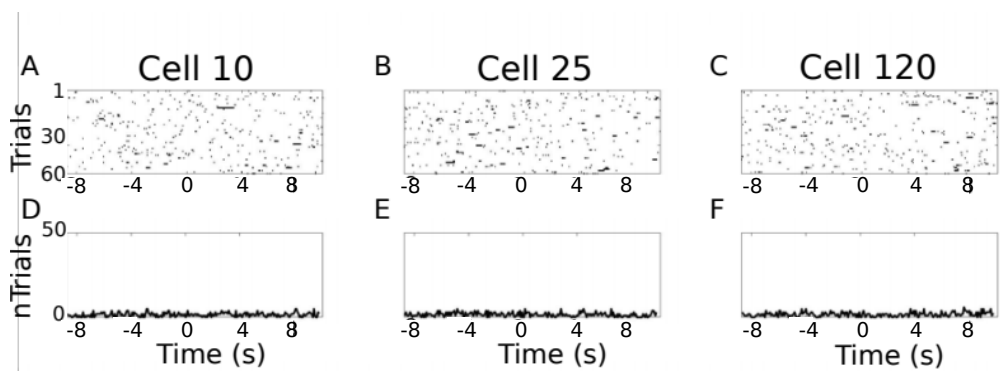


Figure 34: Example Other Cells visualized as event raster plots (A, B, C), along with the trial-summed activity profiles (D, E, F) for cells 10, 25, and 120 from Session 1 (session type 5) with mouse M26.

2537 Considering only the classified time cells, we sorted cells based on the
 2538 time of the peak of the trial-average activity and a spatiotemporal
 2539 sequence was visualized (Figure 35; also see “Chapter 4 - Analysis
 2540 Figure 7H”).

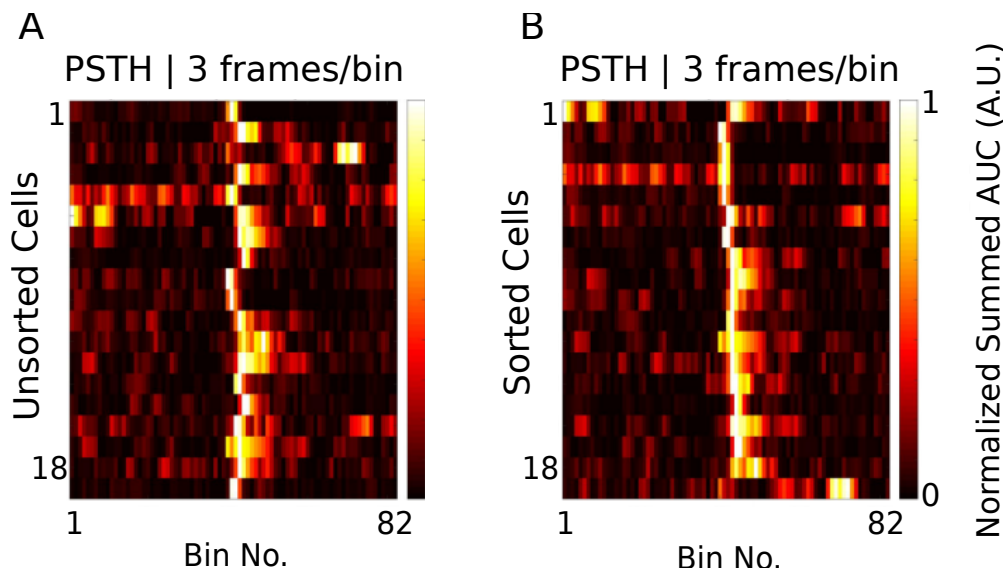


Figure 35: Event Time Histograms or tuning curves for Identified Time-Locked Cells with trial-summed peaks in session 4 of training (session type 5) with mouse M26. (A) Unsorted list of Time cells. (B) Peak-sorted list of the same cells. Here, 1 bin = 3 frames = ~210 ms (sampling rate 14.5 Hz without binning; ~5 Hz with binning). As per the (legacy) session type 5 protocol, the CS (50 ms Blue LED flash) was presented in frame bin 39, followed by a stimulus-free trace interval during frame bins 40 and 41, and then the US (50 ms airpuff to ipsilateral eye) was presented in frame bin 42.

2542 We did not observe any obvious trend in the temporal information of
 2543 time cells with peak times. For the same cells (as in Figure 35), we
 2544 now look at the actual Temporal Information estimates plotted against
 2545 sorted time cells (Figure 36) .

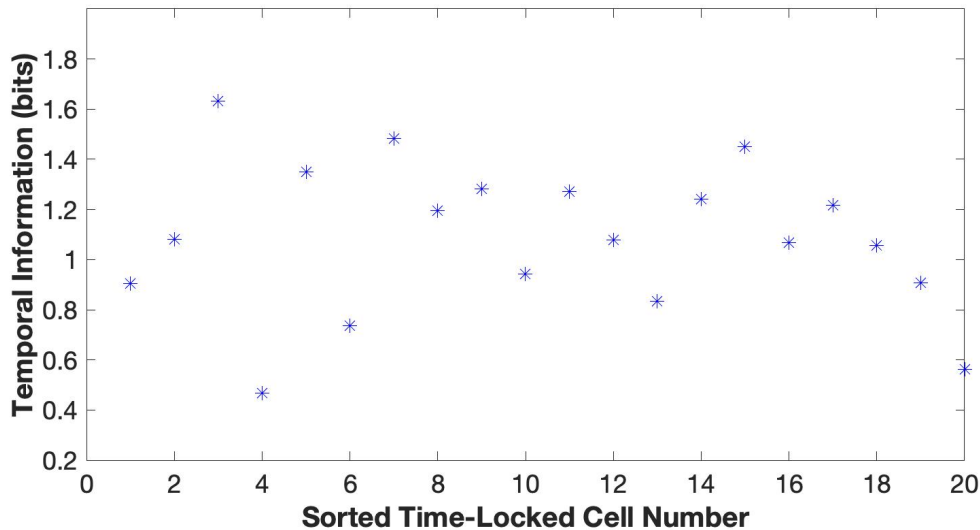


Figure 36: Temporal Information (bits) vs Sorted time cell number from the analytically identified Time Cells in Session 4 (session type 5) with mouse M26. No clear trend was observed.

2547 **Tuning, re-tuning, and de-tuning of time cells across
2548 sessions**

2549

2550 A crucial advantage of the chronic preparation was that many
2551 anatomically aligned and classified cells (as cell ROIs), could be
2552 recorded from over several days and sessions, to look for possible
2553 changes in calcium activity profiles across sessions in the same set of
2554 cells.

2555

2556 We noticed some evidence for an expansion of the set of identified
2557 time cells with sessions, up to a reliable pool of ~20% time cells.

2558 Altogether, from the pool of chronically aligned cells (across sessions),

2559 there was an increase from 7.7% to 23.1% of time cells. Considering
2560 the full cohort cells (irrespective of tracking across multiple training
2561 sessions) the increase was from 7.2% to 21.1% time cells. Here are
2562 the classified time cells between two independent recording sessions,
2563 early in training (Figure 37).

2564

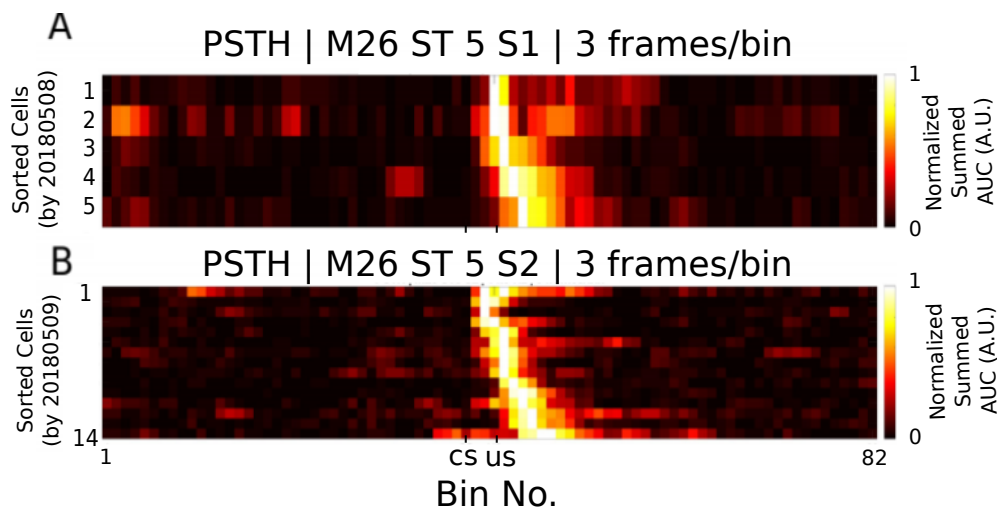


Figure 37: More time cells observed to attain tuning as training sessions. Event Time Histograms of the identified set of time cells between A) Sessions 1 and (B) Session 2, with mouse M26 (session type 5).

2566

2567 The same may also be visualized as trial-averaged calcium activity
2568 profiles for all recorded cells across independent recording sessions
2569 (Figure 38). Here, we see the development of the CA1 sequence with
2570 behavioural training sessions.

2571

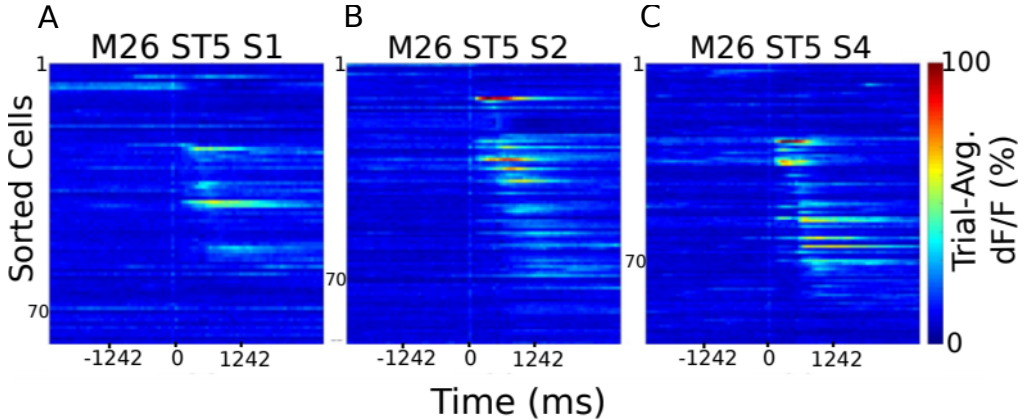


Figure 38: Sorted Time Cells form Sequences that develop with learning. Trial-Averaged calcium activity traces for all recorded cells across A) Session 1, B) Session 2, and C) Session 4, with mouse M26 (sessiontype 5). Time 0 ms was aligned to the CS. The CS + Trace + US interval lasted from 0-600 ms, here.

2573 Chronically tracked time cells that showed reliable tuning across
2574 sessions were then compared to look for any shifts in the peak tuning
2575 bin. We observed examples of cells that maintained their tuning across
2576 pairs of sessions (Figure 39).

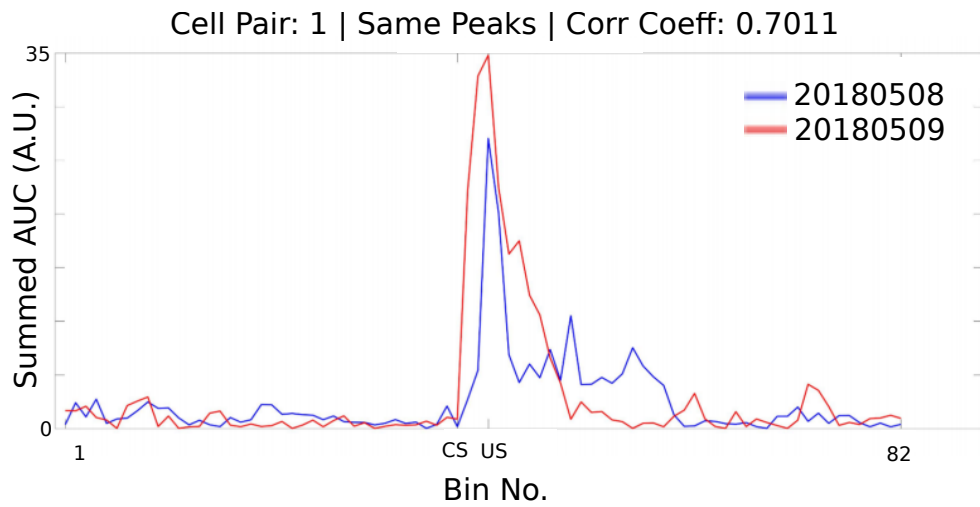


Figure 39: Same/similar tuning across session 1 and session 2 for this example time cell. Blue Event Time Histograms represent the tuning curve for the cell for session 1 (date: 20180508) and Red represent the same but for session 2 (date: 20180509). Pearson's correlation coefficient between the two session pairs was 0.7011.

2578 Here are examples wherein the tuning curve peaks shift to earlier time
 2579 points, across sessions (Figure 40) for Mouse M26, session type 5,
 2580 session 1 vs 2.
 2581

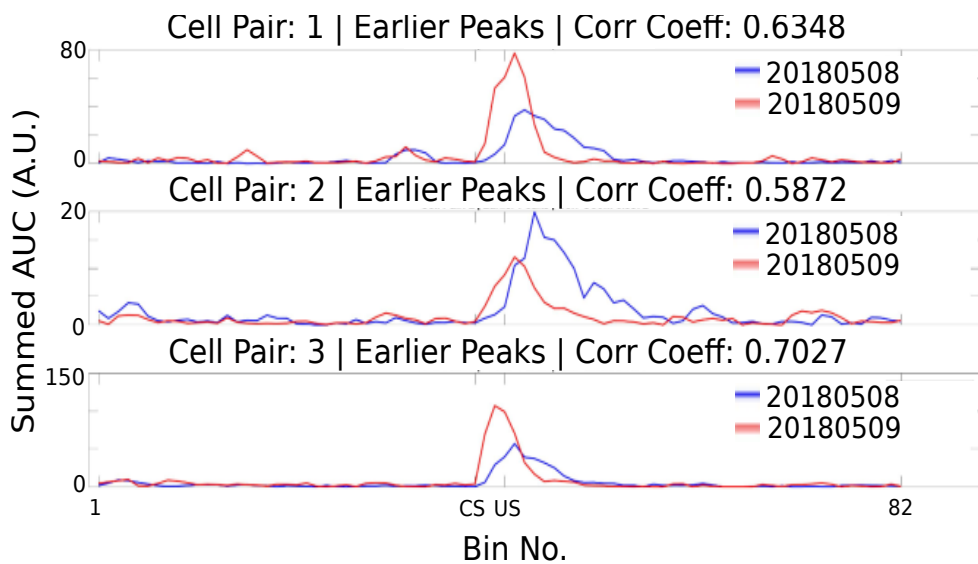


Figure 40: Three example chronically tracked cell pairs with tuning peaks arriving earlier with training sessions (rows). Blue Event Time Histograms represent the tuning curve for any cell for session 1 (date: 20180508) and Red represent the same but for session 2 (date: 20180509). Pearson's correlation coefficient between the session pairs was 0.6348, 0.5872 and 0.7027 for A) cell pair 1, B) cell pair 2, and C) cell pair3, respectively.

2583 Here is an example of a cell showcasing de-tuning for the CS-US
 2584 interval, across sessions (Figure 41), potentially with a new, delayed
 2585 peak almost 100 frames later.

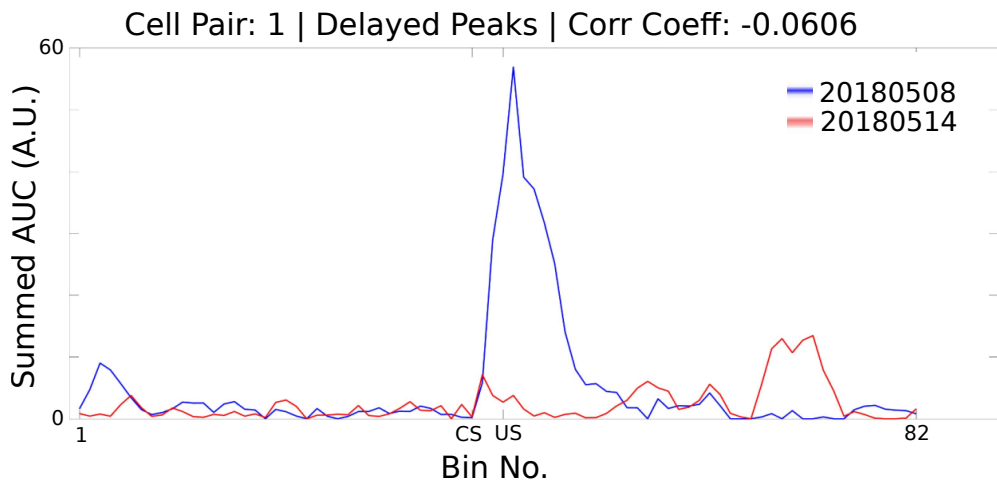


Figure 41: Example chronically tracked cell pair with de-tuning between session 1 and 4. Blue Event Time Histograms represent the tuning curve for the example cell for session 1 (date: 20180508) and Red represent the same but for session 4 (date: 20180514). Pearson's correlation coefficient between the two curves was -0.0606.

2587 A full summary of the correlation based peak timing analysis for
 2588 chronically identified time cells with mouse M26 is shown (Figure 42).
 2589 Across all same cell pairs, there was positive correlation (>0.2) in 71%
 2590 of Time Cells. Also a comparison of the tuning curve peaks between
 2591 the same time cell pairs revealed that a majority of the re-tuned peaks
 2592 occurred earlier in time, going across sessions (71%), with an equal
 2593 proportion of cells without much re-tuning (14%) or de-tuning to later
 2594 time points (14%).

2595

2596

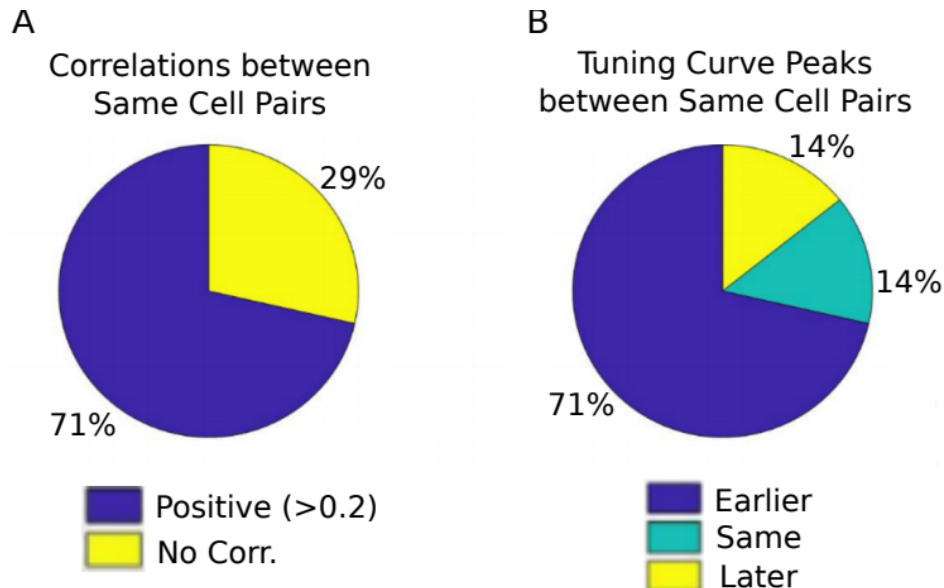


Figure 42: Comparing chronically tracked time cells across sessions for all matched cell pairs by (A) Correlation Analysis, and (B) Timing of peaks.

2598 A summary of the key preliminary results observed using real
 2599 physiology data is as follows.
 2600 1. Time cell tuning curve peaks typically began only after the
 2601 presentation of the CS.
 2602 2. The width of the tuning curve peaks for time cells increased with
 2603 tuning to later frame bins. This was consistent with the recordings
 2604 presented in literature under physiological conditions (B. Kraus et al.,
 2605 2013; MacDonald et al., 2011, 2013; Mau et al., 2018; Modi et al.,
 2606 2014; Pastalkova et al., 2008).
 2607 3. Pairwise time cell tuning curves for different time cells may have
 2608 some overlap in timing, but peaks were observed in all frame bins
 2609 between the CS and the US. This particular observation is confounded
 2610 by the short number of Trace period frames recorded and the
 2611 requirement to consider 3 recording frames to every bin (Mau et al.,

2612 2018), decreasing the effective sampling rate even further (14.5 Hz
2613 without binning, to ~5 Hz with binning). However, the observation is still
2614 consistent with previous literature (B. Kraus et al., 2013; B. J. Kraus et
2615 al., 2015; MacDonald et al., 2011, 2013; Mau et al., 2018; Modi et al.,
2616 2014; Pastalkova et al., 2008).

2617 4. A surprisingly large number of time cells could be identified with
2618 tuning peaks for frame bins occurring after the termination of the US.

2619 5. Considering all chronically tracked cells, the classified and sorted
2620 time cells formed sequences that were dynamic across learning
2621 sessions. Many time cells developed tuning curves with sessions while
2622 some time cells lost their tuning.

2623 6. For the majority of time cells, re-tuning occurred with initial tuning
2624 to the timing of the US in earlier sessions, followed by a shift to earlier
2625 time points for the tuning peak, as training progressed through
2626 sessions.

2627

2628 Future directions to be explored in the lab include studying the
2629 reliability of a larger pool of chronically tracked cells with switches in
2630 the inter-stimulus interval (ISI) between the CS and the US as well as
2631 with a larger palette of different stimuli testing out a battery of
2632 Conditioned Stimuli (CS1, CS2, etc.) and Unconditioned Stimuli (US1,
2633 US2, etc.). The goal is to understand how well the internal neural
2634 spatiotemporal CA1 sequence maps to the external behavioural
2635 protocol parameters, *in vivo*.

2636

2637 Bibliography

- 2638 Abe, R., Sakaguchi, T., Matsumoto, N., Matsuki, N., & Ikegaya, Y.
2639 (2014). Sound-induced hyperpolarization of hippocampal neurons.
2640 *Neuroreport*, 25(13), 1013–1017.
2641 <https://doi.org/10.1097/WNR.0000000000000206>
- 2642 Andersen, P., Morris, R., Amaral, D., Bliss, T., & O'Keefe, J. (Eds.).
2643 (2006). *The Hippocampus Book*. Oxford University Press.
2644 <https://doi.org/10.1093/acprof:oso/9780195100273.001.0001>
- 2645 Attardo, A., Fitzgerald, J. E., & Schnitzer, M. J. (2015). Impermanence
2646 of dendritic spines in live adult CA1 hippocampus. *Nature*,
2647 523(7562), 592–596. <https://doi.org/10.1038/nature14467>
- 2648 Bellistri, E., Aguilar, J., Brotons-Mas, J. R., Foffani, G., & de la Prida, L.
2649 M. (2013). Basic properties of somatosensory-evoked responses
2650 in the dorsal hippocampus of the rat. *The Journal of Physiology*,
2651 591(10), 2667–2686. <https://doi.org/10.1113/jphysiol.2013.251892>
- 2652 Dhawale, A. K. (2013). *Temporal and spatial features of sensory
2653 coding in the olfactory bulb and hippocampus*. Tata Institute of
2654 Fundamental Research.
- 2655 Dombeck, D. A., Harvey, C. D., Tian, L., Looger, L. L., & Tank, D. W.
2656 (2010). Functional imaging of hippocampal place cells at cellular
2657 resolution during virtual navigation. *Nature Neuroscience*, 13(11),
2658 1433–1440. <https://doi.org/10.1038/nn.2648>
- 2659 Fanselow, M. S., & Dong, H.-W. (2010). Are the dorsal and ventral
2660 hippocampus functionally distinct structures? *Neuron*, 65(1), 7–19.
2661 <https://doi.org/10.1016/j.neuron.2009.11.031>
- 2662 Harvey, C. D., Collman, F., Dombeck, D. A., & Tank, D. W. (2009).
2663 Intracellular dynamics of hippocampal place cells during virtual
2664 navigation. *Nature*, 461(7266), 941–946.
2665 <https://doi.org/10.1038/nature08499>
- 2666 Hjorth-Simonsen, A., & Jeune, B. (1972). Origin and termination of the
2667 hippocampal perforant path in the rat studied by silver

- 2668 impregnation. *The Journal of Comparative Neurology*, 144(2),
2669 215–232. <https://doi.org/10.1002/cne.901440206>
- 2670 Itskov, P. M., Vinnik, E., & Diamond, M. E. (2011). Hippocampal
2671 representation of touch-guided behavior in rats: persistent and
2672 independent traces of stimulus and reward location. *PLoS One*,
2673 6(1), e16462. <https://doi.org/10.1371/journal.pone.0016462>
- 2674 Kaifosh, P., Lovett-Barron, M., Turi, G. F., Reardon, T. R., & Losonczy,
2675 A. (2013). Septo-hippocampal GABAergic signaling across
2676 multiple modalities in awake mice. *Nature Neuroscience*, 16(9),
2677 1182–1184. <https://doi.org/10.1038/nn.3482>
- 2678 Kamondi, A. (1998). *Theta Oscillations in Somata and Dendrites of*
2679 *Hippocampal Pyramidal Cells In Vivo: Activity-Dependent Phase-*
2680 *Precession of Action Potentials*. 261(March), 244–261.
- 2681 Kraus, B. J., Brandon, M. P., Robinson, R. J., Connerney, M. A.,
2682 Hasselmo, M. E., & Eichenbaum, H. (2015). During Running in
2683 Place, Grid Cells Integrate Elapsed Time and Distance Run.
2684 *Neuron*, 88(3), 578–589.
2685 <https://doi.org/10.1016/j.neuron.2015.09.031>
- 2686 Kraus, B., Robinson, R., White, J., Eichenbaum, H., & Hasselmo, M.
2687 (2013). Hippocampal “Time Cells”: Time versus Path Integration.
2688 *Neuron*, 78(6), 1090–1101.
2689 <https://doi.org/10.1016/j.neuron.2013.04.015>
- 2690 Lovett-Barron, M., Kaifosh, P., Kheirbek, M. A., Danielson, N.,
2691 Zaremba, J. D., Reardon, T. R., Turi, G. F., Hen, R., Zemelman,
2692 B. V., & Losonczy, A. (2014). Dendritic inhibition in the
2693 hippocampus supports fear learning. *Science (New York, N.Y.)*,
2694 343(6173), 857–863. <https://doi.org/10.1126/science.1247485>
- 2695 MacDonald, C. J., Carrow, S., Place, R., & Eichenbaum, H. (2013).
2696 Distinct hippocampal time cell sequences represent odor
2697 memories in immobilized rats. *The Journal of Neuroscience : The*
2698 *Official Journal of the Society for Neuroscience*, 33(36), 14607–
2699 14616. <https://doi.org/10.1523/JNEUROSCI.1537-13.2013>

- 2700 MacDonald, C. J., Lepage, K. Q., Eden, U. T., & Eichenbaum, H.
2701 (2011). Hippocampal “time cells” bridge the gap in memory for
2702 discontiguous events. *Neuron*, 71(4), 737–749.
2703 <https://doi.org/10.1016/j.neuron.2011.07.012>
- 2704 Mau, W., Sullivan, D. W., Kinsky, N. R., Hasselmo, M. E., Howard, M.
2705 W., & Eichenbaum, H. (2018). The Same Hippocampal CA1
2706 Population Simultaneously Codes Temporal Information over
2707 Multiple Timescales. *Current Biology*, 28(10), 1499-1508.e4.
2708 <https://doi.org/10.1016/j.cub.2018.03.051>
- 2709 McHugh, T. J., Jones, M. W., Quinn, J. J., Balthasar, N., Coppari, R.,
2710 Elmquist, J. K., Lowell, B. B., Fanselow, M. S., Wilson, M. A., &
2711 Tonegawa, S. (2007). Dentate gyrus NMDA receptors mediate
2712 rapid pattern separation in the hippocampal network. *Science*
2713 (New York, N.Y.), 317(5834), 94–99.
2714 <https://doi.org/10.1126/science.1140263>
- 2715 Min, E., Ban, S., Wang, Y., Bae, S. C., Popescu, G., Best-Popescu, C.,
2716 & Jung, W. (2017). Measurement of multispectral scattering
2717 properties in mouse brain tissue. *Biomedical Optics Express*, 8(3),
2718 1763–1770. <https://doi.org/10.1364/BOE.8.001763>
- 2719 Mizrahi, A. (2004). High-Resolution In Vivo Imaging of Hippocampal
2720 Dendrites and Spines. *Journal of Neuroscience*, 24(13), 3147–
2721 3151. <https://doi.org/10.1523/JNEUROSCI.5218-03.2004>
- 2722 Modi, M. N., Dhawale, A. K., & Bhalla, U. S. (2014). CA1 cell activity
2723 sequences emerge after reorganization of network correlation
2724 structure during associative learning. *eLife*, 3, e01982–e01982.
2725 <https://doi.org/10.7554/eLife.01982>
- 2726 Moser, M.-B., & Moser, E. I. (1998). Distributed encoding and retrieval
2727 of spatial memory in the hippocampus. In *The Journal of*
2728 *Neuroscience* (Vol. 18, pp. 7535–7542). Society for Neuroscience.
- 2729 Nakashiba, T., Young, J. Z., McHugh, T. J., Buhl, D. L., & Tonegawa,
2730 S. (2008). Transgenic inhibition of synaptic transmission reveals
2731 role of CA3 output in hippocampal learning. *Science* (New York,

- 2732 *N.Y.*), 319(5867), 1260–1264.
2733 <https://doi.org/10.1126/science.1151120>
- 2734 Pachitariu, M., Stringer, C., Dipoppa, M., Schröder, S., Rossi, L. F.,
2735 Dalgleish, H., Carandini, M., & Harris, K. D. (2017). Suite2p:
2736 beyond 10,000 neurons with standard two-photon microscopy.
2737 *BioRxiv*, 61507. <https://doi.org/10.1101/061507>
- 2738 Pastalkova, E., Itskov, V., Amarasingham, A., & Buzsaki, G. (2008).
2739 Internally Generated Cell Assembly Sequences in the Rat
2740 Hippocampus. *Science*, 321(5894), 1322–1327.
2741 <https://doi.org/10.1126/science.1159775>
- 2742 Peron, S. P., Freeman, J., Iyer, V., Guo, C., & Svoboda, K. (2015). A
2743 Cellular Resolution Map of Barrel Cortex Activity during Tactile
2744 Behavior. *Neuron*, 86(3), 783–799.
2745 <https://doi.org/10.1016/j.neuron.2015.03.027>
- 2746 Poort, J., Khan, A. G., Pachitariu, M., Nemri, A., Orsolic, I., Krupic, J.,
2747 Bauza, M., Sahani, M., Keller, G. B., Mrsic-Flogel, T. D., & Hofer,
2748 S. B. (2015). Learning Enhances Sensory and Multiple Non-
2749 sensory Representations in Primary Visual Cortex. *Neuron*, 86(6),
2750 1478–1490. <https://doi.org/10.1016/j.neuron.2015.05.037>
- 2751 Sheffield, M. E. J., & Dombeck, D. A. (2014). Calcium transient
2752 prevalence across the dendritic arbour predicts place field
2753 properties. *Nature*, 517(7533), 200–204.
2754 <https://doi.org/10.1038/nature13871>
- 2755 Siegel, J. J., Taylor, W., Gray, R., Kalmbach, B., Zemelman, B. V.,
2756 Desai, N. S., Johnston, D., & Chitwood, R. A. (2015). Trace
2757 Eyeblink Conditioning in Mice Is Dependent upon the Dorsal
2758 Medial Prefrontal Cortex, Cerebellum, and Amygdala: Behavioral
2759 Characterization and Functional Circuitry. *ENeuro*, 2(4),
2760 ENEURO.0051-14.2015. <https://doi.org/10.1523/ENEURO.0051-14.2015>
- 2762 Sofroniew, N. J., Flickinger, D., King, J., & Svoboda, K. (2016). A large
2763 field of view two-photon mesoscope with subcellular resolution for

- 2764 in vivo imaging. *eLife*, 5(JUN2016), 1–20.
2765 <https://doi.org/10.7554/eLife.14472>
- 2766 Stosiek, C., Garaschuk, O., Holthoff, K., & Konnerth, A. (2003). In vivo
2767 two-photon calcium imaging of neuronal networks. *Proceedings of
2768 the National Academy of Sciences of the United States of
2769 America*, 100(12), 7319–7324.
2770 <https://doi.org/10.1073/pnas.1232232100>
- 2771 Suh, J., Rivest, A. J., Nakashiba, T., Tominaga, T., & Tonegawa, S.
2772 (2011). Entorhinal cortex layer III input to the hippocampus is
2773 crucial for temporal association memory. *Science (New York,
2774 N.Y.)*, 334(6061), 1415–1420.
2775 <https://doi.org/10.1126/science.1210125>
- 2776 Vinogradova, O. S. (2001). Hippocampus as comparator: Role of the
2777 two input and two output systems of the hippocampus in selection
2778 and registration of information. *Hippocampus*, 11(5), 578–598.
2779 <https://doi.org/https://doi.org/10.1002/hipo.1073>

2780 **Chapter 4 – Analysis**

2781

2782

2783 Our efforts to identify the best use cases for the various implemented
2784 time cell analysis algorithms on the basis of a testbed of user-defined,
2785 categorically labeled synthetic data with known ground truth (Project
2786 III), have been consolidated into a publication. The early access
2787 version of our paper (along with supplementary figures) has been
2788 attached.

Novel Tools and Methods

Synthetic Data Resource and Benchmarks for Time Cell Analysis and Detection Algorithms

Kambadur G. Ananthamurthy and Upinder S. Bhalla

<https://doi.org/10.1523/ENEURO.0007-22.2023>

National Centre for Biological Sciences - Tata Institute of Fundamental Research, Bellary Road, Bengaluru - 560065, Karnataka, India

Abstract

Hippocampal CA1 cells take part in reliable, time-locked activity sequences in tasks that involve an association between temporally separated stimuli, in a manner that tiles the interval between the stimuli. Such cells have been termed time cells. Here, we adopt a first-principles approach to comparing diverse analysis and detection algorithms for identifying time cells. We generated synthetic activity datasets using calcium signals recorded *in vivo* from the mouse hippocampus using two-photon (2-P) imaging, as template response waveforms. We assigned known, ground truth values to perturbations applied to perfect activity signals, including noise, calcium event width, timing imprecision, hit trial ratio and background (untuned) activity. We tested a range of published and new algorithms and their variants on this dataset. We find that most algorithms correctly classify over 80% of cells, but have different balances between true and false positives, and different sensitivity to the five categories of perturbation. Reassuringly, most methods are reasonably robust to perturbations, including background activity, and show good concordance in classification of time cells. The same algorithms were also used to analyze and identify time cells in experimental physiology datasets recorded *in vivo* and most show good concordance.

Significance Statement

Numerous approaches have been developed to analyze time cells and neuronal activity sequences, but it is not clear whether their classifications match, nor how sensitive they are to various sources of data variability. We provide two main contributions to address this: (1) a resource to generate ground truth labeled synthetic two-photon (2-P) calcium activity data with defined distributions for confounds such as noise and background activity, and (2) a survey of several methods for analyzing time cell data using our synthetic data as ground truth. As a further resource, we provide a library of efficient C++ implementations of several algorithms with a Python interface. The synthetic dataset and its generation code are useful for profiling future methods, testing analysis toolchains, and as input to computational and experimental models of sequence detection.

Introduction

The mammalian hippocampus is important for the formation of several kinds of memory, one of which is the association between stimuli occurring separately in time. Time cells were originally described using tuning curves from single-unit recordings of cellular activity when rats ran on a running wheel in between behavioral decisions (Pastalkova et al., 2008). These cells exhibited time tuning of the order of seconds. Several further studies have shown that small populations of hippocampal CA1 cells

fire in time-locked sequences, “bridging” the time gap between stimulus and response in temporal delay tasks lasting several seconds (Pastalkova et al., 2008; MacDonald et al., 2011, 2013; Kraus et al., 2013). Cellular calcium imaging studies have also been used to report time cells, albeit at slower sampling rate (Modi et al., 2014; Mau et al., 2018). For example, similar interval tiling properties of hippocampal CA1 neurons were observed on much shorter, 500 ms timescales in a Trace Eyeblink Conditioning (TEC) task (Modi et al., 2014). Spontaneous sequential activity

Received January 2, 2022; accepted February 9, 2023; First published February 23, 2023.

The authors declare no competing financial interests.

Author contributions: K.G.A. and U.S.B. designed research; K.G.A. performed research; K.G.A. and U.S.B. analyzed data; K.G.A. and U.S.B. wrote the paper.

has also been reported in free-running animals (Villette et al., 2015). Such cells with a well-defined temporal firing field are commonly termed time cells (MacDonald et al., 2011; Eichenbaum, 2017). However, there is a wide diversity of methods used to detect and characterize time cells, and it is not clear how consistent these methods are in classifying cells as time cells. It is also unclear how sensitive each method may be to a range of physiological sources of variability and noise. A consistent set of benchmarks of classification performance is necessary to draw accurate and comparable conclusions from real physiology data across different methods and different laboratories. Our approach in the current study is not prescriptive, but pragmatic: we ask how existing methods work when we already know exactly which cells are time cells, and we determine how well each method deals with imperfect data.

The major approaches used to identifying time cells are tuning curves (peristimulus time histograms), temporal information (TI), principal component analysis with time offset, support vector machines, and bootstrap analysis of activity peaks. Several studies have used a temporal delay task lasting several seconds, in which a rat runs on a treadmill during the delay period. A temporal information metric (Mau et al., 2018) has been used to find individual time cells in such tasks. A distinct task involves monitoring recurrent sequences of activity during free-running treadmill recordings. Such datasets have been analyzed using offset principal component analysis (Kaifosh et al., 2013; Villette et al., 2015; Malvache et al., 2016), to first denoise two-photon (2-P) data, establish correlation coefficients, and detect hippocampal CA1 sequences. Time cells have also been reported for much shorter duration tasks (~500 ms) such as hippocampus-dependent trace conditioning (Tseng et al., 2004; Modi et al., 2014). Time cells in these 2-P datasets were identified using yet another method, in which bootstrapping was used to determine whether peak activity at a given time was different from chance. This method was termed ratio of ridge/background (Modi et al., 2014). Yet other methods have utilized support vector machines to categorize time cells (Ahmed et al., 2020). Additionally, while the applicability of a variety of algorithms for place cell detection has been previously compared (Souza et al., 2018), we have

K.G.A. and the experiments received support from the Department of Biotechnology Grant BT/PR12255/MED/122/8/2016 (to U.S.B.). National Centre for Biological Sciences-Tata Institute of Fundamental Research (NCBS-TIFR) provided resources for analysis equipment and support to U.S.B. through intramural funds supported by the Department of Atomic Energy, Government of India, Project Identification No. TRI 4006.

Acknowledgments: We thank Daniel Dombeck for help with the chronic preparation for physiological 2-P calcium recording of hippocampal CA1 cells and William Mau for his Temporal Information calculation code. We also thank Vinu Varghese and Bhanu Priya Somashekhar for helpful comments on this manuscript.

Correspondence should be addressed to Upinder S. Bhalla at bhalla@ncbs.res.in.

<https://doi.org/10.1523/ENEURO.0007-22.2023>

Copyright © 2023 Ananthamurthy and Bhalla

This is an open-access article distributed under the terms of the Creative Commons Attribution 4.0 International license, which permits unrestricted use, distribution and reproduction in any medium provided that the original work is properly attributed.

focused on methods which are fully automatable and which scale well to large datasets, specifically comparing algorithms to detect time cells.

Time cell detection is closely related to sequence detection, which has been fraught with statistical challenges. For example, detection of synfire chains has been the subject of some debate (Ikegaya et al., 2004; Lee and Wilson, 2004; Mokeichev et al., 2007; Schrader et al., 2008). Time cell detection is usually easier, in that in most experiments there is a well-defined initiating stimulus and a known delay or trace phase (however, see Villette et al., 2015). For any cell identified as a time cell, it is desirable to define a score to measure quality or reliability along with decodable time. Hence it is also valuable to be able to compare the score of a time cell across recordings and even between groups, using well defined, analog measures. Each algorithm currently used in the literature implements a different scoring method and it is as yet unclear whether comparable results would be observed with other metrics.

In the current study, we compare these diverse methods by estimating their performance on synthetic test datasets where we controlled all features of the data, including the identity and timing of each time cell. The development of a synthetic dataset serves two purposes. First, it facilitates principled comparison of different methods, since the ground truth is known. Second, it facilitates an analysis over many dimensions of input variance, corresponding to very different experimental and neural circuit contexts. Richness in variety of input data allows for better sampling of the performance of the analyses under many potential conditions. We have explored variance along the key dimensions of noise, timing imprecision, signal widths, frequency of occurrence, as well as several others. To strengthen the applicability of this synthetic data resource to real data, our generated output uses sampled experimental data.

Our experimental data, synthetic dataset, and code base are intended to be a resource for algorithm testing and optimization.

Materials and Methods

Animals, chronic implants, and behavioral training

All animal procedures were performed in accordance with the National Centre for 114 Biological Sciences Institutional Animal Ethics Committee (project ID NCBS115 IAE-2016/20(M)), in accordance with the guidelines of the Government of India (Animal Facility CPCSEA registration number 109/1999/CPCSEA) and equivalent guidelines of the Society for Neuroscience.

To chronically monitor the activity of the same population of hippocampal CA1 cells, we implanted two- to four-month-old male and female GCaMP6f mice [Tg(Thy1-GCaMP6f)GP5.17Dkim JAX stock #025393] with an optical window and head-bar using a protocol adapted from previously published methods (Dombeck et al., 2010). Briefly, anesthesia was induced with 2–3% isoflurane in a chamber, and subsequently maintained (breathing rate of ~1 Hz) with 1–2% isoflurane, directly to the mouse's nose using an inverted pipette tip. Surgery was performed on a

temperature-controlled table, maintained at 36.5°C, while the anaesthetized animal was cheek-clamped. After a haircut, a ~5 cm piece of scalp was cut open to reveal the skull. A ~3 mm circular craniotomy was then performed at a position 2 mm caudal and ~1.5 mm lateral to bregma, on the left hemisphere. After gently tearing off the dura, the underlying cortex was carefully aspirated till the corpus callosum (CC) layer, clearing out any blood using repeated washes of cortex buffer (Modi et al., 2014). A small thickness of corpus callosum fibers were then carefully aspirated till horizontal CC fibers were sparse but visible. The cortex buffer was then carefully suctioned out to dry the exposure till tacky. The exposure was then quickly sealed using a thin layer of Kwik-Sil and a coverslip attached to the bottom of a 3 mm steel cannula. This preparation left the CA1 cell body layer ~200 μm below the most exposed tissue. Finally, an imaging head-bar was surgically implanted and fixed to the scalp, using dental cement and skull screws, before the animal was brought out of anesthesia.

The animals were allowed to recover for 1–5 d after implantation, with a further 3–4 d of habituation to the rig. Following this simultaneous behavioral training and 2-P *in vivo* imaging was conducted.

Trace Eyeblink Conditioning (TEC)

We standardized a multi-session Trace Eyeblink Conditioning (TEC) paradigm to train head-fixed mice, based on previous literature (Siegel et al., 2015). TEC involves an association between a previously neutral conditioned stimulus (CS) with an eyeblink inducing unconditioned stimulus (US), across an intervening, stimulus-free, trace interval. Training involved 60 trials per session, one session a day, for approximately two weeks. The CS was a 50 ms blue LED flash while the US was a 50 ms air-puff to the left eye. The stimulus-free trace interval was 250–750 ms long, depending on the session. Additionally, a pseudorandom 10% of the trials were CS-only probe trials (no US) to test for learning. All behavior routines were controlled by programmed Arduinos. Eyeblinks were measured for every trial, by video camera (Point Gray Chameleon3 1.3 MP Monochrome USB3.0) based detection.

The conditioned response (CR) is observed as a preemptive blink before the US is delivered, in animals that learn the task. The analysis of the behavioral data was performed using custom written MATLAB scripts. In brief, each frame for every trial was:

1. Cropped to get the eye;
2. Binarized to get the pixels defining just the eye, and finally;
3. Given an FEC score from 0 to 1 (see below).

Every trial was then scored as a hit or miss, using the result of a two-sample Kolmogorov-Smirnov test between the FEC during the trace and pre-CS period (1% significance). The performance of an animal for a session was then established as the percentage of hit trials/total trials.

Definitions:

FEC: The fraction of eye-closed is estimated by counting the pixels defining the eye in every image of a time series, normalized by the maximum number of pixels defining the eye, in that session. Thus, every frame was given an analog score from 0 to 1, where,

- 0: fully opened eye
- 1: fully closed eye

CR: The conditioned response is the eye-closing transition during the trace period.

UR: The unconditioned response is the eye-closing transition when the US is delivered.

Performance: Percentage of hit trials/total trials. This allowed us to observe how the animals perform during and across sessions.

Two-photon imaging

We used a custom-built two photon laser-scanning microscope (Modi et al., 2014) to record calcium activity from 100–150 hippocampal CA1 cell bodies *in vivo*, at cellular resolution. We performed galvo-scans through the imaging window, over a field of view of ~100 × 100 μm², at 14.5 Hz, during TEC (Fig. 1A). An Arduino microcontroller was used to control the behavior routines, and it additionally sent a TTL trigger to initiate the imaging trials. The behavior and imaging were conducted simultaneously to record calcium activity when the animal was learning the task.

Time-series fluorescence data for various cells was extracted using Suite2P (Pachitariu et al., 2017). All further analysis and code development was done on MATLAB R2017b and batch analysis runs were performed on MATLAB R2021a. The average of the fluorescence values for cell specific pixels is then converted into the fold change relative to the baseline (dF/F₀; F₀ as 10th percentile), for every marked cell, in every trial (Fig. 1B). These dF/F traces were used for the rest of the analysis.

Curating a library of calcium events

For all synthetic data experiments, we used one good quality 2-P recording session's worth of data from one animal. We mapped our imaging dataset into a matrix of dF/F values for all cells, trials, and frames. We then identified calcium events as signal deviations that were above a threshold (mean ± 2*SD) for more than four consecutive frames (frame rate: 14.5 Hz or ~70 ms per frame). Once identified, we curated a library for each event by a cell, and saved the respective start indices and widths. Using this library, we generated synthetic data by inserting experimental calcium events into the time series for each simulated cell. This approach just uses a time series of signal bins and amplitudes, hence is signal-agnostic and could be applied to other imaging and recording modalities. In the interests of data integrity, our synthetic datasets were watermarked to be distinguishable from real physiology datasets.

Generating synthetic data

Synthetic data were generated using a custom-written MATLAB function script “generateSyntheticData()” in the provided code repository. We preallocated and set up a 3-D matrix of zeros (as cells, trials, frames), and added

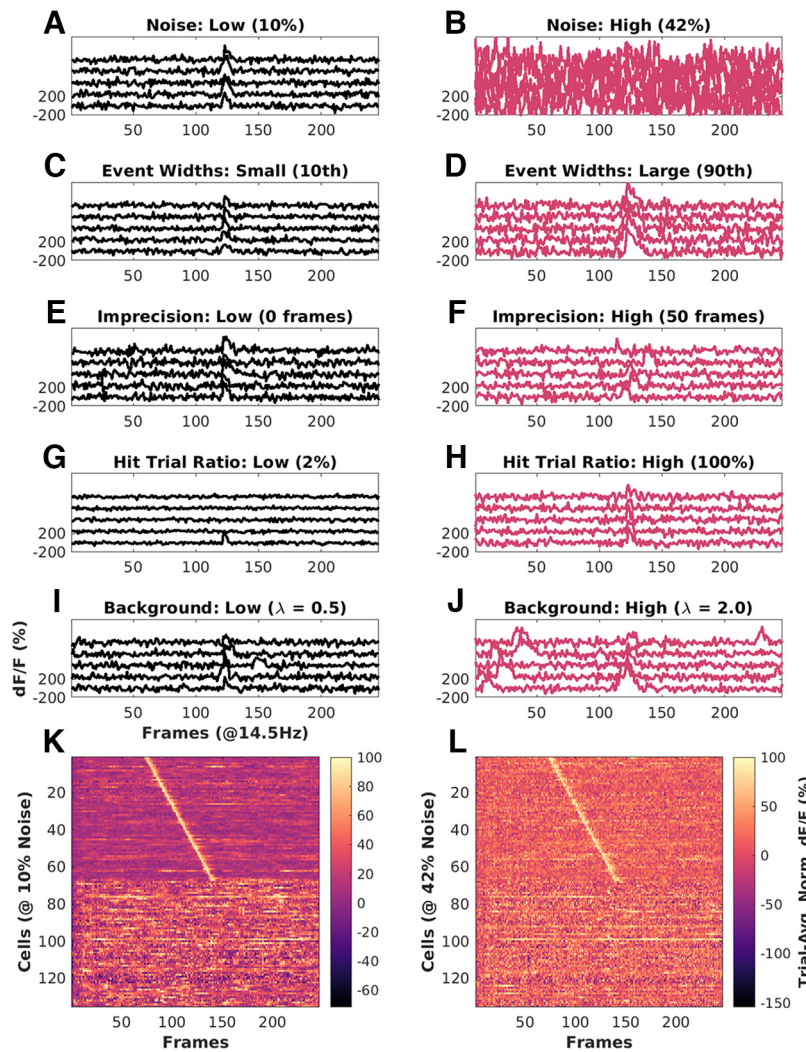


Figure 1. Key features of synthetic datasets. Left, Black panels, Low range of features. Right, Red panels, High range of features. **A**, Noise = 10%. **B**, Noise = 42%. **C**, Event width: 10th percentile ± 1 SD. **D**, Event width 90th percentile ± 1 SD. **E**, Imprecision at 0 frames FWHM. **F**, Imprecision at 50 frames FWHM. **G**, Hit trial ratio from 0% to 2%. **H**, Hit trial ratio from 0% to 100%. **I**, **J**, Background activity with the number of background spikes per background sampled from a Poisson distribution for with mean (λ), for **I**: $\lambda = 0.5$ (low), and **J**: $\lambda = 2.0$ (high). **K**, **L**, Trial-averaged Calcium traces from example synthetic datasets of 135 neurons, displayed as heatmap sorted by time of peak Ca signal. **K**, Baseline physiology synthetic data trial-average with 10% noise (low) and high background activity ($\lambda = 2$ to 3 events/trial). **L**, Same as **K** with 42% noise (high) and comparable background activity ($\lambda = 2$ to 3 events/trial). In both cases, 50% of the cells (top 67) are time cells and the remainder are not. Extended Data Figure 1-1 describes the most important parameters modulated for datasets in each of the three parameter regimes, “Unphysiological,” “Canonical,” and “Physiological,” along with the false positives and false negatives, for each of the 10 implemented algorithms.

calcium events sampled from the Calcium Event Library at frames (time) determined by the synthesis algorithm. The input parameters to this algorithm included timing, noise, imprecision, event width selection, hit trial ratio, background activity, and several others. We aimed to cover the most likely conditions to affect timing and other experiment design properties. In more detail, we generated synthetic datasets using the following control parameters:

- Time cell percent

Value: Number between 0 and 100. This sets the number of cells that are assigned tuned calcium activity as a

percentage of total cells, and controls the number of positive and negative class cells in the dataset.

- Cell order

Value: ‘basic’ or ‘random.’ In ‘basic’ mode, time cells are indexed lower than other cells. In ‘random’ mode, the indices of time cells and other cells are randomly selected. This should have no impact on algorithm detection but is useful for visualization.

- Max hit trial percent

Value: Number between 0 and 100. This sets the maximum possible fraction of total trials, during which a Time Cell will exhibit tuned calcium activity.

- Hit trial percent assignment

Value: ‘fixed’ or ‘random.’ In ‘fixed’ mode, the number of hit trials is set as defined by max hit trial percent. In ‘random’ mode, the number of hit trials is calculated by randomly picking a value from a range ($\frac{1}{2} \times \text{max hit trials}$, max hit trials).

- Trial order

Value: ‘basic’ or ‘random.’ In ‘basic’ mode, the hit trials are indexed lower than miss trials. In ‘random’ mode, the indices of hit and miss trials are randomly selected. Specific patterns of hit and miss trials for a session have not been reported in physiology, so this feature is not implemented.

- Event width

Value: {0–100 percentile value, Integer N}. For each cell, this defines the selection of events based on width in frames. The percentile value is estimated from the histogram of all event widths. The variance of this selection is set by “N,” which adds N^*SD to the selection. All synthetic cells exhibit a range of different calcium events. This is considered an important parameter.

- Event amplification factor

Value: Number from 0 to $+\infty$. This allows additional control to multiplicatively amplify any chosen calcium event, before incorporation. Our library was curated from physiologically recorded signals. The default value is 1.

- Event timing

Value: ‘sequential’ or ‘random.’ In ‘sequential’ mode, the time of peak calcium activity is reflected by the indexing of the time cells. In ‘random’ mode, the time of peak calcium activity is randomly dispersed over the trial frame points.

- Start frame

Value: Number from 0 to total number of frames. This sets the timing of the first cell in a time cell sequence.

- End frame

Value: Number from 0 to total number of frames. This sets the timing of the last cell in a time cell sequence.

- Imprecision full width at half max (FWHM)

Value: Number from 0 to total number of frames. This sets the lower and upper bounds for the difference in timing of calcium activity across trial pairs for a time cell. We use this parameter to model trial to trial variability and is considered an important parameter to test.

- Imprecision type

Value: ‘none,’ ‘uniform,’ or ‘normal.’ In ‘uniform’ and ‘normal’ modes, the trial pair Imprecision is picked from a normal and uniform distribution, respectively. In ‘none’ mode, the trial pair Imprecision defaults to 0.

- Noise

Value: ‘Gaussian’ or ‘none.’ In ‘Gaussian’ mode, the noise is sampled as a time-series vector with points from

a Gaussian distribution. In ‘none’ mode, the noise percent defaults to 0.

- Noise percent

Value: Number from 0 to 100. This allows scaling for any sample noise point, based on the max signal value for any cell.

- Add background spikes for time cells

Value: Boolean 0 or 1. This switch controls the incorporation of background (untuned) activity for putative time cells.

- Add background spikes for other cells

Value: Boolean 0 or 1. This switch controls the incorporation of background (untuned) activity for other (nontime) cells.

- Background distribution mean

Value: Number from 0 to $+\infty$. This sets the mean (λ) of the Poisson distribution to sample from when selecting how many background events to add per trial, for any given cell.

Implementation of a reference quality measure, Q

In order to compare the readouts from the various time-cell detection methods, we implemented a reference measure of quality (Q) of synthetic time cells that used the known inputs to the generation algorithm.

Based on preliminary analysis, we selected following five parameters as the most likely to affect the behavior and detection of time cells:

1. Noise
2. Event width
3. Imprecision
4. Hit trial ratio
5. Background activity

Accordingly, we were able to calculate a reference quality measure, using the following equation:

$$\text{RefQ} = \text{HTR} \times \exp\left(-\{\alpha \times \text{MNP}/100 \times \text{EAF} + \beta \times \text{std. dev. EW}/\text{meanEW} + \gamma \times \text{std. dev. Imp}/\text{Stim Win}\}\right), \quad (1)$$

where HTR: hit trial ratio

MNP: max noise percent (%)

EAF: event amplification factor

EW: event widths (frames)

Imp: imprecision (frames)

Stim Win: stimulus window (frames)

α : 1

β : 1

γ : 10

The values of α , β , and γ , were set to have comparable effects of each of the terms inside the exponent. This reference Q was useful for debugging code and was the basis for a further metric for time cell classification discussed below. A representative synthetic activity trace for ‘low’ and ‘high’ values of each of these five parameters is shown in Figure 1.

All modulations for the datasets in this study along with the estimates for false positives and false negatives, across all algorithms are shown in Extended Data Figure 1-1.

Separate analysis modules were developed for three categories of analysis

We implemented three analysis modules: *ti*, *r2b*, and *peq*, shorthand for temporal information, ridge-to-background, and parametric equations. The *ti* module implements three algorithms from Mau et al. (2018). The *r2b* module implements two algorithms from Modi et al. (2014). The *peq* module computes estimates for noise, hit trial ratio, event width and imprecision, and estimates a Q score as above. All three methods were implemented in C++ with a PyBind11 interface to Python. This combination is fast and efficient in memory use, and also has the ease-of-use of Python. Thanks to the native MATLAB interface to Python, all three methods can also be called from MATLAB.

Synthetic datasets generated and analyzed in batch mode

We generated datasets pertaining to parameter sensitivity analysis by modulating one of the four main parameters and setting the others to noninterference levels. In this manner, we devised 99 cases to study in which one of the main parameters was varied. Note that in these cases the resultant activity was in an unphysiological regime because other sources of variation were kept to low levels so as not to interfere with the parameter of interest. With three randomized shuffles, we generated 297 unique datasets.

We wanted to use more realistic datasets, where we would modulate one of the four parameters while keeping the others to ranges typical of physiological data. We devised 12 canonical cases. With 10 randomized shuffles each, we generated 120 additional unique datasets in the canonical regime. Finally, we devised 12 physiological regime cases, identical to those in the canonical regime, with the addition of background (untuned) activity. This yielded another 150 datasets, with randomization.

Altogether, we had 567 unique datasets for our tests, each with 135 cells (total: 76,545 cells), 60 trials, and 246 frames/trial. Except when the percent time cells were modulated, all datasets featured 50% time cells.

We next implemented an analysis pipeline to run all the datasets through the time cell detection algorithms, yielding scores and predictions for each case. Finally, all the scores and predictions were collated for comparison and benchmarks as shown in the schematic (Fig. 2).

Metrics for time cell classification performance

Recall is inversely proportional to the number of false negatives (Type II error) and is the fraction of true positive class predictions over all positive class ground labels.

$$\text{Recall} = \text{TPR}/(\text{TPR} + \text{FNR}) \quad (2)$$

Precision is inversely proportional to the number of false positives (Type I error) and is the fraction of true positive class predictions over all positive class predictions.

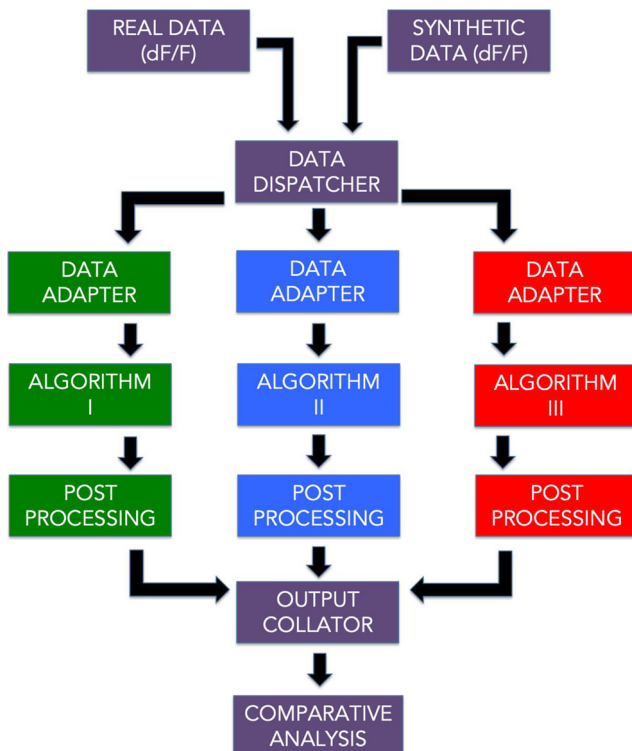


Figure 2. A schematic representation of the analysis pipeline. Physiology data as well as synthetic data were analyzed by 10 different implemented algorithms and the output was collated for comparative benchmarks.

$$\text{Precision} = \text{TPR}/(\text{TPR} + \text{FPR}). \quad (3)$$

F1 Score is the harmonic mean of recall and precision.

$$\text{F1 Score} = 2 * \text{Precision} * \text{Recall}/(\text{Precision} + \text{Recall}), \quad (4)$$

where

TPR: true positive rate

FNR: false negative rate

FPR: false positive rate

Here are the definitions for predictive/classification performance evaluation (Table 1).

Here are the important functions provided in the code base (Table 2).

Here are the MATLAB scripts running the comparative analysis and figure generation (Table 3).

Code and resource availability

The code/software described in the paper is freely available online at <https://github.com/BhallaLab/TimeCellAnalysis>. The code is available as Extended Data 1.

Results

We developed a pipeline (Fig. 2) with 10 different algorithm implementations for time cell detection, which involve scoring and then classifying cells.

Here, we describe the implementation of each of the methods.

Table 1: Definitions for predictive/classification performance evaluation

Ground truth	Prediction/classification	Remark
0/false/other cell	0/false	True negative (TN)
0/false/other cell	1/true	False positive (FP)
1/true/time cell	0/false	False negative (FN)
1/true/time cell	1/true	True positive (TP)

For each detection algorithm, the classification results were compared with known ground truth values to get the total number of true positive (TP), true negative (TN), false positive (FP), and false negative (FN) cases.

Time cell scoring methods and classification

Temporal information: *tiBoot*, *tiMean*, *tiBoth*, *tiMean-O*, *tiBase-O* (Mau et al., 2018)

Here, we used the algorithm from Mau et al. (2018) as follows. There was an initial criterion of cells to have activity in at least 25% of trials. Their activity was summed into event time histograms with a bin size of three frames. The temporal information (TI) was estimated using Equation 5,

$$TI = 1 \times \lambda_j \times \log_2 \lambda_j \times P_j, \quad (5)$$

where, λ is the average transient rate for each cell;

λ_j is the average transient rate for each cell in bin “j”; P_j is the probability that the mouse was in time bin “j.”

Bootstrapping was used to determine whether each cell had a TI greater than chance. We circularly randomized the frame points to develop a random activity model (1000 iterations) and classified cells as time cells if $\lambda > \lambda_{rand}$ in >99% of the models for at least two consecutive bins. We implemented the activity filter from Mau et al. (2018); by considering the trial-averaged peak of the calcium traces for each of the cells, and testing for significance using bootstrapping (*tiMean*). A logical AND operation between the prediction lists for *tiBoot* and *tiMean*, provided us with the full Mau et al., 2018 Temporal Information based detection algorithm (*tiBoth*).

Additionally, we used Otsu’s threshold (Otsu, 1979) on the temporal information scores as well as the trial-averaged peaks to get *tiBase-O* and *tiMean-O* using the MATLAB function “graythresh()” (<https://in.mathworks.com/help/images/ref/graythresh.html>). The purpose of adding the Otsu’s threshold-based classification step was to study how well the scores could be classified with a fast thresholding method, rather than the computationally expensive bootstrap.

Table 2: List of important functions provided in the code base

Name	Description	Command line	Location	Language
synthesis Demo.m	Command line demo, output to file: “synthData-demo.mat”. Generates a synthetic 2-P time cell dataset file	\$ cd TimeCellAnalysis/rho-matlab/demos && matlab -nodisplay -nosplash -r “synthesisDemo; quit”	rho-matlab/demos	MATLAB
ti_demo.py	Command-line demo, output to console.	\$ python TcPy(ti_demo.py sampleData/sample_synth_data.mat	TcPy	Python interface and C++ numerics
r2b_demo.py	Command-line demo, output to console. Runs Ridge-to-Background analysis from Modi et al. (2014). Reports R2B Mean and R2B Bootstrap classifications	\$ python TcPy(r2b_demo.py sampleData/sample_synth_data.mat	TcPy	Python interface and C++ numerics
peq_demo.py	Command-line demo, output to console. Runs parametric equation analysis from current study. Reports PEQ threshold classification, and estimates for noise, event width, imprecision, and hit trial ratio for dataset	\$ python TcPy(peq_demo.py sampleData/sample_synth_data.mat	TcPy	Python interface and C++ numerics
ground_truth_check.py	Command-line demo, output to console. Uses synthetic data files to assess accuracy of classification by the various Mau and Modi algorithms	\$ python TcPy/ground-truth_check.py sampleData/sample_synth_data.mat	TcPy	Python interface and C++ numerics
Benchmark.py	Command-line demo, output to console. Simple time and memory benchmarks for the Mau, Modi, or PEQ algorithms	\$ python TcPy/run_batch_analysis.py sampleData/sample_synth_data.mat	TcPy	Python interface and C++ numerics
run_batch_analysis.py	Command-line production script, output to CSV files. Runs a batch analysis using all methods on a data file. Generates .csv files for TI, R2B, PEQ, and ground truth classifications	\$ python TcPy(ti_demo.py sampleData/sample_synth_data.mat	TcPy	Python interface and C++ numerics
pyBindMap.py	Provides an interface for MATLAB programmers, to the python/C__ fuctions using two wrapper functions: runTlAnalysis and runR2Banalysis	Utility function, not run from command line	TcPy	Python
dodFbF.m	Utility function to convert experimental raw 2p calcium activity data from Suite2P to df/F form.	Utility function, not run from command line	rho-matlab/CustomFunctions	MATLAB

All these functions should be run from the cloned repository, TimeCellAnalysis.

Table 3: List of paper figure generating scripts

Name	Description	Command line
paperFigures	Plots all figures estimating algorithm performance for synthetic data analysis (paper Figs. 1, 4–6, and 8)	\$ matlab -r "paperFiguresSynth"
Synth.m		
paperFigures	Plots all figures estimating algorithm performance for real physiology data analysis (paper Fig. 7)	\$ matlab -r "paperFiguresReal"
Real.m		
paperFigures	For diagnostics; plots figures estimating algorithm performance over all the regimes (unphysiological, canonical, and physiologic)	\$ cd .. /src && matlab -r "paperFiguresSplits"
Splits.m		

All these functions should be run from the cloned repository, TimeCellAnalysis/p-matlab/paperFigures.

Ratio of ridge/background, *r2bMean*, *r2bBoot*, *r2bBase-O* (Modi et al., 2014)

Here, we re-implemented the algorithm from Modi et al., 2014. The time of peak response for each cell was identified in averaged, nonoverlapping trials' worth of $\Delta F/F$ traces, in the CS-onset to US-onset period, or as specified. The rest of the trials were averaged and the summed area under the time of peak was estimated. The ridge was then defined to be a 200 ms window centered at the peak. Next, we calculated the summed area in the ridge window as well as the background (non-ridge frames) to get the ridge to background ratio. As a control condition, these traces were given random time-offsets and then averaged. An independent time of peak was identified for each random-offset, averaged trace and ridge to background ratio calculated for it. This bootstrapping was repeated 1000 times for each cell's data and averaged. The reliability score was then calculated individually, for each cell, as the ratio of the ridge to background ratio for aligned traces to the mean of that of the random-offset traces (*r2bMean*).

We also studied the significance of each cell's raw *r2b* values by comparing them to each of the *r2b* values of the randomized datasets, thresholding significance at the 99th percentile (*r2bBoot*). Finally, the raw *r2b* values were also thresholding using Otsu's Thresholding (*r2bBase-O*; Otsu 1979).

Parametric equations, *peqBase* and *peqBase-O* (in-house)

We developed this method to score cells in a manner similar to the reference quality, which uses the known ground truth of the input parameters given to the generator functions for the synthetic dataset. Rather than using the known inputs, this method computes the corresponding parameters read out or estimated from the dataset, whether synthetic or real. It is applicable to labeled or unlabeled datasets. It is defined as:

$$Q = \text{HTR} \times \exp - \{\alpha \times N/S + \beta \times \text{std. dev. EW} / \text{mean EW} + \gamma \times \text{std. dev. Imp/Stim Win}\}, \quad (6)$$

where HTR: hit trial ratio

N/S: estimated noise/signal

EW: read out event widths (frames)

Imp: estimated imprecision (frames)

Stim Wind: stimulus window (frames)

$\alpha: 10$

$\beta: 1$

$\gamma: 10$

While $10 \times \alpha$ was required, β , and γ , were inspired by the same used for reference Q. Classification was then performed using Bootstrapping (as described above) as well as Otsu's threshold.

All of these implemented algorithms can handle unlabeled (real) or ground truth labeled (synthetic) data.

A schematic to describe the steps involved in each algorithm is shown (Fig. 3). We were then able to run all our synthetically generated datasets through each of the 10 implemented algorithms and perform comparative benchmarks.

Good predictive power in time cell quality scores despite different distributions

We ran each of the analysis methods on our synthetic datasets to assess how they scored the (known) time cells. There were four methods that provided a scoring function for time-cell classification: *tIMean*, *tIBase*, *r2bBase*, and *peqBase* (Fig. 4A–D). By inspection, these methods appeared to have distinct distributions. Below we describe how we compare the distributions using correlation analysis. In subsequent sections we describe other methods in our study that used these scores to generate a categorization through thresholding or bootstrap.

In these synthetic experiments, time cells were generated with a single calcium event per hit trial. Event insertions into the synthetic datasets were subject to noise, variable selection of event widths, trial-pair or timing imprecision, and hit trial ratio. We generated 99 unique unphysiological combinations (3 \times randomized shuffles) 12 unique canonical regime combinations (10 \times randomized shuffles), as well as 15 unique physiological regime combinations featuring background activity (10 \times randomized shuffles). In all, we performed our comparative analysis studies using 567 datasets, each with 135 cells, 60 trials/session, and 246 frames/trial at 14.5 Hz). We found that only *tIMean* and *tIBase* had a correlation coefficient of ~ 0.6 , whereas other pairs were correlated below 0.4 (Fig. 4E).

Generalized linear regression (GLM) models were generated to look for the ideal thresholding value for the best classification predictions by each method. We used the MATLAB implementation of GLMs (*fitglm*); <https://in.mathworks.com/help/stats/fitglm.html>). This is a linear model assuming a binomial distribution of categories (0 or 1, i.e., other cell or time cell; Collett, 2002). We obtained good predictive power for the four methods that provided a scoring function for time-cell classification. We generated Receiver Operating Characteristic (ROC) curves by going over the full range of thresholds for the range of scores for each method

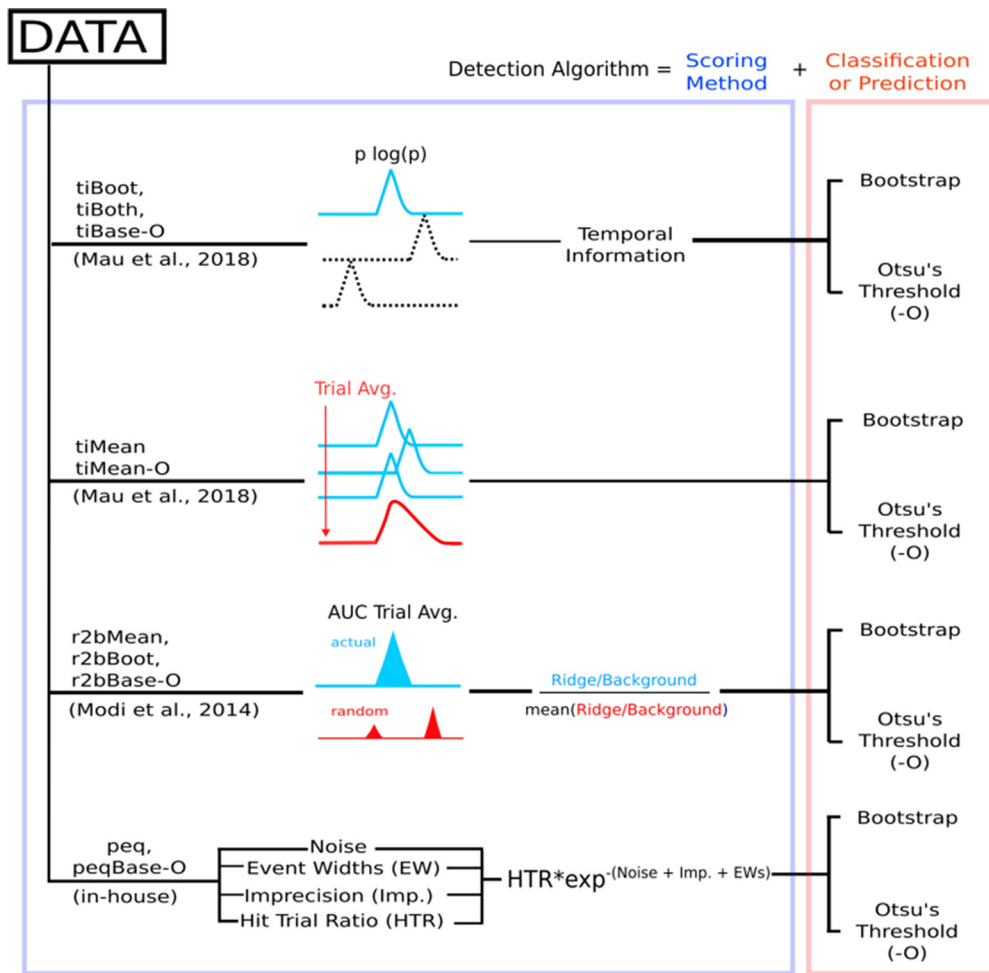


Figure 3. Schematic representation of the implemented algorithms, involving four different scoring methods followed by a classification step (bootstrapping or Otsu's automatic threshold) to have 10 complete time cell detection algorithms.

(ROC curves; Fig. 4F). We found that each distribution of scores had good predictive power, since ideal thresholds could be found to maximize TPR/FPR in all cases. We used the *tiBoth* categorization to distinguish time cells (Fig. 4G) from other cells (Fig. 4H), and plotted trial-averaged calcium traces to visually assess quality of classification as seen from raw data. Overall, each of our methods had distinct distributions of their base scores, but all had good predictive power for classification. The outcome of the classification steps is described in the next sections.

All algorithms exhibit near perfect precision with good recall

Next, we used the scores to classify the cells in our synthetic datasets, compared the predictions to ground truth, and established summaries for true and false cases. Confusion matrices were estimated to compare the predictions (classifications) for each algorithm, with reference to ground truth, and are shown (Fig. 5A,B). All methods exhibit very good precision (true positive classifications over the sum of all positive classifications), suggesting low false positive rates (Type I error; Fig. 5C). Most algorithms also generate good values for recall (true positive

classifications over ground-truth positives). We observed F1 scores (harmonic mean of recall and precision) >0.75 , all the way to 1 (perfect score), for most of the algorithms, as shown (Fig. 5C), suggesting overall usability.

We noticed moderate to strong correlation (>0.8) between the Boolean prediction lists for *tiMean*, *tiBoot*, *tiBoth*, *r2bMean*, and *r2bBoot* (Fig. 5D), but only weak to moderate correlation (<0.6) between the other pairs of predictions. The *tiMean-O* method does slightly better (correlation ~ 0.7 with the first five methods).

Algorithms differ in memory use and speed

Hardware and runtime requirements are a secondary, but practical concern when designing analysis of large datasets, and are specially relevant for experiment designs that require online analysis. We therefore looked at how memory use and runtime scaled on a per dataset basis when considering 67 or 135 cells per dataset ($2\times$).

We ran the memory usage and runtime experiments on a gaming laptop (Lenovo Ideapad 3 Gaming) with a 6 core AMD Ryzen 5 4600H, 16 GB DDR4 RAM (3200 MHz) running MATLAB R2021a on Ubuntu 20.04. Note, however, that we have implemented all the time cell algorithms in

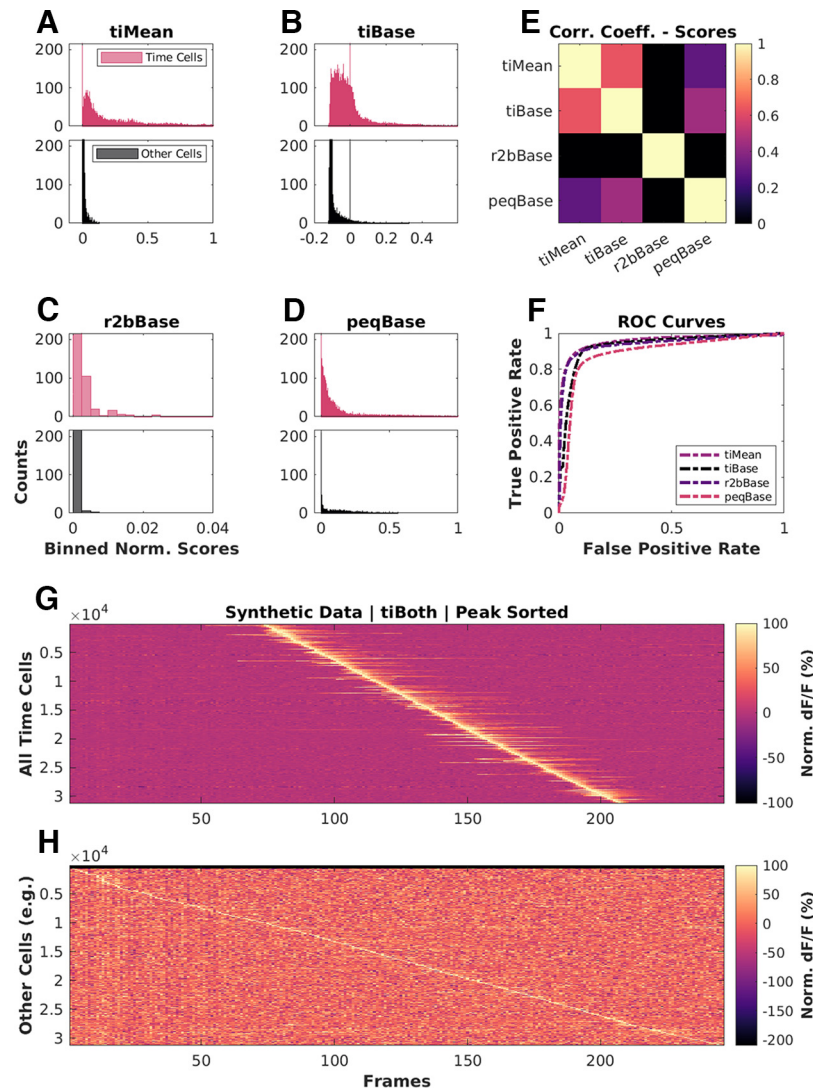


Figure 4. Base scores for different methods differ in their distributions but all have good predictive power. Scores for top (blue): time cells; bottom (red): other cells, across **A**, **tiMean**; **B**, **tiBase**; **C**, **r2bBase**; **D**, **peqBase**. **E**, Pairwise correlation coefficients between the distributions of analog scores (pooling time cells and other cells) by each of the four scoring methods. **F**, Receiver-operator characteristic (ROC) curves after generalized linear regression using the respective distributions of scores and comparisons with known ground truth. **G**, **H**, Trial-averaged calcium activity traces for cells classified as **G**, time cells; **H**, other cells.

serial and these do not use the additional cores. We found that most algorithms ran to completion requiring \sim 15 MB/dataset at a rate of \sim 1–4 s/dataset (135 cells/dataset). With 67 cells/dataset, the memory requirement and runtimes are approximately halved, suggesting that computational costs in memory and time were roughly linear with dataset size. We note that the analysis algorithms work independently for each cell. Thus, in principle, the analysis could be run in an embarrassingly parallel manner and should scale well on multicore architectures.

The synthesis of the main benchmarking datasets ($N=567$ datasets or 76,545 total cells) required a more powerful analysis machine, running a 6 core AMD Ryzen 5 3600, 32GB of DDR4 RAM, running MATLAB R2021a on Ubuntu 20.04. Dataset batches up to \sim 30 datasets ($N=40,500$ cells), however, could be easily handled by a less powerful laptop. The memory usage and runtime for

135 cells per dataset were accordingly, \sim 30 MB/dataset requiring \sim 1 s to complete. Thus, the methods scale readily to handle large datasets on modern hardware.

Physiologic range tests show sensitivity to noise but not to other features of the dataset

We next set out to see how these methods would work in estimated physiological ranges of signal confounds. Given our categorical labels on the synthetic data, we were able to split the datasets to look for the effects of the five main parameters: noise, event widths, imprecision, hit trial ratio, and background activity. We first computed the baseline physiology readouts keeping noise to 10%, event widths to the 60th percentile (± 1 SD), imprecision to 0 frames, hit trial ratios to a range of 33–66%, and background activity to 0.9–1.2 events/trial for time cells

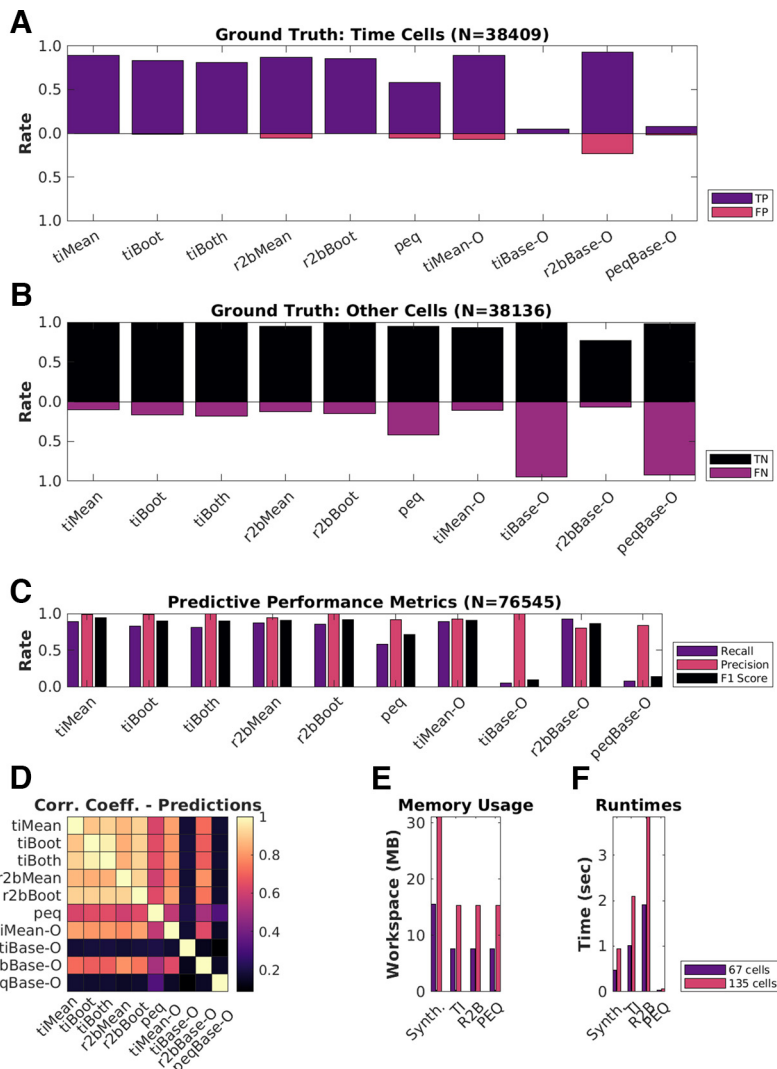


Figure 5. Good predictive performance by all algorithms. **A, B,** Classification performance of each of the 10 implemented detection algorithms. **A,** True positives (TP; purple), false positives (FP; red). **B,** True negatives (TN; black), false negatives (FN; purple). **C,** Predictive performance metrics [Recall = TP/(TP + FN), Precision = TP/(TP + FP), and F1 Score = Harmonic mean of Recall and Precision] to consolidate the confusion matrices. **D,** Pairwise correlation coefficients between the Boolean prediction lists by each of the 10 detection algorithms. Note that the first six methods correlate strongly. **E,** Average memory usage per dataset by the implemented algorithms on datasets with either 67 cells (purple) or 135 cells (red). **F,** Average runtimes per dataset by the implemented algorithms on datasets with either 67 cells (purple) or 135 cells (red).

(~50% of all synthetically generated cells, $N=50$ baseline datasets, 135 cells/dataset, 60 trials/dataset). Next, we established dependency slopes for each of the algorithms, based on their predictions ($N=10$ randomized shuffles for each case; Fig. 6B–F; Extended Data Figs. 6-1, 6-2).

Most methods exhibited a negative dependence of noise (range: 10% to 70%) on prediction F1 score (Fig. 6B). Although many methods are designed with some form of denoising strategy (trial-averaging, etc.), as expected all algorithms ran into classification difficulties at higher Noise levels. This reinforces the value of relatively high signal-to-noise recordings.

The relative insensitivity to event widths (Fig. 6C) is potentially useful for calcium imaging datasets where events may be slow, and in cases where slower tuning curves are

expected. However, this criterion may need to be stringent for analyses that need to precisely identify fine differences in cell responses.

We observed that most algorithms were insensitive to how frequently time cells were active across trials in a session (HTR). This is possibly the reason for the potential confusion among physiologists with regard to how many time cells were expected in a recorded dataset.

We found that the first six algorithms (tiMean, tiBoot, tiBoth, r2bMean, r2bBoot, and peq) gave equivalent predictions in ~66% of cases (Extended Data Fig. 6-1A). Next, we considered the various prediction lists across these top six algorithms and looked for consensus in time cell predictions from the most lenient threshold (“ ≥ 1 ” algorithm), incrementally through the most stringent threshold (“ $=10$ ” algorithms). We thus established a

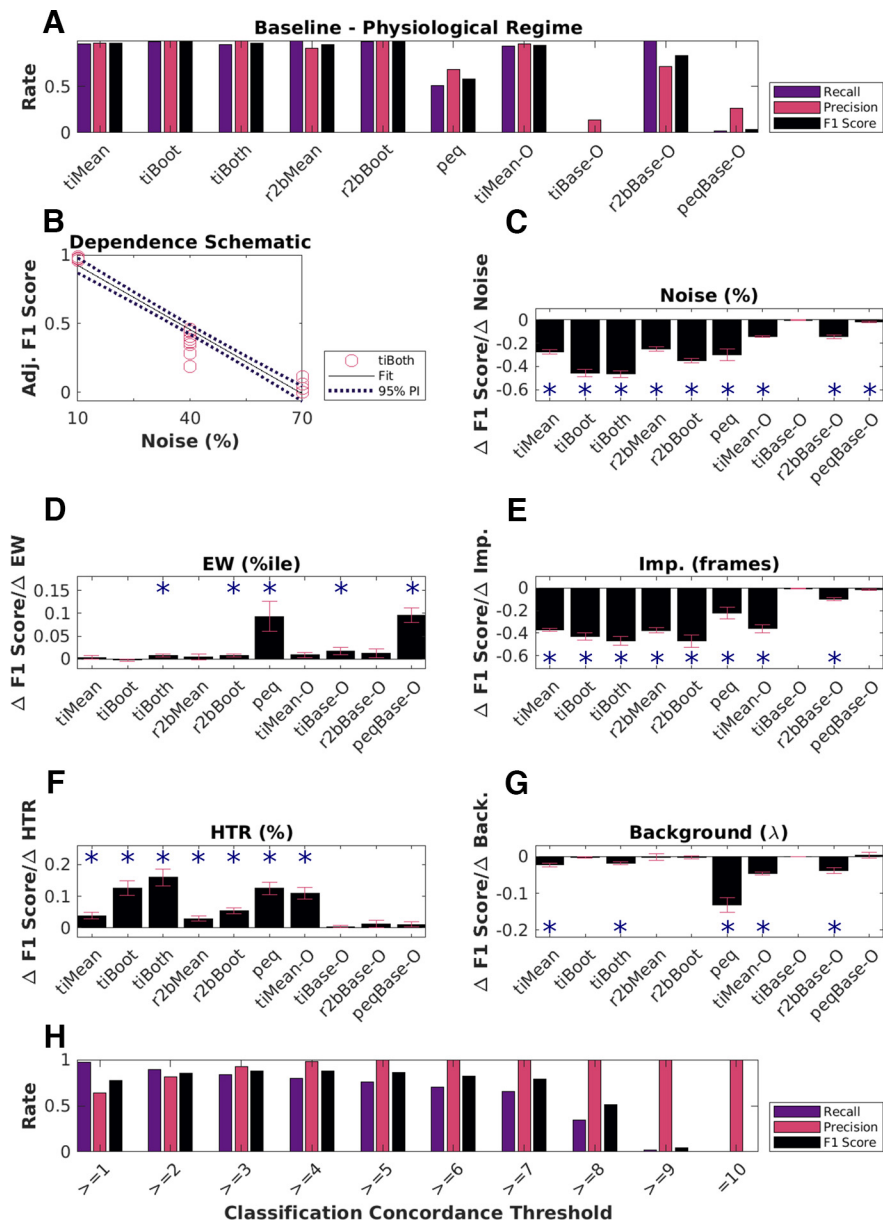


Figure 6. Physiological sensitivity analysis and concordance. **A**, Classification performance scores for all algorithms with the baseline physiology synthetic datasets ($N=6750$ cells). The first five methods perform well. Peq does poorly by all measures when confronted with physiology-range activity variability. Otsu's threshold method for score classification also does not work well for any method under physiological conditions. **B**, Dependence of F1 score on noise as a schematic. This has an overall negative slope (dashed line) which was used for panel **C**, TI-both. A similar calculation was performed for each method. Panels **C–G**, Parameters were systematically modulated one at a time with respect to baseline and the impact on classification score for each algorithm was estimated by computing the slope, using repeats over 10 datasets each with an independent random seed. Significant dependence on the perturbing parameter was determined by testing whether the slope differed from 0 at $p < 0.01$, indicated by asterisks using the MATLAB function `coeffTest()`. Plotted here are bar graphs with mean and error as RMSE normalized by the square root of N ($N=10$ datasets). **C**, Dependence on noise %. **D**, Dependence on event width percentiles. **E**, Dependence on imprecision frames. **F**, Dependence on hit trial ratio (HTR; %). **G**, Background activity (Poisson distribution mean, λ). **H**, Classification performance using concordance for a range of classification thresholds. Extended Data Figure 6-1 describes the three-point line plot dependency curves for the F1 score for each of the implemented algorithms against each of the five main parameters modulated, as the mean of $N=10$ datasets for each case, with error bars as SD. Extended Data Figure 6-2 showcases the linear regression fits for the same, with 95% prediction intervals (PIs), used to estimate the slopes of the various dependency curves.

Concordance based metric for time cell classification. We tested the predictive power of this Concordance based metric, which considers time cells based on consensus among the predictions from all the 10 implemented algorithms.

We identified differences in the classification performance, across the full range of concordance thresholds (Fig. 6H). With lower threshold values (“ $>=4$ ” and below), we notice a slight drop in the Precision, indicating an

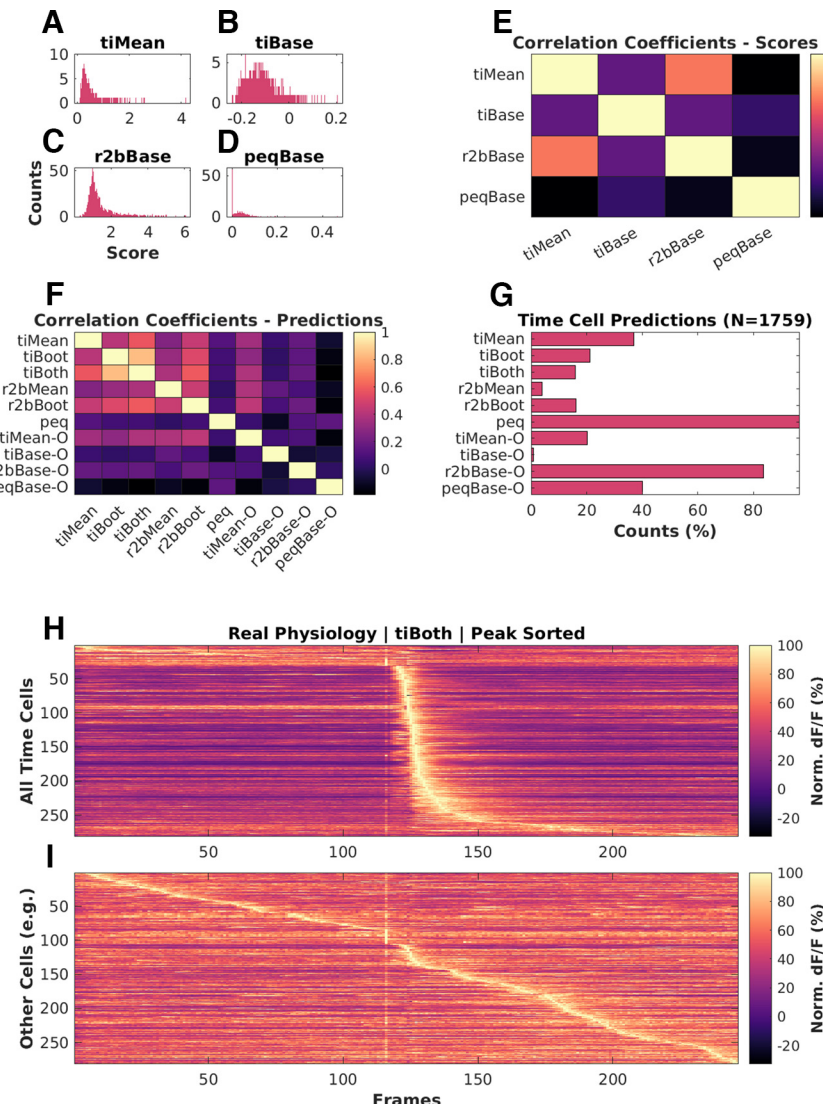


Figure 7. Analysis of experimental 2-P recordings of Ca^{2+} signals. **A–D**, Histograms of scores for physiologically recorded *in vivo* calcium activity from hippocampal CA1 cells (total $N = 1759$), by (A) tiMean, (B) tiBase, (C) r2bBase, and (D) peqBase. **E**, Pairwise correlation coefficients between the distributions of analog scores by the four scoring methods. **F**, Pairwise correlation coefficients between the Boolean prediction lists by the 10 detection algorithms. **G**, Numbers of positive class (time cell) predictions by each of the detection algorithms. **H, I**, Trial-averaged calcium activity traces for (**H**) time cells and (**I**) other cells. LED conditioned stimulus (CS) is presented at frame number 116, as seen by the bright band of the stimulus artifact. Most cells classified as time cells are active just after the stimulus. There is a characteristic broadening of the activity peak for classified time cells at longer intervals after the stimulus. Some of the cells at the top of panel **H** may be false positives because their tuning curve is very wide or because of picking up the stimulus transient. Similarly, some of the cells in the middle of panel **I** may be false negatives because of stringent cutoffs, although they appear to be responsive to the stimulus.

increase in false positive rate (Type I error). On the other hand, with increasing threshold values it is the Recall that drops, suggesting a higher false negative rate (Type II error). We find that a concordance threshold of “ $>=4$ ” achieves the best recall, precision, and F1 scores, for time cell prediction (Fig. 6F). The utility of this approach is subject to the availability of resources to apply multiple algorithms to each dataset.

Time cells identified in real physiology recordings

We used the 10 different implemented algorithms on *in vivo* 2-P calcium recordings ($N = 13$ datasets, namely,

1759 isolated cells from three animals across chronically recorded datasets), to compare time cell classification between the algorithms. As we observed for the synthetic data, experimental 2-P Ca traces also yielded different base scores from the four different methods (Fig. 7A–D). Again, consistent with the synthetic data, the pairwise correlation was weak to moderate (Fig. 7E). When we consider the boolean prediction lists (Fig. 7F), we observed moderate pairwise correlation between tiMean, tiBoot, tiBoth, r2bMean, and r2bBoot (>0.5), and low or weak correlation between the other pairs (<0.5). This was consistent with observations for the synthetic data but the correlations were overall slightly

weaker. The total number of time cells predicted were also different across the implemented algorithms (Fig. 7G). Algorithms such as *r2bBase-O* and *peq*, which had more false positives (Fig. 5B) also had more cells classified as time cells. The converse was not true. *r2bMean*, which had moderate false negatives as well as false positives on the synthetic dataset, classified very few of the experimental set as time cells. The trial-averaged activity of the detected time cells (Fig. 7H; including false positives) and other cells (Fig. 7I), based on the predictions by *tiBoth*, are shown. The experimentally recorded time cells exhibited a characteristic widening of tuning curves (Pastalkova et al., 2008; MacDonald et al., 2011, 2013; Kraus et al., 2013; Mau et al., 2018) with tuning to later time points (Fig. 7H).

Overall, four of the algorithms from the literature seemed consistent in their classifications as well as having reasonable numbers of classified time cells. These were the three algorithms from Mau et al. (2018; *tiMean*, *tiBoot*, and *tiBoth*), and the *r2bBoot* method derived from Modi et al. (2014). This is broadly in agreement with their performance on the synthetic datasets.

Discussion

We have developed a full pipeline for comparing time cell detection algorithms. This starts with synthetic datasets for benchmarking, in which we program in the ground truth of cell identity and timed activity, and a range of perturbations characteristic of experiments. These include noise, event widths, trial-pair timing imprecision, hit trial ratio, and background activity. This resource is, in itself, a key outcome of the current study, and though it is designed for 2-P calcium imaging data it can be extended to rate-averaged single-unit recordings. We built a pipeline for running and comparing the outcome from five methods derived from two previous studies, and one from the current work. These algorithms were applied to synthetic and experimental datasets and compared against each other and, where possible, against ground truth. We observed that most algorithms perform well and substantially agree in their time cell classification, but there were different degrees of sensitivity to different forms of signal variability, notably noise and imprecision.

The value of synthetic data in experimental science

Synthetic neural activity datasets are valuable in at least two main ways: evaluating algorithms for detection of important activity features, and for delivering stimuli to *in vitro* and simulated neurons, so as to provide a more physiological context in which to study input-output properties (Abbasi et al., 2020). While we have deployed our synthetic dataset for the specific purpose of comparing time cell detection algorithms, we suggest that it could also be useful for evaluating sequence analysis algorithms (Ikegaya et al., 2004; Foster and Wilson, 2006; Villette et al., 2015). Beyond the domain of neuronal data analysis, such synthetic datasets act as a test-bed for critique and development of analysis algorithms meant for deployment on real-world or typical use case data. They have been used previously to benchmark unsupervised outlier detection

(Steinbuss and Bohm, 2020), explainable machine learning (Liu et al., 2021), intrusion detection systems (Iannucci et al., 2017), 3D reconstruction algorithms (Koch et al., 2021), among several others. We report the first use of synthetic data pertaining to cellular physiology in the context of identifying time cells from network recordings. Moreover, our experiments study important operational differences across several previously published and new detection algorithms.

Our dataset may also be valuable for the second use case, stimulus delivery. There is a growing body of work on network detection of sequences (Ikegaya et al., 2004; Foster and Wilson, 2006; Csicsvari et al., 2007; Jadhav et al., 2012; Villette et al., 2015; Malvache et al., 2016) or even single-neuron sequence selectivity (Branco et al., 2010; Bhalla, 2017). More realistic input activity patterns with a range of physiological perturbations may be useful probes for such experimental and theoretical studies. Further, experimenter-defined neural activity inputs through optogenetic stimulation has already begun to use more complex temporal patterns than static or periodic illumination (Schrader et al., 2008; Dhawale et al., 2010; Bhatia et al., 2021). Our approaches to synthetic sequential neuronal activity generation may be useful to add more physiological dimensions to the sequential activity employed in such studies.

Further dimensions of time cell modulation

Our experiments allowed us to probe for parametric dependence systematically across published and new algorithms. We observed little or no dependence of the predictive performance (F1 score) of the various algorithms to event widths, hit trial ratios, and background activity. We did observe the F1 scores for most algorithms to be negatively dependent on noise and imprecision. On the one hand, this is a useful outcome in that different methods yield similar time-cell classification. It is a limitation, however, if the network uses such response features for coding, since it means that these methods are insensitive to relevant response changes. Further potential coding dimensions were not explored. Thus, several potential behavioral correlates of tuned cells (Ranck, 1973), could not be studied in our experiments. Such correlates include but are not limited to measurements of spatial navigation (O'Keefe and Dostrovsky, 1971; O'Keefe and Nadel, 1978; Wilson and McNaughton, 1993) and decision-making (Foster and Wilson, 2006; Csicsvari et al., 2007; Diba and Buzsáki, 2007; Davidson et al., 2009; Karlsson and Frank, 2009; Gupta et al., 2010; MacDonald et al., 2013; Villette et al., 2015), as well as navigation across tone frequencies (Aronov and Tank, 2014). While each of these further inputs would be interesting to incorporate into synthetic datasets, this requires that the time cell generation algorithm itself incorporate some form of simulation of the neural context. This is beyond the scope of the current study.

A specific limitation of our dataset is that it assumes that time is encoded by individual neurons. This leaves out population encoding schemes in which no one cell responds with the level of precision or consistency that would clear the criteria we use. For example, many of the same studies that use the methods tested here also use

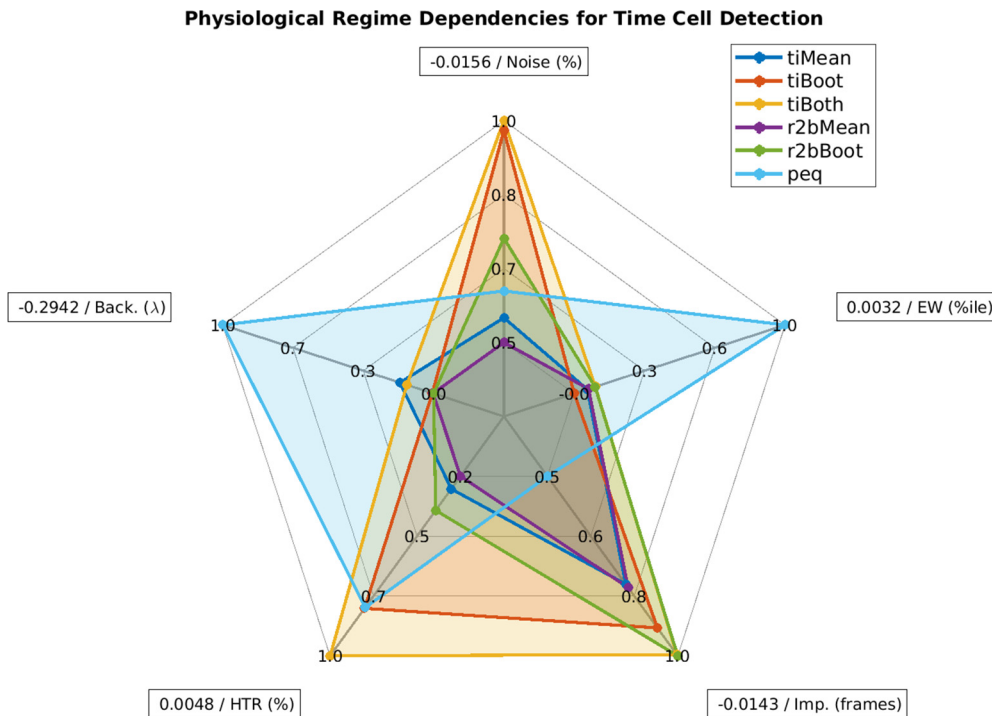


Figure 8. Spider plot summary. Relative sensitivity of the six best detection algorithms (*tiMean*, *tiBoot*, *tiBoth*, *r2bMean*, *r2bBoth*, and *peq*) to the five main parameters for data variability, noise (%), event widths (%ile), imprecision (frames), hit trial ratio (%), and background activity (λ). A perfect algorithm would have very small values (i.e., low sensitivity) for each of the parameters and, thus, occupy only the smallest pentagon in the middle. Note that even the maximal absolute value of sensitivity for most parameters (outer perimeter) is quite small, indicated in boxes at the points of the spider plot.

neural network decoders to report time (Mau et al., 2018). Such decoders might detect time encoding without time cells. A similar situation of individual versus network coding appears for the closely related problem of sequence representation. Place cell replay sequences have been shown to be modulated by the prevalence of location specific aversive (Wu et al., 2017) as well as appetitive stimuli (Bhattarai et al., 2020). Such physiological findings have been the subject of theoretical models of behavior planning (Foster, 2017; Mattar and Daw, 2018), and have been reported to improve performance on multiple Atari games by artificial neural networks (Mnih et al., 2015) featuring salience detection and experience mapping. We suggest that synthetic data for such higher-order encoding schemes might be a useful tool, and could draw on the approaches in the current study.

Comparative analysis benchmarks and concordance

A particularly challenging time cell classification problem is when the same cells may play different timing roles, such as forward and reverse replay. This is made more difficult because of the relative rarity of forward replay sequences over the more typical reverse replay (Diba and Buzsáki, 2007; Foster, 2017). Preplay is also a topic of some debate (Dragoi and Tonegawa, 2013; Foster, 2017). At least one possible problem in such debates is the degree of consistency between time cell or sequence classifiers. Our pipeline allows for (1) error correction in case of nonconcordant classifications, (2) suggest candidate algorithms

with a dependence on dataset features like event widths, imprecision, and hit trial ratio, as well as (3) the possibility to expand the detection regime in more realistic physiological datasets using concordance.

Which algorithms to use?

We did not set out to rank algorithms, but our analysis does yield suggestions for possible use domains based on sensitivity to experimental perturbations (Fig. 8). In cases where runtime and compute resource use is a concern, we recommend using the temporal information method with Bootstrap along with the activity filter (*tiBoth*). Combinations of *tiBoth* with *r2bBoth* may be useful where there are rare and potentially multimodally tuned time cells (Pastalkova et al., 2008; Villette et al., 2015), either to combine their classification for stringent time cell identification, or to pool their classified cells. While it is tempting to use Otsu's threshold as a very fast alternative to bootstrapping, we found that none of the Otsu variants of these methods did a good job of classification. Ultimately, five of our algorithms *tiMean*, *tiBoot*, *tiBoth*, *r2bMean*, and *r2bBoth*: all based on either Mau et al. (2018) or Modi et al. (2014), have very good Precision, and classify with very few false positives (low Type I error). Many methods are susceptible to classification errors if the dataset has high noise.

Here we also implemented the parametric equation (*peq*) algorithm. It is not very good for time cell classification per se, as it is prone to false positives and is susceptible to noise and low hit trial ratios. However, it generates useful

additional estimates of the four key parameters of real data, namely, noise, hit trial ratio, event width and imprecision. This is useful for a first-pass characterization of the properties of the dataset.

Sequence detection in large-scale recordings and scaling of analysis runs

The discovery of replay over the past two decades, has benefitted from the technological advances made in increasing the cellular yield of network recordings and has been reviewed previously (Foster, 2017). Further advances such as with the large scale recordings of $\sim 10^3$ single units by electrical recording using Neuropixels (Jun et al., 2017), fast volumetric fluorescence scanning with up to $\sim 10^4$ cells using resonant electro-optic imaging (Poort et al., 2015; Pachitariu et al., 2017; Bowman and Kasevich, 2021), $\sim 10^3$ mesoscopes (Sofroniew et al., 2016), as well as advances in automated cell region of interest (ROI) detection, denoising, and neuropil subtraction (Pachitariu et al., 2017; Pnevmatikakis et al., 2016) only increase the scale and size of datasets, likely leading to longer analysis runtimes. In addition to our recommendations above for the temporal information/boot method for scalable time-cell analysis, our C++/Python implementations may also be useful in further optimizing these methods. Our implementations allow for relatively fast analysis of the same datasets with multiple algorithms.

References

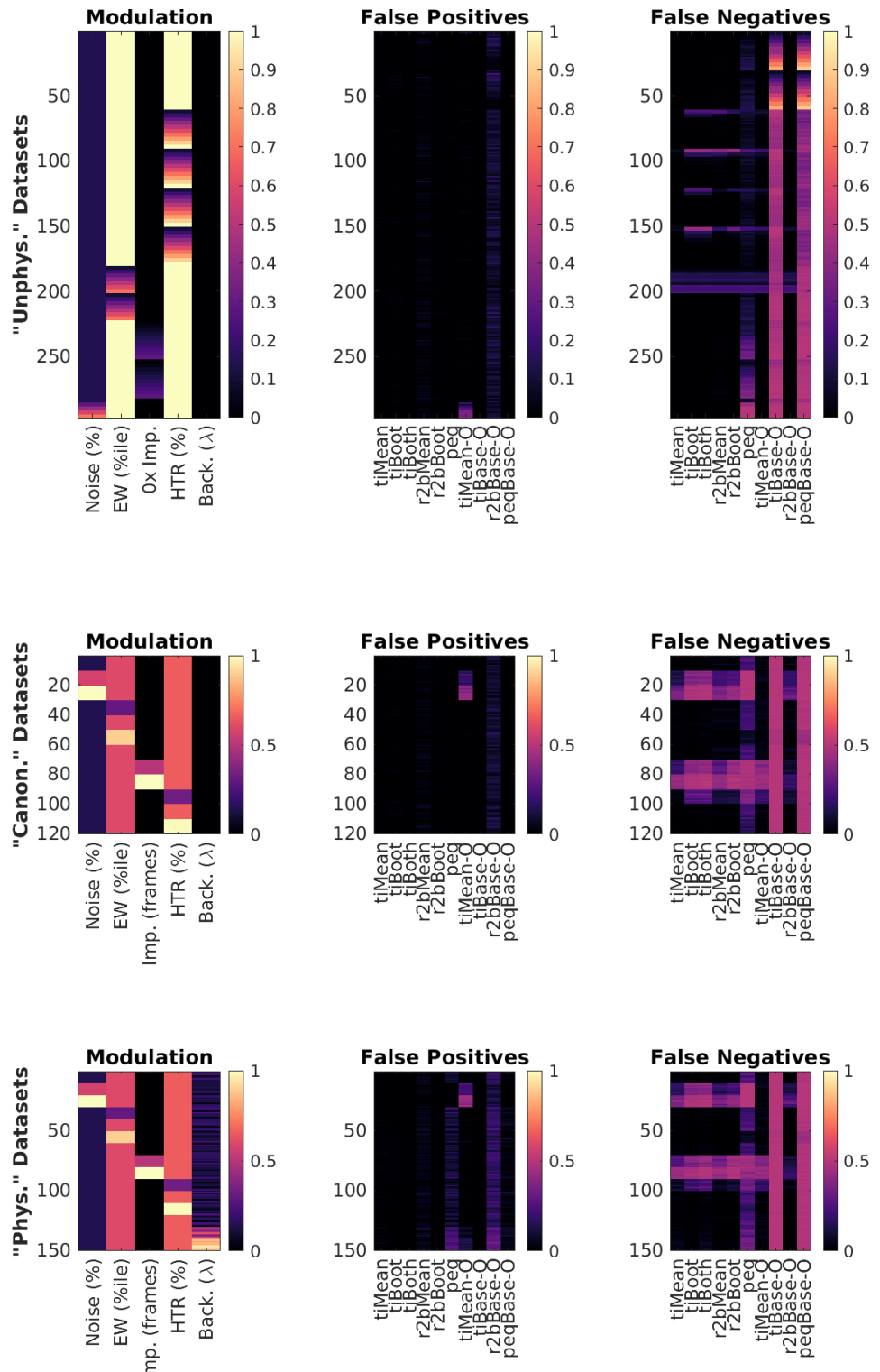
- Abbasi S, Maran S, Jaeger D (2020) A general method to generate artificial spike train populations matching recorded neurons. *J Comput Neurosci* 48:47–63.
- Ahmed MS, Priestley JB, Castro A, Stefanini F, Solis Canales AS, Balough EM, Lavoie E, Mazzucato L, Fusi S, Losonczy A (2020) Hippocampal network reorganization underlies the formation of a temporal association memory. *Neuron* 107:283–291.e6.
- Aronov D, Tank DW (2014) Engagement of neural circuits underlying 2D spatial navigation in a rodent virtual reality system. *Neuron* 84:442–456.
- Bhalla US (2017) Synaptic input sequence discrimination on behavioral timescales mediated by reaction-diffusion chemistry in dendrites. *Elife* 6:e25827.
- Bhatia A, Moza S, Bhalla US (2021) Patterned optogenetic stimulation using a DMD projector. *Methods Mol Biol* 2191:173–188.
- Bhattarai B, Lee JW, Jung MW (2020) Distinct effects of reward and navigation history on hippocampal forward and reverse replays. *Proc Natl Acad Sci U S A* 117:689–697.
- Bowman AJ, Kasevich MA (2021) Resonant electro-optic imaging for microscopy at nanosecond resolution. *ACS Nano* 15:16043–16054.
- Branco T, Clark BA, Häusser M (2010) Dendritic discrimination of temporal input sequences in cortical neurons. *Science* 329:1671–1675.
- Collett D (2002) Modeling binary data. London: Chapman and Hall.
- Csicsvari J, O'Neill J, Allen K, Senior T (2007) Place-selective firing contributes to the reverse-order reactivation of CA1 pyramidal cells during sharp waves in open-field exploration. *Eur J Neurosci* 26:704–716.
- Davidson TJ, Kloosterman F, Wilson MA (2009) Hippocampal replay of extended experience. *Neuron* 63:497–507.
- Dhawale AK, Hagiwara A, Bhalla US, Murthy VN, Albeau DF (2010) Non-redundant odor coding by sister mitral cells revealed by light addressable glomeruli in the mouse. *Nat Neurosci* 13:1404–1412.
- Diba K, Buzsáki G (2007) Forward and reverse hippocampal place-cell sequences during ripples. *Nat Neurosci* 10:1241–1242.
- Dombeck DA, Harvey CD, Tian L, Looger LL, Tank DW (2010) Functional imaging of hippocampal place cells at cellular resolution during virtual navigation. *Nat Neurosci* 13:1433–1440.
- Dragoi G, Tonegawa S (2013) Distinct preplay of multiple novel spatial experiences in the rat. *Proc Natl Acad Sci U S A* 110:9100–9105.
- Eichenbaum H (2017) On the integration of space, time, and memory. *Neuron* 95:1007–1018.
- Foster DJ (2017) Replay comes of age. *Annu Rev Neurosci* 40:581–602.
- Foster DJ, Wilson MA (2006) Reverse replay of behavioural sequences in hippocampal place cells during the awake state. *Nature* 440:680–683.
- Gupta AS, van der Meer MAA, Touretzky DS, Redish AD (2010) Hippocampal replay is not a simple function of experience. *Neuron* 65:695–705.
- Iannucci S, Kholidy HA, Ghimire AD, Jia R, Abdelwahed S, Banicescu I (2017) A comparison of graph-based synthetic data generators for benchmarking next-generation intrusion detection systems. 2017 IEEE International Conference on Cluster Computing (CLUSTER), Honolulu, HI, pp. 278–289, <https://doi.org/10.1109/CLUSTER.2017.54>.
- Ikegaya Y, Aaron G, Cossart R, Aronov D, Lampl I, Ferster D, Yuste R (2004) Synfire chains and cortical songs: temporal modules of cortical activity. *Science* 304:559–564.
- Jadhav SP, Kemere C, German PW, Frank LM (2012) Awake hippocampal sharp-wave ripples support spatial memory. *Science* 336:1454–1458.
- Jun JJ, et al. (2017) Fully integrated silicon probes for high-density recording of neural activity. *Nature* 551:232–236.
- Kaifosh P, Lovett-Barron M, Turi GF, Reardon TR, Losonczy A (2013) Septo-hippocampal GABAergic signaling across multiple modalities in awake mice. *Nat Neurosci* 16:1182–1184.
- Karlsson MP, Frank LM (2009) Awake replay of remote experiences in the hippocampus. *Nat Neurosci* 12:913–918.
- Koch S, Worcel M, Silva C, Alexa M (2021) Hardware Design and Accurate Simulation of Structured-Light Scanning for Benchmarking of 3D Reconstruction Algorithms (Vol. 2021). Proceedings of the Neural Information Processing Systems Track on Datasets and Benchmarks 1 (NeurIPS Datasets and Benchmarks 2021). Retrieved from <https://openreview.net/forum?id=bNL5VfTe3p>.
- Kraus B, Robinson R, White J, Eichenbaum H, Hasselmo M (2013) Hippocampal “time cells”: time versus path integration. *Neuron* 78:1090–1101.
- Lee AK, Wilson MA (2004) A combinatorial method for analyzing sequential firing patterns involving an arbitrary number of neurons based on relative time order. *J Neurophysiol* 92:2555–2573.
- Liu Y, Khandagale S, White C, Neiswanger W (2021) Synthetic benchmarks for scientific research in explainable machine learning. <https://github.com/abacusai/xai-bench>.
- MacDonald CJ, Lepage KQ, Eden UT, Eichenbaum H (2011) Hippocampal “time cells” bridge the gap in memory for discontinuous events. *Neuron* 71:737–749.
- MacDonald CJ, Carrow S, Place R, Eichenbaum H (2013) Distinct hippocampal time cell sequences represent odor memories in immobilized rats. *J Neurosci* 33:14607–14616.
- Malvache A, Reichinnek S, Villette V, Haimerl C (2016) Awake hippocampal reactivations project onto orthogonal neuronal assemblies. *353:1280–1283*.
- Mattar MG, Daw ND (2018) Prioritized memory access explains planning and hippocampal replay. *Nat Neurosci* 21:1609–1617.
- Mau W, Sullivan DW, Kinsky NR, Hasselmo ME, Howard MW, Eichenbaum H (2018) The same hippocampal CA1 population simultaneously codes temporal information over multiple time-scales. *Curr Biol* 28:1499–1508.e4.
- Mnih V, Kavukcuoglu K, Silver D, Rusu AA, Veness J, Bellemare MG, Graves A, Riedmiller M, Fidjeland AK, Ostrovski G, Petersen S, Beattie C, Sadik A, Antonoglou I, King H, Kumaran D, Wierstra D,

- Legg S, Hassabis D (2015) Human-level control through deep reinforcement learning. *Nature* 518:529–533.
- Modi MN, Dhawale AK, Bhalla US (2014) CA1 cell activity sequences emerge after reorganization of network correlation structure during associative learning. *Elife* 3:e01982.
- Mokeichev A, Okun M, Barak O, Katz Y, Ben-Shahar O, Lampl I (2007) Stochastic emergence of repeating cortical motifs in spontaneous membrane potential fluctuations in vivo. *Neuron* 53:413–425.
- O'Keefe J, Dostrovsky J (1971) The hippocampus as a spatial map. Preliminary evidence from unit activity in the freely-moving rat. *Brain Res* 34:171–175.
- O'Keefe J, Nadel L (1978) The hippocampus as a cognitive map. Oxford: Clarendon Press.
- Otsu N (1979) A threshold selection method from gray level histograms. *IEEE Trans Syst Man Cyber* 9:62–66.
- Pachitariu M, Stringer C, Dipoppa M, Schröder S, Rossi LF (2017) Suite2p: beyond 10,000 neurons with standard two-photon microscopy. *BioRxiv* 061507. <https://doi.org/https://doi.org/10.1101/061507>.
- Pastalkova E, Itskov V, Amarasingham A, Buzsáki G (2008) Internally generated cell assembly sequences in the rat hippocampus. *Science* 321:1322–1327.
- Pnevmatikakis EA, Soudry D, Gao Y, Machado TA, Merel J, Pfau D, Reardon T, Mu Y, Lacefield C, Yang W, Ahrens M, Bruno R, Jessell TM, Peterka DS, Yuste R, Paninski L (2016) Simultaneous denoising, deconvolution, and demixing of calcium imaging data. *Neuron* 89:285–299.
- Poort J, Khan AG, Pachitariu M, Nemri A, Orsolic I, Krupic J, Bauza M, Sahani M, Keller GB, Mrsic-Flogel TD, Hofer SB (2015) Learning enhances sensory and multiple non-sensory representations in primary visual cortex. *Neuron* 86:1478–1490.
- Ranck JB, J (1973) Studies on single neurons in dorsal hippocampal formation and septum in unrestrained rats. I. Behavioral correlates and firing repertoires. *Exp Neurol* 41:461–531.
- Schrader S, Grün S, Diesmann M, Gerstein GL (2008) Detecting synfire chain activity using massively parallel spike train recording. *J Neurophysiol* 100:2165–2176.
- Siegel JJ, Taylor W, Gray R, Kalmbach B, Zemelman BV, Desai NS, Johnston D, Chitwood RA (2015) Trace eyeblink conditioning in mice is dependent upon the dorsal medial prefrontal cortex, cerebellum, and amygdala: behavioral characterization and functional circuitry. *eNeuro* 2:ENEURO.0051-14.2015.
- Sofroniew NJ, Flickinger D, King J, Svoboda K (2016) A large field of view two-photon mesoscope with subcellular resolution for in vivo imaging. *Elife* 5:e14472.
- Souza BC, Pavão R, Belchior H, Tort ABL (2018) On information metrics for spatial coding. *Neuroscience* 375:62–73.
- Steinbuss G, Bohm K (2020) Generating artificial outliers in the absence of genuine ones—a survey. *arXiv*. <https://doi.org/10.48550/arXiv.2006.03646>.
- Tseng W, Guan R, Disterhoft JF, Weiss C (2004) Trace eyeblink conditioning is hippocampally dependent in mice. *Hippocampus* 14:58–65.
- Villette V, Malvache A, Tressard T, Dupuy N, Cossart R (2015) Internally recurring hippocampal sequences as a population template of spatiotemporal information. *Neuron* 88:357–366.
- Wilson MA, McNaughton BL (1993) Dynamics of the hippocampal ensemble code for space. *Science* 261:1055–1058.
- Wu CT, Haggerty D, Kemere C, Ji D (2017) Hippocampal awake replay in fear memory retrieval. *Nat Neurosci* 20:571–580.

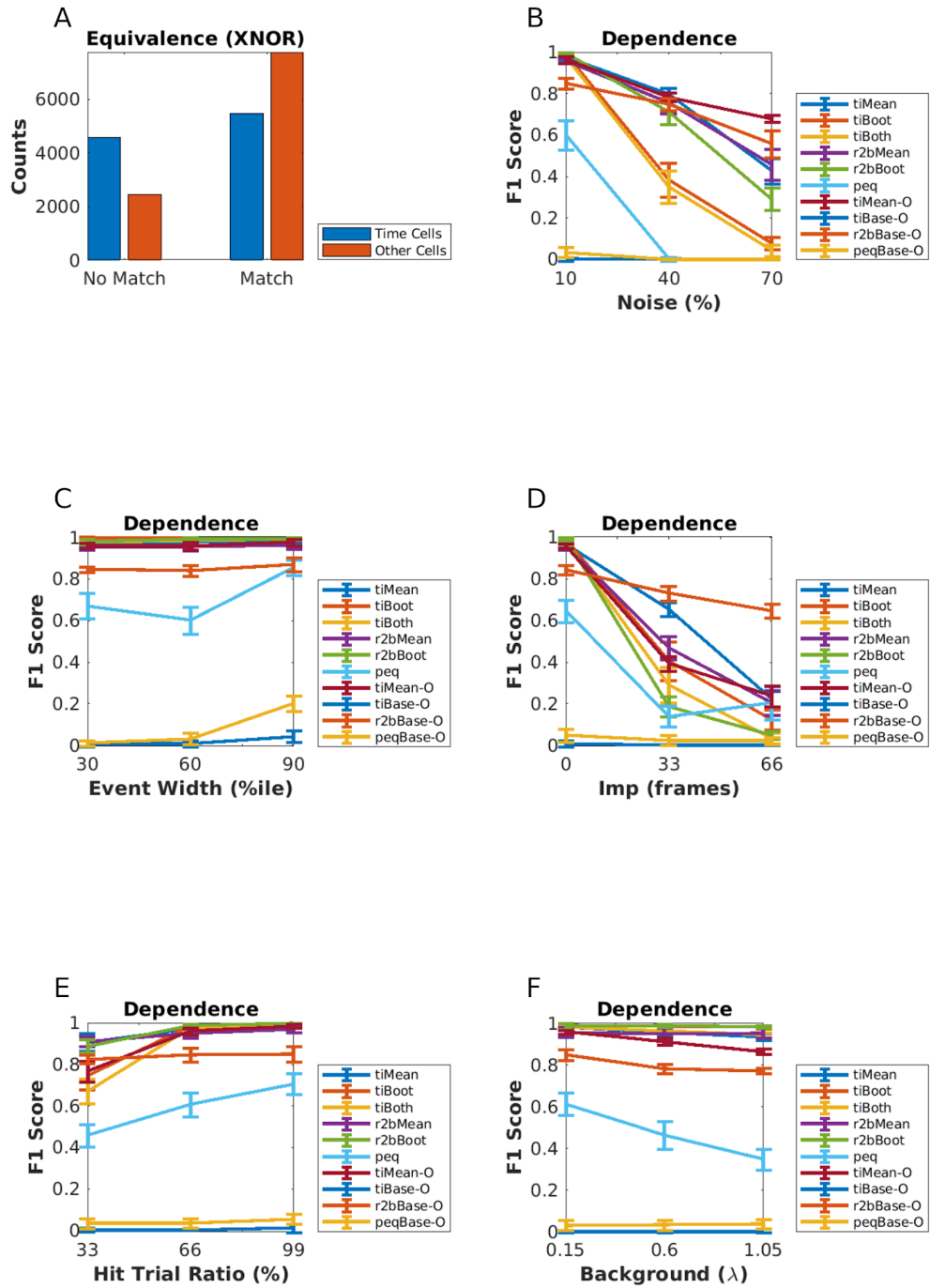
2789 **Extended Data Figures (Supplementary)**

2790

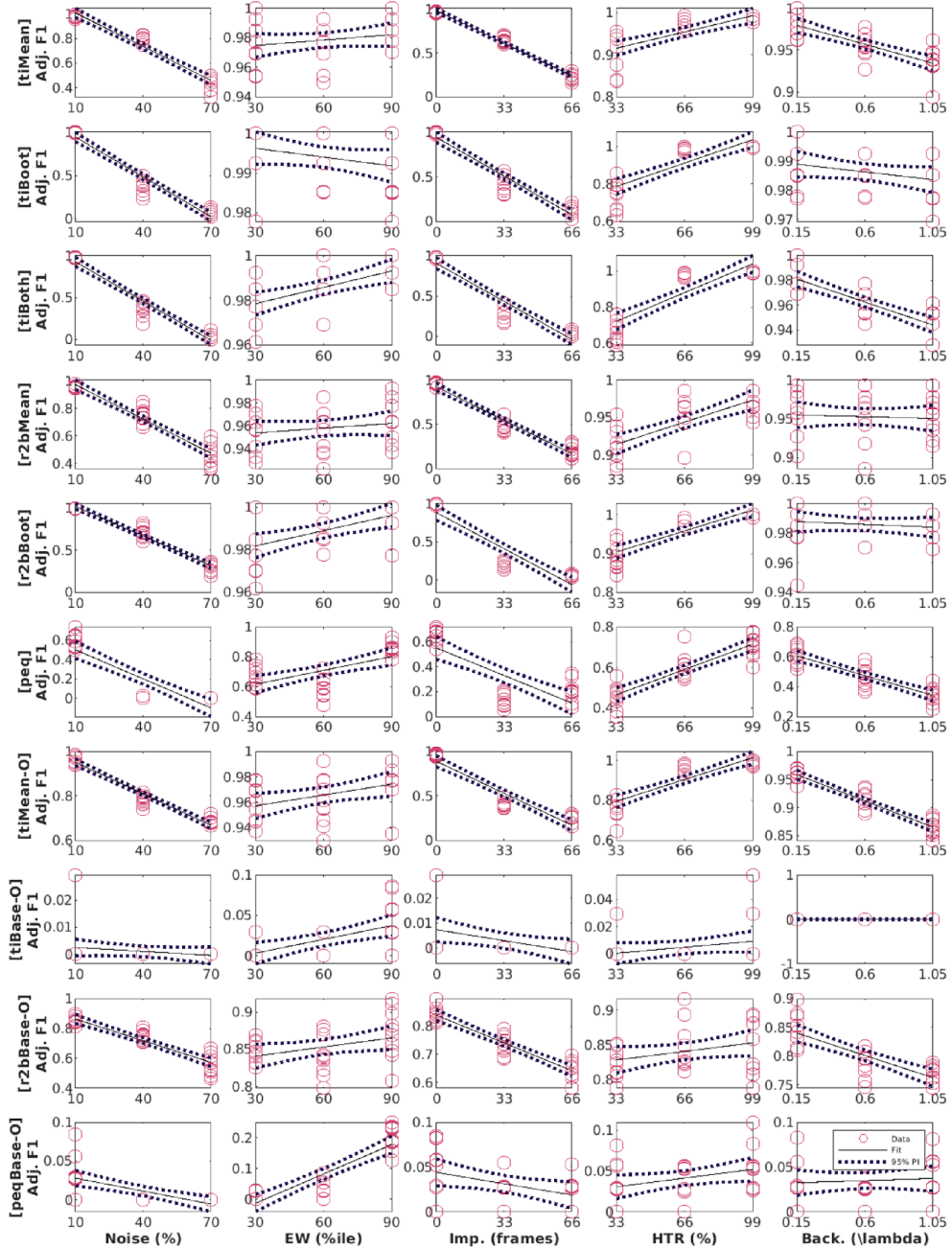
2791 **Figure 1-1.** Modulation profile along with the False Positive and False
2792 Negative rates per dataset, for important parameters configured in each of
2793 the 567 synthetic datasets generated. A-C: “Unphysiological Regime”, D-F:
2794 “Canonical Regime”, G-I: “Physiological Regime”.



2796 **Figure 6-1.** A: Equivalence by XNOR matching the prediction lists from the
2797 top six detection algorithms (Blue: Time Cells; Red: Other Cells). B-F:
2798 Dependence of the predictive performance (F1 Score) on the various
2799 important synthetic dataset configuration parameters, B: Noise (%), C: Event
2800 Width (%ile), D: Imprecision (frames), E: Hit Trial Ratio (%), and F:
2801 Background Activity (λ).



2803 Figure 6-2: Linear Regression fits for all algorithm parameter dependence
2804 curves with data points (red circles), best fit line (black), and the 95%
2805 prediction interval (PI; dotted black lines). The columns represent the
2806 physiology regime modulation parameter (out of the 5 main parameters
2807 tested), and the rows represent the various implemented algorithms for time
2808 cell detection.



2810 **Chapter 5 – Discussion**

2811 **The study of hippocampal CA1 sequences**

2812

2813 The standardized protocols described in the thesis are expected to aid
2814 in future experiments studying hippocampal CA1 sequences. Our
2815 simultaneous 2-photon calcium imaging recordings and behavioural
2816 training provided us the platform to study neural activity from ~100-150
2817 cells/animal at behaviourally relevant timescales (~70 ms per frame).

2818

2819 We standardized a multi-day Trace Eye-Blink Conditioning ("Chapter 2
2820 - Behaviour") training system for mice based on previous literature
2821 (Modi et al., 2014; Siegel et al., 2015) and could demonstrate several
2822 types of behavioural adaptations that experimental animals could learn
2823 under a variety of experiment conditions and modulations. Notably,

2824 1. The animals typically learnt the tasks quickly, within 1-2 weeks of
2825 training.

2826 2. Modulating the inter-stimulus interval (ISI) between the CS and
2827 US results affected the expression of the conditioned response (CR).

2828 3. A wide palette of stimuli may now be incorporated into existing
2829 protocols as either of the presented stimuli

2830

2831 Simultaneous large-scale recordings have been fundamental to the
2832 discovery of long spatiotemporal activity patterns with several
2833 participant CA1 neurons (Davidson et al., 2009; Foster, 2017).
2834 Electrical recordings provide many orders of magnitude better temporal
2835 resolution, not to mention being a direct readout of action potentials.

2836 However at the time of the design of the thesis, imaging based
2837 approaches could yield more recorded neurons per experiment animal.
2838 We standardized 2-photon fluorescence based chronic imaging of
2839 hippocampal CA1 neurons to allow calcium imaging based recording of
2840 the spatiotemporal sequences across multiple days ("Chapter 3 -
2841 Imaging"). This gave us the ability to,
2842 1. Record neurophysiology over a large population of neurons
2843 (~100), in conjunction with temporally relevant behavioural contexts
2844 and modulations, albeit at ~100 ms temporal resolution.
2845 2. Chronically track cells across various behaviour sessions without
2846 ambiguity.
2847 3. Allow for scalability in the per animal yield of recording neurons with
2848 the use of faster and modern 2-photon microscope hardware utilizing
2849 Resonant Scanning instead of Galvo-Scanning, as well as multi-
2850 channel imaging.

2851

2852 We could identify time cells with the ability to retain, de-tune, or even
2853 re-tune, over the course of multiple sessions. Given no change in the
2854 behaviour protocol variables, it is unlikely we would have found such
2855 adaptations without scaling up the yield of cells or improving our
2856 temporal resolution while recording each individual session. Since the
2857 behaviour task is typically learnt to ~70-80% performance levels over
2858 the course of multiple sessions, our methodology gives us the ability to
2859 look into learning mechanisms utilized by the CA1 in the interim.

2860 Production quality datasets were quickly obtained by colleagues in the
2861 lab, following the protocols standardized and described here.

2862

2863 From our preliminary data, the largest proportion of re-tuned cells had
2864 tuning peaks shift to earlier time points (Chapter 3 – "Imaging", Figure

2865 37), with subsequent sessions. Early in training, the timing of tuning
2866 peaks would typically occur near the time of the Unconditioned
2867 Stimulus (US; air-puff to eye). Our experiments presenting stimuli to
2868 naive animals (in accordance with Dhawale, 2013) suggested that
2869 somatosensory stimuli may be able to modulate CA1 responses, while
2870 many neutral stimuli may not (Chapter 3 – “Imaging”, Figure 29),
2871 without training. These results do allow for speculation on how initially
2872 neutral Conditioned Stimuli (CS; Light LED pulse) could develop
2873 behavioural valence for the animal, viz., the selective suppression of
2874 Response Inhibition to the previously neutral CS. An as yet unknown
2875 fraction of time cells may initially be triggered by the Unconditioned
2876 Stimulus (US; air-puff), but over the course of multiple training
2877 sessions, shift tuning fields to respond to the CS at the level of the CA1
2878 network. However, many more datasets would be required to firmly
2879 establish any mechanistic insight into the phenomenon.
2880

2881 **Mapping sequences to abstract variables**

2882
2883 Visual cues are typically considered important to place cell activity and
2884 tuning. The specific requirement of vision, however, was tested in a
2885 study published in 2015. Experimenters switched off the lights as their
2886 animals navigated a maze. The animals were provided only olfactory
2887 cues at specific locations in the maze, yet place cell activity and tuning
2888 could be recorded. This suggested that the hippocampus could use
2889 non-visuospatial resources to generate spatial representations, when
2890 vision was compromised (Zhang & Manahan-Vaughan, 2015).
2891

2892 In a sound manipulation task (SMT) rats changed the frequency of
2893 auditory tones in their environment, by self-initiated joystick control,
2894 ramping logarithmic sweeps of frequency space. The rate of change in
2895 frequency could be manipulated either by the animal or
2896 pseudorandomly by the experimenter. This study describes neural
2897 activity recorded from the medial entorhinal cortex (MEC) as well as
2898 the hippocampal CA1 with sub-populations that were found tuned to
2899 specific frequency “landmarks” during the auditory sequence (Aronov
2900 et al., 2017). The CA1 were, thus, argued to be capable of tuning to
2901 abstract variables and were designed to map out sequences of
2902 events/stimuli in their own spatiotemporal patterns of activity.

2903

2904 The ubiquity of neural sequences in a wide variety of systems has
2905 been discussed previously (Bhalla, 2019; Conen & Desrochers, 2022;
2906 S. Zhou et al., 2020) and over a century of research has discovered
2907 remarkable physiological features that may be used to identify neurons
2908 that participate in these sequences. However, research is still required
2909 to carefully dissect out the contribution that each participant neuron
2910 has to behaviour, an important goal in neuroscience (Ranck, 1973,
2911 1975).

2912

2913 The use of user-configurable, categorically labeled synthetic calcium
2914 activity profiles allowed us to probe and compare a range of different
2915 time cell detection algorithms, identifying strategies to best classify
2916 time cells. We were able to identify Temporal Information as a strong
2917 contender for the choice of algorithm for such classification (“Chapter 4
2918 - Analysis”; Ananthamurthy & Bhalla, 2023). The algorithms developed
2919 along the way were tested within the time scales of ~100 ms, that
2920 correspond to Replay Sequences or other behaviour timescale

2921 sequences. We expect the analysis routines to be useful in a variety of
2922 different experiments that could potentially help describe the neural
2923 code in more detail.

2924 **Does the brain create or predict?**

2925
2926 Predictive coding has been considered as a way for the brain to
2927 ultimately use external sensory information to minimize prediction
2928 errors during tasks (Doya et al., 2007; Rao & Ballard, 1999). One of
2929 the core ideas of Bayesian approaches to neurophysiology and
2930 behaviour is that the brain could be modeled as a prediction machine
2931 that is constantly modeling the change of variables. These variables
2932 may be external or internal yet salient concepts to any experimental
2933 animal, arguably expressed in neurophysiology as the dynamics of
2934 engrams. The ability of the mammalian hippocampus to bind both
2935 information streams to create new, more elaborate engrams, is likely
2936 crucial to the learning of new concepts behaviourally (N. J. Cohen &
2937 Eichenbaum, 1993; Eichenbaum, 2017).

2938
2939 Attentional states have been shown to have a bidirectional relationship
2940 with the expression of memory and learning (Chun & Johnson, 2011;
2941 Hutchinson & Turk-Browne, 2012; Uncapher et al., 2011). Specifically,
2942 Trace Eye-Blink Conditioning (TEC) performance has been suggested
2943 to be positively correlated with attention (Manns et al., 2000). The
2944 question of the effect of attentional states on the dynamics of the
2945 associated engram motivated an important milestone for the thesis,
2946 *viz.*, to combine stable, adaptable behaviour studies with large-scale
2947 neurophysiology.

2948
2949 We were able to train head-fixed mice to TEC and confirm adaptable
2950 conditioned responses to task variables. We were also able to
2951 simultaneous record from ~100 hippocampal CA1 cell bodies as the
2952 animals acquired top behavioural performance. We observed in our
2953 preliminary results that many identified time cells showcased the ability
2954 to tune to different time points across sessions or days, as has been
2955 previously reported (Mau et al., 2018). This standardization of
2956 simultaneous behaviour and imaging ensured that colleagues from our
2957 lab were able to generate production quality data, quickly.
2958
2959 Several more high quality recordings and behaviour modulations would
2960 be required to conclusively describe time cells physiology and engram
2961 dynamics, at least at the level of a sub-population of hippocampal CA1.
2962 However, progress has been made to suggest the best time cell
2963 detection algorithm(s) based on their sensitivity to different recording
2964 parameters (Ananthamurthy & Bhalla, 2023). We hope that the thesis
2965 is of aid to future research on the neural mechanisms of Learning and
2966 Memory by the nervous system.
2967

2968 **Bibliography**

- 2969 Ananthamurthy, K. G., & Bhalla, U. S. (2023). Synthetic Data Resource
2970 and Benchmarks for Time Cell Analysis and Detection Algorithms.
2971 *ENeuro*, ENEURO.0007-22.2023.
2972 <https://doi.org/10.1523/ENEURO.0007-22.2023>
- 2973 Aronov, D., Nevers, R., & Tank, D. W. (2017). Mapping of a non-spatial
2974 dimension by the hippocampal-entorhinal circuit. *Nature*,
2975 543(7647), 719–722. <https://doi.org/10.1038/nature21692>

- 2976 Bhalla, U. S. (2019). Dendrites, deep learning, and sequences in the
2977 hippocampus. *Hippocampus*, 29(3), 239–251.
2978 <https://doi.org/https://doi.org/10.1002/hipo.22806>
- 2979 Chun, M. M., & Johnson, M. K. (2011). Memory: enduring traces of
2980 perceptual and reflective attention. *Neuron*, 72(4), 520–535.
2981 <https://doi.org/10.1016/j.neuron.2011.10.026>
- 2982 Cohen, N. J., & Eichenbaum, H. (1993). *Memory, amnesia, and the*
2983 *hippocampal system*.
- 2984 Conen, K. E., & Desrochers, T. M. (2022). *The Neural Basis of*
2985 *Behavioral Sequences in Cortical and Subcortical Circuits*. Oxford
2986 University Press.
2987 <https://doi.org/10.1093/acrefore/9780190264086.013.421>
- 2988 Davidson, T. J., Kloosterman, F., & Wilson, M. A. (2009). Hippocampal
2989 replay of extended experience. *Neuron*, 63(4), 497–507.
2990 <https://doi.org/10.1016/j.neuron.2009.07.027>
- 2991 Dhawale, A. K. (2013). *Temporal and spatial features of sensory*
2992 *coding in the olfactory bulb and hippocampus*. Tata Institute of
2993 Fundamental Research.
- 2994 Doya, K., Ishii, S., Pouget, A., & Rao, R. P. N. (2007). Bayesian brain:
2995 Probabilistic approaches to neural coding. In K. Doya, S. Ishii, A.
2996 Pouget, & R. P. N. Rao (Eds.), *Bayesian brain: Probabilistic*
2997 *approaches to neural coding*. MIT Press.
- 2998 Eichenbaum, H. (2017). On the Integration of Space, Time, and
2999 Memory. *Neuron*, 95(5), 1007–1018.
3000 <https://doi.org/10.1016/j.neuron.2017.06.036>
- 3001 Foster, D. J. (2017). Replay Comes of Age. *Annual Review of*
3002 *Neuroscience*, 40, 581–602. <https://doi.org/10.1146/annurev-neuro-072116-031538>
- 3004 Hutchinson, J. B., & Turk-Browne, N. B. (2012). Memory-guided
3005 attention: control from multiple memory systems. *Trends in*
3006 *Cognitive Sciences*, 16(12), 576–579.
3007 <https://doi.org/10.1016/j.tics.2012.10.003>

- 3008 Manns, J. R., Clark, R. E., & Squire, L. R. (2000). Parallel acquisition
3009 of awareness and trace eyeblink classical conditioning. *Learning*
3010 & *Memory* (Cold Spring Harbor, N.Y.), 7(5), 267–272.
3011 <https://doi.org/10.1101/lm.33400>
- 3012 Mau, W., Sullivan, D. W., Kinsky, N. R., Hasselmo, M. E., Howard, M.
3013 W., & Eichenbaum, H. (2018). The Same Hippocampal CA1
3014 Population Simultaneously Codes Temporal Information over
3015 Multiple Timescales. *Current Biology*, 28(10), 1499-1508.e4.
3016 <https://doi.org/10.1016/j.cub.2018.03.051>
- 3017 Modi, M. N., Dhawale, A. K., & Bhalla, U. S. (2014). CA1 cell activity
3018 sequences emerge after reorganization of network correlation
3019 structure during associative learning. *eLife*, 3, e01982–e01982.
3020 <https://doi.org/10.7554/eLife.01982>
- 3021 Ranck, J. B. (1973). Studies on single neurons in dorsal hippocampal
3022 formation and septum in unrestrained rats: Part I. Behavioral
3023 correlates and firing repertoires. *Experimental Neurology*, 41(2),
3024 462–531. [https://doi.org/https://doi.org/10.1016/0014-4886\(73\)90290-2](https://doi.org/10.1016/0014-4886(73)90290-2)
- 3025
- 3026 Ranck, J. B. (1975). *Behavioral Correlates and Firing Repertoires of
3027 Neurons in the Dorsal Hippocampal Formation and Septum of
3028 Unrestrained Rats BT - The Hippocampus: Volume 2:
3029 Neurophysiology and Behavior* (R. L. Isaacson & K. H. Pribram
3030 (Eds.); pp. 207–244). Springer US. https://doi.org/10.1007/978-1-4684-2979-4_7
- 3031
- 3032 Rao, R. P. N., & Ballard, D. H. (1999). Predictive coding in the visual
3033 cortex: a functional interpretation of some extra-classical
3034 receptive-field effects. *Nature Neuroscience*, 2(1), 79–87.
3035 <https://doi.org/10.1038/4580>
- 3036 Siegel, J. J., Taylor, W., Gray, R., Kalmbach, B., Zemelman, B. V.,
3037 Desai, N. S., Johnston, D., & Chitwood, R. A. (2015). Trace
3038 Eyeblink Conditioning in Mice Is Dependent upon the Dorsal
3039 Medial Prefrontal Cortex, Cerebellum, and Amygdala: Behavioral
3040 Characterization and Functional Circuitry. *ENeuro*, 2(4),

- 3041 ENEURO.0051-14.2015. <https://doi.org/10.1523/ENEURO.0051-14.2015>
- 3043 Uncapher, M. R., Hutchinson, J. B., & Wagner, A. D. (2011).
3044 Dissociable effects of top-down and bottom-up attention during
3045 episodic encoding. *The Journal of Neuroscience : The Official
3046 Journal of the Society for Neuroscience*, 31(35), 12613–12628.
3047 <https://doi.org/10.1523/JNEUROSCI.0152-11.2011>
- 3048 Zhang, S., & Manahan-Vaughan, D. (2015). Spatial olfactory learning
3049 contributes to place field formation in the hippocampus. *Cerebral
3050 Cortex (New York, N.Y. : 1991)*, 25(2), 423–432.
3051 <https://doi.org/10.1093/cercor/bht239>
- 3052 Zhou, S., Masmanidis, S. C., & Buonomano, D. V. (2020). Neural
3053 Sequences as an Optimal Dynamical Regime for the Readout of
3054 Time. *Neuron*, 108(4), 651-658.e5.
3055 <https://doi.org/https://doi.org/10.1016/j.neuron.2020.08.020>

3056 All Bibliography

- 3057
- 3058 Abe, R., Sakaguchi, T., Matsumoto, N., Matsuki, N., & Ikegaya, Y.
3059 (2014). Sound-induced hyperpolarization of hippocampal neurons.
3060 *Neuroreport*, 25(13), 1013–1017.
3061 <https://doi.org/10.1097/WNR.0000000000000206>
- 3062 Abeles, M. (1982). *Local Cortical Circuits: An Electrophysiological Study*. Springer-Verlag. <https://books.google.co.in/books?id=s25lwwEACAAJ>
- 3063
- 3064
- 3065 Abeles, M. (1991). *Corticonics: Neural Circuits of the Cerebral Cortex*.
3066 Cambridge University Press. <https://doi.org/DOI:10.1017/CBO9780511574566>
- 3066
- 3067
- 3068 Abeles, M. (2004). Time Is Precious. *Science*, 304(5670), 523–524.
3069 <https://doi.org/10.1126/science.1097725>
- 3070 Abeles, M. (2009). *Synfire Chains* (L. R. B. T.-E. of N. Squire (Ed.); pp.
3071 829–832). Academic Press.
3072 <https://doi.org/https://doi.org/10.1016/B978-008045046-9.01437-6>
- 3073 Abeles, M., Hayon, G., & Lehmann, D. (2004). Modeling
3074 compositionality by dynamic binding of synfire chains. *Journal of
3075 Computational Neuroscience*, 17(2), 179–201.
3076 <https://doi.org/10.1023/B:JCNS.0000037682.18051.5f>
- 3077 Ananthamurthy, K. G., & Bhalla, U. S. (2023). Synthetic Data Resource
3078 and Benchmarks for Time Cell Analysis and Detection Algorithms.
3079 *ENeuro*, ENEURO.0007-22.2023.
3080 <https://doi.org/10.1523/ENEURO.0007-22.2023>
- 3081 Andermann, M. L., Gilfoy, N. B., Goldey, G. J., Sachdev, R. N. S.,
3082 Wölfel, M., McCormick, D. A., Reid, R. C., & Levene, M. J. (2013).
3083 Chronic Cellular Imaging of Entire Cortical Columns in Awake
3084 Mice Using Microprisms. *Neuron*, 80(4), 900–913.
3085 <https://doi.org/10.1016/j.neuron.2013.07.052>

- 3086 Andersen, P., Morris, R., Amaral, D., Bliss, T., & O'Keefe, J. (Eds.).
3087 (2006). *The Hippocampus Book*. Oxford University Press.
3088 <https://doi.org/10.1093/acprof:oso/9780195100273.001.0001>
- 3089 Andersen, R. A., Snyder, L. H., Li, C.-S., & Stricanne, B. (1993).
3090 Coordinate transformations in the representation of spatial
3091 information. *Current Opinion in Neurobiology*, 3(2), 171–176.
3092 [https://doi.org/https://doi.org/10.1016/0959-4388\(93\)90206-E](https://doi.org/https://doi.org/10.1016/0959-4388(93)90206-E)
- 3093 Aronov, D., Nevers, R., & Tank, D. W. (2017). Mapping of a non-spatial
3094 dimension by the hippocampal-entorhinal circuit. *Nature*,
3095 543(7647), 719–722. <https://doi.org/10.1038/nature21692>
- 3096 Attardo, A., Fitzgerald, J. E., & Schnitzer, M. J. (2015). Impermanence
3097 of dendritic spines in live adult CA1 hippocampus. *Nature*,
3098 523(7562), 592–596. <https://doi.org/10.1038/nature14467>
- 3099 Barreto, R. P. J., Messerschmidt, B., & Schnitzer, M. J. (2009). In vivo
3100 fluorescence imaging with high-resolution microlenses. *Nature
Methods*, 6(7), 511–512. <https://doi.org/10.1038/nmeth.1339>
- 3102 Barreto, R. P. J., & Schnitzer, M. J. (2012). In vivo optical
3103 microendoscopy for imaging cells lying deep within live tissue.
3104 *Cold Spring Harbor Protocols*, 2012(10), 1029–1034.
3105 <https://doi.org/10.1101/pdb.top071464>
- 3106 Bellistri, E., Aguilar, J., Brotons-Mas, J. R., Foffani, G., & de la Prida, L.
3107 M. (2013). Basic properties of somatosensory-evoked responses
3108 in the dorsal hippocampus of the rat. *The Journal of Physiology*,
3109 591(10), 2667–2686. <https://doi.org/10.1113/jphysiol.2013.251892>
- 3110 Bhalla, U. S. (2019). Dendrites, deep learning, and sequences in the
3111 hippocampus. *Hippocampus*, 29(3), 239–251.
3112 <https://doi.org/https://doi.org/10.1002/hipo.22806>
- 3113 Bienenstock, E. (1995). A model of neocortex. *Network: Computation
3114 in Neural Systems*, 6(2), 179–224. [https://doi.org/10.1088/0954-898X_6_2_004](https://doi.org/10.1088/0954-
3115 898X_6_2_004)

- 3116 Bjerknes, T. L., Moser, E. I., & Moser, M.-B. (2014). Representation of
3117 Geometric Borders in the Developing Rat. *Neuron*, 82(1), 71–78.
3118 <https://doi.org/10.1016/j.neuron.2014.02.014>
- 3119 Brown, G. D. (1998). Nonassociative learning processes affecting
3120 swimming probability in the seashell Tritonia diomedea:
3121 habituation, sensitization and inhibition. *Behavioural Brain
3122 Research*, 95(2), 151–165.
3123 [https://doi.org/https://doi.org/10.1016/S0166-4328\(98\)00072-2](https://doi.org/https://doi.org/10.1016/S0166-4328(98)00072-2)
- 3124 Buzsáki, G., & Llinás, R. (2017). Space and time in the brain. *Science
3125 (New York, N.Y.)*, 358(6362), 482–485.
3126 <https://doi.org/10.1126/science.aan8869>
- 3127 Cai, D. J., Aharoni, D., Shuman, T., Shobe, J., Biane, J., Song, W.,
3128 Wei, B., Veshkini, M., La-Vu, M., Lou, J., Flores, S. E., Kim, I.,
3129 Sano, Y., Zhou, M., Baumgaertel, K., Lavi, A., Kamata, M.,
3130 Tuszyński, M., Mayford, M., ... Silva, A. J. (2016). A shared neural
3131 ensemble links distinct contextual memories encoded close in
3132 time. *Nature*, 534(7605), 115–118.
3133 <https://doi.org/10.1038/nature17955>
- 3134 Caporale, N., & Dan, Y. (2008). Spike timing-dependent plasticity: a
3135 Hebbian learning rule. *Annual Review of Neuroscience*, 31, 25–
3136 46. <https://doi.org/10.1146/annurev.neuro.31.060407.125639>
- 3137 Carew, T. J., Castellucci, V. F., & Kandel, E. R. (1971). An Analysis of
3138 Dishabituation and Sensitization of The Gill-Withdrawal Reflex In
3139 Aplysia. *International Journal of Neuroscience*, 2(2), 79–98.
3140 <https://doi.org/10.3109/00207457109146995>
- 3141 Chen, T.-W., Wardill, T. J., Sun, Y., Pulver, S. R., Renninger, S. L.,
3142 Baohan, A., Schreiter, E. R., Kerr, R. A., Orger, M. B., Jayaraman,
3143 V., Looger, L. L., Svoboda, K., & Kim, D. S. (2013). Ultrasensitive
3144 fluorescent proteins for imaging neuronal activity. *Nature*,
3145 499(7458), 295–300. <https://doi.org/10.1038/nature12354>
- 3146 Chun, M. M., & Johnson, M. K. (2011). Memory: enduring traces of
3147 perceptual and reflective attention. *Neuron*, 72(4), 520–535.
3148 <https://doi.org/10.1016/j.neuron.2011.10.026>

- 3149 Cohen, M. R., & Kohn, A. (2011). Measuring and interpreting neuronal
3150 correlations. *Nature Neuroscience*, 14(7), 811–819.
3151 <https://doi.org/10.1038/nn.2842>
- 3152 Cohen, N. J., & Eichenbaum, H. (1993). *Memory, amnesia, and the*
3153 *hippocampal system.*
- 3154 Conen, K. E., & Desrochers, T. M. (2022). *The Neural Basis of*
3155 *Behavioral Sequences in Cortical and Subcortical Circuits*. Oxford
3156 University Press.
3157 <https://doi.org/10.1093/acrefore/9780190264086.013.421>
- 3158 Csicsvari, J., O'Neill, J., Allen, K., & Senior, T. (2007). Place-selective
3159 firing contributes to the reverse-order reactivation of CA1
3160 pyramidal cells during sharp waves in open-field exploration. *The*
3161 *European Journal of Neuroscience*, 26(3), 704–716.
3162 <https://doi.org/10.1111/j.1460-9568.2007.05684.x>
- 3163 Davidson, T. J., Kloosterman, F., & Wilson, M. A. (2009). Hippocampal
3164 replay of extended experience. *Neuron*, 63(4), 497–507.
3165 <https://doi.org/10.1016/j.neuron.2009.07.027>
- 3166 Denk, W., Strickler, J. H., & Webb, W. W. (1990). Two-photon laser
3167 scanning fluorescence microscopy. *Science (New York, N.Y.)*,
3168 248(4951), 73–76. <https://doi.org/10.1126/science.2321027>
- 3169 Deshmukh, S. S., & Bhalla, U. S. (2003). Representation of odor
3170 habituation and timing in the hippocampus. *The Journal of*
3171 *Neuroscience : The Official Journal of the Society for*
3172 *Neuroscience*, 23(5), 1903–1915.
3173 <https://doi.org/10.1523/JNEUROSCI.23-05-01903.2003>
- 3174 Dhawale, A. K. (2013). *Temporal and spatial features of sensory*
3175 *coding in the olfactory bulb and hippocampus*. Tata Institute of
3176 Fundamental Research.
- 3177 Dhawale, A. K., Poddar, R., Wolff, S. B. E., Normand, V. A.,
3178 Kopelowitz, E., & Ölveczky, B. P. (2017). Automated long-term
3179 recording and analysis of neural activity in behaving animals.
3180 *eLife*, 6, e27702. <https://doi.org/10.7554/eLife.27702>

- 3181 Diba, K., & Buzsáki, G. (2007). Forward and reverse hippocampal
3182 place-cell sequences during ripples. *Nature Neuroscience*, 10(10),
3183 1241–1242. <https://doi.org/10.1038/nn1961>
- 3184 Dickinson, A., Nicholas, D. J., & Mackintosh, N. J. (1983). A re-
3185 examination of one-trial blocking in conditioned suppression. *The
3186 Quarterly Journal of Experimental Psychology B: Comparative
3187 and Physiological Psychology*, 35, 67–79.
3188 <https://doi.org/10.1080/14640748308400914>
- 3189 Dombeck, D. A., Graziano, M. S., & Tank, D. W. (2009). Functional
3190 clustering of neurons in motor cortex determined by cellular
3191 resolution imaging in awake behaving mice. *The Journal of
3192 Neuroscience : The Official Journal of the Society for
3193 Neuroscience*, 29(44), 13751–13760.
3194 <https://doi.org/10.1523/JNEUROSCI.2985-09.2009>
- 3195 Dombeck, D. A., Harvey, C. D., Tian, L., Looger, L. L., & Tank, D. W.
3196 (2010). Functional imaging of hippocampal place cells at cellular
3197 resolution during virtual navigation. *Nature Neuroscience*, 13(11),
3198 1433–1440. <https://doi.org/10.1038/nn.2648>
- 3199 Doya, K., Ishii, S., Pouget, A., & Rao, R. P. N. (2007). Bayesian brain:
3200 Probabilistic approaches to neural coding. In K. Doya, S. Ishii, A.
3201 Pouget, & R. P. N. Rao (Eds.), *Bayesian brain: Probabilistic
3202 approaches to neural coding*. MIT Press.
- 3203 Dragoi, G., & Buzsáki, G. (2006). Temporal encoding of place
3204 sequences by hippocampal cell assemblies. *Neuron*, 50(1), 145–
3205 157. <https://doi.org/10.1016/j.neuron.2006.02.023>
- 3206 Dragoi, G., Carpi, D., Recce, M., Csicsvari, J., & Buzsáki, G. (1999).
3207 Interactions between hippocampus and medial septum during
3208 sharp waves and theta oscillation in the behaving rat. *The Journal
3209 of Neuroscience : The Official Journal of the Society for
3210 Neuroscience*, 19(14), 6191–6199.
3211 <http://www.ncbi.nlm.nih.gov/pubmed/10407055>

- 3212 Dragoi, G., & Tonegawa, S. (2011). Preplay of future place cell
3213 sequences by hippocampal cellular assemblies. *Nature*,
3214 469(7330), 397–401. <https://doi.org/10.1038/nature09633>
- 3215 Dragoi, G., & Tonegawa, S. (2013). Distinct preplay of multiple novel
3216 spatial experiences in the rat. *Proceedings of the National
3217 Academy of Sciences of the United States of America*, 110(22),
3218 9100–9105. <https://doi.org/10.1073/pnas.1306031110>
- 3219 Eichenbaum, H. (2004). Hippocampus: Cognitive processes and
3220 neural representations that underlie declarative memory. *Neuron*,
3221 44(1), 109–120. <https://doi.org/10.1016/j.neuron.2004.08.028>
- 3222 Eichenbaum, H. (2017). On the Integration of Space, Time, and
3223 Memory. *Neuron*, 95(5), 1007–1018.
3224 <https://doi.org/10.1016/j.neuron.2017.06.036>
- 3225 Fanselow, M. S., & Dong, H.-W. (2010). Are the dorsal and ventral
3226 hippocampus functionally distinct structures? *Neuron*, 65(1), 7–19.
3227 <https://doi.org/10.1016/j.neuron.2009.11.031>
- 3228 Fassihi, A., Akrami, A., Pulecchi, F., Schönfelder, V., & Diamond, M. E.
3229 (2017). Transformation of Perception from Sensory to Motor
3230 Cortex. *Current Biology : CB*, 27(11), 1585-1596.e6.
3231 <https://doi.org/10.1016/j.cub.2017.05.011>
- 3232 Ferbinteanu, J., & Shapiro, M. L. (2003). Prospective and retrospective
3233 memory coding in the hippocampus. *Neuron*, 40(6), 1227–1239.
3234 [https://doi.org/10.1016/s0896-6273\(03\)00752-9](https://doi.org/10.1016/s0896-6273(03)00752-9)
- 3235 Ferbinteanu, J., Shirvalkar, P., & Shapiro, M. L. (2011). Memory
3236 Modulates Journey-Dependent Coding in the Rat Hippocampus.
3237 *The Journal of Neuroscience*, 31(25), 9135 LP – 9146.
3238 <https://doi.org/10.1523/JNEUROSCI.1241-11.2011>
- 3239 Foster, D. J. (2017). Replay Comes of Age. *Annual Review of
3240 Neuroscience*, 40, 581–602. <https://doi.org/10.1146/annurev-neuro-072116-031538>

- 3242 Foster, D. J., & Wilson, M. A. (2006). Reverse replay of behavioural
3243 sequences in hippocampal place cells during the awake state.
3244 *Nature*, 440(7084), 680–683. <https://doi.org/10.1038/nature04587>
- 3245 Foster, D. J., & Wilson, M. A. (2007). Hippocampal theta sequences.
3246 *Hippocampus*, 17(11), 1093–1099.
3247 <https://doi.org/10.1002/hipo.20345>
- 3248 Francis, M., Qian, X., Charbel, C., Ledoux, J., Parker, J. C., & Taylor,
3249 M. S. (2012). Automated region of interest analysis of dynamic
3250 Ca²⁺ signals in image sequences. *American Journal of*
3251 *Physiology. Cell Physiology*, 303(3), C236-43.
3252 <https://doi.org/10.1152/ajpcell.00016.2012>
- 3253 Frank, L. M., Brown, E. N., & Wilson, M. (2000). Trajectory encoding in
3254 the hippocampus and entorhinal cortex. *Neuron*, 27(1), 169–178.
3255 [https://doi.org/10.1016/s0896-6273\(00\)00018-0](https://doi.org/10.1016/s0896-6273(00)00018-0)
- 3256 Fyhn, M., Molden, S., Witter, M. P., Moser, E. I., & Moser, M.-B.
3257 (2004). Spatial representation in the entorhinal cortex. *Science*
3258 (*New York, N.Y.*), 305(5688), 1258–1264.
3259 <https://doi.org/10.1126/science.1099901>
- 3260 Giovannucci, A., Badura, A., Deverett, B., Najafi, F., Pereira, T. D.,
3261 Gao, Z., Ozden, I., Kloth, A. D., Pnevmatikakis, E., Paninski, L.,
3262 De Zeeuw, C. I., Medina, J. F., & Wang, S. S.-H. (2017).
3263 Cerebellar granule cells acquire a widespread predictive feedback
3264 signal during motor learning. *Nature Neuroscience*, 20(5), 727–
3265 734. <https://doi.org/10.1038/nn.4531>
- 3266 Grün, S. (2009). Data-Driven Significance Estimation for Precise Spike
3267 Correlation. *Journal of Neurophysiology*, 101(3), 1126–1140.
3268 <https://doi.org/10.1152/jn.00093.2008>
- 3269 Guo, Z. V., Hires, S. A., Li, N., O'Connor, D. H., Komiyama, T., Ophir,
3270 E., Huber, D., Bonardi, C., Morandell, K., Gutnisky, D., Peron, S.,
3271 Xu, N., Cox, J., & Svoboda, K. (2014). Procedures for Behavioral
3272 Experiments in Head-Fixed Mice. *PLOS ONE*, 9(2), e88678.
3273 <https://doi.org/10.1371/journal.pone.0088678>

- 3274 Gupta, A. S., van der Meer, M. A. A., Touretzky, D. S., & Redish, A. D.
3275 (2010). Hippocampal Replay Is Not a Simple Function of
3276 Experience. *Neuron*, 65(5), 695–705.
3277 <https://doi.org/https://doi.org/10.1016/j.neuron.2010.01.034>
- 3278 Hafting, T., Fyhn, M., Molden, S., Moser, M.-B., & Moser, E. I. (2005).
3279 Microstructure of a spatial map in the entorhinal cortex. *Nature*,
3280 436(7052), 801–806. <https://doi.org/10.1038/nature03721>
- 3281 Han, J.-H., Kushner, S. A., Yiu, A. P., Hsiang, H.-L. L., Buch, T.,
3282 Waisman, A., Bontempi, B., Neve, R. L., Frankland, P. W., &
3283 Josselyn, S. A. (2009). Selective erasure of a fear memory.
3284 *Science (New York, N.Y.)*, 323(5920), 1492–1496.
3285 <https://doi.org/10.1126/science.1164139>
- 3286 Harvey, C. D., Collman, F., Dombeck, D. A., & Tank, D. W. (2009).
3287 Intracellular dynamics of hippocampal place cells during virtual
3288 navigation. *Nature*, 461(7266), 941–946.
3289 <https://doi.org/10.1038/nature08499>
- 3290 Hebb, D. O. (1949). The organization of behavior; a
3291 neuropsychological theory. In *The organization of behavior; a*
3292 *neuropsychological theory*. Wiley.
- 3293 Helmchen, F., & Denk, W. (2005). *Deep tissue two-photon microscopy*.
3294 2(12), 9. <https://doi.org/10.1038/nmeth818>
- 3295 Heys, J. G., Rangarajan, K. V., & Dombeck, D. A. (2014). The
3296 Functional Micro-organization of Grid Cells Revealed by Cellular-
3297 Resolution Imaging. *Neuron*, 84(5), 1079–1090.
3298 <https://doi.org/10.1016/j.neuron.2014.10.048>
- 3299 Hjorth-Simonsen, A., & Jeune, B. (1972). Origin and termination of the
3300 hippocampal perforant path in the rat studied by silver
3301 impregnation. *The Journal of Comparative Neurology*, 144(2),
3302 215–232. <https://doi.org/10.1002/cne.901440206>
- 3303 Hubel, D. H., & Wiesel, T. N. (1962). Receptive fields, binocular
3304 interaction and functional architecture in the cat's visual cortex.
3305 *The Journal of Physiology*, 160(1), 106–154.
3306 <https://doi.org/10.1113/jphysiol.1962.sp006837>

- 3307 Hutchinson, J. B., & Turk-Browne, N. B. (2012). Memory-guided
3308 attention: control from multiple memory systems. *Trends in*
3309 *Cognitive Sciences*, 16(12), 576–579.
3310 <https://doi.org/10.1016/j.tics.2012.10.003>
- 3311 Ikegaya, Y., Aaron, G., Cossart, R., Aronov, D., Lampl, I., Ferster, D.,
3312 & Yuste, R. (2004). Synfire chains and cortical songs: temporal
3313 modules of cortical activity. *Science (New York, N.Y.)*, 304(5670),
3314 559–564. <https://doi.org/10.1126/science.1093173>
- 3315 Itskov, P. M., Vinnik, E., & Diamond, M. E. (2011). Hippocampal
3316 representation of touch-guided behavior in rats: persistent and
3317 independent traces of stimulus and reward location. *PloS One*,
3318 6(1), e16462. <https://doi.org/10.1371/journal.pone.0016462>
- 3319 Itskov, V., Pastalkova, E., Mizuseki, K., Buzsaki, G., & Harris, K. D.
3320 (2008). Theta-mediated dynamics of spatial information in
3321 hippocampus. *The Journal of Neuroscience : The Official Journal*
3322 *of the Society for Neuroscience*, 28(23), 5959–5964.
3323 <https://doi.org/10.1523/JNEUROSCI.5262-07.2008>
- 3324 Jadhav, S. P., Kemere, C., German, P. W., & Frank, L. M. (2012).
3325 Awake hippocampal sharp-wave ripples support spatial memory.
3326 *Science (New York, N.Y.)*, 336(6087), 1454–1458.
3327 <https://doi.org/10.1126/science.1217230>
- 3328 Jaramillo, S., & Zador, A. M. (2014). Mice and rats achieve similar
3329 levels of performance in an adaptive decision-making task . In
3330 *Frontiers in Systems Neuroscience* (Vol. 8).
3331 <https://www.frontiersin.org/articles/10.3389/fnsys.2014.00173>
- 3332 Josselyn, S. A., & Tonegawa, S. (2020). Memory engrams: Recalling
3333 the past and imagining the future. *Science (New York, N.Y.)*,
3334 367(6473). <https://doi.org/10.1126/science.aaw4325>
- 3335 Jun, J. J., Steinmetz, N. A., Siegle, J. H., Denman, D. J., Bauza, M.,
3336 Barbarits, B., Lee, A. K., Anastassiou, C. A., Andrei, A., Aydin, Ç.,
3337 Barbic, M., Blanche, T. J., Bonin, V., Couto, J., Dutta, B., Gratiy,
3338 S. L., Gutnisky, D. A., Häusser, M., Karsh, B., ... Harris, T. D.
3339 (2017). Fully integrated silicon probes for high-density recording of

- 3340 neural activity. *Nature*, 551(7679), 232–236.
3341 <https://doi.org/10.1038/nature24636>
- 3342 Kaifosh, P., Lovett-Barron, M., Turi, G. F., Reardon, T. R., & Losonczy,
3343 A. (2013). Septo-hippocampal GABAergic signaling across
3344 multiple modalities in awake mice. *Nature Neuroscience*, 16(9),
3345 1182–1184. <https://doi.org/10.1038/nn.3482>
- 3346 Kalmbach, B. E., Davis, T., Ohyama, T., Riusech, F., Nores, W. L., &
3347 Mauk, M. D. (2010). Cerebellar Cortex Contributions to the
3348 Expression and Timing of Conditioned Eyelid Responses. *Journal*
3349 *of Neurophysiology*, 103(4), 2039–2049.
3350 <https://doi.org/10.1152/jn.00033.2010>
- 3351 Kalmbach, B. E., Ohyama, T., & Mauk, M. D. (2010). Temporal
3352 Patterns of Inputs to Cerebellum Necessary and Sufficient for
3353 Trace Eyelid Conditioning. *Journal of Neurophysiology*, 104(2),
3354 627–640. <https://doi.org/10.1152/jn.00169.2010>
- 3355 Kamondi, A. (1998). *Theta Oscillations in Somata and Dendrites of*
3356 *Hippocampal Pyramidal Cells In Vivo: Activity-Dependent Phase-*
3357 *Precession of Action Potentials*. 261(March), 244–261.
- 3358 Khan, A. G., Parthasarathy, K., & Bhalla, U. S. (2010). Odor
3359 representations in the mammalian olfactory bulb. *Wiley*
3360 *Interdisciplinary Reviews. Systems Biology and Medicine*, 2(5),
3361 603–611. <https://doi.org/10.1002/wsbm.85>
- 3362 Kraus, B. J., Brandon, M. P., Robinson, R. J., Connerney, M. A.,
3363 Hasselmo, M. E., & Eichenbaum, H. (2015). During Running in
3364 Place, Grid Cells Integrate Elapsed Time and Distance Run.
3365 *Neuron*, 88(3), 578–589.
3366 <https://doi.org/10.1016/j.neuron.2015.09.031>
- 3367 Kraus, B., Robinson, R., White, J., Eichenbaum, H., & Hasselmo, M.
3368 (2013). Hippocampal “Time Cells”: Time versus Path Integration.
3369 *Neuron*, 78(6), 1090–1101.
3370 <https://doi.org/10.1016/j.neuron.2013.04.015>

- 3371 Kropff, E., Carmichael, J. E., Moser, M.-B., & Moser, E. I. (2015).
3372 Speed cells in the medial entorhinal cortex. *Nature*, 523(7561),
3373 419–424. <https://doi.org/10.1038/nature14622>
- 3374 Krupa, D., & Thompson, R. (2003). Inhibiting the Expression of a
3375 Classically Conditioned Behavior Prevents Its Extinction. *The
3376 Journal of Neuroscience : The Official Journal of the Society for
3377 Neuroscience*, 23, 10577–10584.
3378 <https://doi.org/10.1523/JNEUROSCI.23-33-10577.2003>
- 3379 Lever, C., Burton, S., Jeewajee, A., O'Keefe, J., & Burgess, N.
3380 (2009). Boundary Vector Cells in the Subiculum of the
3381 Hippocampal Formation. *The Journal of Neuroscience*, 29(31),
3382 9771 LP – 9777. <https://doi.org/10.1523/JNEUROSCI.1319-09.2009>
- 3384 Lovett-Barron, M., Kaifosh, P., Kheirbek, M. A., Danielson, N.,
3385 Zaremba, J. D., Reardon, T. R., Turi, G. F., Hen, R., Zemelman,
3386 B. V., & Losonczy, A. (2014). Dendritic inhibition in the
3387 hippocampus supports fear learning. *Science (New York, N.Y.)*,
3388 343(6173), 857–863. <https://doi.org/10.1126/science.1247485>
- 3389 Luo, L., Callaway, E. M., & Svoboda, K. (2018). Genetic Dissection of
3390 Neural Circuits: A Decade of Progress. *Neuron*, 98(2), 256–281.
3391 <https://doi.org/https://doi.org/10.1016/j.neuron.2018.03.040>
- 3392 MacDonald, C. J., Carrow, S., Place, R., & Eichenbaum, H. (2013).
3393 Distinct hippocampal time cell sequences represent odor
3394 memories in immobilized rats. *The Journal of Neuroscience : The
3395 Official Journal of the Society for Neuroscience*, 33(36), 14607–
3396 14616. <https://doi.org/10.1523/JNEUROSCI.1537-13.2013>
- 3397 MacDonald, C. J., Lepage, K. Q., Eden, U. T., & Eichenbaum, H.
3398 (2011). Hippocampal “time cells” bridge the gap in memory for
3399 discontiguous events. *Neuron*, 71(4), 737–749.
3400 <https://doi.org/10.1016/j.neuron.2011.07.012>
- 3401 Manns, J. R., Clark, R. E., & Squire, L. R. (2000). Parallel acquisition
3402 of awareness and trace eyeblink classical conditioning. *Learning*

- 3403 & Memory (*Cold Spring Harbor, N.Y.*), 7(5), 267–272.
3404 <https://doi.org/10.1101/lm.33400>
- 3405 Maruyama, R., Maeda, K., Moroda, H., Kato, I., Inoue, M., Miyakawa,
3406 H., & Aonishi, T. (2014). Detecting cells using non-negative matrix
3407 factorization on calcium imaging data. *Neural Networks : The
3408 Official Journal of the International Neural Network Society*, 55,
3409 11–19. <https://doi.org/10.1016/j.neunet.2014.03.007>
- 3410 Mau, W., Sullivan, D. W., Kinsky, N. R., Hasselmo, M. E., Howard, M.
3411 W., & Eichenbaum, H. (2018). The Same Hippocampal CA1
3412 Population Simultaneously Codes Temporal Information over
3413 Multiple Timescales. *Current Biology*, 28(10), 1499-1508.e4.
3414 <https://doi.org/10.1016/j.cub.2018.03.051>
- 3415 McHugh, T. J., Jones, M. W., Quinn, J. J., Balthasar, N., Coppari, R.,
3416 Elmquist, J. K., Lowell, B. B., Fanselow, M. S., Wilson, M. A., &
3417 Tonegawa, S. (2007). Dentate gyrus NMDA receptors mediate
3418 rapid pattern separation in the hippocampal network. *Science
(New York, N.Y.)*, 317(5834), 94–99.
3419 <https://doi.org/10.1126/science.1140263>
- 3420
- 3421 McLelland, D., & Paulsen, O. (2007). Cortical Songs Revisited: A
3422 Lesson in Statistics. *Neuron*, 53(3), 319–321.
3423 <https://doi.org/https://doi.org/10.1016/j.neuron.2007.01.020>
- 3424 McNaughton, N., & Gray, J. A. (2000). Anxiolytic action on the
3425 behavioural inhibition system implies multiple types of arousal
3426 contribute to anxiety. *Journal of Affective Disorders*, 61(3), 161–
3427 176. [https://doi.org/10.1016/s0165-0327\(00\)00344-x](https://doi.org/10.1016/s0165-0327(00)00344-x)
- 3428 Medina, J. F., Garcia, K. S., Nores, W. L., Taylor, N. M., & Mauk, M. D.
3429 (2000). Timing mechanisms in the cerebellum: testing predictions
3430 of a large-scale computer simulation. *The Journal of
3431 Neuroscience : The Official Journal of the Society for
3432 Neuroscience*, 20(14), 5516–5525.
3433 <https://doi.org/10.1523/JNEUROSCI.20-14-05516.2000>
- 3434 Meeks, J. P., Arnson, H. A., & Holy, T. E. (2010). Representation and
3435 transformation of sensory information in the mouse accessory

- 3436 olfactory system. *Nature Neuroscience*, 13(6), 723–730.
3437 <https://doi.org/10.1038/nn.2546>
- 3438 Miller, A. M. P., Jacob, A. D., Ramsaran, A. I., De Snoo, M. L.,
3439 Josselyn, S. A., & Frankland, P. W. (2023). Emergence of a
3440 predictive model in the hippocampus. *Neuron*.
3441 <https://doi.org/10.1016/j.neuron.2023.03.011>
- 3442 Min, E., Ban, S., Wang, Y., Bae, S. C., Popescu, G., Best-Popescu, C.,
3443 & Jung, W. (2017). Measurement of multispectral scattering
3444 properties in mouse brain tissue. *Biomedical Optics Express*, 8(3),
3445 1763–1770. <https://doi.org/10.1364/BOE.8.001763>
- 3446 Mizrahi, A. (2004). High-Resolution In Vivo Imaging of Hippocampal
3447 Dendrites and Spines. *Journal of Neuroscience*, 24(13), 3147–
3448 3151. <https://doi.org/10.1523/JNEUROSCI.5218-03.2004>
- 3449 Modi, M. N., Dhawale, A. K., & Bhalla, U. S. (2014). CA1 cell activity
3450 sequences emerge after reorganization of network correlation
3451 structure during associative learning. *eLife*, 3, e01982–e01982.
3452 <https://doi.org/10.7554/eLife.01982>
- 3453 Mokeichev, A., Okun, M., Barak, O., Katz, Y., Ben-Shahar, O., &
3454 Lampl, I. (2007). Stochastic Emergence of Repeating Cortical
3455 Motifs in Spontaneous Membrane Potential Fluctuations In Vivo.
3456 *Neuron*, 53, 413–425.
3457 <https://doi.org/10.1016/j.neuron.2007.01.017>
- 3458 Mollinedo-Gajate, I., Song, C., & Knöpfel, T. (2021). Genetically
3459 Encoded Voltage Indicators. *Advances in Experimental Medicine
3460 and Biology*, 1293, 209–224. https://doi.org/10.1007/978-981-15-8763-4_12
- 3462 Morris, R. G. M., Garrud, P., Rawlins, J. N. P., & O’Keefe, J. (1982).
3463 Place navigation impaired in rats with hippocampal lesions.
3464 *Nature*, 297(5868), 681–683. <https://doi.org/10.1038/297681a0>
- 3465 Moser, M.-B., & Moser, E. I. (1998). Distributed encoding and retrieval
3466 of spatial memory in the hippocampus. In *The Journal of
3467 Neuroscience* (Vol. 18, pp. 7535–7542). Society for Neuroscience.

- 3468 Moyer, J. R., Deyo, R. A., & Disterhoft, J. F. (1990). Hippocampectomy
3469 disrupts trace eye-blink conditioning in rabbits. *Behavioral*
3470 *Neuroscience*, 104(2)(Apr 1990), 243–252.
3471 <https://doi.org/10.1037/0735-7044.104.2.243>
- 3472 Mukamel, E. A., Nimmerjahn, A., & Schnitzer, M. J. (2009). Automated
3473 analysis of cellular signals from large-scale calcium imaging data.
3474 *Neuron*, 63(6), 747–760.
3475 <https://doi.org/10.1016/j.neuron.2009.08.009>
- 3476 Muller, R. U., & Kubie, J. L. (1989). The firing of hippocampal place
3477 cells predicts the future position of freely moving rats. *The*
3478 *Journal of Neuroscience : The Official Journal of the Society for*
3479 *Neuroscience*, 9(12), 4101–4110.
3480 <https://doi.org/10.1523/JNEUROSCI.09-12-04101.1989>
- 3481 Murray, T. A., & Levene, M. J. (2012). Singlet gradient index lens for
3482 deep in vivo multiphoton microscopy. *Journal of Biomedical*
3483 *Optics*, 17(2), 021106. <https://doi.org/10.1117/1.JBO.17.2.021106>
- 3484 Nakashiba, T., Young, J. Z., McHugh, T. J., Buhl, D. L., & Tonegawa,
3485 S. (2008). Transgenic inhibition of synaptic transmission reveals
3486 role of CA3 output in hippocampal learning. *Science (New York,*
3487 *N.Y.*), 319(5867), 1260–1264.
3488 <https://doi.org/10.1126/science.1151120>
- 3489 O'Keefe, J., & Burgess, N. (1996). Geometric determinants of the
3490 place fields of hippocampal neurons. *Nature*, 381(6581), 425–428.
3491 <https://doi.org/10.1038/381425a0>
- 3492 O'Keefe, J., & Dostrovsky, J. (1971). The hippocampus as a spatial
3493 map. Preliminary evidence from unit activity in the freely-moving
3494 rat. *Brain Research*, 34(1), 171–175. [https://doi.org/10.1016/0006-8993\(71\)90358-1](https://doi.org/10.1016/0006-8993(71)90358-1)
- 3496 O'Keefe, J., & Nadel, L. (1978). The Hippocampus as a Cognitive Map.
3497 In *Philosophical Studies* (Vol. 27).
3498 <https://doi.org/10.5840/philstudies19802725>
- 3499 O'Keefe, J., & Recce, M. L. (1993). Phase relationship between
3500 hippocampal place units and the EEG theta rhythm.

- 3501 *Hippocampus*, 3(3), 317–330.
3502 <https://doi.org/10.1002/hipo.450030307>
- 3503 Ohyama, T., Nores, W. L., Murphy, M., & Mauk, M. D. (2003). What
3504 the cerebellum computes. *Trends in Neurosciences*, 26(4), 222–
3505 227. [https://doi.org/10.1016/S0166-2236\(03\)00054-7](https://doi.org/10.1016/S0166-2236(03)00054-7)
- 3506 Ozden, I., Lee, H. M., Sullivan, M. R., & Wang, S. S.-H. (2008).
3507 Identification and Clustering of Event Patterns From In Vivo
3508 Multiphoton Optical Recordings of Neuronal Ensembles. *Journal*
3509 *of Neurophysiology*, 100(1), 495–503.
3510 <https://doi.org/10.1152/jn.01310.2007>
- 3511 Pachitariu, M., Stringer, C., Dipoppa, M., Schröder, S., Rossi, L. F.,
3512 Dalgleish, H., Carandini, M., & Harris, K. D. (2017). Suite2p:
3513 beyond 10,000 neurons with standard two-photon microscopy.
3514 *BioRxiv*, 61507. <https://doi.org/10.1101/061507>
- 3515 Paredes, R. M., Etzler, J. C., Watts, L. T., Zheng, W., & Lechleiter, J.
3516 D. (2008). Chemical calcium indicators. *Methods (San Diego,*
3517 *Calif.)*, 46(3), 143–151.
3518 <https://doi.org/10.1016/j.ymeth.2008.09.025>
- 3519 Pastalkova, E., Itskov, V., Amarasingham, A., & Buzsaki, G. (2008).
3520 Internally Generated Cell Assembly Sequences in the Rat
3521 Hippocampus. *Science*, 321(5894), 1322–1327.
3522 <https://doi.org/10.1126/science.1159775>
- 3523 Pavlov, I. P. (1927). Conditioned reflexes: an investigation of the
3524 physiological activity of the cerebral cortex. In *Conditioned*
3525 *reflexes: an investigation of the physiological activity of the*
3526 *cerebral cortex*. Oxford Univ. Press.
- 3527 Peron, S. P., Freeman, J., Iyer, V., Guo, C., & Svoboda, K. (2015). A
3528 Cellular Resolution Map of Barrel Cortex Activity during Tactile
3529 Behavior. *Neuron*, 86(3), 783–799.
3530 <https://doi.org/10.1016/j.neuron.2015.03.027>
- 3531 Petersen, C. C. H. (2019). Sensorimotor processing in the rodent
3532 barrel cortex. *Nature Reviews. Neuroscience*, 20(9), 533–546.
3533 <https://doi.org/10.1038/s41583-019-0200-y>

- 3534 Pfeiffer, B. E., & Foster, D. J. (2013). Hippocampal place-cell
3535 sequences depict future paths to remembered goals. *Nature*,
3536 497(7447), 74–79. <https://doi.org/10.1038/nature12112>
- 3537 Pfeiffer, B. E., & Foster, D. J. (2015). Autoassociative dynamics in the
3538 generation of sequences of hippocampal place cells. *Science*,
3539 349(6244), 180–183. <https://doi.org/10.1126/science.aaa9633>
- 3540 Pnevmatikakis, E. A., Soudry, D., Gao, Y., Machado, T. A., Merel, J.,
3541 Pfau, D., Reardon, T., Mu, Y., Lacefield, C., Yang, W., Ahrens, M.,
3542 Bruno, R., Jessell, T. M., Peterka, D. S., Yuste, R., & Paninski, L.
3543 (2016). Simultaneous Denoising, Deconvolution, and Demixing of
3544 Calcium Imaging Data. *Neuron*, 89(2), 285–299.
3545 <https://doi.org/https://doi.org/10.1016/j.neuron.2015.11.037>
- 3546 Poort, J., Khan, A. G., Pachitariu, M., Nemri, A., Orsolic, I., Krupic, J.,
3547 Bauza, M., Sahani, M., Keller, G. B., Mrsic-Flogel, T. D., & Hofer,
3548 S. B. (2015). Learning Enhances Sensory and Multiple Non-
3549 sensory Representations in Primary Visual Cortex. *Neuron*, 86(6),
3550 1478–1490. <https://doi.org/10.1016/j.neuron.2015.05.037>
- 3551 Ranck, J. B. (1973). Studies on single neurons in dorsal hippocampal
3552 formation and septum in unrestrained rats: Part I. Behavioral
3553 correlates and firing repertoires. *Experimental Neurology*, 41(2),
3554 462–531. [https://doi.org/https://doi.org/10.1016/0014-4886\(73\)90290-2](https://doi.org/https://doi.org/10.1016/0014-4886(73)90290-2)
- 3556 Ranck, J. B. (1975). *Behavioral Correlates and Firing Repertoires of
3557 Neurons in the Dorsal Hippocampal Formation and Septum of
3558 Unrestrained Rats BT - The Hippocampus: Volume 2:
3559 Neurophysiology and Behavior* (R. L. Isaacson & K. H. Pribram
3560 (Eds.); pp. 207–244). Springer US. https://doi.org/10.1007/978-1-4684-2979-4_7
- 3562 Rao, R. P. N., & Ballard, D. H. (1999). Predictive coding in the visual
3563 cortex: a functional interpretation of some extra-classical
3564 receptive-field effects. *Nature Neuroscience*, 2(1), 79–87.
3565 <https://doi.org/10.1038/4580>

- 3566 Reyes, A. D. (2003). Synchrony-dependent propagation of firing rate in
3567 iteratively constructed networks in vitro. *Nature Neuroscience*,
3568 6(6), 593–599. <https://doi.org/10.1038/nn1056>
- 3569 Rogerson, T., Cai, D. J., Frank, A., Sano, Y., Shobe, J., Lopez-Aranda,
3570 M. F., & Silva, A. J. (2014). Synaptic tagging during memory
3571 allocation. *Nature Reviews Neuroscience*, 15(3), 157–169.
3572 <https://doi.org/10.1038/nrn3667>
- 3573 Savelli, F., Yoganarasimha, D., & Knierim, J. J. (2008). Influence of
3574 boundary removal on the spatial representations of the medial
3575 entorhinal cortex. *Hippocampus*, 18(12), 1270–1282.
3576 <https://doi.org/10.1002/hipo.20511>
- 3577 Schreurs, B. G. (1989). Classical conditioning of model systems: A
3578 behavioral review. *Psychobiology*, 17(2), 145–155.
3579 <https://doi.org/10.3758/BF03337830>
- 3580 Scoville, W. B., & Milner, B. (1957). Loss of recent memory after
3581 bilateral hippocampal lesions. In *Journal of Neurology,*
3582 *Neurosurgery & Psychiatry* (Vol. 20, pp. 11–21). BMJ Publishing
3583 Group. <https://doi.org/10.1136/jnnp.20.1.11>
- 3584 Sheffield, M. E. J., & Dombeck, D. A. (2014). Calcium transient
3585 prevalence across the dendritic arbour predicts place field
3586 properties. *Nature*, 517(7533), 200–204.
3587 <https://doi.org/10.1038/nature13871>
- 3588 Siegel, J. J., & Mauk, M. D. (2013). Persistent Activity in Prefrontal
3589 Cortex during Trace Eyelid Conditioning: Dissociating Responses
3590 That Reflect Cerebellar Output from Those That Do Not. *The*
3591 *Journal of Neuroscience*, 33(38), 15272 LP – 15284.
3592 <https://doi.org/10.1523/JNEUROSCI.1238-13.2013>
- 3593 Siegel, J. J., Taylor, W., Gray, R., Kalmbach, B., Zemelman, B. V.,
3594 Desai, N. S., Johnston, D., & Chitwood, R. A. (2015). Trace
3595 Eyeblink Conditioning in Mice Is Dependent upon the Dorsal
3596 Medial Prefrontal Cortex, Cerebellum, and Amygdala: Behavioral
3597 Characterization and Functional Circuitry. *ENeuro*, 2(4),

- 3598 ENEURO.0051-14.2015. <https://doi.org/10.1523/ENEURO.0051-14.2015>
- 3600 Skaggs, W., McNaughton, B., Gothard, K., & Markus, E. (1996). An
3601 Information-Theoretic Approach to Deciphering the Hippocampal
3602 Code. *Neural Inf. Process Syst.*, 5.
- 3603 Sofroniew, N. J., Flickinger, D., King, J., & Svoboda, K. (2016). A large
3604 field of view two-photon mesoscope with subcellular resolution for
3605 in vivo imaging. *eLife*, 5(JUN2016), 1–20.
3606 <https://doi.org/10.7554/eLife.14472>
- 3607 Solstad, T., Boccara, C. N., Kropff, E., Moser, M.-B., & Moser, E. I.
3608 (2008). Representation of Geometric Borders in the Entorhinal
3609 Cortex. *Science*, 322(5909), 1865–1868.
3610 <https://doi.org/10.1126/science.1166466>
- 3611 Souza, B. C., Pavão, R., Belchior, H., & Tort, A. B. L. (2018). On
3612 Information Metrics for Spatial Coding. *Neuroscience*, 375, 62–73.
3613 <https://doi.org/10.1016/j.neuroscience.2018.01.066>
- 3614 Stosiek, C., Garaschuk, O., Holthoff, K., & Konnerth, A. (2003). In vivo
3615 two-photon calcium imaging of neuronal networks. *Proceedings of
3616 the National Academy of Sciences of the United States of
3617 America*, 100(12), 7319–7324.
3618 <https://doi.org/10.1073/pnas.1232232100>
- 3619 Suh, J., Rivest, A. J., Nakashiba, T., Tominaga, T., & Tonegawa, S.
3620 (2011). Entorhinal cortex layer III input to the hippocampus is
3621 crucial for temporal association memory. *Science (New York,
3622 N.Y.)*, 334(6061), 1415–1420.
3623 <https://doi.org/10.1126/science.1210125>
- 3624 Taube, J. S., Muller, R. U., & Ranck, J. B. J. (1990). Head-direction
3625 cells recorded from the postsubiculum in freely moving rats. I.
3626 Description and quantitative analysis. *The Journal of
3627 Neuroscience : The Official Journal of the Society for
3628 Neuroscience*, 10(2), 420–435.
3629 <https://doi.org/10.1523/JNEUROSCI.10-02-00420.1990>

- 3630 Uncapher, M. R., Hutchinson, J. B., & Wagner, A. D. (2011).
3631 Dissociable effects of top-down and bottom-up attention during
3632 episodic encoding. *The Journal of Neuroscience : The Official*
3633 *Journal of the Society for Neuroscience*, 31(35), 12613–12628.
3634 <https://doi.org/10.1523/JNEUROSCI.0152-11.2011>
- 3635 Valero, M., Cid, E., Averkin, R. G., Aguilar, J., Sanchez-Aguilera, A.,
3636 Viney, T. J., Gomez-Dominguez, D., Bellistri, E., & de la Prida, L.
3637 M. (2015). Determinants of different deep and superficial CA1
3638 pyramidal cell dynamics during sharp-wave ripples. *Nature*
3639 *Neuroscience*. <https://doi.org/10.1038/nrn.4074>
- 3640 Velasco, M. G. M., & Levene, M. J. (2014). In vivo two-photon
3641 microscopy of the hippocampus using glass plugs. *Biomedical*
3642 *Optics Express*, 5(6), 1700–1708.
3643 <https://doi.org/10.1364/BOE.5.001700>
- 3644 Vinogradova, O. S. (2001). Hippocampus as comparator: Role of the
3645 two input and two output systems of the hippocampus in selection
3646 and registration of information. *Hippocampus*, 11(5), 578–598.
3647 <https://doi.org/https://doi.org/10.1002/hipo.1073>
- 3648 Voelcker, B., Pancholi, R., & Peron, S. (2022). Transformation of
3649 primary sensory cortical representations from layer 4 to layer 2.
3650 *Nature Communications*, 13(1), 5484.
3651 <https://doi.org/10.1038/s41467-022-33249-1>
- 3652 Wood, E. R., Dudchenko, P. A., Robitsek, R. J., & Eichenbaum, H.
3653 (2000). Hippocampal Neurons Encode Information about Different
3654 Types of Memory Episodes Occurring in the Same Location.
3655 *Neuron*, 27(3), 623–633.
3656 [https://doi.org/https://doi.org/10.1016/S0896-6273\(00\)00071-4](https://doi.org/https://doi.org/10.1016/S0896-6273(00)00071-4)
- 3657 Yiu, A. P., Mercaldo, V., Yan, C., Richards, B., Rashid, A. J., Hsiang,
3658 H.-L. L., Pressey, J., Mahadevan, V., Tran, M. M., Kushner, S. A.,
3659 Woodin, M. A., Frankland, P. W., & Josselyn, S. A. (2014).
3660 Neurons are recruited to a memory trace based on relative
3661 neuronal excitability immediately before training. *Neuron*, 83(3),
3662 722–735. <https://doi.org/10.1016/j.neuron.2014.07.017>

- 3663 Zhang, S., & Manahan-Vaughan, D. (2015). Spatial olfactory learning
3664 contributes to place field formation in the hippocampus. *Cerebral*
3665 *Cortex (New York, N.Y. : 1991)*, 25(2), 423–432.
3666 <https://doi.org/10.1093/cercor/bht239>
- 3667 Zhou, S., Masmanidis, S. C., & Buonomano, D. V. (2020). Neural
3668 Sequences as an Optimal Dynamical Regime for the Readout of
3669 Time. *Neuron*, 108(4), 651-658.e5.
3670 <https://doi.org/https://doi.org/10.1016/j.neuron.2020.08.020>
- 3671 Zhou, Y., Won, J., Karlsson, M. G., Zhou, M., Rogerson, T., Balaji, J.,
3672 Neve, R., Poirazi, P., & Silva, A. J. (2009). CREB regulates
3673 excitability and the allocation of memory to subsets of neurons in
3674 the amygdala. *Nature Neuroscience*, 12(11), 1438–1443.
3675 <https://doi.org/10.1038/nn.2405>
- 3676 Ziv, Y., Burns, L. D., Cocker, E. D., Hamel, E. O., Ghosh, K. K., Kitch,
3677 L. J., El Gamal, A., & Schnitzer, M. J. (2013). Long-term dynamics
3678 of CA1 hippocampal place codes. *Nature Neuroscience*, 16(3),
3679 264–266. <https://doi.org/10.1038/nn.3329>